

Encoding of Odorants by Olfactory Sensory Neurons

Zita Peterlin

Submitted in partial fulfillment of the
requirements for the degree of
Doctor of Philosophy
in the Graduate School of Arts and Sciences

COLUMBIA UNIVERSITY

2012

ABSTRACT

Encoding of Odorants by Olfactory Sensory Neurons

Zita Peterlin

The olfactory system relies on a combinatorial code where a given odorant receptor (OR) detects multiple odorants, and a given odorant is detected by multiple ORs (Malnic, Hirono et al. 1999). Prior attempts to decipher the code have emphasized linking genetic sequence to functional profile, but this approach has led to deorphanization of only ~85 out of ~1200 ORs in mouse (Zhang and Firestein 2007). With such a narrow window onto the combinatorial code, even the deorphaned ORs effectively remain stranded.

High throughput calcium imaging of olfactory sensory neurons (OSNs) can provide the missing context. With this method, it is possible to survey the population response patterns while still preserving information on the individual receptive fields that contribute to the ensemble. I have used this technique to gain a more comprehensive view of the combinatorial code.

Octanal is an odorant capable of recruiting many OSNs, but how functionally diverse are they? Screening with a panel of odorants made the subdivisions among this large suite of OSNs clear, revealing that nearly half uniquely parse the test panel.

Expanding upon this, I show that such rare response patterns can be used like a fingerprint to assess, via physiology, that an OSN expresses a given OR.

Population level analysis of the combinatorial code led me to two driving concepts. One is that the OR repertoire, despite its diversity, is nevertheless markedly constrained in its ability to discriminate certain series of odorants. For example, an OSN cannot respond to an alcohol and acid without also responding to an aldehyde. Exploring potential mechanisms, I used designer aldehydes that were trapped in an intermediate polar anchor state. I found that a previously discounted binding mode correlated with the ability of OSNs to selectively respond to aldehydes while excluding alcohols.

The other key finding is that odorants can often adopt high energy conformations when activating OSNs. Initially, this was noted for aromatic odorants during a general screen. To probe the phenomenon in greater detail, I used a series of cyclized compounds that mimic rarely assumed states of the flexible tail of octanal. Comparing the activation strength of each analog to that elicited by unconstrained octanal demonstrated extensive co-recognition. This suggests that the flexibility of octanal contributes to its promiscuity in terms of recruiting a high number of OSNs.

This study led to the realization that rings could often be treated as merely preserving a particular trajectory of a hydrocarbon backbone. Guided by this concept, I developed new panels with odorants that previously would have been considered discrepant. Hedione is an odorant where a ring imparts specialized geometry that greatly impacts perception. Yet at the OR combinatorial code level, I found that the ring was not critical and flexible but related odorants were still effective. I also demonstrated that OSNs readily accept odorants where an aromatic ring has been substituted with specific

alkyl fragments. Thus, aromatic rings too, despite their unique electronics, are sometimes better viewed from a strictly architectural perspective.

Using population analysis to identify what the ORs deem the important features of odorants can clarify the trends that sculpt the combinatorial code. This knowledge can help us consolidate seemingly broad receptive fields to better understand what information the OR repertoire extracts from the external chemical environment.

TABLE OF CONTENTS

<u>CHAPTER 1 - SECTION 1 : General Introduction</u>	1
Part A : Engaging the external chemical world	
Olfaction provides important information about the external world	2
Odorants are complex stimuli	3
Odorants are diverse despite constraints	5
Part B : The combinatorial code	
The olfactory system manages this complexity via a combinatorial code	7
Estimating the size of the code for a given odorant	8
Part C : Means of monitoring the code	
Heterologous expression has proven insufficient for this task	10
The transduction cascade in OSNs provides a way to monitor the code	13
Some caveats when using OSNs	16
Glomerular imaging is an alternate to using dispersed OSNs for select questions	18
Promise of integrating the two approaches in the future	20
Part D : Development of OSN panel screening	22
Section I : Impact of data selection	
Focus on sequences shunts attention from the full combinatorial code	23
Sequence information does not yet contribute to understanding the code	24
Technical difficulties can lead to partial panels with limited interpretation	26

Emphasis on physical proximity reports on biased OR space	27
Section II : Impact of data display	
Template for the panel format	28
Panels allow reinterpretation as themes in the field evolve	29
Alternate data display formats can inadvertently be constricting	30
Part E : Recent panel screens with novel focus	
A panel designed to evaluate the relationship between code and percept	31
Performing panel screening with mixes	32
Part F : Summary	33
<u>CHAPTER 1 - SECTION 2 : Introduction to reading panels</u>	57
Part A : Introduction to panel organization	58
Horizontal rows reflect the receptive field of unique odorant receptors	58
The importance of inactive odorants in data interpretation	59
Patterns between vertical columns look at population-wise ease of discrimination	60
Supplemental visualization of co-activation patterns	61
Part B : Case Study	62
Composition of the odorant panel	62
Reading 1 : Is there a “biological fovea” for terpenes?	63
Reading 2 : Predicting antagonism	64

Reading 3 : Sensitivity to subtleties of the alkyl scaffold	65
Part C : Conclusion	66
<u>CHAPTER 2 - SECTION 1 : A pharmacological profile of the aldehyde</u>	
receptor repertoire in rat olfactory epithelium	71
Abstract	72
Introduction	73
Methods	
Isolation of sensory neurons	76
Ca ²⁺ imaging recordings	77
Data analysis	78
Results	80
A receptor for aldehydes can discriminate among closely related molecules	81
Geranial can distinguish among different octanal receptors	83
Different receptors exhibit various sensitivities for aldehydes	84
Molecular range of other aldehyde receptors	85
Selectivity is maintained at higher concentrations	88
Discussion	89
Acknowledgements	96

<u>CHAPTER 2 - SECTION 2</u> : Validating the functional fingerprint concept	111
Abstract	112
Introduction	113
Appropriate odor selection can achieve unique profiles	113
The presenting problem	115
Methods	
Panel pruning : a tradeoff between speed and accuracy	116
Marginally activating compounds can compromise a fingerprint	116
Rationale for extracting an I7 fingerprinting panel of odorants	117
Results	119
Discussion	119
Combining adenoviral infection with functional fingerprinting of an alternate receptor allows a direct contrast in chemical parsing strategies	121
<u>CHAPTER 3 - Dual modes of aldehyde recognition by odorant receptors</u>	131
Abstract	132
Introduction	133
Results	136
Proximal alkyl substitution is highly disfavored across the 8AL+ population	137
A diol-mode requisite 8AL+ subpopulation	138

A carbonyl-mode requisite 8AL+ subpopulation	139
Population-specific response broadening of DIF suggests beneficial diol pre-formation	141
Only diol-mode requisite OSNs can selectively discriminate aldehydes	141
Rat I7 is an OR that utilizes diols for both activation and antagonism	142
Discussion	143
Methods	
Isolation of olfactory sensory neurons	146
Calcium imaging of olfactory sensory neurons	147
Acknowledgements	148
<u>CHAPTER 4 - The importance of odorant conformation to the binding and activation of a representative odorant receptor</u>	159
Abstract	160
Introduction	160
Results	163

A series of conformationally restricted eight-carbon aldehydes	164
OR-I7 activation: Octanal uses a semi-extended conformation	165
Small cycloalkyl rings enhance OR-I7 activation	167
An activating octanal conformation	167
Conformational determinants of OR-I7 antagonism	169
Functional group determinants of OR-I7 antagonism	171
Conformational flexibility contributes to the activation range of an odorant	171
Discussion	174
Significance	180
Experimental procedures	
Method to estimate the maximum extended length of aldehydes	181
Synthesis of octanal analogs	181
Isolation of olfactory sensory neurons	181
Calcium imaging of olfactory sensory neurons	182
Acknowledgements	184
<u>CHAPTER 5 - Identification of acyclic, activity-graded Hedione mimics</u>	199
Abstract	200
Introduction	201
Methods	204
Results	
Subclasses among the HED+ population	205

Subclass 1 : The cyclopentanone ring is a required epitope	205
Subclass 2 : Reliably graded activation by unconstrained esters	206
Responsiveness to HED impacts the pattern of MENON/NERAC discrimination	207
The conformer adopted by cis3-HEXAC may depend on the OR's response to MENON	208
Discussion	209
Future Directions	
Rationale for expanding the scope of this study	212
Current status of terpene encoding among other functional groups	212
Proposed modified panel	214
Comparisons of particular note within this panel	214
<u>CHAPTER 6 - Benzene bioisosterism at odorant receptors</u>	235
Abstract	236
Introduction	237
Methods	240
Results	
Alkyl ring substitutions	241
Cyclohexene as an effective alkyl bioisostere for a benzene ring	241
A steric spectrum between three alkyl mimics of benzene	242

Heteraromatic ring substitutions : selection of aromatic cores	243
OR repertoire-wide rejection of nitrogen-containing heteroaromatic cores	244
Thiophene as the best bioisostere for benzene among ORs	244
A suspected polar filter underlying a “spectrum” among heteroaromatic rings	245
Extensive cross-recognition between aliphatic and aromatic space	246
Discussion	246
<u>CHAPTER 7 - Future Directions : Exploring ester encoding</u>	263
Introduction	264
Background	
Reported ester-responsive ORs are broadly tuned	264
OR1G1 and OR1D2 prioritize different features of esters	265
Proposed investigation of ester encoding	266
Does the continuity rule transfer from “1D” space to the esters?	267
Where is the fovea/ae of highest recruitment for esters?	268
Investigating bioisosterism can also reveal arm usage bias	268
Esters as a platform for investigating the structure of chemical space	270
<u>SUMMARY</u>	281
<u>REFERENCES</u>	285

LIST OF FIGURES AND TABLES

CHAPTER 1 - SECTION 1

Figure 1.1 - relationships within a homologous series	35
Figure 1.2 - interactions between the polar group and alkyl scaffold	36
Figure 1.3 - diversity among odorants	37
Figure 1.4 - sparsely activating odorants still do not constitute a labeled line	38
Figure 1.5 - odorants exhibit a range of recruitment levels	40
Figure 1.6 - signal transduction cascade in mammalian OSNs	41
Figure 1.7 - patterned projection of OSNs from olfactory epithelium locations to general locations in the olfactory bulb	43
Figure 1.8 - failure of protein models to predict ligands of rat I7	44
Figure 1.9 - Sato et al.'s foundational template for panel presentation	46
Supplemental Figure 1.1 - inconsistencies between heterologous expression systems	48
Supplemental Figure 1.2 - odorants recognized by both Class I and Class II ORs	50
Supplemental Figure 1.3 - possible class-based bias in recruitment by odorants	52
Supplemental Figure 1.4 - proposed ligand-interacting residues on the rat I7 receptor	55

CHAPTER 1 - SECTION 2

Figure 1.10 - case study in panel reading	68
-------------------------------------------	----

CHAPTER 2 - SECTION 1

Figure 2.1 - panel of odorants used to characterize the pharmacological profiles of receptors for octanal	97
Figure 2.2 - pharmacology of OR-I7-expressing cells and cells expressing other receptors for aldehydes	98
Figure 2.3 - aldehyde receptors can discriminate closely related compounds	100
Figure 2.4 - the isomers geranial and neral reduce the responses to octanal at some aldehyde receptors	102
Figure 2.5 - cells exhibit distinct response profiles to a test panel of odorants	105
Figure 2.6 - cluster analysis reveals several aldehyde receptor types	106
Figure 2.7 - selectivity of aldehyde receptors is maintained at different concentrations	108
Table 2.1 - GFP+ (OR-I7) and GFP- cells tested with different aldehydes and non-aldehyde compounds in OR-I7-infected animals	110

CHAPTER 2 - SECTION 2

Figure 2.8 - distribution of observed response profiles	124
Table 2.2 - frequency of activation by a given odorant given the status of the response to octanal	126
Figure 2.9 - visualization of overlap patterns	127
Figure 2.10 - response patterns in the retrovirally-induced I7 system	128

Supplemental Figure 2.1 - partial receptive fields for rat I7 and hOR17-4	
demonstrate near mutual exclusivity	130

CHAPTER 3

Figure 3.1 - schematic of how proximal fluorination of aldehydes shifts	
the hydration equilibrium	149

Figure 3.2 - panel screen for the mode of octanal binding	150
-----------------------------------------------------------	-----

Figure 3.3 - octanal-responsive OSNs can selectively recognize either form of	
the aldehyde	152

Figure 3.4 - response broadening by DIF appears only among	
diol-mode requisite ORs	154

Figure 3.5 - rat I7 primarily uses the diol form for activation	156
-----------------------------------------------------------------	-----

Figure 3.6 - I7 antagonists must be able to assume a diol form	157
----------------------------------------------------------------	-----

CHAPTER 4

Figure 4.1 - conformationally restricted octanal analogs	185
----------------------------------------------------------	-----

Figure 4.2 - OR-I7 activation by cyclic octanal analogs	186
---------------------------------------------------------	-----

Figure 4.3 - cyclopropyl and cyclobutyl ring-containing analogs are more potent	
than predicted from their maximal lengths	189

Figure 4.4 - a semi-extended octanal conformation activates OR-I7	190
Figure 4.5 - inhibition of OR-I7 activation by short octanal analogs	192
Figure 4.6 - conformational preference among octanal receptors	194
Figure 4.7 - summary of OR-I7 binding and activation by octanal conformation mimics	196
Supplemental Figure 4.1 - OR-I7 activation by longer aldehydes and compounds with a more bulky terminus	197

CHAPTER 5

Figure 5.1 - Hedione stereoisomers	219
Figure 5.2 - ring closing and ring opening relationships	220
Figure 5.3 - structures of compounds used in this study	221
Figure 5.4 - altered polar topology of the ester arm	222
Figure 5.5 - response profiles of cells to the Hedione fragment mimics	224
Figure 5.6 - Venn representation of response trends	227
Figure 5.7 - Structures and relationships within the proposed extension panel	228
Supplemental Figure 5.1 - cis-3-hexenyl acetate as a weak mimic of a benzene ring	230
Supplementary Figure 5.2 - assaying terpene bias in olfactory space	232
Supplementary Figure 5.3 - cis/trans preference for the isomers of citral	233

CHAPTER 6

Figure 6.1 - compounds used and their recruitment frequencies	251
Figure 6.2 - overlap between aromatic and aliphatic odorant space	252
Figure 6.3 - co-recognition among the alkyl scaffolds	253
Figure 6.4 - response profiles for OSNs responding to nitrogen-containing heteroaromatic compounds	255
Figure 6.5 - co-recognition between ACE and other aromatic odorants	256
Figure 6.6 - extensive cross-recognition between aromatic and aliphatic cores	258
Supplementary Figure 6.1 - contrasting classical isosteres with bioisosteres	259
Supplementary Figure 6.2 - aromatic rings and cyclohexene rings in common odorants	261
Supplementary Figure 6.3 - some properties of the heteroaromatic cores used in this study	262

CHAPTER 7

Figure 7.1 - asymmetry of esters sets up a homologous matrix	272
Figure 7.2 - two strategies of ester recognition used by ORs	273
Figure 7.3 - an ester percept violating the continuity rule	274
Figure 7.4 - a series of esters with which to explore bioisosteric relationships	276
Figure 7.5 - how the bioisostere series of esters also probes embedding depth	278

Figure 7.6 - relationship between ketones and esters 279

Figure 7.7 - two ways of conceptualizing the relationship between
regular esters and lactones 280

ACKNOWLEDGEMENTS

Do not go where the path may lead, go instead where there is no path and leave a trail.

- Ralph Waldo Emerson

Each morning this quote reminded me of my duty, and each morning I was proud to serve as a scout at the edge of the unknown in a truly remarkable lab. Stuart Firestein grants each person the freedom to pursue the path they are passionate about. I value what I have learned from each lab member over the many years. I particularly want to thank those who served as guides at critical points. Drs. Ricardo Araneda and Matthew Rogers imparted a strong technical foundation. They also deftly balanced nurturing the enthusiasm of a young graduate student with sculpting that energy towards a more focused target. Alexander Chesler brought humor and optimism to a very challenging experiment. Cen Zhang's patience and expertise in cell culture were of great help. Armen Enikolopov was talented at listening to imaginings about odor space and then generously writing the code to make those visions real. I especially want to thank Drs. Jessica Brann and Dongjing Zou. They have been immensely supportive throughout the thesis process, providing valued perspective and advice.

Outside of the Firestein lab, thanks goes to Prof. Rafael Yuste who granted me my first independent research project. The transition from a bookish undergraduate to an acting scientist took place under his guidance, and I could not have had a better training experience. Prof. Kevin Ryan introduced me to applying medicinal chemistry perspectives to odorants. His student, Yadi Li, synthesized the specialized compounds

that were critical to this work. Dr. Christian Margot engaged in fascinating discussions of the chemical intricacies of odorants, making the olfactory world even more vibrant through stories of psychophysical phenomenon. Dr. Maria Ines also played a formative role. Her insightful question about zonal expression reverberated long after our brief discussion, prompting me to think critically about subsystem encoding.

Most of all, my profound gratitude goes to Stuart Firestein for his stabilizing confidence and unwavering support.

CHAPTER 1 - SECTION 1
GENERAL INTRODUCTION

PART A : ENGAGING THE EXTERNAL CHEMICAL WORLD

Olfaction provides important information about the external world

The olfactory system governs our sense of smell and contributes greatly to our experience of flavor (Doty 2009). Yet among the long-range senses, olfaction is sometimes undervalued, regarded as being ancillary and primarily of hedonic value. Actually, the olfactory system can provide crucial information in situations when visual and auditory cues are insufficient. Odors can alert an organism to the presence of a concealed predator (Hacquemand, Jacquot et al. 2010; Matsukawa, Imada et al. 2011) or unfit, spoiled food (Takahashi, Nagayama et al. 2004). Wafting odors can guide an organism to a food source. Since the complex chemical blend that emanates from many fruits alters with ripeness, the subtleties of the bouquet can provide a gauge of nutritional content (Takahashi, Nagayama et al. 2004).

The odorant receptors (ORs) are GPCRs that bind odorants to initiate the signal transduction cascade. With ~1200 members in mouse and ~1300 members in rat (Zhang and Firestein 2007), the ORs form the main interface with the external volatile chemical world. However, for specialized tasks, other chemoreceptors also participate. Vomeronasal receptors are key in identifying potential mates and their reproductive status (Mucignat-Caretta 2010). The TRPM5 expressing OSNs (Lin, Margolskee et al. 2007) and GC-D expressing OSNs (Juilfs, Fulle et al. 1997) in the main olfactory epithelium also detect semiochemicals. The TAARs assist with amine detection (Liberles

and Buck 2006). Although trigeminal receptors do not project to the olfactory bulb, they integrate detection of several noxious chemical stimuli (Peterlin, Chesler et al. 2007).

Many of the same chemicals detected by these specialized subsystems are also detected by ORs. For example, 2-heptanone is a ligand not only for the vomeronasal receptor V1rb2 (Boschat, Pelofi et al. 2002), but also for the odorant receptor 912-93 (Gaillard, Rouquier et al. 2002). 2-heptanone also activates the odorant receptors MOR139-3 (Yoshikawa and Touhara 2009), MOR271-1 and MOR272-1 (Saito, Chi et al. 2009). Trimethylamine is a ligand of the TAAR receptor mTAAR5, and mTAAR4 detects phenylethylamine (Liberles and Buck 2006). Yet these amines are also ligands for odorant receptors OR1A1 (Schmiedeberg, Shirokova et al. 2007) and OR5 (Kobilka and Deupi 2007) respectively. Comparison with the TRPA1 nociceptor particularly highlights how ORs continue to lend unique contributions to sensation even when there are shared ligands. Cinnamaldehyde activates the trigeminal TRPA1 nociceptor by forming a covalent adduct. This mechanism locks TRPA1 in an active state for hours (Hinman, Chuang et al. 2006; Macpherson, Dubin et al. 2007). Multiple ORs are also activated by cinnamaldehyde but only transiently (Araneda, Peterlin et al. 2004). The capacity of ORs to rapidly reset after a pulse of odorant allows the organism to detect a gradient and thus select a direction for action.

Odorants are complex stimuli

Understanding how the olfactory system can detect thousands of odorants and yet still make nuanced discriminations is a great challenge in sensory physiology. The

stimulus qualities in olfaction are quite different from that of other long-range sensory systems. Vision and audition detect intangible, analog stimuli. The dimensional organization of wavelength / frequency and amplitude are readily defined. Moreover, they are independent of one another. This allows for fine control of the stimulus in experimental settings.

In contrast, odorants are discrete physical entities. They are multifaceted with no clear dimension predominating. Homologous series of n-compounds possess a polar functional group at one terminus and an unbranched alkyl tail of incrementing carbon number (Figure 1.1A). The series might thus seem to have a dimension in terms of tail length. The appeal of this apparent organization led to homologous series being the stimuli of choice in the majority of early studies on olfactory encoding by ORs (Sato, Hirono et al. 1994; Malnic, Hirono et al. 1999; Kaluza and Breer 2000). But while the extended length of the tail in homologous series does increase linearly, the tails are flexible and can assume a number of conformers. The number of conformers scales roughly by $3^{(2n-1)}$ where “n” equals the number of carbons in the tail (Figure 1.1B) With this consideration in mind, how does one order the range of shapes swept out within a given homologous series, let alone order the various polar functional groups at the heads of these series? Even for the most architecturally simple odorants, the organization of chemical space is opaque.

Another complication when working with odorants is that chemical features can be highly context dependent (Figure 1.2). In the citronellyl hydrocarbon scaffold, the methyl proximal to the polar group head is skewed relative to the hydrocarbon backbone. A double bond converts this to a geranyl scaffold where the methyl is now planar.

Examining how frequently other ORs can make this discrimination could be an experimental goal, but the appropriateness of the “lead compound” for the test depends highly on the identity of the polar head group. When the nearby functional group is an aldehyde, the change in methyl orientation results in steric tension as well as an electrical perturbation of the aldehyde group strength. These secondary effects do not occur when the polar head group is an alcohol. Thus, elementary changes are not as readily isolated for olfactory stimuli as in other systems.

Odorants are diverse despite constraints

Odorants need to be volatile and this imposes constraints on their makeup. These constraints, in turn, can make the typical ligands challenging to detect. Molecular weight strongly impacts volatility. Most odorants have a molecular weight below 300 Daltons. As a result, highly interlocked rigid carbon scaffolds are rare with the steroidal odorants, such as androstenone, representing the extreme. More commonly, odorants are much smaller and either fully flexible or only partially constrained.

Although composition of between 6-10 carbons seems a general trend, there are many ways these scaffolds can be arranged (bold numbers that follow refer to Figure 1.3). At one extreme are the compact rigid compounds, such as cyclic terpenes (**1**) and small aromatics (**2**). At the other extreme are the highly flexible n-compounds with a single polar head and an unbranched tail. Volatility is hindered by an overabundance of polar or charged groups if the odorant emanates from an aqueous source. When presented in mineral oil, though, ORs can respond to such odorants (Oka, Katada et al. 2006). Still,

many of the odorants typically studied have but one polar group to provide strong hydrogen bonding, leading the alkyl scaffold to play a particularly important role in ligand recognition and stabilization.

Even with these constraints, known odorants span a gamut of compositions. N-compounds such as octanal (**5**) have only a single terminal polar group, but they can recruit many ORs due to highly flexible alkyl tails that can mold to a variety of shapes (Peterlin, Li et al. 2008). Vanillin (**3**) is a compact rigid aromatic with multiple polar groups that provide a “Velcro-like” set of strong attachments points. Large steroidal odorants such as androstenone (**8**) achieve rigidity through interlocking ring systems, but the tiny diacetyl (**9**) achieves rigidity through electrical repulsion. Many odorants, such as bourgeonal (**4**), have a “ball and chain” architecture with a rigid aromatic ring attached to a distal polar group via a variable flexible linker region. Linear terpenes like citronellal (**6**) have plate-like rigid regions and highly stereotypic branching patterns. This stereotypy may be what allows some terpenes, such as farnesene (**7**) and limonene (**10**), to eschew polar groups completely.

To identify biologically meaningful features and to properly rank relationships within chemical space requires an empirical study of the broad-scale response patterns among the odorant receptors. This is the aim of my thesis.

PART B : THE COMBINATORIAL CODE

The olfactory system manages this complexity via a combinatorial code

Against this diversity of odorants are arrayed the ~1194 ORs in the mouse and ~1284 ORs in rat (Zhang and Firestein 2007). These Class A GPCRs form the largest gene family (Buck and Axel 1991). Yet there is even a greater number of potential odorants, suggesting that each OR must recognize multiple ligands. In their seminal work, Malnic et al. (1999) established that this is indeed the case. Chemical detection and discrimination by ORs is particularly intriguing because all ligands, be they discrepant-looking agonists or even antagonists, appear to utilize the same binding pocket. A structure-activity relationship model of the very broadly tuned OR1G1 receptor could still account for all 95 binding compounds in one molecular overlay (Sanz, Thomas-Danguin et al. 2008). Empirically, only competitive antagonism has ever been demonstrated, even when the odors are highly discrepant as in the case of halothane and citral (Peterlin, Ishizawa et al. 2005). From what seems to be a chemical cacophony, each OR abstracts a unifying suite of features.

Malnic et al. (1999) also demonstrated that the same odorant activates different ORs. Thus, no labeled line seems to exist either in the direction of ligand to receptor or in the direction of receptor to ligand. Instead there is a complex reciprocal combinatorial code. Fascinatingly, this is far from a uniform code. The size of the recruited ensemble of ORs can vary widely between odorants. N-octanal is the most robust recruiter I have studied, activating at least 37 OR types based on differential response patterns but

possibly as high as ~50-60 ORs (Araneda, Peterlin et al. 2004). Diacetyl, however, may activate only ~5-6 ORs (0.6% of n=1015 OSNs tested). Yet even sparsely activating ligands do not appear to constitute a labeled line; the rare diacetyl-responding olfactory sensory neurons were also responsive to various mixtures of alcohols, esters, and aldehydes (Figure 1.4).

Estimating the size of the code for a given odorant

A third critical finding of the Malnic et al. (1999) study was that rodent olfactory sensory neurons (OSNs) express only a single OR. This paves the way for high throughput evaluation of the combinatorial code because cellular activation can be taken as a proxy for OR activation. Combined with the fact that there are 1200+ intact ORs in the genome for mice and rats (Zhang and Firestein 2007), if one makes the simplifying assumption that the ORs are expressed with equal frequency, then the percent of OSNs activated by a given compound in a large sample can provide a rough estimate of the number of ORs activated.

There are recognized caveats to this approximation. Expression frequency actually varies among ORs. MOR28 is expressed at a very high rate (Tsuboi, Yoshihara et al. 1999), and differing degrees in OR expression between the P2, P3, and P4 receptors are clearly seen in whole mount images from transgenic mouse lines (Feinstein and Mombaerts 2004). There is also a developmental time course such that ~30% of intact ORs that were previously expressed at embryonic or immature ages are no longer expressed at 6-8 weeks of age (Zhang, Rogers et al. 2004). Moreover, a handful of ORs

are expressed exclusively in tissues outside the OE (Zhang, Rogers et al. 2004).

However, since it is not feasible to recover the OR sequences for every cell recorded, the assumption of equal expression of the full genomic number of intact ORs is commonly used to translate the percent of cells activated to an approximate number of ORs.

The size of the population that a given odorant recruits will impact the type of experiment which that ligand is best suited for (Figure 1.5). In addition to octanal, some high recruiters I have worked with include gamma-undecalactone (3.9%; n=634 OSNs screened), citral (3.6%; n=553), and hexyl acetate (2.8%; n=634). Such compounds are well suited for panning for trends that shape the code and for presenting challenging discriminations.

In contrast, odorants that are only sparsely recognized by the OR repertoire make amenable targets for RT-PCR retrieval. Gaining a particular sequence multiple times would add a level of assurance of accurate sequence identification (Mizrahi, Matsunami et al. 2004). As few as ~2 ORs were estimated for such compounds as hexyl salicylate, acetoin, 2-acetyl pyridine, and acetyl pyrazine. Hexyl salicylate makes a particularly intriguing target given that it can be viewed as a phenol-appended form of the robust recruiter hexyl acetate. Why the flexible hexyl arm, which would be expected to be a permissive feature, fail in the salicylate context would be an intriguing question that could be probed by computational modeling following RT-PCR retrieval.

In summary, the “one OR is activated by multiple odorants and one odorant activates multiple ORs” arrangement has been dubbed the reciprocal combinatorial code (Malnic, Hirono et al. 1999). This distributed code enables the system to resiliently

detect a broad array of diverse chemicals while retaining the ability to make nuanced discriminations. Studying the combinatorial code is critical since the activity patterns across the OR repertoire form the substrate for all higher olfactory processing. And yet, outside the work presented in this thesis, the full combinatorial code has scarcely received attention.

PART C : MEANS OF MONITORING THE CODE

Heterologous expression has proven insufficient for this task

Admittedly, the biology of the olfactory system has presented some substantial challenges to studying the combinatorial code. OSNs survive only marginally in culture (Gonzales, Farbman et al. 1985; Gangadhar, Firestein et al. 2008). It has also proven notoriously difficult to achieve proper OR trafficking in heterologous systems (Matsunami 2005; Bush and Hall 2008). Various cell lines have been tried, accessory factors and chaperones provided, and assistive tags appended (Von Dannecker, Mercadante et al. 2006; Bush and Hall 2008). Still, reliable expression is far from routine.

The predominant approach to heterologous expression employs HEK cells or tailored variants. Using HEK 293 cells along with one of the promiscuous Galpha subunits, Ga15 or Ga16 (Kajiya, Inaki et al. 2001), to perform calcium imaging has proven quite robust for the MOREG receptor. However, other ORs did not perform as

well. The Hana3A cell line is an HEK 293T derivative that stably expresses Golf and the assistive molecules RTP1, RTP2, and REEP (Saito, Kubota et al. 2004). Supplemented by RTP1S (a short form of RTP), this formed the platform for the impressive large panel deorphanization by Saito et al. (2009). Ric-8B is an adjunct accessory factor that can also be used in HEK systems (Von Dannecker, Mercadante et al. 2006). It is promising because it promotes expression even in the absence of the N-terminal rho tag that is commonly appended to OR sequences.

An important alternate heterologous system is based on HeLa cells. It more completely recapitulates the native olfactory transduction cascade. The HeLa cells are stably transfected with CNGA2 to create homomeric cyclic nucleotide gated channels. They are also stably transfected with Golf and the connexin CX43 (Shirokova, Schmiedeberg et al. 2005; Schmiedeberg, Shirokova et al. 2007). Work with this system demonstrated that the G-protein identity can dramatically shift the apparent receptive field; an antagonist when Golf was used became a robust agonist when Ga15 was used (Shirokova, Schmiedeberg et al. 2005).

Oocytes can also be induced to express ORs, (Katada, Nakagawa et al. 2003; Abaffy, Matsunami et al. 2006; Repicky and Luetje 2009). The oocyte expression technique typically employs RTP1, RTP2, and REEP1. Golf is added along with the CFTR channel. Upon receptor activation, the increase in cAMP directly gates CFTR, leading to chloride flux that can be monitored by voltage recording. The traces appear very stable and many odorants can be tested. However, because the oocyte technique requires individual mRNA injection, it is ill suited for high throughput assays. Thus, it does not present a viable approach to monitoring the full combinatorial code.

Despite intensive efforts, until 2009 only 34 ORs out of the full repertoire of ~1200 mouse ORs had been functionally expressed. These have been scattered over multiple expression systems and tested with different ligand sets, making direct comparison difficult. The study by Saito et al. (2009) is a marked technical achievement that represents the first concerted effort to investigate the combinatorial code using heterologous expression. The authors expressed a panel of 52 mouse ORs, 48 of which were novel. While this sample still only represents ~4% of the total code, they thoughtfully attempted to express a member from each of the full-length sequence-derived phylogenetic families.

Although this is the best performance of a heterologous systems to date, I suggest caution in applying patterns gleaned from this study without additional empirical validation in native OSNs. Firstly, the response profiles only partially matched that from 6 ORs that had previously been tested in other systems (Supplemental Figure 1.1) Secondly, the panel in Saito et al. (2009) is not simply a smaller reflection of the combinatorial code. The number of ORs in each family varies dramatically, with family sizes ranging from 1 through 50 members (Zhang and Firestein 2002). Equal expression of one OR per family will not recapitulate this distribution. Moreover, only 52 (Saito, Chi et al. 2009) of 328 families (Zhang and Firestein 2002) were represented in the final panel.

All these factors may contribute to the pronounced skew in percent activation between what was observed in the heterologous screen versus what we find when monitoring the full OR repertoire as expressed by native OSNs. Strikingly, Saito et al. found only one OR out of 52 (2%) responding to octanal while I find regularly find

~5.5% of OSNs responding to this compound at 30uM (Araneda, Peterlin et al. 2004; Peterlin, Li et al. 2008). Conversely, while Saito et al. found an astounding 29% recruitment by acetophenone (15/52 receptors), I witness more modest 3% activation at 30uM. The trends on display in the heterologous expression panel are indeed intriguing; my pursuit to understand the basis of the high degree of co-recognition between acetophenone and carvone (detailed in Chapter 6) was sparked by this panel. Heterologous systems are finally beginning to show practical promise in generating leads, but they are not quite yet ready to serve as the sole means of deciphering the combinatorial code.

The transduction cascade in OSNs provides a way to monitor the code

At present, the most reliable and robust means of tracking the code is to use the OSNs themselves. Even though the response profiles obtained from acutely prepared OSNs are shorter, in other respects the biology of the olfactory system works in favor of monitoring the full suite of ORs in a high throughput manner.

OSNs possess a single dendrite bearing 15-30 slender cilia (McEwen, Jenkins et al. 2008). The cilia are specialized compartments with low internal volume that promote close proximity of the brigade of signaling factors, thus increasing efficiency (Pifferi, Menini et al. 2010). In its resting state the inactive OR is bound to the heterotrimeric G-protein comprised of GDP-bound Galpha-olf (Jones and Reed 1989) and beta and gamma subunits. Two other major transduction participants, adenylyl cyclase III (ACIII) (Bakalyar and Reed 1990) and phosphodiesterase PDE1C2 (Borisy, Ronnett et al. 1992;

Yan, Zhao et al. 1995), are basally active but in balance. Either of these members can be pharmacologically targeted to assess whether the OSN has retained its cilia post-dissociation and is thus “viable” from a functional perspective. Forskolin upregulates ACIII directly, leading to increased cAMP production and preemptive recruitment of the downstream cascade. IBMX inhibits phosphodiesterases, preventing cAMP breakdown. This leads to accumulation of basally produced cAMP and eventual triggering of the downstream cascade.

Binding of an odorant (Figure 1.6A) leads to presumed conformational changes in the OR. Based on other Class A GPCR models, this may involve adjustment of helices TM5 and TM6 (Deupi and Standfuss 2011). Translated to the C-terminus, these rearrangements induce Golf to exchange its GDP for GTP. Odorants are bound so transiently that mathematical models predict that only a single Golf is activated per odorant binding event (Bhandawat, Reisert et al. 2005). The G-protein dissociates, and Golf upregulates ACIII (Fukuda, Yomogida et al. 2004). The resultant cAMP accumulation directly gates CNG (Kaupp and Seifert 2002). CNG is an ion channel that provides inflow of both sodium and calcium ions (Nakamura and Gold 1987). This initial calcium influx, however, is localized to the narrow cilia. It can be monitored optically, but only via scanning confocal microscopy (Leinders-Zufall, Rand et al. 1997), making this signal unsuited for high-throughput screening. The local rise in calcium activates an outward flowing but depolarizing chloride current (Kleene 1993). Long thought to be critical for signal amplification, the precise role of this current is now in question (Billig, Pal et al. 2011).

The depolarization propagates to the cell soma, recruiting further voltage gated channels and eventually leading to the opening of voltage gated calcium channels. The resultant somatic calcium transient can be readily monitored in a high throughput manner. Unlike the upstream ciliary calcium influx, the somatic calcium signal provides $\sim 80\mu\text{m}^2$ target area that is amenable to conventional fluorescent microscopy using calcium indicators. Fura2-AM is the most commonly used fluorescent calcium indicator (Sato, Hirono et al. 1994; Malnic, Hirono et al. 1999; Kajjya, Inaki et al. 2001; Hamana, Hirono et al. 2003; Araneda, Peterlin et al. 2004; Fukuda, Yomogida et al. 2004; Peterlin, Ishizawa et al. 2005; Oka, Katada et al. 2006; Peterlin, Li et al. 2008), although Fluo3 (Kaluza and Breer 2000) and Calcium Green (Ma and Shepherd 2000) have also been employed. Onset of the somatic calcium transient is fast, already peaking by 4 sec post stimulus application. Decay of the transient is slower, on the order of minutes. It is likely driven by the dynamics of calcium extrusion and sequestration in the soma, but kinetics of the dye also likely contribute to the rate of signal dissipation too.

The signal transduction cascade in the cilia terminates much faster (Figure 1.6B). Apocalmodulin, the calcium free version of calmodulin, is already bound to the CNG channels (Bradley, Bonigk et al. 2004). The calcium flowing through the CNG channels binds to apocalmodulin. This results in rapid modulation of the CNG channel, decreasing its sensitivity to cAMP (Kramer and Siegelbaum 1992) and thereby preventing further influx of calcium. Calcium-bound calmodulin also activates CAM Kinase II, which phosphorylates ACIII to decrease cAMP production (Wei, Zhao et al. 1998). While it was thought that CAMKII also phosphorylated PDE1C2 to upregulate it, this is now in question (Boccaccio, Lagostena et al. 2006). Calcium is primarily extruded by a

Na⁺/Ca²⁺ exchanger (Reisert and Matthews 1998), although the potassium-dependent exchanger NKCX1-3 may assist (Pyrski, Koo et al. 2007). Finally, the chloride gradient needs to be restored. This is achieved by the Na⁺/K⁺/2Cl⁻ cotransporter NKCC1 (Reisert, Lai et al. 2005).

This resetting allows for multiple odorant assays at each OSN. When recording voltage, adaptation can occur if two activating odorant pulses are presented close together, leading to a smaller response amplitude to the second application of the same odor. However, this adaptation has already attenuated by the time the odor pulses are separated by about 7 seconds (Kurahashi and Menini 1997); our stimuli are typically given at least 4-5 minutes apart. Thus, calcium imaging at the soma of the OSNs allows us to test a battery of odorants, maintaining single cell and thus single receptor type resolution, while surveying multiple cells in the field of view. It is this combination of fine resolution and ability to achieve a global survey in a high throughput manner that makes the dispersed cell calcium imaging technique so amenable for studying the combinatorial code.

Some caveats when using OSNs

When interpreting panel data based on OSN responses, it is critical to note how they were prepared. OSNs are consolidated into a dense sheet called the olfactory epithelium (OE) that lines the convoluted turbinate bones of the nasal cavity. While visually featureless, there is intrinsic patterning of the OE in terms of OR expression. Subsets of ORs were once believed to be restricted in expression to one of four, non-

overlapping zones of the OE (Ressler, Sullivan et al. 1993) (Figure 1.7A). Within the zonal limits, the OSNs could select an OR from that subset in a random manner (Imai and Sakano 2009). A strict zonal boundary does seem to apply to the dorsal-most portion of the OE. This zone I region almost exclusively expresses class I ORs, and almost all the class I ORs are expressed in this region (Zhang, Rogers et al. 2004). The more ventral “zones”, however, are now recognized to be far more graded. Any given Class II OR is still locally restricted in a band, but these bands are of variable width and are overlapping (Miyamichi, Serizawa et al. 2005). Thus, due to the anatomical organization, any small portion of OE tissue provides only a biased representation of ORs and thus a distorted view of the code.

This feature impacts studies that utilize tissue printing and septal knob recording methods. In tissue printing, a lightly enzyme-treated piece of OE is gently rolled on a coverslip coated with an adhesive, roughly maintaining the local anatomical relationships from the tissue in the now dispersed cells (Sato, Hirono et al. 1994). This technique is well suited to study whether proximally located OSNs share greater similarities in their receptive field. OSNs treated in this manner also seem to be more robust, making this a technique of choice in studies emphasizing RT-PCR recovery of OR sequence (Malnic, Hirono et al. 1999; Hamana, Hirono et al. 2003). The septal knob preparation uses fully intact pieces of the flat OE from the medial-most region of the nasal cavity. The tips of the dendrites, where they poke through the protective support cell layer, are imaged rather than the soma (Ma and Shepherd 2000). Septal knob imaging has always been a specialized technique to investigate proximal patterning as opposed to the overall combinatorial code, and that constraint has always been clearly stated.

In acute OSN preparations, only short response profiles can typically be obtained. Using the dispersed cell method, I find that OSNs remain reliable for about an hour, allowing assessment of only ~10 different stimuli. Investigators that incorporate RT-PCR subsequent to imaging tend to curtail profile length since successful sequence retrieval plummets to nearly 30% (Malnic, Hirono et al. 1999; Hamana, Hirono et al. 2003) or even down to 7% (Touhara, Sengoku et al. 1999) with prolonged UV excitation (Hamana, Hirono et al. 2003). As I will demonstrate in this thesis, very interesting questions can still be successfully probed using short chemical panels. Still, a means of extending the duration of the recording, and hence the response profile length, would be beneficial.

Glomerular imaging is an alternate to using dispersed OSNs for select questions

Imaging the dorsal olfactory bulb (OB) offers just such a means to investigate a subset of the combinatorial code in greater detail. The axons from OSNs expressing the same OR converge to only two narrowly circumscribed regions on the OB, one located dorsally and one medially (Mombaerts, Wang et al. 1996). The dense neuropil from this cohort of axon terminals is called a glomerulus. There is a rough patterning to the OB that corresponds to the dorsal to ventral progression in the OE (Mombaerts 2004) (Figure 1.7A) What is beneficial to those studying the combinatorial code is that all zone I OSNs, representing the full suite of Class I ORs, project to the dorsal-most surface of the OB (Tsuboi, Miyazaki et al. 2006; Matsumoto, Kobayakawa et al. 2010) (Figure 1.7B). This

region can be readily monitored by optical methods, either through a thinned skull or by removing the skull and adhering a coverslip.

Activity of OSNs projecting to the dorsal OB can thus be tracked in an intact animal, permitting delivery of an extended battery of odorants. Activity has traditionally been monitored by intrinsic signals (Uchida, Takahashi et al. 2000; Takahashi, Kurosaki et al. 2004; Takahashi, Nagayama et al. 2004; Soucy, Albeanu et al. 2009; Tsuboi, Imai et al. 2011). However, recent generation of a transgenic mouse that expresses synapto-pHluorin in all OSNs provides even finer resolution (Bozza, McGann et al. 2004). Synapto-pHluorin is a pH sensitive fluorescent protein fused to a synaptic vesicle protein. Its luminosity increases when vesicles fuse following cell excitation (Miesenbock, De Angelis et al. 1998). The density of axon termini in the glomeruli makes this approach attractive, and it is rapidly being adopted (Bozza, McGann et al. 2004; Soucy, Albeanu et al. 2009).

Imaging of intrinsic signals in the dorsal bulb has a long history under the guidance of K. Mori. A series of studies have characterized the receptive fields of several glomeruli (Uchida, Takahashi et al. 2000; Takahashi, Kurosaki et al. 2004; Takahashi, Nagayama et al. 2004; Tsuboi, Imai et al. 2011). Initially, the panels consisted of simple homologous series and the focus was more descriptive (Uchida, Takahashi et al. 2000). But in later studies, longer response profiles and application of a broader variety of structures shifted emphasis to development of structure-activity relationships (Takahashi, Kurosaki et al. 2004). However, despite the wealth of data, no attempt has been made to extract the general rules governing chemical parsing by ORs, a goal I have tried to achieve in my work. Instead, dorsal bulb imaging remains fixated

either on developing ever refined descriptions of the shared features among “modules” of neighboring glomeruli (Mori, Takahashi et al. 2006) or whether there is a chemotopic map on the OB in the first place (Bozza, McGann et al. 2004; Soucy, Albeanu et al. 2009).

Promise of integrating the two approaches in the future

Why promote dorsal bulb glomerular imaging as a means of investigating discrimination between chemicals? After all, dispersed cell calcium imaging is an efficient and powerful method for monitoring the combinatorial code. The most compelling argument is that the anatomical segregation permits a unique chance to compare and contrast the detection strategies used by the Class I versus Class II ORs. Class I and Class II ORs have no gross topological differences. Still, bioinformatic analysis has revealed a number of short motifs with predicted functional relevance that are class unique or heavily class biased (Liu, Zhang et al. 2003; Zhang and Firestein 2007). Thus, although there are odorants that are indeed recognized by both defined Class I and Class II receptors (Supplementary Figure 1.2), the mechanisms by which they are detected might be intrinsically different.

For example, at their preferred alkyl tail length, all dorsally projecting and putatively Class I expressing ORs that were activated by an n-aldehyde could also be activated by an n-amine (Takahashi, Nagayama et al. 2004). The Class II OR rat I7 clearly prefers eight carbon tails (Zhao, Ivic et al. 1998). But while it is activated by the aldehyde it fails to respond to the amine (Araneda, Kini et al. 2000). This implies that the

two classes of OR employ differential polar group filtering capabilities, but this needs to be evaluated on a much larger scale. The heterologous expression panel screen conducted by Saito et al. (2009) also suggests that some ligands may be restricted in detection to only Class I or Class II ORs (Supplementary Figure 1.4). Given similarities between the suggested “exclusive” sets, however, it is important to evaluate if the trends from their pilot extend to a full survey of natively expressed ORs.

In a collaborative approach to determining if there are pronounced differences in chemical encoding between Class I and Class II ORs, the long response profiles obtained from the glomerular recordings can be used first to rapidly identify the chemical parsing rules operating among the Class I ORs. After a trend is identified, one can then turn to the dispersed full epithelium technique to survey the full complement of Class II ORs, the majority of which are hidden from glomerular imaging (Matsumoto, Kobayakawa et al. 2010) (Figure 1.7A). This assay can also provide a secondary confirmation of any suspected chemical parsing specialization. Microdissection of the dorsal-most part of the OE can provide Class I OR enrichment (Zhang, Rogers et al. 2004), but because there is no visible demarcation of zone boundaries, purity is always somewhat suspect. Furthermore, some class II ORs, such as MOREG (Oka, Katada et al. 2006), are interspersed among the Class I ORs in the dorsal epithelium region. The recent development of a transgenic mouse in which all Class II OR-expressing OSNs are GFP+ permits clear identification of class identity (Matsumoto, Kobayakawa et al. 2010), making these proposed comparative studies reliable for the first time.

Promisingly, a convergence between the concepts being explored in glomerular imaging and those established in dispersed cell calcium imaging seems to already be

underway. We proposed and validated the concept of “functional fingerprinting” as a way to physiologically identify a specific OR and return to it in subsequent assays (see Chapter 2 - Section 2). Soucy et al. (2009) have independently replicated the methodology to identify matched glomeruli on the opposing bulb. Because the two techniques have different strengths and are best suited to probe different OR classes, glomerular imaging and dispersed cell calcium imaging can complement each other. Together, they can greatly enhance our appreciation of the most fundamental aspect of olfactory sensory physiology, the combinatorial code.

PART D : DEVELOPMENT OF OSN PANEL SCREENING

Odor panel screens on large ensembles of OSNs provide a wealth of information from which one can extract multi-tiered relationships between odorants. But a study’s utility as a future resource depends highly on what data is included as well as how it is displayed. All panels may appear similar, but a careful comparison underscores that our panels uniquely incorporate three key elements: a broad and unbiased survey of the OR repertoire, consistent application of odorants to all cells, and preservation of each cell’s response pattern. The form of our panel construction springs from our emphasis on actively engaging the code as opposed to merely describing it. This template has since been adopted by others (Furudono, Sone et al. 2009; Nara, Saraiva et al. 2011). The following literature review tracks the evolution of the modern panel.

Section I : Impact of data selection

Focus on sequences shunts attention from the full combinatorial code

In their foundational work, Malnic et al. (1999) very convincingly demonstrated that RT-PCR retrieved only one OR sequence per OSN. The linking of sequence to activity was indeed crucial to conceptualization of the combinatorial code. But what does not necessarily follow is why the receptive fields were only reported from the cells where an OR sequence had been retrieved. Due to this filter, only a fraction of the code that must have been encountered (given the meager 30% success rate for OR retrieval) was reported.

This approach seemed adopted without question in the RT-PCR-based studies that followed. Because emphasis was placed solely on profiles that could be tagged to sequences, the 70% “failure rate” meant that a vast amount of valid functional information was discarded. One set of studies reported the response profile of only 3 of the 226 OSNs that were activated by a panel of 11 odorants (Kajiya, Inaki et al. 2001; Fukuda, Yomogida et al. 2004). The opportunity for full panel reporting was also lost in Hamana et al.’s 2003 study on carvones; 263 carvone+ OSNs were observed, but the profiles of only 28 OSNs were reported. Valuing OSNs only for their sequence greatly shunted attention away from appreciating the the combinatorial code and how ORs work in concert.

Sequence information does not yet contribute to understanding the code

The appeal of tagging a genetic signature to a functional signature is understandable. The initial expectation was that genetically identified families would represent functional families. If so, knowing the gene sequence would help predict core elements of the receptive field. However, little support currently exists for the notion that phylogenetic organization based on full-length sequences captures functional organization well. Tested in oocytes, the three members of the MOR42 family do all respond to long chain acids. But MOR42-2 is selective for diacids while the other members reject this multipolar ligand (Abaffy, Matsunami et al. 2006). Further, the sequences for carvone-sensitive ORs were found to distribute broadly across the OR repertoire as it was understood at that time (Hamana, Hirono et al. 2003).

More recently, the qualities of a set of 16 amino acids dispersed throughout the receptor sequence have been proposed to be superior to using the full length sequence when predicting receptive fields (Saito, Chi et al. 2009). While this selective focus does result in a 2.5-fold improvement for the ORs in the test set used to build the model, the success rate of predicting ligands for a novel OR plummets to just above chance. Thus, at present, gene sequence is not a ready route to extracting or expanding the receptive field.

Can the OR sequence be used, instead, to generate a model of the protein to predict potential ligands in silico? Results have been mixed. Multiple models of the I7 receptor have been constructed, all proposing different bound conformations of octanal and different “critical” interacting residues (Singer 2000; Hall, Floriano et al. 2004; Lai, Singer et al. 2005; Khafizov, Anselmi et al. 2007; Kurland, Newcomer et al. 2010)

(Supplemental Figure 1,5). Models have predicted activation by fluorooctane and high concentrations of octanoic acid (Singer 2000), and they have predicted binding by linal (Hall, Floriano et al. 2004). None of these predictions have materialized (Figure 1.8) (Hall, Floriano et al. 2004). All the I7 models were built off a rhodopsin template, but there has been a recent and rapid increase in the range of Class A GPCR crystal structures obtained in both active and inactive conformations (Katritch, Cherezov et al. 2012). These can serve as improved templates, but so far even the new templates have left some ambiguity. At hOR17-40 the traditional docking strategy resulted in many spurious “hits” that failed to activate *in vivo* (Anselmi, Buonocore et al. 2011). However, greater reliability has been found with a dynamic modeling strategy applied to hOR2AG1 (Gelis, Wolf et al. 2011), giving hope for this newer approach (Wolf, Bockmann et al. 2008).

In summary, for detailed characterization of a given OR’s receptive field and the mechanism by which it discriminates odorants it is indeed appropriate to retrieve the OR by RT-PCR. This is a necessary first step towards heterologous expression or the generation of transgenic animals (in silico methods are not yet robust enough to operate without one of these *in vivo* methods for confirmation). But if the goal is to extract large scale trends of how receptors work together to encode odorants, the step of adding a tag to an OSN, after its functional properties have already been acquired, is largely extraneous.

Technical difficulties can lead to partial panels with limited interpretation

To understand the combinatorial code is already challenging. To attempt to interpret a fractured code, due to failure to consistently apply the same odorants on all OSNs, can severely limit conclusions. In fairness, these partial panels often arise out of facing pronounced technical challenges.

One challenge is that of retrieving an OR sequence by RT-PCR after imaging. Hamana et al. (2003) ascribed the difficulty to duration of exposure to UV light. They thus took a strategy of curbing the number of odorants assayed. While they consistently applied the two enantiomers of carvone, other related cyclic terpenes and linear terpenes were tested only sporadically. As a result, their panel must be read carefully, for much of what casually appears to be “no response” is really “not tested”.

The technical challenge faced by Bieri et al. (2004) is inherent to the code itself. Sandalwood odorants activate very few OSNs; in our hands, the particular odorant dactanol activates only ~5-6 ORs (0.5%; n=940). One needs to pan through many OSNs to find this signature. We approached the problem by using a lower magnification objective. Bieri et al.’s strategy to deal with the rarity was to continuously move fields, applying a different sandalwood odor on each one, until an active OSN was found. Inexplicably, once a responding OSN was found, the previously presented odors were never re-applied. Thus, none of the sandalwood odorants ended up being tested on all the reported OSNs. As a consequence, this commercially important class of odorants still remains largely uncharacterized.

Emphasis on physical proximity reports on biased OR space

As previously discussed, another caveat when interpreting panels is the source of the OSN population. With the discovery of a zonal expression pattern of ORs came curiosity as to whether ORs within the same zone shared similar response profiles. This question was targeted using both tissue printing (Sato, Hirono et al. 1994) or intact tissue imaging (Ma and Shepherd 2000). These studies were clear in their circumscribed scope, and it is important to respect that. Other studies, however, fail to make this constraint inherent in tissue printing obvious. In most studies a potential mis-reading does not dilute the main conclusions of the work (Malnic, Hirono et al. 1999; Hamana, Hirono et al. 2003). However, it is unclear why this methodology should persist in a recent study that sought to correlate response pattern similarity to perceptual similarity (Furudono, Sone et al. 2009); there, a full epithelial survey would have been more appropriate. Even if fewer OSNs are recorded from a full OE dispersed cell preparation, I feel it provides a better representation of the combinatorial code than a highly oversampled and restricted region.

Section II : Impact of data display

How data is reported can profoundly impact its future utility. The contrast between the display format of Sato et al (1994) and Kaluza and Breer (2000) highlights this difference.

Template for the panel format

Despite being the earliest investigation of the combinatorial code in rodents, Sato et al. (1994) used a very sophisticated panel format for reporting their results (Figure 1.9). The functional data from each cell were preserved, and stacking the response profiles adjacent to one another formed a compact and highly informative matrix. The authors did not use the panel as a mere passive repository for profiles, but instead actively made comparisons within and between cells. The display of the full data set, combined with working to extract organizational principles of the code, marks this as closest to our approach to panel screening. The greatest difference is in repertoire bias and size. Sato et al used the more circumscribed tissue printing method (resulting in Class I bias) and they reported on fewer cells; we harvest the complete epithelium and scan hundreds of viable OSNs.

Intriguingly, Sato et al.'s panel pre-dates the work by Malnic and Buck (1999) and was thus conducted before the emphasis on receptor sequence had become entrenched. It would take five years until Kaluza and Breer (2000) and we (Araneda, Peterlin et al. 2004) would independently shift from the dominant focus on sequences and single receptors to re-discover that the combinatorial code could be profitably studied using OSN responses as endpoints in and of themselves.

Panels allow re-interpretation as themes in the field evolve

Because of the panel format's flexibility and its ability to succinctly preserve all the relationships, the data from Sato et al. (1994) can be re-interpreted in terms of the modern question of deducing order in chemical space. Sato et al. tested OSNs with two parallel homologous series of n-alcohols and n-acids, ranging from carbon chain lengths from three to nine. Their purpose was to observe the rates of functional group discrimination and to identify the preferred tail length at each functional group (if the cell responded to both an alcohol and acid). They found that among such OSNs, the preferred tail length was the same whether the polar group was an acid or alcohol.

But I would argue that this data matrix can be read as a guide for how to establish polar groups' "biological ranking". The dimensionality that orders various polar groups is currently unclear from models of chemical space and is an area of active study (Haddad, Khan et al. 2008; Saito, Chi et al. 2009). In Sato et al.'s panel, two measures of "strength" of the polar group are possible. One is to observe the range of tail lengths tolerated per functional group. A stronger stabilizing group would be predicted to accommodate a larger range of tails. The second is to measure the relative response magnitude between two polar group compounds at a given length. Evaluation of Sato et al.'s panel in this manner shows that the two gauges of "strength" can indeed be used interchangeably to converge on the same assignment. Thus, due to the panel format display, the data can provide a platform for a new way of approaching questions of the organization of the combinatorial code.

Alternate data display formats can inadvertently be constricting

In contrast, without the panel format other means of display may suffice for the question at hand but limit future applications. The study of homologous n-aldehydes by Kaluza and Breer (2000) is contemporary with our first panel screen (Araneda, Peterlin et al. 2004). As the only other study to collect OE tissue from all regions and to monitor a large number of OSNs, it represented one of the first opportunities to assess the full combinatorial code for a series of clearly related odorants.

Kaluza and Breer's primary emphasis was on the discriminatory capabilities between various tail lengths, expanding upon earlier studies with other functional groups that suggested the existence of a "biological fovea" of maximal recruitment (Sato, Hirono et al. 1994; Malnic, Hirono et al. 1999). Extending the tail range tested, they demonstrated maximal recruitment at eight carbons, with levels tapering at higher and lower chain lengths. Kaluza and Breer were also the first to clearly state the "continuity rule", that if an OSN responds to a n-odorant of carbon number X and (X+2), it also will respond to (X+1).

But Kaluza and Breer chose to provide only summary bar graphs as opposed to response profiles from individual cells in a panel format. As a result, one could not witness the "handoff" of the code for aldehydes as the tail length changed. Without the raw data, other interesting features that could have provided a more rounded picture, such as average breadth of the tail range or which direction those ranges tend to extend cannot be addressed or reverse engineered from the bar graphs provided.

In contrast, our study spanned a slightly more restricted range of n-aldehydes but provided much of the same data as a panel (Araneda, Peterlin et al. 2004). This permits more flexible evaluation of the role of alkyl subsidy in the system. Panels are succinct, transparent, and information rich, but perhaps we underestimated how its compactness could affect reader accessibility. For its limitations, the study by Kaluza and Breer highlights that it is useful to supplement the core panel by explicitly extracting and presenting comparisons in auxiliary formats.

PART E : RECENT PANEL SCREENS WITH NOVEL FOCUS

Traditionally, panels have focused on odorant structure. However, recent large scale OR repertoire surveys are investigating the combinatorial code from other perspectives. Because both studies employ the panel format, the data is preserved for alternate readings and applications.

A panel designed to evaluate the relationship between code and percept

Furodono et al. (2009) used a panel of aromatic compounds, selected because they elicit partially overlapping percepts in humans. The aim was to determine if OSN activity patterns across the mouse OR repertoire could predict the groupings made by humans based on percept. Earlier attempts at correlating the combinatorial code at the OR level with percept similarities had been made, but these were secondary analyses that

either simply listed available descriptors from literature (Malnic, Hirono et al. 1999) or used a complex and fairly confusing weighting scheme (Hamana, Hirono et al. 2003). Furodono et al. made percept correlation a primary aim, employing multidimensional scaling and interpretation of the resulting clusters.

Performing panel screening with mixes

The panel screening performed by Nara et al. (2011) is curious in that it employs mixes of odorants, roughly clustered by functional group, instead of pure compounds. Previously, Bozza et al. (2002) had employed mix panels on a very small scale; the response profiles of twenty random OSNs to a series of mixes were shown in order to contrast their functional diversity with the uniformity seen by M71-expressing OSNs. The study by Nara et al. spans the full OR repertoire and focuses on the mix responses patterns as terminal data.

While this does provide a gauge as to functional group frequency of use and co-recognition, because no mix had perfectly matched alkyl scaffolds this panel is difficult to interpret. Our work shows that the alkyl scaffold is an important contributor to the receptive field (Peterlin, Li et al. 2008). Further, there may be stronger potential for intramix antagonism to yield false negatives when alkyl scaffolds are more similar (Peterlin, Li et al. 2008). This omnipresent specter of antagonism when using mixes has been appreciated ever since bourgeonal, a high-potency agonist of the hOR17-4 receptor, was missed in initial screening due to co-presence of the antagonist undecanal in the blend (Spehr, Gisselmann et al. 2003).

Still, the study by Nara et al. is the first to examine neglected classes of odorants such as macrocyclic musks, ethers, and thiols, providing a glimpse of how their codes relate to more commonly studied functional groups.

PART F : SUMMARY

As discrete and multifaceted entities, odorants form a challenging stimulus space to understand. Over 1200+ receptors (Zhang and Firestein 2007) are employed to provide the mouse with the required discriminative capacities. Because these receptors work as an ensemble to parse chemicals, understanding the function of any one receptor is incomplete without appreciation of its context within the repertoire. Large scale screening of olfactory sensory neurons is a robust means of probing how the biological system weights given chemical relationships. Reporting this data in a panel format preserves the richness of the multiple interrelationships.

(this page intentionally left blank)

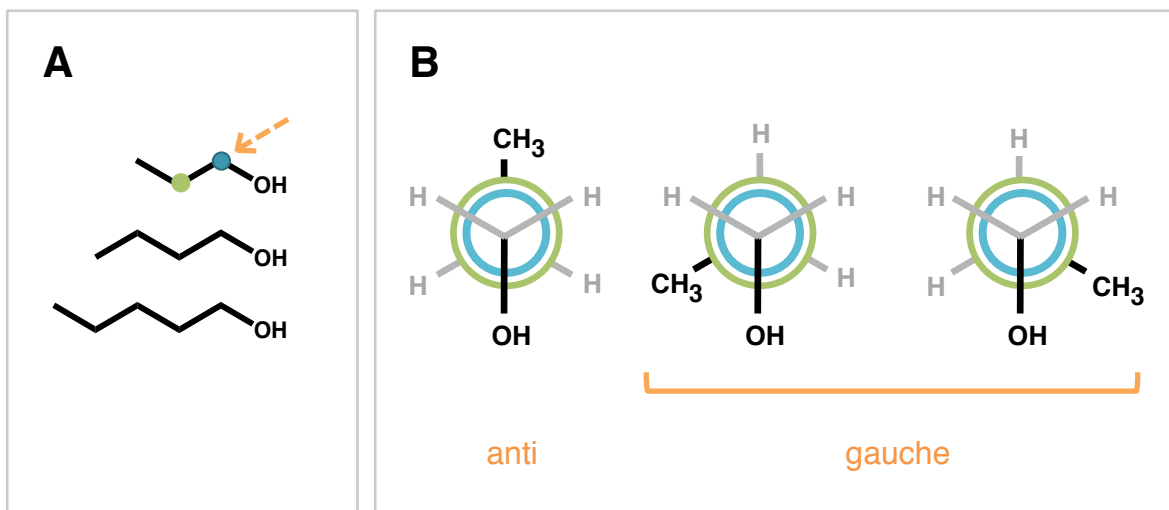


Figure 1.1 - relationships within a homologous series (A) A homologous series of n-alkanols. The polar group is at one terminus, and the unbranched alkyl tail increments in carbon number ranging from $n = 3$ to 5. If the alkyl tail assumes the lowest energy, all “anti” conformation, then the compound length would increase linearly with n . (B) Conformational freedom complicates the dimensionality of even simple homologous series. Newman projection viewing down the carbon 1 (blue) to carbon 2 (green) bond. Carbon 1 is facing front-most towards the reader. The lowest energy form has the methyls on adjacent carbons staggered in the anti conformation (left). However, with only minor energy expenditure the methyl tail can rotate to assume the gauche conformations (right). These three positions are why the number of total conformers scales as approximately $3^{(2n-1)}$ given n carbons in the tail. The actual number is slightly lower as some conformers are symmetrical -- as in this example using propanol.

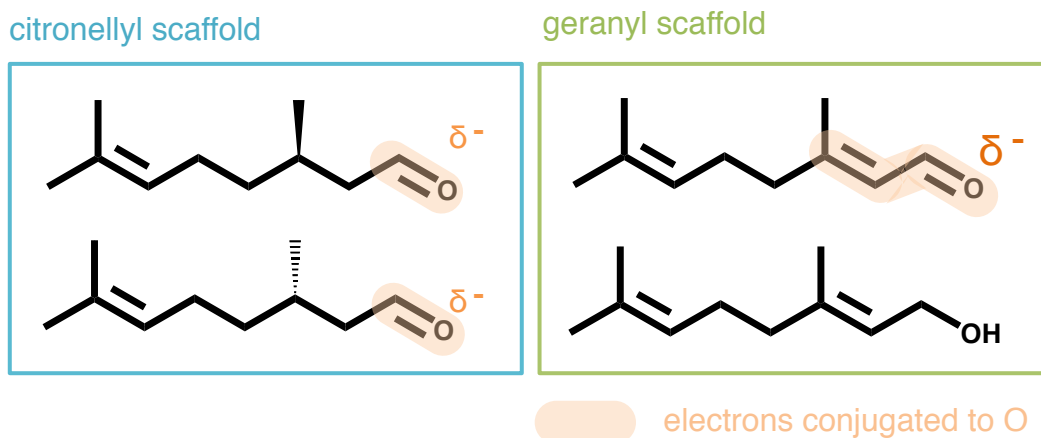


Figure 1.2 - interactions between the polar group and alkyl scaffold. (A) The citronellyl alkyl scaffold shown with an aldehyde functional group. The methyl on carbon 3 is chiral, veering off the axis of the main chain. The aldehyde group electron delocalization (shaded orange) results in a modest partial negative charge on the oxygen. (B) Introducing a double bond between carbon 2 and carbon 3 converts the citronellyl scaffold to a geranyl scaffold. From the alkyl perspective, the only change is making the C3 carbon planar. But when an aldehyde functional group is present (top), there is also extended electrical conjugation, leading to a greater partial negative charge on the oxygen. There is also steric pressure between the planar methyl and the planar aldehyde. Such secondary effects of the scaffold conversion do not occur when the functional group is an alcohol (bottom). Polar group and alkyl scaffold interactions are complex.

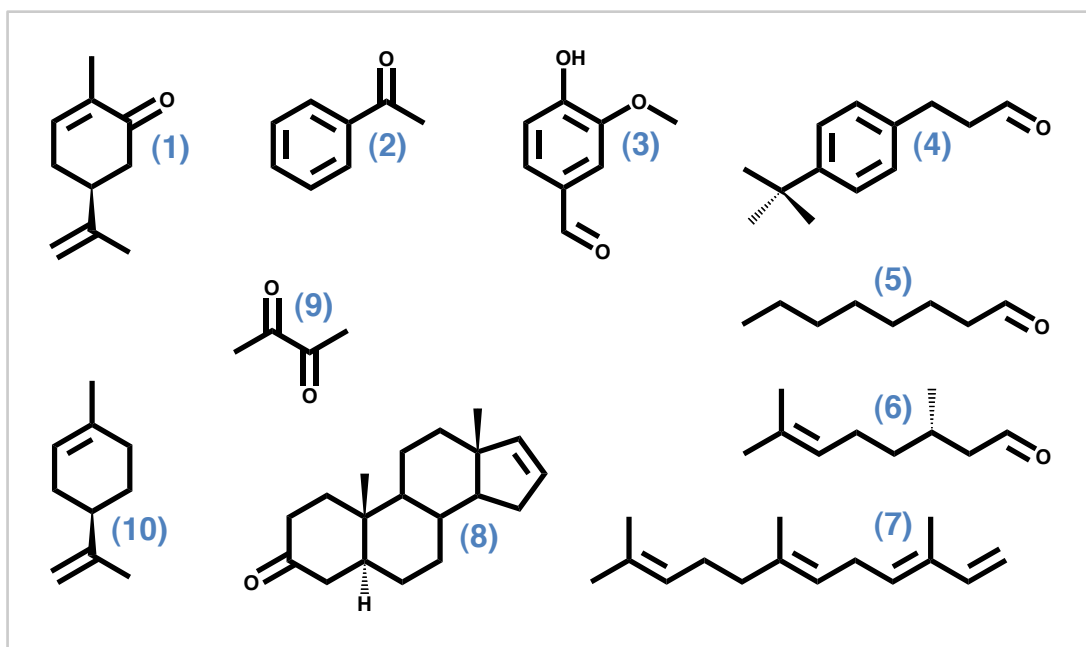


Figure 1.3 - diversity among odorants. Some odorants demonstrating the different challenges facing odorant receptors. Diacetyl (**9**) is one of the smallest odorants while androst-4-en-3-one (**8**) is one of the highest molecular weight compounds. Both are rigid, but they achieve this through different means. The series formed by octanal (**5**), citronellal (**6**) and farnesene (**7**) have an increasing number of rigid “plates” that can pivot around one another. Bourgeonal (**4**) demonstrates a “ball and chain” arrangement with a bulky and rigid terminus separated from the polar functional group by a flexible linker region. Vanillin (**3**) is a compact, multipolar odorant with the potential to make multiple hydrogen bonds, providing a “Velcro” like effect. However, purely hydrocarbon odorants can also be sufficient ligands as in farnesene (**7**) and limonene (**10**). The aromatic acetophenone (**2**) and the branched alkyl carvone (**1**) actually demonstrate surprisingly high levels of co-recognition across the OR repertoire. See chapter 6 for more details on this phenomenon.

Figure 1.4 - sparsely activating odorants still do not constitute a labeled line. (A)

Results of a panel screen conducted on 448 OSNs. Each row denotes the response profile of a given OSN. Shaded boxes indicate that the OSN responded to the odorant blend listed in that column. White boxes indicate that the blend was tested, but did not elicit a response. Given the presence of ~1200 ORs in the mouse genome (Zhang and Firestein, 2007) and only one OR type expressed per OSN (Chess et al. 1994), each row probably reflects the activity of a different OR. That some response profiles are shared by more than one OSN is likely due to the brevity of the odor panel and this particular selection of odorants. **(B)** The components in each blend, each present at 30uM. The blends are formulated roughly by functional group. They were not designed for direct comparison with each other but rather in an attempt to recruit the greatest number of OSNs. Diacetyl (DA), a sparsely activating di-ketone odorant, activated 4 OSNs displaying 2 different response profiles. The DA+ cells can thus respond to at least 3 different odorants from diverse functional group categories. Intriguingly, the mono-ketone KET blend never co-activated the DA+ cells. Names for each component are listed from top to bottom for each blend:

HOL mix

hydroxycitronellal
geraniol
octanol
mayol
coranol

EST mix

3-mercapto hexyl acetate
cis-3-hexenyl acetate
benzyl acetate
methyl anthranilate
geranyl acetate

ALD mix

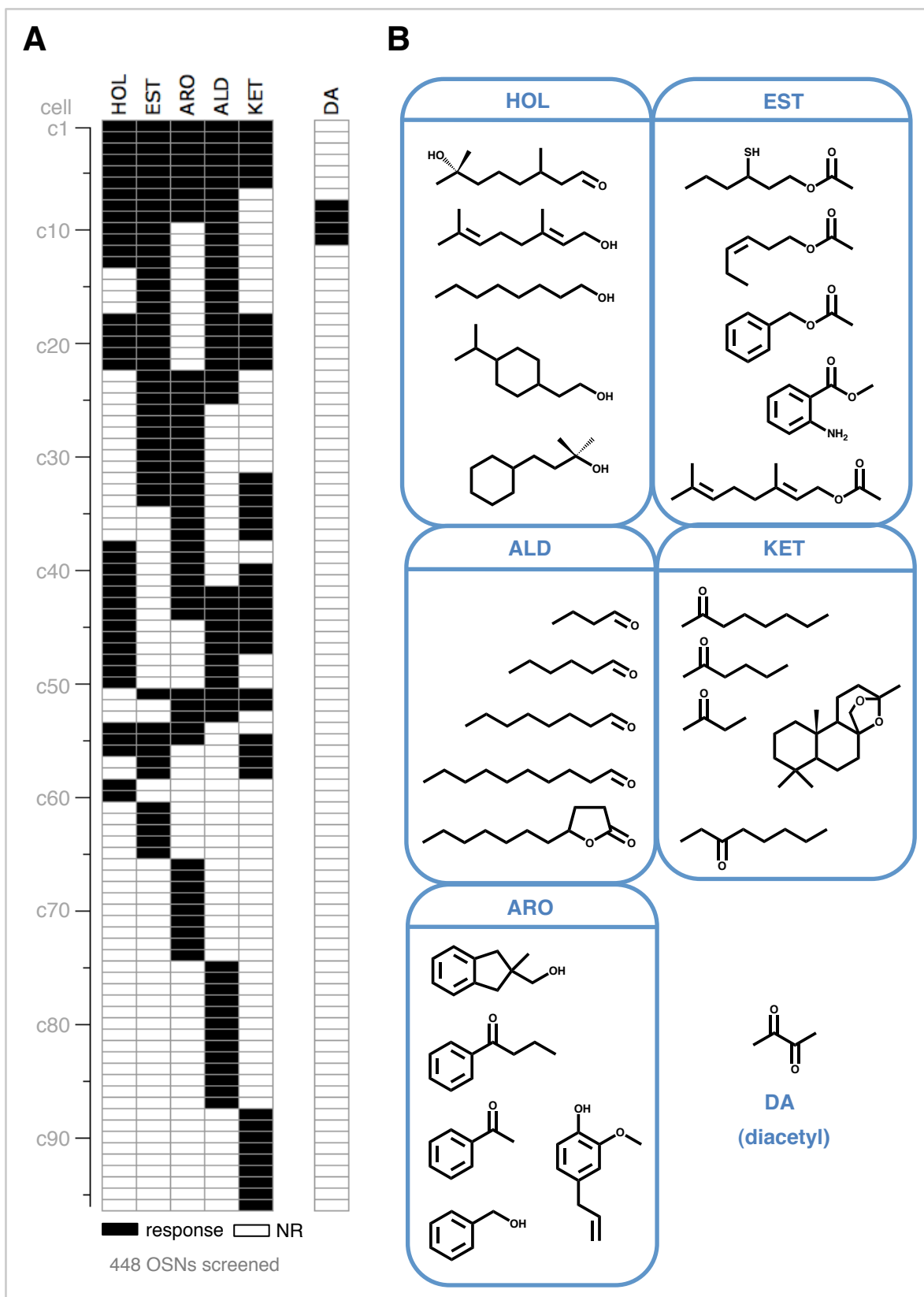
butanal
hexanal
octanal
decanal
gamma-undecalactone

KET mix

2-octanone
2-hexanone
2-butanone
Jeger's Ketal
3-octanone

ARO mix

lilyflore
butyrophenone
acetophenone (*left*)
eugenol (*right*)
benzyl alcohol




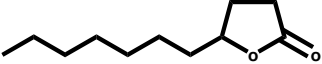
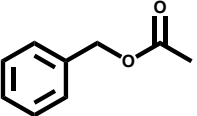
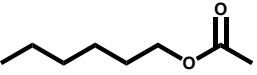
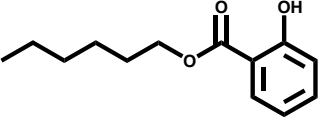
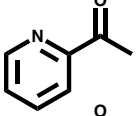
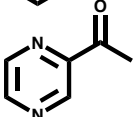
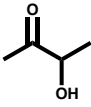
		% OSNs activated by 30 μ M cmpd	# OSNs responding / sample size
	octanal	~5.5%	(various studies)
	γ -undecalactone	3.9%	(25 / 634)
	benzyl acetate	3.0%	(19 / 634)
	hexyl acetate	2.8%	(18 / 634)
	hexyl salicylate	0.2%	(1 / 634)
	2-acetyl pyridine	0.2%	(1 / 664)
	acetyl pyrazine	0.2%	(1 / 501)
	acetoin	0.2%	(2 / 1015)

Figure 1.5 - odorants exhibit a range of recruitment levels. Structures and activation frequencies for some of the most widely activating (top) and sparsely activating (bottom) odorants I have worked with. From the current data, sparse recruiters tend to be rigid and compact, while widely activating odorants often have a flexible tail 7-9 carbons in length. However, note that hexyl salicylate has a flexible 6 carbon appendage; while normally a sign of a broadly recruiting compound (see hexyl acetate), it did not promote widespread recruitment in the salicylate context. Further study is required to refine these impressions.

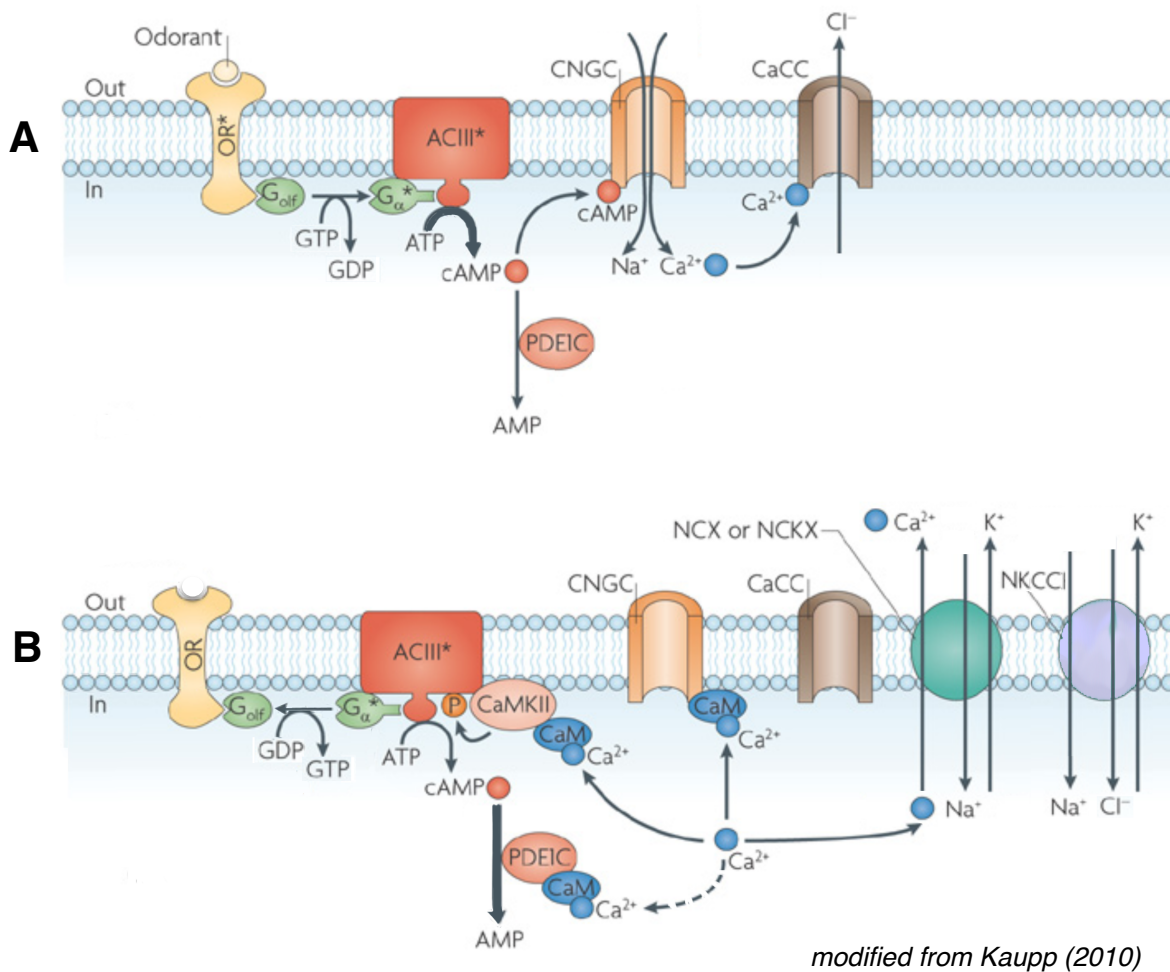


Figure 1.6 – signal transduction cascade in mammalian OSNs. (A) Activation of the cascade upon odorant binding. cAMP production levels by ACIII (thick line) outstrip the degradation rate by PDE1C. **(B)** Calcium-based feedback plays an important role in quenching the cascade. Ion gradients are reset by a number of exchangers. Whether PDE1C activity is upregulated (thick line) is uncertain at this time. See text for details of the cascade and its regulation. *Abbreviations:* OR = odorant receptor, ACIII = adenylyl cyclase III, CNGC = cyclic nucleotide gated channel, CaCC = calcium-activated chloride channel, PDE1C = phosphodiesterase, CaM = calmodulin, CaMKII = calcium-calmodulin kinase II, NCX = sodium/calcium exchanger, NCKX = sodium/calcium/potassium exchanger, NKCC1 = sodium/potassium/chloride exchanger.

(this page intentionally left blank)

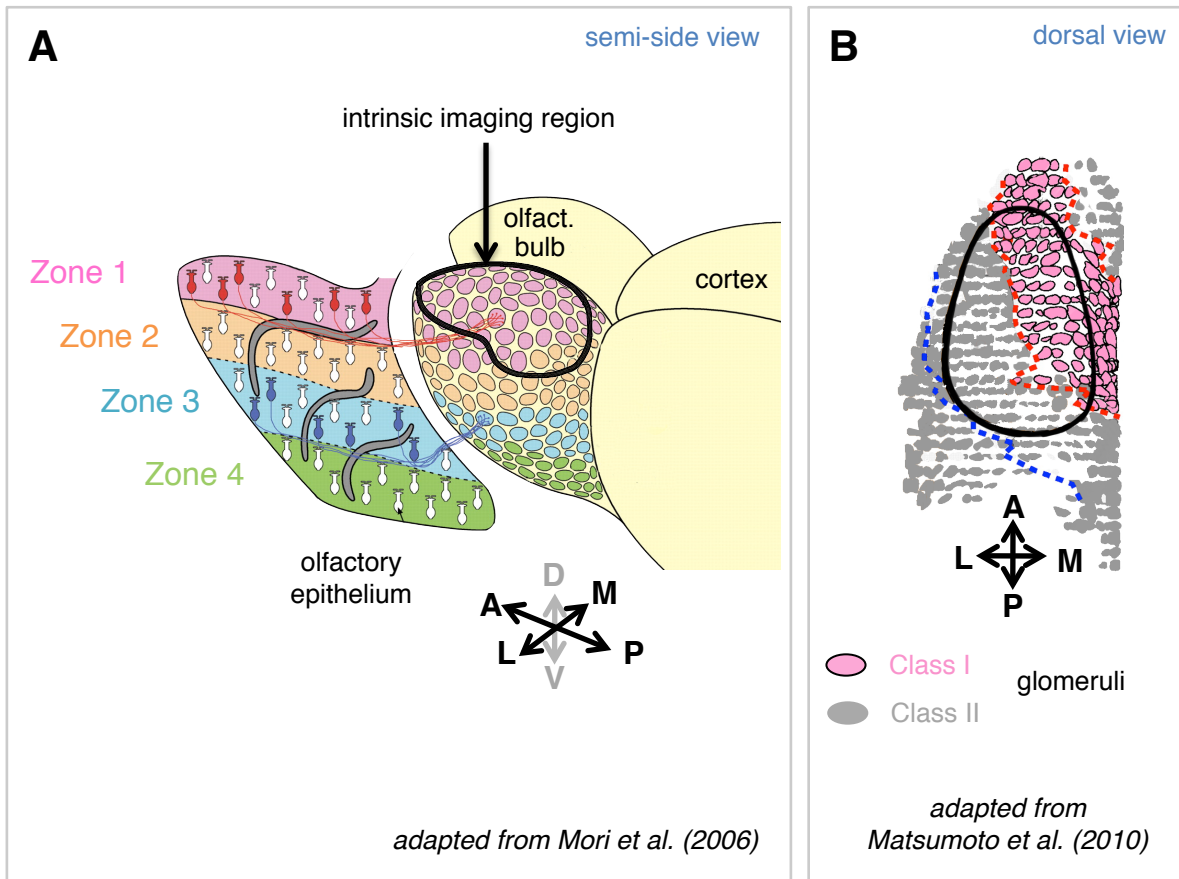


Figure 1.7 - patterned projection of OSNs from olfactory epithelium locations to general locations in the olfactory bulb. (A) The dorsally located Zone I of the olfactory epithelium expresses almost exclusively Class I ORs, and almost all Class I ORs reside in Zone I (Zhang et al. 2004). These OSNs project to the dorsal-most part of the bulb. The circles denote the glomeruli where the axons of all the OSNs expressing the same OR converge. The region of the bulb that is amenable to intrinsic imaging is outlined. Class II ORs residing in the more ventral zones of the epithelium project to increasing lateral and ventral bulb regions that are not amenable to intrinsic imaging; this OR population can only be monitored by calcium imaging. (B) The olfactory bulb viewed dorsally with the surface of the bulb partly unrolled. The outline is the region amenable to intrinsic imaging. The Class I OR glomeruli, now more accurately defined via a transgenic mouse, are in pink. Class II OR glomeruli are in grey.

Figure 1.8 - failure of protein models to predict ligands of rat I7. Fluorooctane (**A**, top) and high concentrations of octanoic acid (**B**) were predicted to be activators of rat I7 by Singer (2000). I7-expressing OSNs were obtained and subjected to calcium imaging as described in Chapter 4. White arrows denote application of the proposed ligand while black arrows denote application of octanal, either at its saturating concentration of 10uM, or a more permissive, approximately mid-level activating concentration of 3uM. Neither of the proposed compounds activated I7 when presented alone. (short traces to left). To check for binding in absence of activation (ie. antagonism) we performed a series of applications in which the combination of octanal with the proposed ligand was flanked on either side by octanal presented alone. The dashed line between the octanal flanks shows the predicted magnitude if the proposed compound failed to compete with octanal and was thus fully “ignored” by I7. Neither fluorooctane nor octanoic acid significantly altered the response magnitude, thus indicating lack of binding. Two compounds related to fluorooctane ((**A**) middle and bottom) also showed no evidence of being an agonist or antagonist.

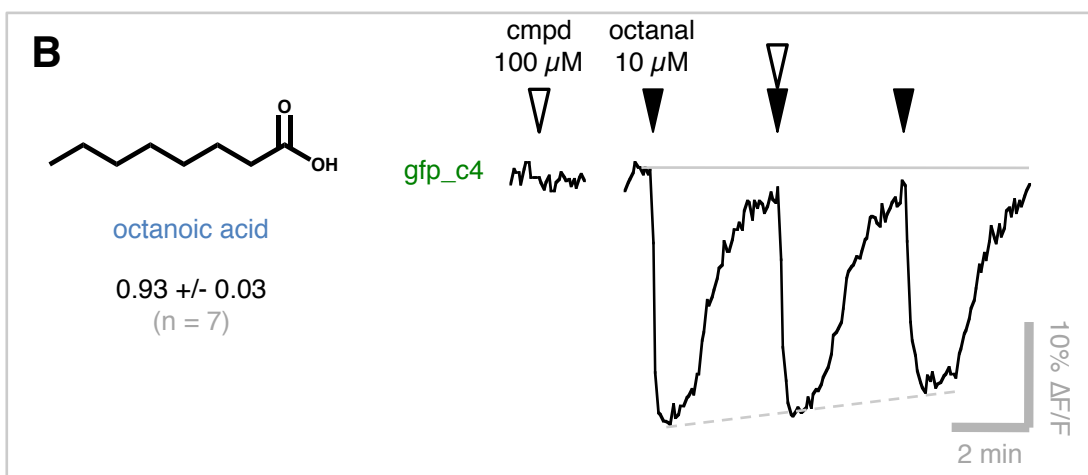
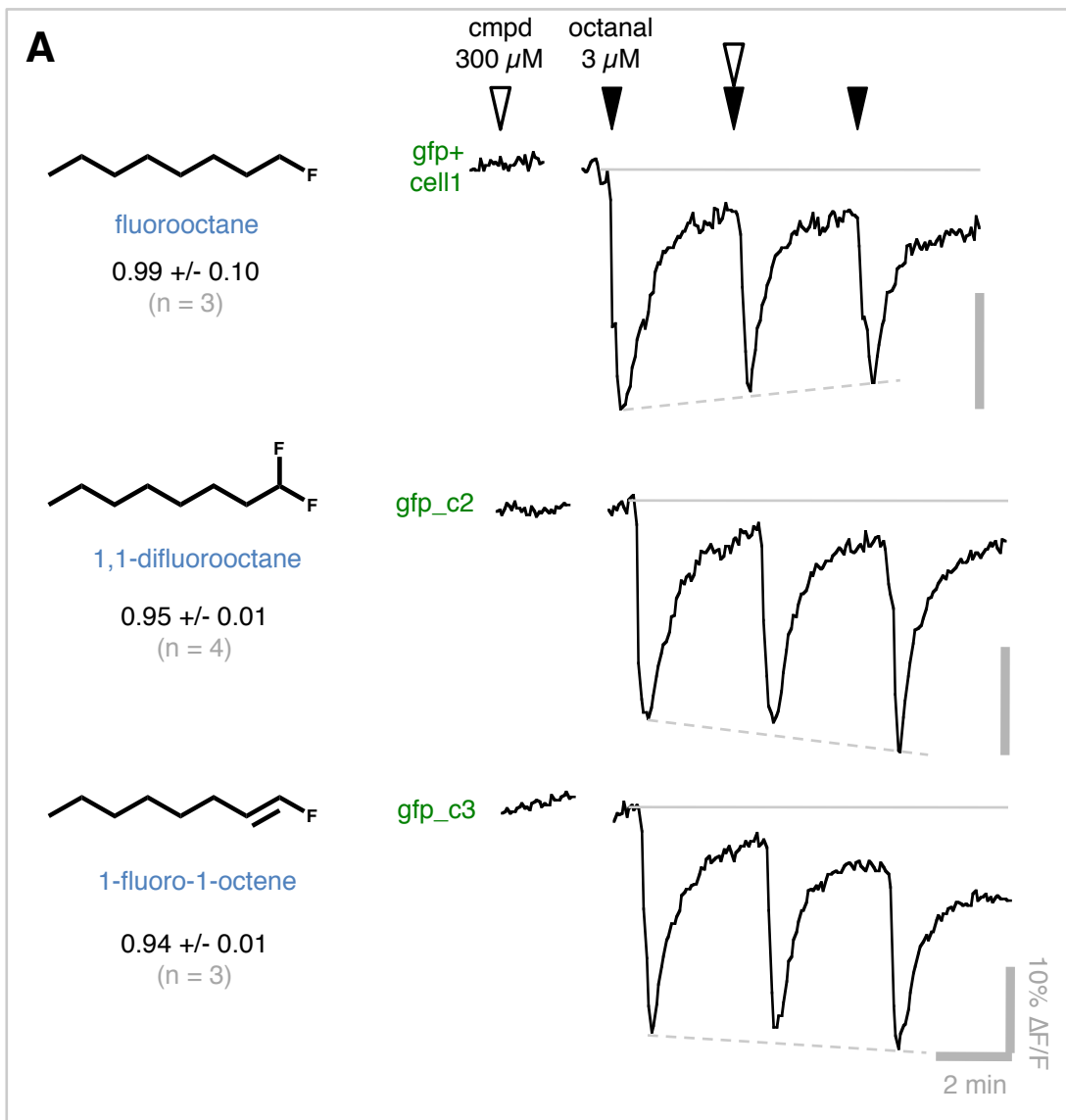
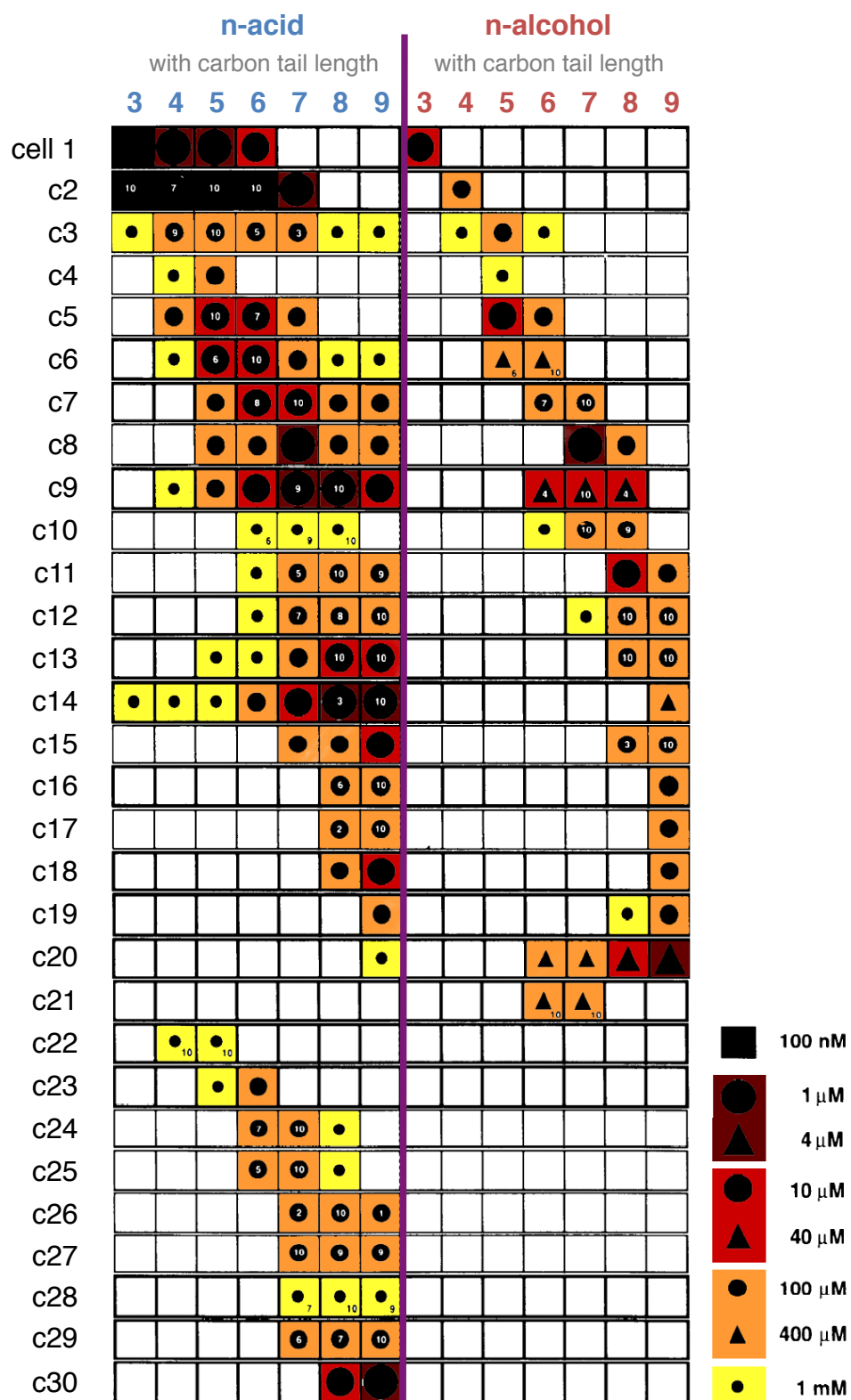


Figure 1.9 - Sato et al.'s foundational template for panel presentation. The first true panel screen format as conducted by Sato et al. (1994), reporting the response profiles observed from calcium imaging of tissue-printed OSNs. This important organization is reproduced here with color-coding to assist comparison between analog magnitude responses. The transparency and thoroughness of the format allows new hypotheses to be derived from the data. Only cell 10 cannot be assigned a functional group preference based on the range of tails it can accommodate, and only cell 11 shows discrepancy in assignment of the “stronger” functional group when based on tail range versus on response magnitude at one tail length. For 73/78 odorant pairs the functional group preference as assigned by single tail response magnitude matched that assigned by breadth of the tail range. My reading of this panel suggests that either method can be used to help rank functional group “strength” in biologically relevant chemical space.



adapted from Sato et al. (1994)

Supplemental Figure 1.1 - inconsistencies between heterologous expression systems.

5 ORs expressed in the broad scale screen described in Saito et al (2009) had previously been characterized in other systems. Red shading indicates where there are conflicting results using these odorants. Note that not all odorants were used in all studies, and so this measure is a lower estimate.

The other groups which have characterized these ORs are as follows:

MOR23-1, MOR33-1, and MOR40-1 : Malnic et al. (1999)

MOR203-1 : Saito et al. (2004)

OR1A1 : Schmiedeberg et al. (2007)

OR51E2 : Neuhaus et al. (2009)

odorant receptor

	MOR23-1	MOR33-1	MOR40-1	MOR203-1	OR1A1	OR51E2
coumarin						
acetophenone						
4-chromanone						response
allyl phenylacetate						response
dihydrojasmane						response
nonanoic acid	response	response	response	response		
octanoic acid	response	response	response	response		
decanoic acid		response	response	response		
cyclohexanone						
heptanoic acid	response	response	response	response		
vanillic acid						
camphor ; (S)-(-) ; (L)						
camphor ; (R)-(+); (D)						
benzophenone						response
dihydrocarvone : (+)						response
carvone (L) ; (R)-(-)				response	response	
carvone (D) ; (S)-(+)				response	response	
prenyl acetate				response		
hexanal						
lyral						
propionic acid						
geraniol				response	response	
citronellol ; (S)-(-)				response	response	
octanethiol				response	response	
nonanethiol				response	response	
2-coumaranone						
allyl benzene						
phenyl acetate					response	
benzyl acetate					response	response
hexanoic acid		response				
fenchone ; (-) ; (L)						
ethyl isobutyrate						
fenchone ; (+) ; (D)						
nonanal		response	response			
decanal						
octanol	response	response	response	response		
heptanol		response	response	response		
nonanol		response	response	response		
decanol				response	response	
butyl butyrylactate						
2-phenylbutyric acid ; (R)-(-)						
2-phenylbutyric acid ; (S)-(+)						
gamma-caprolactone				response		
2-octanone				response	response	
2-nonanone				response	response	
3-octanone				response	response	
3-heptanone				response	response	
2-heptanone				response	response	
pentanoic acid						
3,4-hexanedione						
2,3-hexanedione						
hexanol						
amyl hexanoate						
benzene						
2-pentanone						
2-hexanone						
4-hydroxycoumarin						
pentanol						
allyl heptanoate					response	
hexyl acetate						
heptanal					response	
octanal	response			response	response	
butyl formate						

no response
 response
 contested

Supplemental Figure 1.2 - odorants proven to be recognized by both Class I and Class II ORs. Deorphaned mouse Class I receptors are listed at top in blue, Class II in green at bottom. Due to lack of a standardized test panel in the olfactory field, different odorants are assayed in each study. Thus, this panel is biased towards the most commonly chosen odorants: the simple n-aldehydes, n-alcohols, and n-acids.

Source data for the ORs listed is as follows:

All ORs tested with 8-bromooctanoic acid, regardless of whether this compound elicited a response, are from Malnic et al. (1999). All ORs whose name end in “1”, in addition to MOR256-17, were tested by Saito et al. (2009). MOR41-1, 41-2, and 41-3 were tested Abaffy et al. (2006), validating and extending earlier work conducted by Malnic et al. (1999). MOR139-3 was characterized by Yoshikawa et al. (2009).

Class I ORs

	heptanol	octanol	nonanol	hexanal	octanal	nonanal	decanal	heptanoic acid	octanoic acid	nonanoic acid	decanoic acid	8-bromooctanoic acid	2-coumaranone	allyl phenylacetate
MOR1-1														(nt)
MOR2-1														(nt)
MOR4-1														(nt)
MOR5-1														(nt)
MOR8-2				(nt)	(nt)	(nt)	(nt)				(nt)		(nt)	(nt)
MOR18-1														(nt)
MOR13-6				(nt)	(nt)	(nt)	(nt)				(nt)		(nt)	(nt)
MOR22-2				(nt)	(nt)	(nt)	(nt)				(nt)		(nt)	(nt)
MOR23-1														
MOR25-1														(nt)
MOR30-1														(nt)
MOR31-1														(nt)
MOR31-2				(nt)		(nt)	(nt)						(nt)	(nt)
MOR31-4														(nt)
MOR32-4				(nt)		(nt)							(nt)	(nt)
MOR32-5				(nt)	(nt)		(nt)					(nt)	(nt)	(nt)
MOR32-11														(nt)
MOR33-1														
MOR37-1														(nt)
MOR40-1														
MOR40-4														(nt)
MOR41-1														(nt)
MOR42-2														(nt)
MOR42-3														(nt)

Class II ORs

MOR103-15			(nt)										(nt)	(nt)	(nt)
MOR105-1														(nt)	
MOR106-1				(nt)	(nt)	(nt)	(nt)					(nt)		(nt)	(nt)
MOR106-13				(nt)	(nt)	(nt)	(nt)					(nt)		(nt)	(nt)
MOR125-1												(nt)	(nt)	(nt)	(nt)
MOR139-1														(nt)	
MOR139-3														(nt)	(nt)
MOR203-1														(nt)	(nt)
MOR204-32				(nt)	(nt)	(nt)	(nt)					(nt)		(nt)	(nt)
MOR222-1														(nt)	
MOR223-1														(nt)	
MOR236-1														(nt)	
MOR256-17														(nt)	
MOR258-1														(nt)	
MOR258-5												(nt)		(nt)	(nt)
MOR259-1														(nt)	
MOR260-1														(nt)	
MOR261-1														(nt)	
MOR268-1														(nt)	
MOR271-1														(nt)	
MOR272-1														(nt)	

(nt) not tested
 no response response
 no response contested

Supplemental Figure 1.3 - possible class-based bias in recruitment by odorants.

Regrouping the data from the heterologous expression study by Saito et al. (2009) to segregate odorants based on the Class identity of the ORs they activated. On the top, Class I ORs are shaded in blue (left) and Class II ORs are shaded in green (right). On the left-hand side, the top-most list (dark blue bar) were odorants that exclusively activated Class I ORs in this sample. The bottom-most list (dark green) are odorants that exclusively activated Class II ORs. The list directly above (light green) could tentatively be included among the Class II odorants as well, given that only a single Class I OR (MOR41-1) violated what is otherwise a strong bias. With such a marked discrepancy in MOR41-1's profile, I suggest that this OR may have been misclassified or misidentified at some point and should be re-evaluated. The middle list (red) are odorants that clearly activate both classes, although the acids do appear to activate Class I more frequently.

Supplemental Figure 1.4 - proposed ligand-interacting residues on the rat I7

receptor. This table shows the variability in assignment of the “critical” residues of the I7 receptor for interacting with octanal. The discrepancy highlights the challenges of building consistent OR models for in silico evaluation of receptive fields. The left-most column provides the Ballesteros-Weinstein index number for each amino acid. Residues listed and shaded in green are based on models generated specifically to rat I7. Residues in black are predictions that were generally proposed for all ORs. Lys 164 (black arrow) and asp 204 (white arrow) are the only highly conserved predicted residues in the I7-specific modeling studies. Lys 164 may interact with the aldehyde carbonyl, and asp 204 may form an ionic lock with lys 164 for when the receptor is in a ligand-free state.

The references corresponding to each column, listed left to right:

specific I7 models

Singer (2000)

Hall et al. (2004)

Lai et al. (2005)

Khafizov et al. (2007)

Kurland et al. (2010)

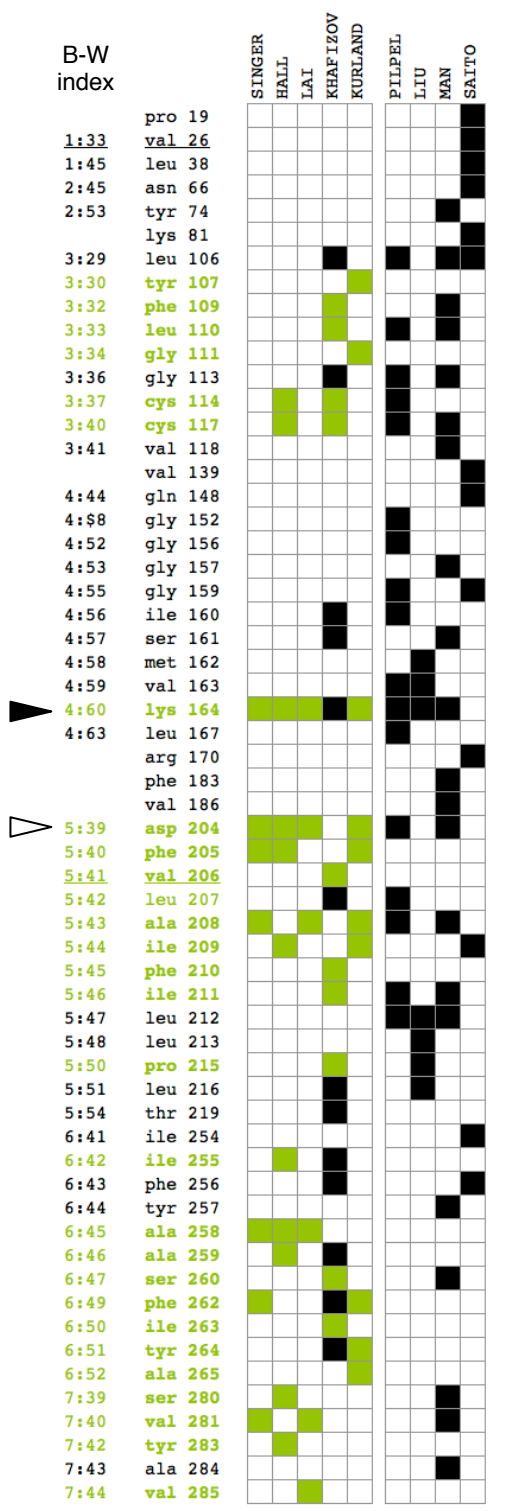
general OR models

Pilpel et al. (1999)

Liu et al. (2003)

Man et al. (2004)

Saito et al. (2009)



■ predicted based on I7 model
■ predicted based on general model
 not predicted in this study

(this page intentionally left blank)

CHAPTER 1 - SECTION 2

INTRODUCTION TO READING PANELS

PART A : INTRODUCTION TO PANEL ORGANIZATION

In the panel data display (Figure 1.10A), the odorants that were tested are arrayed in columns and each row reflects the response pattern of a given olfactory sensory neuron (OSN) to those probe odorants. Despite their simplicity, panels are information dense and many relationships can be extracted. This section will discuss some features to particularly attend to when interpreting panels. It will conclude with a case study that demonstrates how the horizontal and vertical reading of the panel can be integrated to query preferred chemical detection strategies by odorant receptors (ORs) and predict likely antagonist pairs.

Horizontal rows reflect the receptive field of unique odorant receptors

In the dispersed olfactory epithelium preparation, OSNs are the only cells that respond selectively to odorants at the micromolar concentrations that we use. In an OMP-GFP transgenic mouse where mature OSNs were visually labeled (Bozza, Feinstein et al. 2002), only GFP+ cells responded to 30uM octanal. Each OSN is believed to express only a single OR type (Chess, Simon et al. 1994; Malnic, Hirono et al. 1999), and so the cellular response is a proxy of the receptor response. Although ORs are not expressed with equal frequencies, at ~1200 members (Zhang and Firestein 2007) the OR family is so large that in the screens presented here it is unlikely that the same OR will be recruited more than once. Each row of the panel represents the response pattern of an individual cell, presumed to be an OSN and hence the bearer of a different OR. Because

of these tight relationships, the terms “cell”, “OSN”, and “OR” are sometimes used interchangeably.

The importance of inactive odorants in data interpretation

The pattern of activity in a horizontal row displays a portion of that OR's receptive field. Activation by an odorant is denoted by a shaded box, while boxes corresponding to odorants that were tested but found inactive are white. While attention may be naturally drawn to the activating odorants, the identity of inactive odorants can provide crucial information to help rank auxiliary stabilizing motifs and highlight non-permitted paths for structure activity models. A great benefit of the panel display format is that it preserves this information and makes it eminently visible.

Granted, the absence of a response (which I like to call “whitespace” based on its appearance) is somewhat ambiguous. It could reflect true lack of binding but it might also hide silent binding by an antagonist. The distinction can only be revealed through testing with mixes. Panel-wide tests of antagonism, however, are uncommon. To properly conduct an antagonism test the activating odorant should be applied at its just saturating concentration. In a mixed population this first requires determining the dose response curve of the target cell. Acquisition of such curves can be challenging, particularly if there are multiple targets in a field. It can thus be useful to narrow down which “whitespace” is more likely to represent an OR susceptible to antagonism.

Panel interpretation can guide this endeavour. One method strictly relies on “vertical” reading of the population response pattern to identify OSNs whose inactivity to

a given compound violates a robust trend of co-activation by the two compounds. The idea is that if an overwhelming majority of OSNs are co-activated by odorants A and B, such that either is rarely recognized in isolation, it suggests that it might be challenging to construct an OR to parse these chemicals. The A+/B- OSN, then, would be expected to have a high probability of still binding B but as an antagonist. A second method of using panel screening data to predict antagonism, uses both “horizontal” and “vertical” reading. This approach will be presented in the case study.

Patterns between vertical columns look at population wide ease of discrimination

Considering each row individually is the classical way of examining receptor response patterns. But in a family of 1000+ receptors, it becomes even more interesting to view a particular receptor’s role in context. One can compare the target cell’s activity profile against that of OSNs that also recognize the same odorant or that can make a given discrimination. Such appreciation is gained through “vertical” reading, which emphasizes the frequency with which a given detection or discrimination is made across the population. The panel format thus encourages appreciation of a unique receptor’s contribution to the larger combinatorial code.

As the number of odorants in the response profile increases, more and more subdivisions of the population ensue. As the subset of OSNs performing that particular parsing becomes smaller, this procedure merges into development of a functional fingerprint. This specialized application is discussed in detail in Chapter 2 - Section 2.

Supplemental visualization of co-activation patterns

While reading directly from the panel is the most accurate approach, sometimes comparisons of interest may not immediately be apparent. The odorant columns may not be juxtaposed or the cell subpopulation making the target discrimination may be dispersed along the published array order. Venn diagrams can provide supplemental visualizations of simple global comparisons. The Venn diagrams viscerally convey the relative sizes of the responding populations and the ratio of the discriminating population versus the co-responding one. Venn diagrams are also useful for displaying the frequency of mini-fingerprints three odorants long since the absence of a sector immediately flags an intriguing violation in chemical detection that warrants further study.

Sometimes direct panel reading or noting deep embedding in the Venn diagrams highlights that the ability to respond to one odorant greatly impacts the ability to respond to another. This is seen in the responses to octanal and trans-2-octenal (Figure 1.10C, top). The ability to respond to one of these odorants nearly assures the ability to respond to the other.

Sometimes, embedding results in a “spectrum” (ex: A,B,C) where an OR cannot respond to both flanks (A+/C+) without also responding to the odorant in the middle. This manifests as the absence of an A+/B-/C+ profile. A spectrum organization was first recognized for the oxidation series for alcohols, aldehydes, and acids (Chapter 2). Other examples involve alkyl ring geometry among octanal analogs (Chapter 4), steric size of an alkyl moiety (Chapter 6), and polarity among aromatic rings (Chapter 6). Such spectra underscore that the parsing capabilities of ORs are constrained, even despite the great

size and diversity of this receptor family. In these instances, if one ability is enabled then performing another distinction is prevented. These “rules” are intriguing both from a mechanistic standpoint and because they flag important boundaries in the combinatorial code.

PART B : CASE STUDY

Figure 1.10 extracts data from Chapter 2, which has previously been published (Araneda, Peterlin et al. 2004). It provides an example of reading “vertically” to evaluate the probability of finding a given profile, in an integrated manner to predict likely antagonists, and backwards from Venn diagrams to identify fine aspects of alky scaffold discrimination. Hopefully, this exercise will underscore the flexibility available when data is preserved in the panel format.

Composition of the odorant panel

The odorants, whose structures are provided in Figure 1.10B, center around the bare n-aldehyde octanal (OAL). Trans-2-octenal (2-TO) alters the local electronics, and citronellal (CTR) alters the alkyl scaffold. Citral (CIT) incorporates both these changes at once. These odorants were all delivered at the equimolar concentration of 30uM, so differences in activity can be ascribed to chemical makeup.

All the cells that responded to at least one panel member are arrayed as horizontal rows in Figure 1.10A. Recall that this sample panel is extracted from a larger one.

Although some profiles are present multiple times, they do not reflect the same OR; each cell responded uniquely when challenged with the full panel of 9 odorants. This can be confirmed using the original cell ID numbers shaded in gray for cross reference to Figure 2.3.

The linear terpenes CTR and CIT share the bulk of their hydrocarbon scaffold. Both provide an epitope-rich prenyl terminus with a predictable structure and a high hydrophobic surface area. CTR and CIT both possess a methyl on carbon C3. However, CTR has a chiral methyl while CIT's C3 methyl is planar. The double bond that holds CIT's C3 methyl planar also creates a conjugated aldehyde. This conjugation, present also in 2-TO, leads to a slightly larger partial negative charge on the carbonyl oxygen. In theory, this should improve the anchoring strength of the aldehyde. However, the conjugation also stiffens the proximal portion of the aldehyde. The inability to completely isolate features speaks to the challenges inherent when working with multidimensional odorant stimuli.

Reading 1 : Is there a “biological fovea” for terpenes?

A simple “vertical” reading in this panel can be used to evaluate if there is a preference for terpene scaffolds over the octane scaffold in aldehyde chemical space. Multiple studies using n-compounds have demonstrated a biological “fovea” of markedly larger recruitment by eight carbon tails as opposed to longer or shorter tails. The terpene scaffold takes this eight-carbon backbone and appends stereotyped features. Would the terpenes, as both prevalent components in natural products and epitope rich odorants in

their own right, be more effective in recruiting ORs than OAL? As can be seen from global recruitment, obtained by counting the shaded boxes in each column, fewer cells were activated by the terpene CTR than by the n-aldehyde OAL. The relative sizes of these recruited populations, and the extent to which they are co-recognized (which adds a second layer to the basic counts) is shown in the Venn diagram in Figure 1.10D. Thus, any benefit of CTR's predictable terminal prenyl group and defined inter-methyl distance seems to be offset by the increased bulk and reduced flexibility.

Reading 2 : Predicting antagonism

Rat I7 responds to OAL but not to CIT at the assayed concentrations. However, I7 can be antagonized by CIT and thus this “whitespace” of a CIT- designation actually hides silent binding. How common is such antagonism? The OAL+ population is large and nearly two thirds fail to respond to CIT (Figure 1.10A (cells ra9 to ra-20, ra-23, ra-34 to ra-41) and Figure 1.10C bottom, red and yellow sectors). Going on this signature alone, there are far too many cells to assay for antagonism.

Reading “horizontally” to examine the 2-TO and CTR signatures of each OAL+/CIT- cell can be used to focus the experiment. 24% of OAL+ cells have the signature of 2-TO+/CTR+/CIT- (8/34; Figure 1.10A cells ra-34 to ra-41, orange box). This signature demonstrates that the ORs can accommodate either the electronic conjugation or alkyl branching components of CIT in isolation but just not when co-present. A different sub-group of cells display a 2-TO+/CTR-/CIT- profile that demonstrates acceptance of electronic conjugation but rejection of the terpene scaffold

regardless of its C3 methyl orientation (Figure 1.10A cells ra-12 to ra-20; blue box). These orange and blue OAL+/CIT- subgroups are of equal sizes, but I would predict that they would exhibit different frequencies of antagonism by CIT. All cells of the orange subgroup have proven that they can accommodate the distal alkyl portion of the terpene scaffold. They can potentially leverage this large and rigid hydrophobic surface area to provide auxiliary stabilization of CIT, even should the planar bond in CIT disrupt the preferred geometry of the polar group tether. The blue subgroup shows no evidence of even accepting, let alone utilizing the terpene scaffold in this way. Thus, I predict the rates of antagonism by CIT would be higher among the OSNs of the orange versus the blue subgroup. I7's profile does indeed place it into the orange subgroup.

Reading 3 : Sensitivity to subtleties of the alkyl scaffold

One nuanced contribution of the alkyl scaffold to ligand activation was first noted in the simplified Venn analysis. To further explore the role of terpenes in odor space, CTR and CIT were overlaid with OAL (Figure 1.10D). CTR and CIT both have OAL as a backbone, so any OSN responding to CTR or CIT is physically capable of accommodating OAL. But as demonstrated in the three-way Venn, a small set of terpene-activated OSNs absolutely require the full terpene skeleton (green, cyan, and blue sectors). Returning to the original panel data, it was found that even the electronically stronger 2-TO polar anchor cannot compensate for stripping away the terpene steric epitopes (Figure 1.10A, (cells ra-1 to ra-8). 20% (5/25) of CTR+ OSNs and 23% (4/17) of CIT+ OSNs thus require the subsidy afforded by these alkyl features. Intriguingly,

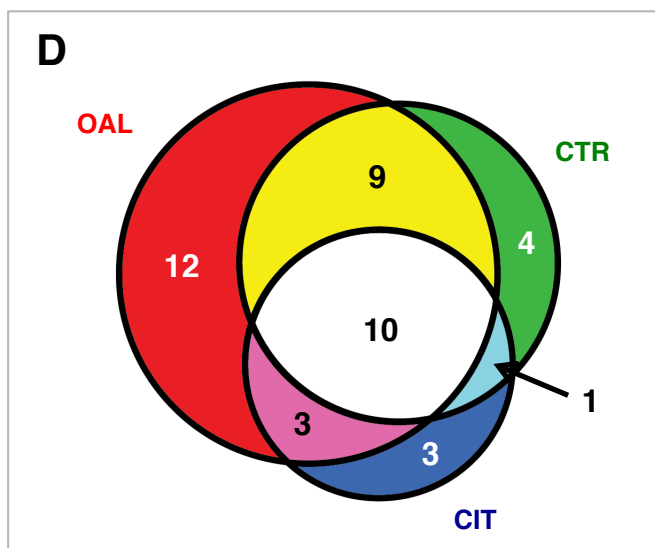
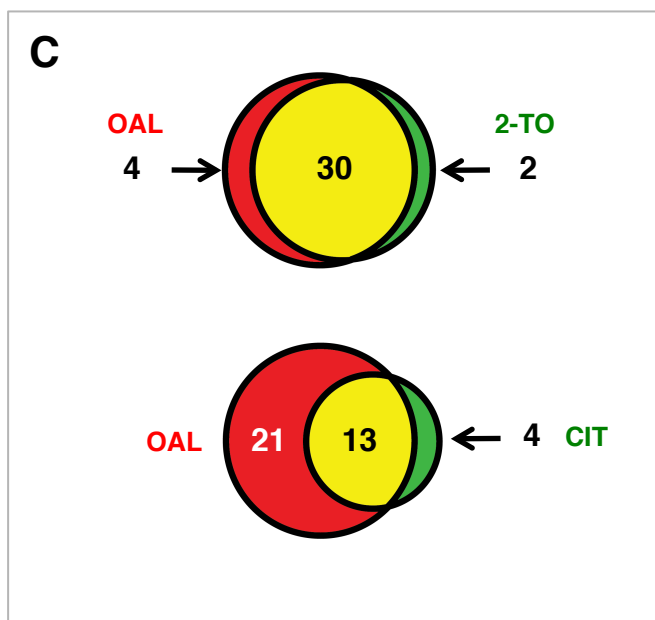
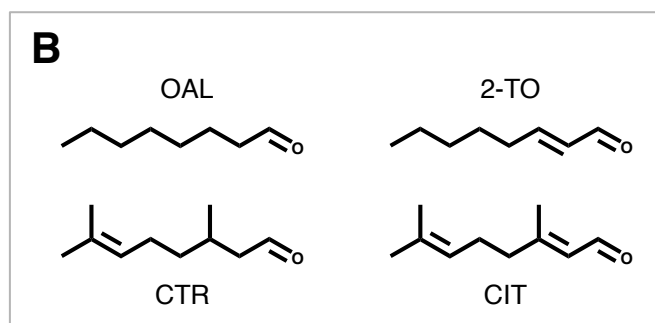
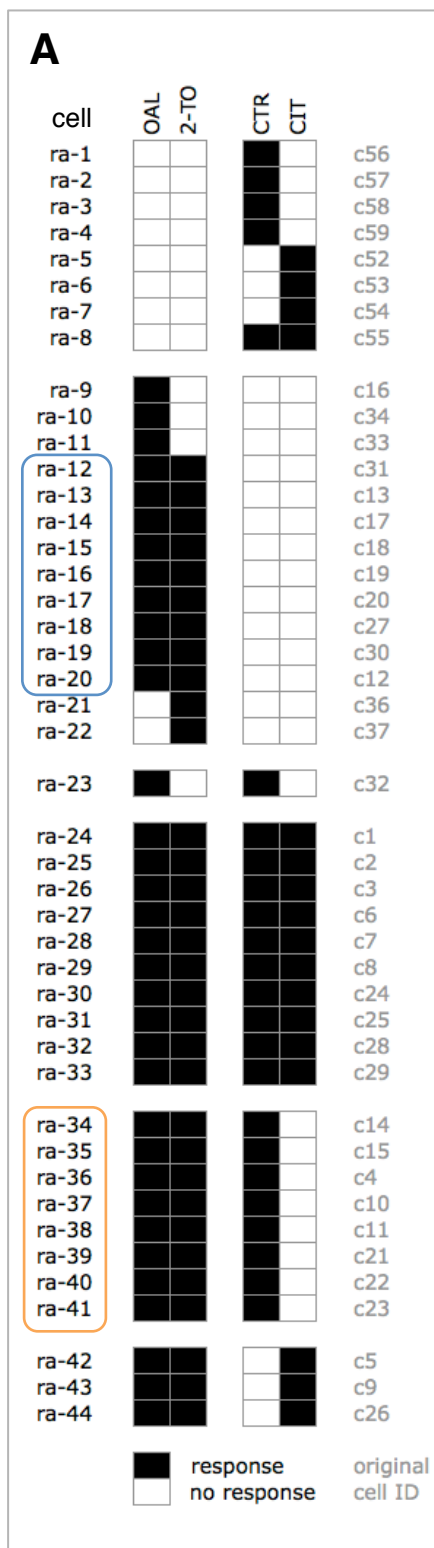
of these 8 cells, only one was CTRN+/CIT+. My interpretation is that the remaining 7 ORs are explicitly reading the orientation of the C3 methyl as the driving feature for activation.

PART C : CONCLUSION

The panel format could casually be viewed as a convenient way of stacking receptive field reports. However, once “vertical” reading to integrate population trends is appreciated a wealth of questions can be profitably addressed. By fluidly combining analysis of chemical features with identification of OSN functional subpopulations, studying the combinatorial code becomes more approachable.

(this page intentionally left blank)

Figure 1.10 - case study in panel reading. This panel is a subset of the data originally presented in Araneda et al. (2004). The odorants tested are shown in **(B)**. All were delivered at 30uM. (OAL, octanal; 2-TO, trans-2-octenal; CTR, citronellal; CIT, citral). **(A)** Results of the screen arrayed in panel format. Each row represents the response profile of an individual OSN to the odorants listed in the columns. A shaded box indicates that the OSN responded to that odorant; a white box indicates that the compound was tested, but it did not elicit a response. For clarity, the cells have been rearranged and assigned new ID numbers (ra-#), with the original ID numbers listed in grey at left. The cluster of cells outlined in orange are those where I predict the non-activating citral is likely to be an antagonist, while the cluster of cells outlined in blue I predict will ignore citral and not be antagonized. See text for rationale. **(C) (top)** Venn diagram showing the recruitment patterns by octanal and trans-2-octenal. These two odorants differ only subtly in electrical strength and proximal backbone stiffening. The numbers indicate the number of OSNs with that profile. The extensive yellow sector and near absence of red and green sectors shown how the OAL+ and 2-TO+ populations are almost identical. **(bottom)** In contrast, nearly 2/3rds of the OAL+ population fails to respond to CIT. **(D)** Overlay the recruitment by the two terpene aldehydes along with the bare octanal backbone that they both must physically be able to accommodate. There is a small subset of cells that can recognize a terpene but find octanal insufficient (green, cyan, and blue sectors).



(this page intentionally left blank)

CHAPTER 2 - SECTION 1

**A PHARMACOLOGICAL PROFILE OF THE ALDEHYDE RECEPTOR
REPERTOIRE IN RAT OLFACTORY EPITHELIUM**

this section has previously been published as

“A pharmacological profile of the aldehyde receptor repertoire in rat olfactory epithelium.” Araneda RC, Peterlin Z, Zhang X, Chesler A, Firestein S. *J Physiology*. 2004 Mar 16;555(Pt 3):743-56. PMID: 14724183

ABSTRACT

Several lines of evidence suggest that odorants are recognized through a combinatorial process in the olfactory system; a single odorant is recognized by multiple receptors and multiple odorants are recognized by the same receptor. However few details of how this combinatorial process might actually function for any particular odor set or receptor family are available. Approaching the problem from the ligands rather than the receptors, we used the response to a common odorant, octanal, as the basis for defining multiple receptor profiles. Octanal and other aldehydes induce large electroolfactogram responses in the rodent olfactory epithelium, suggesting that these compounds activate a large number of odor receptors (ORs). Here, we have determined and compared the pharmacological profile of different octanal receptors using Ca^{2+} imaging in isolated olfactory sensory neurons (OSNs). It is believed that each OSN expresses only one receptor, thus the response profile of each cell corresponds to the pharmacological profile of one particular receptor. We stimulated the cells with a panel of nine odorants, which included octanal, octanoic acid, octanol, and cinnamaldehyde among others (all at $30\mu\text{m}$). Cluster analysis revealed several distinct pharmacological profiles for cells that were all sensitive to octanal. Some receptors had a broad molecular range, while others were activated only by octanal. Comparison of the profiles with that of the one identified octanal receptor, OR-I7, indicated several differences. While OR-I7 is activated by low concentrations of octanal and blocked by citral, other receptors were less sensitive to octanal and not blocked by citral. A lower estimate for the maximal number of octanal receptors is between 33 and 55. This large number of receptors for

octanal suggests that, although the peripheral olfactory system is endowed with high sensitivity, discrimination among different compounds probably requires further central processing.

INTRODUCTION

Terrestrial vertebrates occupy an odor-rich environment of considerable variety and complexity. Olfactory systems have evolved to meet the numerical and physical challenges of chemical detection and discrimination. They operate over a dynamic range of several orders of stimulus magnitude and can recognize an enormous array of low to medium molecular weight organic compounds. Theoretically, there is no limit to the number and variety of compounds that can be considered odorants. If a receptor expressed in a primary olfactory sensory neuron (OSN) binds a compound, that compound will be, by definition, an odor. The large number of receptors used in olfactory systems and the combinatorial strategy of overlapping affinities assures that the number of possible receptor combinations is larger, by several orders of magnitude, than the number of known chemicals. In some ways this is analogous to vision in which it is possible to see thousands, perhaps millions, of hues with only three receptors of overlapping bandwidth. However, it also differs from vision, hearing, and other sensory systems in that the stimulus does not vary along a single physical dimension (i.e. wavelength, frequency). Rather, the stimulus varies along multiple dimensions including, but not limited to, molecular shape and size, functional group, charge, hydrophobicity, and atomic composition.

Olfaction utilizes a large family of G-protein-coupled receptors (GPCRs) expressed in specialized primary sensory neurons residing in a thin neuro-epithelium in the nose (Buck 1992). The odor receptor (OR) family of genes, comprising some 1100 functional genes in the mouse, is the largest family of GPCRs in the mammalian genome (Mombaerts 1999; Zhang and Firestein 2002). Nonetheless, this is nowhere near the number of compounds possessing an odor quality. Thus, it is generally accepted that a combinatorial strategy must be employed, in which most odorants are recognized by several receptors and most receptors recognize multiple related compounds ((Malnic, Hirono et al. 1999); but see (Hamana, Hirono et al. 2003)). A particular odor percept is then produced in higher brain centers that ‘decode’ the combination of activated receptors.

It is clear from this model that the primary event of receptor–odorant interaction is critical in determining the range of odorant sensitivities. Several lines of evidence suggest that, with a few exceptions (Rawson, Eberwine et al. 2000), each OSN expresses only one OR gene (Serizawa, Miyamichi et al. 2003). All cells expressing the same receptor converge onto one or a few restricted targets, known as glomeruli, in the olfactory bulb (Mombaerts 1999). This suggests that the molecular range, or pharmacological profile, of each OR defines the receptive field of each glomerular unit. As with other sensory systems, defining the receptive field of olfactory neurons would provide critical information about the manner in which the stimulus is encoded.

Progress in this area has been slowed by the lack of a reliable high-throughput OR expression system in which a pharmacological program of ligand screening could be carried out on many receptors. Thus, there are only a handful of identified mammalian

receptors for which a few cognate ligands have been determined and confirmed (Krautwurst, Yau et al. 1998; Zhao, Ivic et al. 1998; Murrell and Hunter 1999; Wetzel, Oles et al. 1999; Kajiya, Inaki et al. 2001; Touhara 2001; Gaillard, Rouquier et al. 2002). Previously, using an adenovirus expression system, we were able to drive the expression of OR-I7 in a large number of OSNs (Zhao, Ivic et al. 1998). This enabled us to make a comprehensive investigation of the molecular receptive range of this receptor and to identify critical chemical attributes of the ligands that predict the likelihood of receptor-ligand activity. This exercise has allowed us to define an OR-I7 profile based on function rather than gene sequence (Araneda, Kini et al. 2000). We found that OR-I7 displays a high specificity for certain molecular features (e.g. only aldehydes were active), and a high tolerance for others (e.g. unsaturated 8-carbon aldehydes were as effective as the saturated octanal in activating the receptor).

Here we take a different approach to the same problem. Using a set of compounds that were chosen for their chemical disparity, we asked if it were possible to identify distinct chemical profiles of receptors by screening a large number of cells with the same compound set. Even though we are ignorant of the genetic identity of the OR protein expressed, we can rely on the principle that only one OR gene is being expressed by any given neuron, and the response of that neuron is a faithful reflection of the receptive range of the receptor it is expressing. With this strategy we have been able to distinguish at least 33 distinct types of receptors, all of which bind octanal, but each of which differs in its sensitivity to other test compounds.

METHODS

Isolation of sensory neurons

All animal procedures conformed to Columbia University guidelines for care and use of animals. Sensory neurons were isolated from 6 to 8-week old Sprague-Dawley rats of both sexes. Two experimental groups of animals were used to compare the pharmacological profile of OR-I7 to that of other octanal receptors. These included animals that were infected with adenovirus containing the OR-I7, following the same protocol previously used (Zhao, Ivic et al. 1998; Araneda, Kini et al. 2000), as well as uninfected animals.

Animals were overdosed with anesthetics (ketamine, 90mg/kg; xylazine, 10mg/kg, i.p.) and decapitated. The head was cut open sagittally and the septum was removed to expose the medial surface of the olfactory turbinates. The epithelium was dissected out and placed in an oxygenated divalent-free rat Ringer solution (mm: 145 NaCl, 5.6 KCl, 10 Hepes, 10 glucose, 4 EGTA, pH 7.4). For infected animals, the epithelium was dissected under a fluorescent microscope (see below). The tissue was then incubated at 37°C for 45min in 5ml of divalent-free Ringer solution containing 5mg/ml⁻¹ bovine serum albumin (Sigma-Aldrich, St Louis, MO, USA), 0.5mg/ml collagenase, 22U/ml dispase (Gibco BRL, Grand Island, NY, USA) and 50µg/ml deoxyribonuclease II (Sigma). The tissue was then transferred to a normal rat Ringer solution (mm: 138 NaCl, 5 KCl, 1 CaCl₂, 1.5 MgCl₂, 10 Hepes, 10 d-glucose, pH 7.4) and the cells were dissociated by tapping the tube containing the tissue. Cells (in 400µl

volume) were plated onto concanavalin A (Sigma-Aldrich, 10mg/ml)-coated glass coverslips and placed in 35 mm Petri dishes. After allowing the cells to settle for 20min, 2ml of culture medium was added to each dish and the dishes were placed at 37°C in a CO₂ incubator for at least 1h. The culture medium consisted of DMEM/F12 (Gibco BRL) supplemented with 10% fetal bovine serum, 100µm ascorbic acid, 1X insulin–transferrin–selenium (Gibco BRL), 2mm glutamine, 100U/ml penicillin and 100µg/ml streptomycin (Gibco BRL).

Ca²⁺ imaging recordings

Calcium imaging recordings were performed as described elsewhere (Yuste R. 2000). After incubation, the culture medium was removed and the cells were loaded with Fura-2 AM (5µm) plus pluronic acid F127 (80µg/ml; Molecular Probes, Eugene, OR, USA) in rat Ringer solution. Cells were loaded in the dark for 45min, at room temperature. After washing with fresh Ringer solution, the coverslip was mounted onto a recording chamber. Imaging was carried out at room temperature on an inverted fluorescence microscope (IMT-2 Olympus, Tokyo, Japan) equipped with a SIT camera (C2400-08, Hamamatsu Photonics, Hamamatsu, Japan) connected to a frame grabber (LG-3, Scion, Frederick, MD, USA) on a Macintosh computer. The NIH Image software was used for data acquisition and analysis (NIH, Bethesda, MD, USA). Customized macros were written for shutter control (Uniblitz, Vincent Associates, Rochester, NY, USA) and time-lapse imaging. Recordings were made at 380nm excitation and 510nm emission. Images were taken every 4s and 3 frames were averaged. The recording

chamber was continuously perfused with oxygenated Ringer solution by means of a peristaltic pump. Odorant solutions were freshly prepared in rat Ringer solution by dilutions from odorant stocks made in DMSO and applied through syringes connected to the perfusion system via a manifold. Odors were applied for 8s in enough volume to completely replace the solution in the chamber (200 μ l). The odorant concentration, unless otherwise noted, was 30 μ m and stimuli were applied at intervals of at least 1min. Data is shown as the fractional change in fluorescent light intensity: $\Delta F/F_0$ or $(F - F_0)/F_0$, where F is the fluorescent light intensity at each point and F_0 is the value of emitted fluorescent light before the stimulus application (baseline). Odorants were applied randomly; however, in most of the figures the order of odor presentation was modified for illustrative purposes. All odorants were purchased from Sigma-Aldrich, except 2,5,7-trimethyl-2-octenal, neral, and geranial.

Data analysis

Isolated OSNs were stimulated with a panel of odorants that included saturated, unsaturated, and branched aldehydes and some non-aldehyde odorants (Figure 2.1) while responses were monitored with Ca^{2+} imaging. Some of these molecules were previously used to define the molecular range of one of the receptors for octanal, OR-I7, using electroolfactogram (EOG) recordings (Araneda, Kini et al. 2000). To compare the profile of OR-I7 with that of other putative receptors for octanal we infected OSNs with a bicistronic adenoviral construct encoding both OR-I7 and green fluorescent protein (GFP) (Zhao, Ivic et al. 1998; Araneda, Kini et al. 2000). Thus, cells expressing OR-I7

could be identified by expression of the GFP marker (GFP+ cells). Although infected OSNs also express their endogenous receptor, these will be a random selection from among the approximately 1200 rat ORs (S. Firestein, unpublished observations). For example, although citral is not an OR-17 agonist, 37% of the GFP+ cells responded to citral (Table 2.1). However, the size of the response to citral in GFP+ cells did not correlate with the size of the response to octanal (data not shown) and a similar fraction of the GFP- cells (34%) also responded to citral (Table 2.1). Moreover, even upon increasing the concentration of citral to 500 μ m, in the same group of cells the percentage of GFP+ and GFP- cells responding to citral was comparable (data not shown). Taken together these results indicate that the citral response observed in a subset of GFP+ cells is likely to be due to the activation of endogenous receptors sensitive to citral (and other compounds as well), which are prevalent among OSNs, and hence were present in some of the randomly infected OSNs (see also Figures 2.4 and 2.5).

Responses were quantified using macros included in the Igor Pro software (WaveMetrics, Lake Oswego, OR, USA). An odorant was considered to elicit a response only if the change in $\Delta F/F_0$ was higher than two times the value of the standard deviation of the baseline and the decrease in $\Delta F/F_0$ lasted more than 20s. For most of the experiments the amplitude of the responses was measured as the difference between the values of $\Delta F/F_0$ of the peak of the response and the baseline. For the data shown in Figure 2.2B and 2.4B the amplitude of the response was obtained by integrating the area under the curve, using a window of 90s starting at the peak of the response. Statistical significance was assessed using the Student's unpaired *t* test. For the dose-response relations the data were fitted to the Hill equation. Data are shown as means \pm s.e.m. of

least three different cells. In preliminary experiments we found that on average 20% of the cells in the recording field were viable OSNs, as measured by the response to both a high-KCl stimulus (50mM) and the phosphodiesterase inhibitor 3-iso-butyl-1-xanthine (IBMX, 2mM). In most of the experiments odorant responses were compared to the responses to octanal, and repeated applications of octanal allowed us to check for the possible rundown of the responses. Those cells in which the response to octanal decreased more than 60% were discarded.

For cluster analysis the data were analyzed using the EPICLUST software by directly loading spreadsheets made with the Excel software into the <http://ep.ebi.ac.uk/EP/server>. For each cell a response was assigned a value of 1 and no response a value of 0. Thus, all the responses, regardless of their size compared with that of octanal, had the same value. The same data transformation was applied for the cells shown in Figure 2.3.

RESULTS

The odorant octanal and other aldehydes produce activation of a large number of glomeruli in the olfactory bulb (Johnson, Ho et al. 2002; Xu, Liu et al. 2003), suggesting that these compounds activate a large number of ORs. We have used this wide-ranging response to aldehydes, in particular octanal, as the basis for identifying and defining multiple receptor profiles in isolated OSNs. In a first set of experiments we identified different receptors by their sensitivity to closely related aliphatic aldehydes. Many of these compounds were previously used to define the molecular range of an identified

receptor for aldehydes, OR-I7 (Araneda, Kini et al. 2000). In addition, we further extended the distinction between different aldehyde receptors by using a panel that includes distinct molecules.

A receptor for aldehydes can discriminate among closely related molecules

Several studies have proposed that ORs can recognize odorants with very different structures (Sicard and Holley 1984; Duchamp-Viret, Chaput et al. 1999; Ma and Shepherd 2000). However, a thorough characterization of the receptive field of one receptor, OR-I7, shows clear discrimination among aliphatic aldehydes with only subtle modifications in the vicinity of the carbonyl group (Araneda, Kini et al. 2000). Still other studies have shown varying degrees of selectivity in mammalian OSNs (Sato, Hirono et al. 1994; Bozza and Kauer 1998; Kaluza and Breer 2000). In a first set of experiments we determined the receptive field of OR-I7 using Ca^{2+} imaging and found that the profiles of responses were in accord with our previous EOG studies (Araneda, Kini et al. 2000). Thus, cells expressing OR-I7 responded to octanal and other aldehydes with 7- to 11-carbon backbones (30 μm , Figure 2.2A cell a, upper trace) but did not respond to the shorter (<7) or longer (>11) aldehydes (Table 2.1). Similarly, cells expressing OR-I7 also responded to the unsaturated 8-carbon aldehydes, trans-2-octenal and trans,trans-2,4-octadienal, and the unsaturated and branched citronellal (Figure 2.2A cell a, lower trace). None of the cells expressing OR-I7 responded to 8-carbon molecules bearing different functional groups such as octanoic acid or octanol (both at 1mm, Figure 2.2A cell a, lower trace) Also, none of the cells expressing OR-I7 responded to the aldehydes 2,5,7-

trimethyl-trans-2-octenal or cinnamaldehyde, which has been recently described as an agonist for this receptor in mouse (Bozza, Feinstein et al. 2002). This discrepancy may be due to differences in the level of receptor expression achieved with the adenovirus and in the gene targeting experiments. We did find a large number of cells that responded to octanal but which otherwise had pharmacological profiles that were distinct from OR-I7. Some of those cells were less discriminatory and they will be discussed below; for illustration one such aldehyde-responsive cell is shown in Figure 2.2A cell b.

To test the possibility that other receptors for aldehydes could also discriminate among closely related compounds we challenged OSNs with a set of nine aliphatic aldehydes, including octanal. The stimulating panel included saturated aldehydes of increasing carbon chain length (C7–C11), 8-carbon unsaturated (trans-2-octenal and trans,trans-2,4-octadienal), and unsaturated-branched (citral and citronellal) aldehydes. The response profiles of a group of 59 cells activated by at least one member of the panel are shown in Figure 2.3. In this group, cell 4 was the only one to exhibit the expected profile of OR-I7 (Figure 2.3, arrow, green shading). 25 cells did not respond to octanal but did respond to another component of the panel. In general these cells were rather narrowly tuned to one or a few odorants; 20/25 cells responded to only a single odorant in the panel.

Inspection of the profiles of the responding cells revealed some surprising selectivity among these receptors. The unsaturated aldehydes trans-2-octenal and trans,trans-2,4-octadienal, and the unsaturated-branched aldehydes citral and citronellal, differ only by the presence of one extra double bond, yet several cells were able to distinguish between these aldehydes despite being activated by all or most of the

saturated aldehydes in the series C7–C11. Moreover, a set of these cells (28, 29, 32, 33) was activated strictly by 8-carbon aldehydes. Also, notice that cells 52–59 were activated by the unsaturated and unsaturated-branched 8-carbon aldehydes, but not by octanal. Overall, analysis of the pharmacological profiles of cells tested with this panel of aliphatic aldehydes distinguished at least two different types of aldehyde receptor: those that behave like OR-I7 (i.e. are activated by saturated and unsaturated aldehydes) and those that are more narrowly tuned (i.e. are not activated by the unsaturated analogues, or are activated only by aldehydes with an 8-carbon chain).

Geranial can distinguish among different octanal receptors

We have previously shown that citral reduced responses to octanal in OR-I7 (Araneda, Kini et al. 2000). Thus, we tested the possibility that citral could exert differential effects in other receptors for aldehydes. Citral is a mixture of two isomers, geranial and neral, which differ in the orientation of the methyl group at carbon-3, raising the possibility that these isomers might contribute differently to the antagonizing effect. First, we tested each isomer (100 μ m) against octanal (10 μ m) in cells expressing OR-I7. Both isomers almost completely abolished the response to octanal in a reversible fashion (Figure 2.4A). Although neral had a slightly smaller antagonistic effect compared to geranial (Figure 2.4B, left) the difference was not significant ($P < 0.8$), suggesting that at OR-I7 both isomers are equally effective antagonists. In contrast, in other cells that responded to octanal the responses to geranial varied between 6 and 80% of the response to octanal (average, $25 \pm 13\%$). In these cells coapplication of geranial with octanal

resulted in responses that were additive or only slightly reduced ($110 \pm 25\%$, Figure 2.4B, right). In two cells in which geranial did not exhibit a response, the responses to octanal in the presence of geranial were 39 and 100% of the responses to octanal alone (not shown). These results indicate that in different receptors for aldehyde, the citral aldehydes either do not bind the receptor, or their binding produces different degrees of antagonism, further delineating differences in the pharmacology of these receptors.

Different receptors exhibit various sensitivities for aldehydes

Responses to octanal in cells expressing OR-I7 were dose dependent, exhibiting a threshold for response between 0.1 and 0.3 μm and saturation between 10 and 30 μm . For five cells with complete data, a fit of the Hill equation yielded an EC_{50} of $1.9 \pm 0.5\mu\text{m}$ and a Hill coefficient of 2.8 ± 0.1 (Figure 2.2B, green). Compared with the EC_{50} obtained for other receptors using similar recording techniques, this value is relatively low and suggests that OR-I7 may be a high affinity receptor for octanal (Kajiya, Inaki et al. 2001; Bozza, Feinstein et al. 2002). In some cells we observed a decrease in responses at high concentrations of octanal, which could be due to desensitization of the receptor at higher concentrations (i.e. 30 μm). Similarly, we found that in other cells responding to octanal its effect was also dose dependent, with thresholds for octanal responses ranging from 0.1 to 30 μm . As these cells correspond to a heterogeneous group of ORs the data could not be averaged, but the response from one cell, which had a threshold for octanal at 10 μm , is plotted in Figure 2.2B (black) for comparison. These results indicate that multiple receptors bind aldehydes, albeit with different affinities (see below).

In a group of 2301 GFP– isolated OSNs (see Methods) we found 144 (6%) octanal-responding cells at 30 μ m (a saturating concentration for OR-I7). Assuming there is a more or less equal representation of ORs in sensory neurons, and that each OSN expresses only 1 out of ~1200 receptors in the rat (S. Firestein, unpublished observations), we might expect that ~70 receptors are activated by octanal at 30 μ m (Ma and Shepherd 2000; Hamana, Hirono et al. 2003)). Increasing the concentration of octanal to 1000 μ m elicited a response in 47/220 cells (21%), corresponding to ~250 octanal sensitive receptors, representing the recruitment of 180 additional ORs (data not shown). These findings are in general agreement with observations using optical imaging and fMRI, which show that high concentrations of aldehydes activate a large number of glomeruli in the olfactory bulb (Wachowiak and Cohen 2001; Fried, Fuss et al. 2002; Xu, Liu et al. 2003).

Molecular range of other aldehyde receptors

Given this apparently large number of receptors that can detect aldehydes it would be of interest to determine if they can be discriminated pharmacologically. To further distinguish the profile of different receptors for aldehydes we challenged a group of octanal-responding neurons to a select panel of eight other odorants. This panel consisted of aliphatic and aromatic aldehydes, as well as non-aldehyde compounds (see Figure 2.1). All of the compounds were tested at 30 μ m. Based on our dose–response relation for OR-I7 and other receptors (see above), this concentration should allow us to detect both low and high affinity receptors. While some of these odorants might activate the receptors at

lower concentrations, the issue of specificity is better addressed at mid-range concentrations where a non-response indicates significant selectivity of the receptors.

Analysis of the response profiles of 55 cells reveals several receptor types, all of which are activated by octanal, but otherwise possess clearly distinct pharmacological profiles. Examples of odorant responses for some of those cells are shown in Figure 2.5. Some receptors, illustrated by cell 1, have a broad spectrum of activity, responding to all the compounds in this panel. In contrast, other receptors were activated only by octanal, suggesting that they are very narrowly tuned as even *trans,trans*-2,4-octadienal failed to activate them (cell 47). The remaining cells were distributed along a continuum of profiles, from those activated by at least two molecules to those cells that were activated by several compounds (cells 37 and 8, respectively). In addition to differences in the pattern of activation between OSNs there were also differences in the size of the responses to the various odorants in the same OSN. For example cell 8 exhibited responses to citral or octanol that were smaller than octanal, while its response to cinnamaldehyde was larger (Figure 2.5). This suggests differences in affinity and/or efficacy for these compounds at a particular receptor.

To classify the pharmacological profiles from a large number of cells and thus gain further insight into the structure–activity relations among these different receptors we employed cluster analysis, similar to that utilized in analysis of DNA microarrays. Each member of the panel, acting as a molecular probe, is analogous to a gene in an array. Because the components of the panel were compared at a uniform concentration, the profile of each cell was expressed in a binary code as presence or absence of a response (see Methods). As shown in Figure 2.6, inspection of the cluster analysis for this

set of cells revealed two distinct groups, possessing broadly (cluster A) and narrowly (cluster D) tuned molecular ranges. Furthermore, 10 of the response patterns were observed in more than one cell, suggesting that these cells express the same or a very closely related receptor. Altogether we observed 33 profiles and, based on patterns that appeared just once, we can distinguish at least 23 distinct octanal receptor types using only this panel of eight odorants. Like the group of cells shown in the lower half of Figure 2.3, 67 cells that did not respond to octanal but responded to other components of the panel exhibited particularly narrow tuning (not shown). Overall, of 122 cells that responded to at least one component of the panel, 3% of the cells responded to all the compounds while 39% of the cells responded to only one compound.

Cell 27, activated only by octanal and its unsaturated analog *trans,trans*-2,4-octadienal, exhibited the expected profile of OR-I7 based on our previous work (Figure 2.6, arrow, green shading). However, unlike OR-I7, nearly half of the octanal-responding cells (28/55) discriminated between octanal and *trans,trans*-2,4-octadienal. Those receptors were more narrowly tuned, with 27/28 cells responding to three or fewer additional components of the panel. Once again many cells responded to citral (22/55), and most of them had a broad tuning profile, with the exception of cell 38, which (besides octanal) was activated only by citral and 3-phenyl propanal. Cell 20 exhibited a similar profile to that described by Bozza et al. (Bozza, Feinstein et al. 2002) for an OR-I7 expressed in transgenic mice; it was activated by octanal, citral, cinnamaldehyde, and *trans,trans*-2,4-octadienal (though these authors did not test the latter). Also, cluster B was activated by octanal and cinnamaldehyde, but not by *trans,trans*-2,4-octadienal or citral. We suggest that these receptors may be closely related to OR-I7.

The alcohol (27/55) and the acid (10/55), which did not activate OR-I7, did activate several octanal-sensitive receptors and in general these receptors had broader tuning profiles. Interestingly, we found that the majority of the receptors activated by octanoic acid were also activated by octanol (8/10) but the opposite was not generally true. Half of the cells activated by cinnamaldehyde did not recognize the saturated bond at carbon 2 in 3-phenyl propanal. This suggests that other aldehyde receptors, like OR-I7, are sensitive to modifications near the aldehyde group, although differences in the polarization of the aromatic ring in these two molecules could also play a role. It is interesting to note that three cells responded only to octanal and 2,5,7-trimethyl-trans-2-octenal, a compound that does not bind to OR-I7 (Figure 2.6, cluster C), indicating that in those receptors the methyl group at carbon 2 did not interfere with activity although the methyl at C3 in citral was not tolerated.

Selectivity is maintained at higher concentrations

We reasoned that a 10-fold increase in concentration would allow us to detect the majority of aldehyde-sensitive receptors in our sample and would reveal broadly tuned receptors by their response to most or all of the sample components. Indeed, out of 479 cells tested at 300 μ m, 94 (20%) responded to this higher concentration of octanal. However, even at this 10-fold higher concentration, the profiles exhibited a distribution ranging from narrow to wide tuning: at 300 μ m 1% of the cells responded to all the components of the panel, while 24% of the cells responded to only one component, suggesting the occurrence of a population of highly selective receptors (data not shown).

In Figure 2.7 we show the combined profiles of cells tested at 30 μ m (in light blue) or at 300 μ m (dark blue), for selected components of the panel. Analysis of the response profiles to the 8-carbon aldehydes present in the panel reveals that all clusters but one (*C*) contained responsive cells from both concentrations (Figure 2.7A). These clusters included cells that had narrow, intermediate, and broad tuning (*D*, *B* and *A*, respectively). Thus, at both concentrations there remained cells that could discriminate among these related aldehydes.

The response profiles of OSNs to the 8-carbon molecules that differ only in the functional group (octanol, octanal, and octanoic acid), revealed an additional level of unexpected selectivity. We observed cells stimulated by octanoic acid, octanal, and octanol (broadly tuned cells), or by a combination of the alcohol and aldehyde, or the aldehyde and the acid (Figure 2.7B). However, cells stimulated by only octanol and octanoic acid while excluding octanal were never observed. These findings suggest that the interaction of these molecules with the receptor is affected by electronegativity at carbon-1 since the three compounds form a series of increasing electronegativity from octanol to octanoic acid.

DISCUSSION

The problem of detecting and discriminating a large and unpredictable universe of chemical compounds is solved in the olfactory system by using receptors belonging to a family that are better known for their high level of specificity for a small number of hormones and neurotransmitters. The collection of G-protein-coupled receptors (GPCRs)

expressed in the olfactory epithelium is numerically large and presumably structurally diverse, but nonetheless seems likely to participate in a combinatorial signaling strategy to produce odor percepts. This notion was in vogue even before the cloning of odorant receptors, but has since gained experimental support from observations in both the olfactory epithelium and the olfactory bulb. In the epithelium Malnic et al. (1999) showed that molecules differing only in their functional group activated overlapping but not identical sets of receptors. In the olfactory bulb recent recordings with optical imaging techniques (Rubin and Katz 1999; Uchida, Takahashi et al. 2000; Wachowiak and Cohen 2001; Fried, Fuss et al. 2002) have confirmed and extended earlier work with 2-deoxyglucose (Leon and Johnson 2003) and mitral cell recordings (Mori, Nagao et al. 1999) to demonstrate that related odors cause the activation of large and partially overlapping receptor populations.

We have presented data here that largely support these observations and then ask what are the actual numbers of receptors that may be involved in detecting a particular odorant? We have taken a pharmacological approach, using a panel of compounds that differ in specific chemical features, to define receptors by their binding profile, rather than by their nucleotide sequence or synaptic target. In doing so we have been able to approach the more general questions of how many receptors may recognize a particular compound, and how many compounds are recognized by a particular receptor.

To facilitate this analysis we first extended our characterization of a single receptor, OR-17, using a panel of odorants that had a range of activities, extending from none, to partial, to full. An advantage of the calcium imaging recordings is that, unlike the EOG, we were able to compare different odorants at the same concentration. Nevertheless, we

found that compounds that were inactive in the EOG recordings were also inactive in the Ca^{2+} imaging experiments and vice versa, further supporting the reliability of the imaging recording for determining the receptive field of ORs. One characteristic of OR-I7 was the ability of aldehydes unsaturated at carbon 2 to activate this receptor. We found that among the unsaturated aldehydes trans,trans-2,4-octadienal had a larger response than octanal in the majority of the cells and that trans-2-octenal was very effective as well, suggesting that a double bond at this position increases affinity or efficacy (or both). Interestingly, the addition of a double bond to a fragrance compound often results in an increased intensity. Assuming that the efficacies for the different aldehydes are similar, we suggest the following affinity ranking for OR I7: trans,trans-2,4-octadienal > octanal > trans-2-octenal > heptanal.

Only a few studies have analyzed the dose–response relation for a single odorant at a mammalian OR; in general the values of EC_{50} obtained are > $10\mu\text{m}$ (Kajiya, Inaki et al. 2001; Bozza, Feinstein et al. 2002). We find that for octanal this relationship was typically steep, with a threshold concentration for responses at $\sim 0.1\text{--}0.3\mu\text{m}$ and maximal activity within a narrow concentration range (1 log unit). This type of steep relationship has been found in other systems as well, and it may be related to the efficacy of the coupling between the receptor and the transduction pathway in OSNs (Firestein, Picco et al. 1993). The value of the EC_{50} ($\sim 2\mu\text{m}$) is the lowest published for a mammalian OR, using Ca^{2+} imaging techniques ((Kajiya, Inaki et al. 2001; Bozza, Feinstein et al. 2002) but see (Levasseur, Persuy et al. 2003)), suggesting that this receptor has a high affinity for aldehydes. However, this value may not reflect the true affinity of octanal for the receptor as the observed responses in Ca^{2+} imaging depend on the activation of second

messenger pathways, and their stoichiometric relation to the Ca^{2+} signal is unknown. Furthermore, the thresholds for detection of some compounds in mammals are very low (~ 3.5 p.p.b. for octanal in humans (Cometto-Muniz, Cain et al. 1998)), suggesting that the higher concentrations necessary to activate the receptors in the imaging experiments may reflect technical limitations rather than true receptor kinetics.

In our experiments, citral failed to activate the I7 receptor, but did block the response to octanal, indicating that analogs of octanal can bind to the receptor while possessing lower, or no efficacy at the receptor. This highlights an important and often overlooked feature of ORs, that of antagonism. While well documented in other GPCRs, antagonism has not been regularly reported for ORs (Araneda, Kini et al. 2000; Spehr, Gisselmann et al. 2003; Oka, Omura et al. 2004). However, since olfactory stimuli are commonly a complex mixture of chemicals, the quality of a given stimulus, i.e. its code, will in fact be a combination of activated, partially activated, and antagonized receptors. Indeed, commercial fragrances often contain compounds that have no detectable odor of their own but are known to add to the quality of the mixture. Antagonism at the level of the receptor cells could also explain suppression or inhibition in mixtures of odorants (Laing, Legha et al. 2003). From the perspective of a neural code both agonistic and antagonistic effects should be considered, especially for complex mixtures containing odorants with related structures – a potential difficulty for assay systems that rely solely on activity for their signal. Finally, pharmacologically the use of antagonists could be useful in classifying receptors, in analogy with their use in other GPCRs.

In regard to the number of receptors that recognize a particular set of ligands we focused on aldehydes because chemicals in this class tend to produce large responses in

EOG recordings, suggesting the activation of a large number of receptors. In addition we used a few compounds that were similar in structure to the aldehydes but with different functional groups. With this panel of nine odors we were able to distinguish a surprisingly large number of pharmacological profiles. Overall two types of receptors were present, those with relatively broader tuning profiles, and those that appeared more narrowly responsive. One finding of interest was that half of the responding cells responded to both aldehydes and alcohols, suggesting that many receptors cannot distinguish between these two functional groups, although both compounds maintain a distinctive odor quality, even at high concentrations. This result could explain the observation, in studies with 2-deoxyglucose labeling, that aldehydes and alcohols of the same carbon chain length activated overlapping glomerular modules (Johnson, Ho et al. 2002). In addition, activation of receptors shared by structurally related or unrelated odorants could explain the phenomenon of cross-adaptation (Dalton 2000).

From cluster analysis we estimated that the number of octanal-sensitive receptors could be no lower than 33. This number is higher than that estimated in mice (10–20) by optical imaging of the bulb (Fried, Fuss et al. 2002). The difference could be due to the slightly higher number of predicted functional receptors in rat (S. Firestein, unpublished observations). Adding a few more odors to the panel would probably enable us to pharmacologically distinguish additional receptor types. It is also important to note that in our analysis responses were classified as binary, either yes or no, and no account was taken of different levels of activation. Adding this dimension would further help to discriminate between different receptors. Thus, in the limit we could have identified 55 octanal responsive odor receptors, assuming that every response pattern we observed was

representative of a different receptor. Other functional groups, of course, may not be as widely represented in the receptor repertoire.

Our data appear to be inconsistent with a model in which most, if not all, of the receptors are broadly tuned and thus able to recognize molecules with very different chemical structures (Duchamp-Viret, Chaput et al. 1999; Ma and Shepherd 2000). Indeed we find that the opposite is more likely the case, with many receptors showing surprising levels of selectivity, even among the most similar molecules in the panel. Thus we find selectivity among 8-carbon aldehydes with different degrees of unsaturation or branching, as well as among saturated 8-carbon molecules with different functional groups. Most strikingly we find an apparent selectivity for electronegativity at these functional groups. Another possibility is that this selectivity reflects the nature of hydrogen bonding in the binding pocket. For example, all three functional groups are potential proton acceptors, but only the alcohol and acid can act as proton donors, suggesting a model in which the hydrogen-bonded protons are donated by residues within the receptor protein rather than by the ligand.

These observations lead us to propose a model in which receptors are relatively specific for particular chemical features and any given compound is discriminated based on its recognition by a large number of receptors, each with an affinity for a particular feature. While this may be a general principle of coding we also expect that there may be compounds recognized with very high affinity by only a few highly specific receptors. These might include burning odors or those of decomposition, which are known to be recognized at very low concentrations. From an evolutionary perspective, recognition of these sorts of odors by a dedicated labeled-line type of strategy may be more appropriate.

Moreover, recognition of the odorant (discrimination threshold) occurs at higher concentrations than the detection threshold (Dalton 2002) and it may be that high affinity receptors act to signal the presence of an odorant, but determination of the quality requires the combination and recruitment of other receptors.

How can a combinatorial code for odor recognition remain faithful over changes in stimulus concentration? For several compounds odor quality is known to change with concentration. A recent study has shown that in humans the odor quality of three molecules homologous to those included in our panel, heptanal, heptanol and heptanoic acid, changed as their concentration was increased, and none of the odors shared a common quality at high concentrations (Laing, Legha et al. 2003). However, most odors retain a constant quality over many orders of concentration. We found that octanal activates a large number of receptors and that the number increases appreciably with increasing concentration. This is consistent with data from intrinsic and magnetic resonance imaging studies showing a large number of glomeruli in the bulb activated by aldehydes (Uchida, Takahashi et al. 2000; Wachowiak and Cohen 2001; Fried, Fuss et al. 2002; Xu, Liu et al. 2003). Increasing concentrations activate additional glomeruli suggesting that additional, presumably lower affinity receptors, are being recruited (Uchida, Takahashi et al. 2000; Fried, Fuss et al. 2002). However, this clearly changes the activation pattern and the combinatorial code for that odor. We observe that although more cells respond at higher concentrations, indicating recruitment of new receptors, several cells continue to exhibit narrow profiles, even at high concentrations. This suggests an alternative coding model in which some receptors signify specificity while other receptors may signal concentration. For example there may be receptors with a low

affinity and broad sensitivity to many odors. These receptors are only activated by high concentrations, but are not particularly discriminative. Thus the inclusion of these receptors in any pattern of activated receptors simply signals the presence of that odor at a high concentration.

In summary, our evidence supports the notion that the olfactory system probably uses an array of receptors with different pharmacological tuning, from very specific to quite broad. This places the locus for understanding the code at the olfactory bulb, or higher centers. Whether a glomerular map that reflects an odor code exists in the bulb (Leon and Johnson 2003), and how the intrinsic circuits within the olfactory bulb modify the signal (Mori, Nagao et al. 1999), are now questions that can be profitably investigated using a relatively compact stimulus set.

ACKNOWLEDGEMENTS

We thank the Takasago Company (Kanagawa, Japan) for providing neral and geranial, Givaudan-Roure (Vernier, Switzerland) for 2,5,7-trimethyl-2-octenal, and Dr. Christian Margot for helpful comments. This work was supported by the NIDCD.

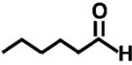
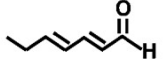
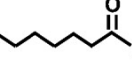
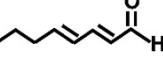
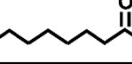
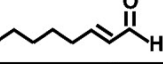
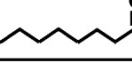
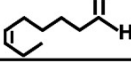
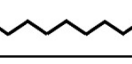
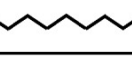
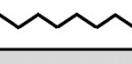
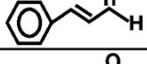
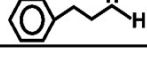
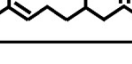
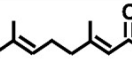
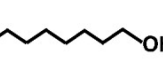
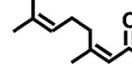
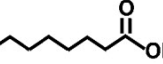
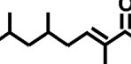
Saturated Aliphatic			Unsaturated Aliphatic		
hexanal	HEX		trans,trans-2,4-heptadienal	2,4-HD	
heptanal	C7		trans,trans-2,4-octadienal	2,4-OD	
octanal	OAL		trans-2-octenal	2-TO	
nonanal	C9		cis-6-nonenal	CNO	
decanal	C10				
undecanal	C11		Aromatic		
dodecanal	C12		cinnamaldehyde	CIN	
Unsaturated Branched			3-phenyl-propanal	3-PP	
citronellal	CTR				
citral	CIT	(Mix of NER and GER)	Non Aldehyde		
neral	NER		octanol	OOL	
geranial	GER		octanoic acid	OAC	
2,5,7-trimethyl-2-octenal	TMO				

Figure 2.1 - panel of odorants used to characterize the pharmacological profiles of receptors for octanal. The abbreviation given for each compound is that used in the subsequent figures.

Figure 2.2 - pharmacology of OR-I7-expressing cells and cells expressing other receptors for aldehydes. (A) Comparison of the responses to octanal and other odorants in cells expressing OR-I7. For this and the following figures odorants were applied for 8s, beginning at the time indicated by the arrow. (top, green) GFP+ cells were activated by C7–C11 aldehydes. (middle, green) They were also activated by the unsaturated aldehydes, CTR, 2-TO and 2,4-OD, but not by CIT, TMO, OAC and OOL (bottom, black) Activity profile for a GFP– cell. This cell also responded to octanal and 2-TO, but unlike the I7-expressing cell, this cell also responded to OAC and OOL and did not respond to CTR and 2,4-OD. All compounds were tested at 30 μ m, except OAC and OOL (at 1mm). The calibration bar is 6% Δ F/F (vertical) and 1min (horizontal) and is the same for both cells. **(B)** Dose–response relation for OAL in cells expressing OR-I7 (•, green) and a GFP– cell (■, black). Responses were normalized to the largest response (10 and 100 μ m, respectively) and fitted to the Hill equation. Responses in OR-I7 are shifted to the left, indicating greater sensitivity for octanal. (inset) Dose-dependent increases in calcium signal induced by OAL in a cell expressing OR-I7. The calibration bar is 4% Δ F/F (vertical) and 1min (horizontal).

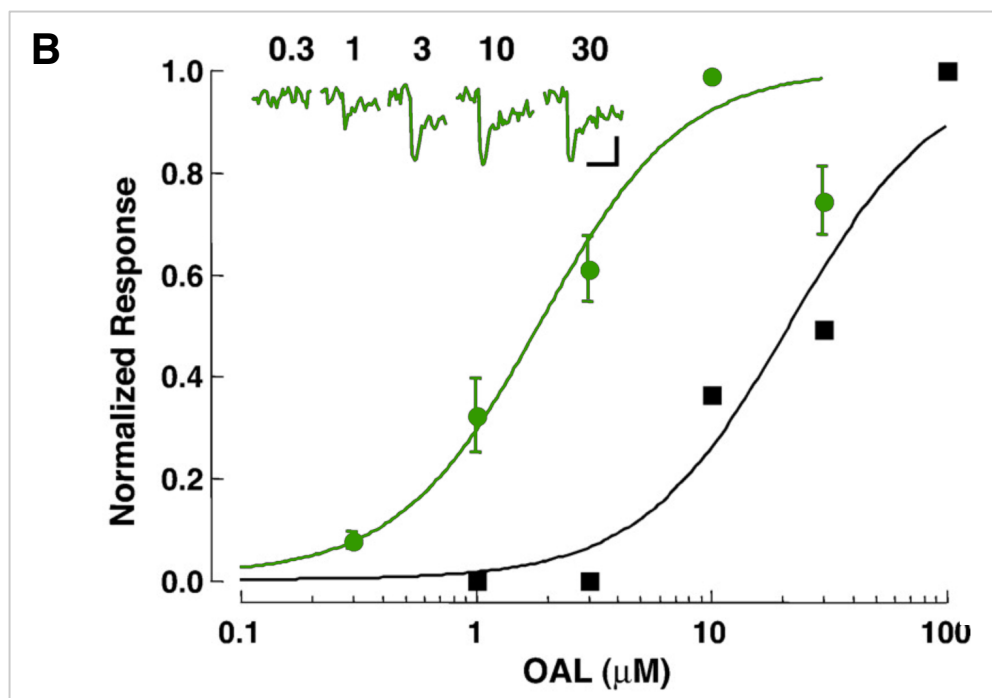
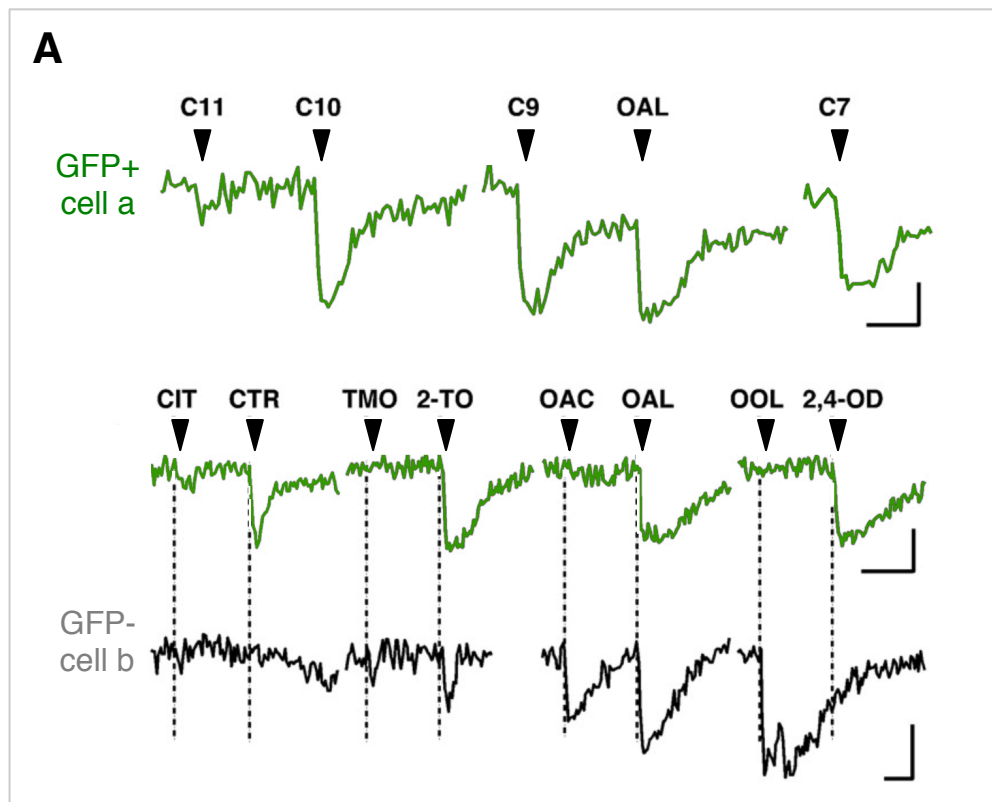


Figure 2.3 - aldehyde receptors can discriminate closely related compounds.

Pharmacological profiles of 59 GFP⁻ cells, tested with a panel of 9 aldehydes. A response is indicated by a shaded box and no response, by a white box. In this group only cell 4, shaded using green, exhibited the pharmacological profile of OR-I7; it was activated by all aldehydes tested except CIT. Other cells exhibited varying patterns of responses. The lower section of the panel shows a group of 25 cells that did not respond to OAL, but responded to other aldehydes in the panel. These cells were all rather narrowly tuned. All compounds were tested at 30 μ m.

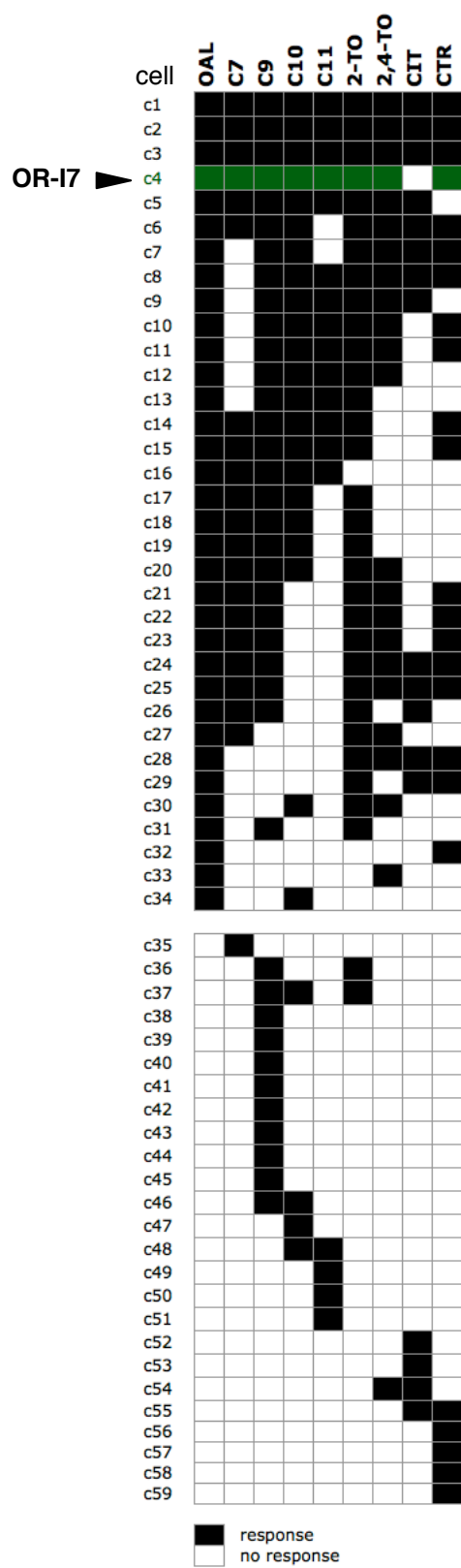
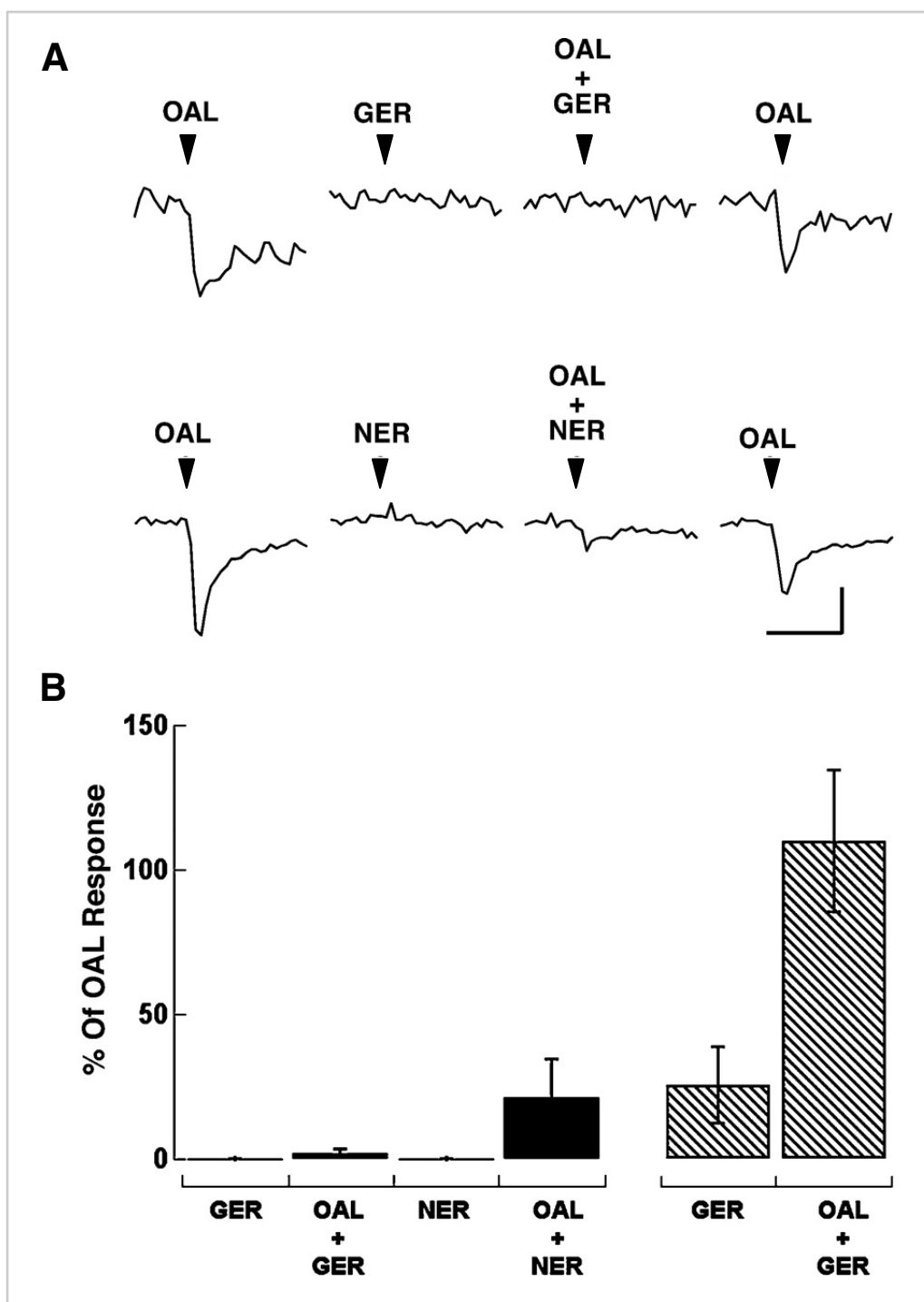


Figure 2.4 - the isomers geranial and neral reduce the responses to octanal at some aldehyde receptors. (A) GER (top traces) and NER (bottom traces) reversibly reduced the responses to octanal in cells expressing OR-I7. Both isomers were tested at 100 μ m, and in the cells shown here they did not generate a response (see Methods). Calibration bar, 6% $\Delta F/F$ (vertical) and 1min (horizontal). (B) Not all receptors for aldehydes were blocked by the isomers. Both isomers almost completely reduced the response to octanal in GFP+ cells (solid bars, left). In contrast, in GFP- cells, GER produced a small response and failed to inhibit the response to octanal (hatched bars, right).



(this page intentionally left blank)

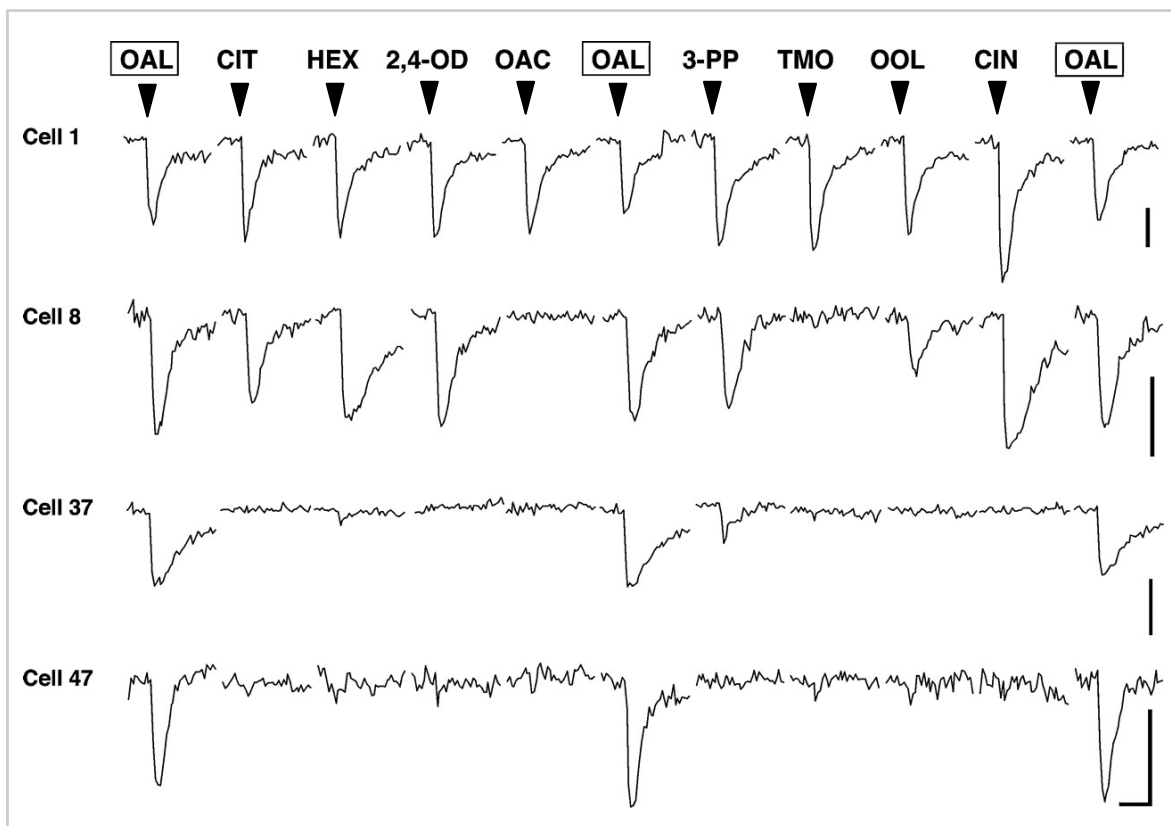


Figure 2.5 - cells exhibit distinct response profiles to a test panel of odorants.

Odorant responses of a selected group of OAL+ cells challenged with a second panel of 9 odorants. The full cohort of OAL+ cells from this screen are shown in Figure 2.6. Responses to the different odorants were compared to a test application of OAL. Cells exhibited various profiles of activity, from narrowly tuned (cell 47) to broadly tuned (cell 1). In a few cells some of the components in the panel produced larger responses than octanal (i.e. CIN in cells 1 and 8). All odorants were tested at 30 μ m. For all cells the calibration bar is 6% $\Delta F/F$ (vertical) and 1min (horizontal).

Figure 2.6 - cluster analysis reveals several aldehyde receptor types. Cluster analysis of 55 octanal responding cells. Cell responses as a binary profile were used for the cluster analysis (see Methods). Responses are indicated in black and no response in white. Cell 27 had the expected profile of OR-I7; responses of this cell are shaded green. There were 33 distinct response profiles; 10 of these profiles appeared in more than one cell. A few cells responded to all the odorants (cluster A), and a large number only to OAL (cluster D). Cluster C was stimulated only by octanal and TMO. All odorants were tested at 30 μ m.

Figure 2.7 - selectivity of aldehyde receptors is maintained at different concentrations. Cluster analysis for cells tested at 30 μ m (light blue) or 300 μ m (dark blue) with a selected group of compounds from the panel. The number of cells included in the analysis is indicated by the labeled grid at the left of each panel. There are 178 cells in **(A)** and 146 cells in **(B)**. **(A)** Cluster analysis of the response profiles to 8-carbon compounds with different degrees of unsaturation and branching. All of the clusters, except one, included cells from both groups (30 or 300 μ m). **(B)** Cluster analysis of the response profiles to 8-carbon compounds with different functional groups. Cells that responded both to OOL and OAC and yet excluded OAL were not observed at either concentration.

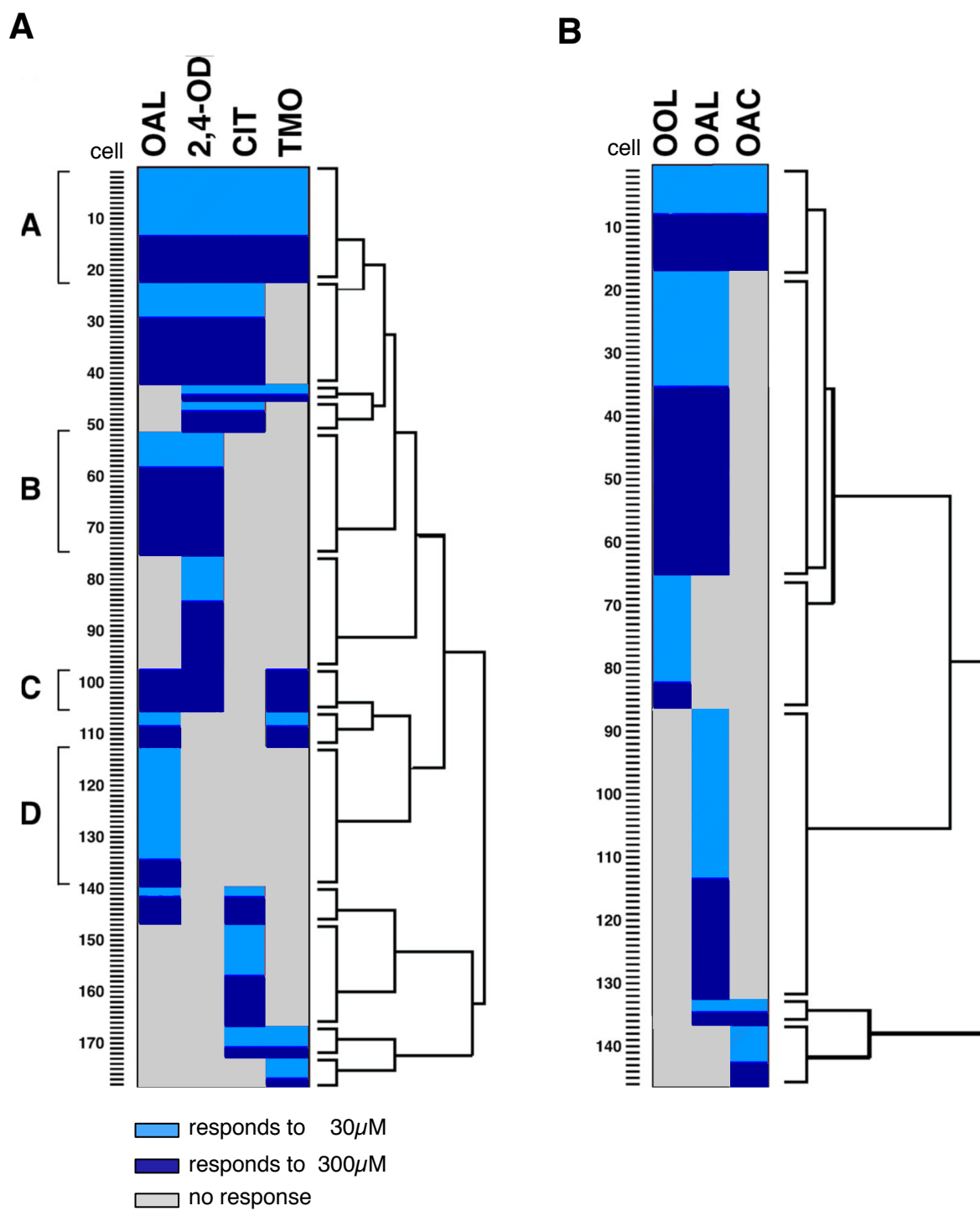


Table 2.1

GFP+ (OR-I7) and GFP- cells tested with different aldehydes and non-aldehyde compounds in OR-I7-infected animals

		NR	<50%	50-100%	>100%	Total	% Responding
GFP+	HEX	3	0	0	0	3	0
	C7	3	8	12	0	23	87
	OAL	-	-	-	-	73	-
	C9	8	11	10	2	31	82
	C10	20	6	1	1	28	29
	C11	21	2	1	0	24	13
	C12	5	0	0	0	5	0
	CIT	22	11	2	0	35	37
	CTR	3	4	25	5	37	92
	2,4-HD	0	3	3	5	11	100
	2-TO	1	0	17	7	25	96
	2,4-OD	1	0	7	25	33	97
	TMO	11	0	0	0	11	0
	CNO	0	2	1	1	4	100
	OAC	7	0	0	0	7	0
	OOL	6	0	0	0	5	0
	CIN	5	0	0	0	5	0
	GFP-	HEX	5	0	0	0	5
C7		20	18	15	7	60	67
OAL		-	-	-	-	-	-
C9		10	12	27	9	58	83
C10		23	15	9	10	57	60
C11		31	9	4	5	49	37
C12		3	0	0	0	3	0
CIT		58	12	10	8	88	54
CTR		37	18	22	4	81	54
2,4-HD		12	12	7	4	81	54
2-TO		16	9	25	18	66	76
2,4-OD		24	9	15	23	71	66
TMO		23	3	0	2	28	18
CNO		0	0	2	1	3	100
OAC		9	2	3	6	20	55
OOL		13	1	4	4	22	41
CIN		2	1	0	1	4	50

CHAPTER 2 - SECTION 2

VALIDATING THE FUNCTIONAL FINGERPRINTING CONCEPT

ABSTRACT

In our prior study (Araneda, Peterlin et al. 2004) we suggested that a distinctive physiological signature could, in lieu of genetic sequence, be used as an alternate means of identifying an olfactory sensory neuron (OSN) expressing a given odorant receptor (OR). A panel of 8 odorants was able to parse a large population of 55 octanal (OAL) responsive OSNs into 23 uniquely occurring response patterns. One of these profiles matched that previously established for rat I7. In this brief communication, we describe successful implementation of this concept of functional fingerprinting. Following a novel procedure in which GFP and I7 were co-infected into OSN precursor cells (Chesler, Zou et al. 2007), we needed a method to establish that mature GFP+ OSNs continued to express I7 and that decoupling of the visual marker and functional expression of the receptor had not occurred. We detail how a mini-panel of odorants was extracted from the original panel with consideration given to both activation probabilities and literature reports. We cross-checked this proposed “mini-fingerprint” across the OAL+ OSN population to establish the baseline ambiguity introduced by the truncation of the odor panel. We then applied this pruned panel to OSNs retrieved from the novel expression system and observed the frequency of the target fingerprint among both GFP- and GFP+ OAL+ OSNs. We confirm that the functional fingerprinting method was highly effective, with the expected physiological profile present in all the GFP+ OSNs but only at the previously predicted residual levels among GFP- OSNs.

INTRODUCTION

In panel screens a large number of OSNs that sample the full OR repertoire are challenged with a series of odorants. High throughput calcium imaging permits an efficient assay of activity while preserving cellular identity. Due to expression of only one OR type per OSN (Chess, Simon et al. 1994; Malnic, Hirono et al. 1999), the cellular activity is taken as a proxy for receptor activity. With ~1200 ORs predicted for the rat (Zhang and Firestein 2007), every OSN in a screen is likely to express a different OR. The response profiles are reported in a matrix format, offering the ability to note the discriminations achieved by each cell as well as patterns that are conserved across the population.

It is this ability to leverage a cell's response profile against the trends observed among the population that converts what would otherwise be a mere description of a portion of a cell's receptive field into a useful diagnostic tool. Emphasis thus shifts from the makeup of a given functional profile to the frequency of finding that profile. Primarily, this technique is used to gain insight as to how readily certain chemical discriminations are made by ORs. But if it is rare, a functional profile can serve as an identifying signature for the OR that generated it.

Appropriate odor selection can achieve unique profiles

In part, the number of unique response profiles in a panel will depend on the choice of odorants used during screening. Should too many of the odorants fail to

activate the population, response patterns consisting of only one activating odorant may appear at high frequencies. This is seen in Figure 2.8, particularly among the OAL- population. High frequency profiles are ambiguous in the sense that they likely result from multiple receptors. This interpretation is based off the low frequency of expression of any given OR and the high number of ORs involved. A plausible explanation for this occurrence is that this panel of odorants samples a region of chemical space that only marginally overlaps that preferred by these receptors. It is also possible that some of these ORs are very highly tailored receptors with narrow receptive fields.

The histogram in Figure 2.8 also underscores how the appropriateness of the panel will depend on the targeted subpopulation. With this set of 8 odorants the OAL+ OSNs were readily parsed into a number of unique signatures, but the OAL- cells were not. The presence of such a well-defined split suggests some architectural constraint in building a receptor such that the ability to exclude OAL also limits the ability to recognize odors that are common co-activators alongside OAL.

At present, we do not have a guide for choosing odorants specifically with the aim of eliciting a unique profile that can serve as a functional fingerprint for a given OR. However we suggest that a useful approach may be to plot a ligand of interest in the recently developed models of multidimensional chemical space (Haddad, Khan et al. 2008; Saito, Chi et al. 2009).

From 55 OAL+ OSNs, only one profile matched that observed in our system for ratI7 when the remaining 8 odorants were considered (Figure 2.8, pro_19, arrow and green shading). Because of the uniqueness of the response profile, it can be taken as a signature of an I7-expressing cell. This set of odorants and the pattern they elicited thus

constitute a “functional fingerprint”. Finding this fingerprint proved fortuitous when the need arose to clarify the behavior of I7 in a novel expression system.

The presenting problem

Instead of the established technique of using adenovirus to infect mature OSNs (Zhao, Ivic et al. 1998), the new system used embryonically injected retrovirus to target the precursor cells that would give rise to OSNs (Chesler, Zou et al. 2007). As a result, immature OSNs should express I7 well before any OR would normally be chosen during development. The fate of this ectopic I7 was highly uncertain. At the normal developmental time-point, would the maturing OSN shut down the expression of ectopic I7 and select instead a different OR? If so, GFP+ OSNs would express a diversity of ORs and thus exhibit an array of functional profiles. If I7 expression persisted, this could result in GFP+ OSNs continuing to express just I7 or I7 along with a second receptor. Either scenario should result in GFP+ OSNs carrying a functional signature of I7.

The possibility of uncoupling the fluorescent marker from OR expression, combined with OAL being a robust recruiter, created a reasonable chance that a cell could be GFP+ and OAL+ but I7-. Had GFP+ cells been prevalent, uncoupling would have been readily apparent. But the success rate of the in utero retroviral transfection procedure was exceedingly low, making viable GFP+ cells rare. A truncated fingerprinting panel of odorants was needed to rapidly confirm whether an OAL+/GFP+ cell indeed had the functional characteristics of I7 expression.

METHODS

Panel pruning : a tradeoff between speed and accuracy

The utility of a functional fingerprint is enhanced if odorants can be eliminated and yet the truncated profile remains rare among the population. This is best achieved by removing column-wise redundancies. The extent to which any fingerprint can be pruned into a “mini-fingerprint” will vary depending on population trends and which elements have been retained in the fingerprint. Pruning, even with the introduction of some ambiguity, can offer practical advantages. Any preparation using acutely dissociated OSNs will have limited viability. A shorter fingerprint will decrease the time spent delivering odorants while panning for the appropriate functional signature. In our application, a mini-print for I7 was required as some of the original stimulus lines needed to be re-dedicated to apply blends of odorants to screen for a second functional OR.

Marginally activating compounds can compromise a fingerprint

When deciding which odorants to prune from a signature, one guideline is to strip odorants that may give a marginal response at the concentration in question. This is because sensitivities are mixed even within the same OR-expressing population. For example, M71 displays a bell shaped distribution in sensitivity to acetophenone (Bozza, Feinstein et al. 2002). Such an effect could convert a very weak positive response to a negative one or vice versa. For this reason, we considered the reliability of the response,

based on multiple prior experiments, as a factor if two options were otherwise closely matched.

We also chose to avoid odorants where the response patterns were contested. In our adenoviral infection system, cinnamaldehyde and citral (CIT) were not I7 agonists at 30uM. However when ratI7 was expressed in transgenic mice, those OSNs responded to both odorants at 10uM (Bozza, Feinstein et al. 2002). The discrepancy may be due to details of the perfusion systems that impact the effective concentration of odorant reaching the plated cells, or it may be related to level of receptor expression. For this second reason in particular, we were wary of including these odorants in the diagnostic mini-fingerprint. Although this decision compromised our flexibility in selecting odorants for the mini-fingerprint, we felt it important to utilize only the more reliable elements from the larger profile.

Rationale for extracting an I7 fingerprinting panel of odorants

Table 2.2 provides the frequency with which OAL+ cells were co-activated by each odorant in the survey panel. To initiate the mini-fingerprint, it would be ideal to add the I7-activating odorant which activated the fewest general OAL+ cells. The simple +/- signature would thus already indicate that the observed cell was worth pursuing. By the probability table CIT was the preferred candidate. However, since CIT's signature at I7 was contested, we selected trans, trans-2,4-octadienal (2,4-OD) as the second element for the fingerprinting panel. A odorant that failed to activate I7 was also desired because it could serve as a control to rule out non-specific responses while also improving the

significance of the fingerprint. It would be ideal for the odor, that fails to activate I7, to recruit as many general OAL+ cells as possible. Octanol (OOL) matched this criterion, resulting in a mini-fingerprint with the target I7 pattern of OAL+ / 2,4-OD+ / OOL-.

Using the probability table, if the ability to detect each chemical was independent of each other, then this activation pattern should occur with 26% frequency among OAL+ cells (ie: $1.00 * 0.49 * (1-0.47)$). However, analysis of the large scale panel screen revealed that the OAL+ / 2,4-OD+ / OOL- signature was found in only 13% (7/55) of OAL+ OSN profiles (Figure 2.8, grey shading). This uneven partitioning can also be seen in the Venn diagram (Figure 2.9). OOL and 2,4-OD could each recruit ~45-50% of the OAL+ population. However, an OSN responding to any two of the odorants was highly likely to respond to all three, leading to sparser than predicted occupancy of the yellow and magenta sectors. This bias worked in favor of the mini-fingerprint being a better diagnostic tool for I7.

The 13% ambiguity could have been eliminated with the addition of cinnamaldehyde, but because it was a contested odorant we supplemented the mini-fingerprint with hexanal (HEX). While inclusion of HEX provides only minor benefit in reducing the chance of mistaken attribution of I7 to 9%, HEX has value as an I7 antagonist (Peterlin, Li et al. 2008). There was the chance that retrovirally infected OSNs might select a second OR in addition to retaining I7. If a ligand for this second OR could be found among the screening mixes, one could investigate if HEX could inhibit activation by this second ligand. The ability to do so might suggest heterodimerization between the second OR and the ectopic I7.

RESULTS

The retroviral infection resulted in dispersed, small patches of GFP+ cells within the olfactory epithelium. These regions were microdissected, dissociated, and the cells subjected to odor application and calcium imaging following published procedures (Araneda, Peterlin et al. 2004). Once located, a GFP+ cell was first screened with octanal. If the OSN was responsive, the remainder of the mini-fingerprint panel of odorants was applied. The responses of both GFP+ and GFP- OAL+ OSNs that were present in the same visual field are shown in Figure 2.10. Among the GFP- / OAL+ OSNs, of which we assume none truly express I7, the I7 mini-print profile was misattributed with 13% frequency, which is near what we had predicted. The slight increase over a 9% misattribution rate (with HEX inclusion) could reflect either the small sample size or bias in receptor expression arising from the very uneven sampling of the olfactory epithelium. As hoped, among GFP+ / OAL+ OSNs the I7 mini-print profile of OAL+ / 2,4-OD+ / OOL- / HEX- was present 100% of the time, confirming both the continued expression of I7 in the system and the utility of the functional fingerprinting method.

DISCUSSION

Because each OR generates a hallmark functional signature, adequate odor selection can result in a brief and yet unique response profile that can be used to physiologically identify a cell as expressing that OR. Though a simple concept, functional fingerprinting can be an expedient and useful tool. For example, a profile

demonstrating an unexpected discrimination pattern might be identified during broad panel screening. Indeed, this profile might only be recognized after the experiment has been completed, analyzed, and the population trends are evident. How best to confirm and extend the discriminations made by this OR, particularly if the investigation is only at a preliminary stage?

Traditional means require significant investment of labor and resources. After rescreening for a cell matching that functional profile, the OR sequence would need to be retrieved by RT-PCR. This is a difficult proposition with groups regularly reporting 30% failure rates (Malnic, Hirono et al. 1999; Kajiya, Inaki et al. 2001; Hamana, Hirono et al. 2003) or worse (Touhara, Sengoku et al. 1999). Re-expression of the retrieved OR is also an investment, requiring either preparation of an adenoviral vector and recurrent acute surgery or the generation of transgenic animals.

An adequate functional fingerprint can obviate these difficulties; one simply pans for the unique physiological signature as opposed to visually panning for GFP. Ranking the order of the stimulus delivery can assist with expediency. For example, the activating odorant in the fingerprint that is the most rarely activating among the general OR population should be given first. This is followed by the odorant that would best parse the remaining ambiguous population and so forth until the accepted level of certainty is achieved. The greatest challenge is deriving a unique functional signature, but we have shown that a panel of 9 partially-related odorants could generate 36 signatures which occurred only once out of 1115 OSNs screened. Any of those ORs are amenable to further pursuit by functional fingerprinting.

Combining adenoviral infection with functional fingerprinting of an alternate receptor allows a direct contrast in chemical parsing strategies

Another potential application of functional fingerprinting is to investigate whether functional orthologs are indeed genetic orthologs. A promising case study would be human hOR17-4. Aside from sharing citronellal as an agonist, the hOR17-4 (Triller, Boulden et al. 2008) and I7 (Zhao, Ivic et al. 1998; Araneda, Kini et al. 2000) receptive fields are near mirror-images for the odorants that have been tested at both ORs (Supplemental Figure 2.1). As not all hOR17-4 agonists require an aromatic ring, I suspect that the ring may serve a scaffolding function to shunt the tail into a particular conformation. This bend occurs just slightly more distal than where we conclude I7 prefers for its agonists (Peterlin, Li et al. 2008). Identification of the rat version of hOR17-4 could provide an interesting opportunity to compare steric tolerance and preferred geometric path of the odorant through the mid-portion of the binding pocket.

The hOR17-4 discrimination profile of OAL- / cinnamaldehyde- / 3-phenyl propanal+ was noted only one time in our panel conducted on rat OSNs (Figure 2.8, pro_51). The simple cinnamaldehyde- /3-phenyl propanal+ discrimination itself is exceedingly rare. It can thus be used as the core for rapidly panning for the hOR17-4-like fingerprint. To pan for the OSN with this profile in tissue dissociated from an I7 adenovirally infected rat has an added benefit. Once an hOR17-4-like rat OSN is found, there is a high probability that GFP+/I7+ OSNs will be co-present in the field due to exuberance of the adenoviral infection. The previously reported compounds from literature will need to be assayed to establish how similar the rat hOR17-4-like OSN truly

functionally mimics hOR17-4; the presence of GFP+/ I7+ OSNs in the same field allows for a report on the same odorant panel in parallel. The hOR17-4-like rat OSNs can then be retrieved for RT-PCR with both degenerate and ortholog-tailored specific primers to determine if the genetic ortholog indeed corresponds to the functional one.

In conclusion, functional fingerprinting identifies a specific OR-expressing cell through physiological means. Odorants that comprise the fingerprinting panel are strategically chosen from analysis of population trends established in preliminary broader panel screens. Functional fingerprinting can free the experimenter from the challenging, and often unnecessary, constraint of simply adding a genetic tag to a receptor that is interesting because of its function and not its sequence per se. Functional fingerprinting focuses on the elements that make that receptor distinct among the population. In doing so, it permits a more rapid approach to extended characterization of a given receptor and appreciation of its specialized contribution to the combinatorial code.

(this page intentionally left blank)

Figure 2.8 - distribution of observed response profiles. All the unique response profiles from a panel screen on 1115 rat OSNs using 30uM each of the indicated odors: OAL, octanal; 2-4-OD, trans,trans-2,4-octadienal; CIT, citral ; TMO, 2,5,7-trimethyl-2-octenal ; OOL, octanol; OAC, octanoic acid; HEX, hexanal; CIN, trans-cinnamaldehyde; 3-PP, 3-phenyl propanal. The profiles for the OAL+ population have previously been reported in Areneda et al. (2004). Horizontal rows show the response profile for a given cell with shaded boxes indicating that the cell responded to that odorant. White boxes indicate that the odorant was tested, but it did not elicit a response. The I7 profile (pro_19) is shaded using green and marked by an arrowhead. Grey shaded profiles (pro 8, 10, 13-15) are those that cannot be disambiguated from I7 if only the abbreviated panel of the mini-fingerprint is employed. 58 unique profiles were observed. This is far less than the 512 profiles possible if detection of each odorant is independent of each other. Dots at right mark how many times a given profile was observed.

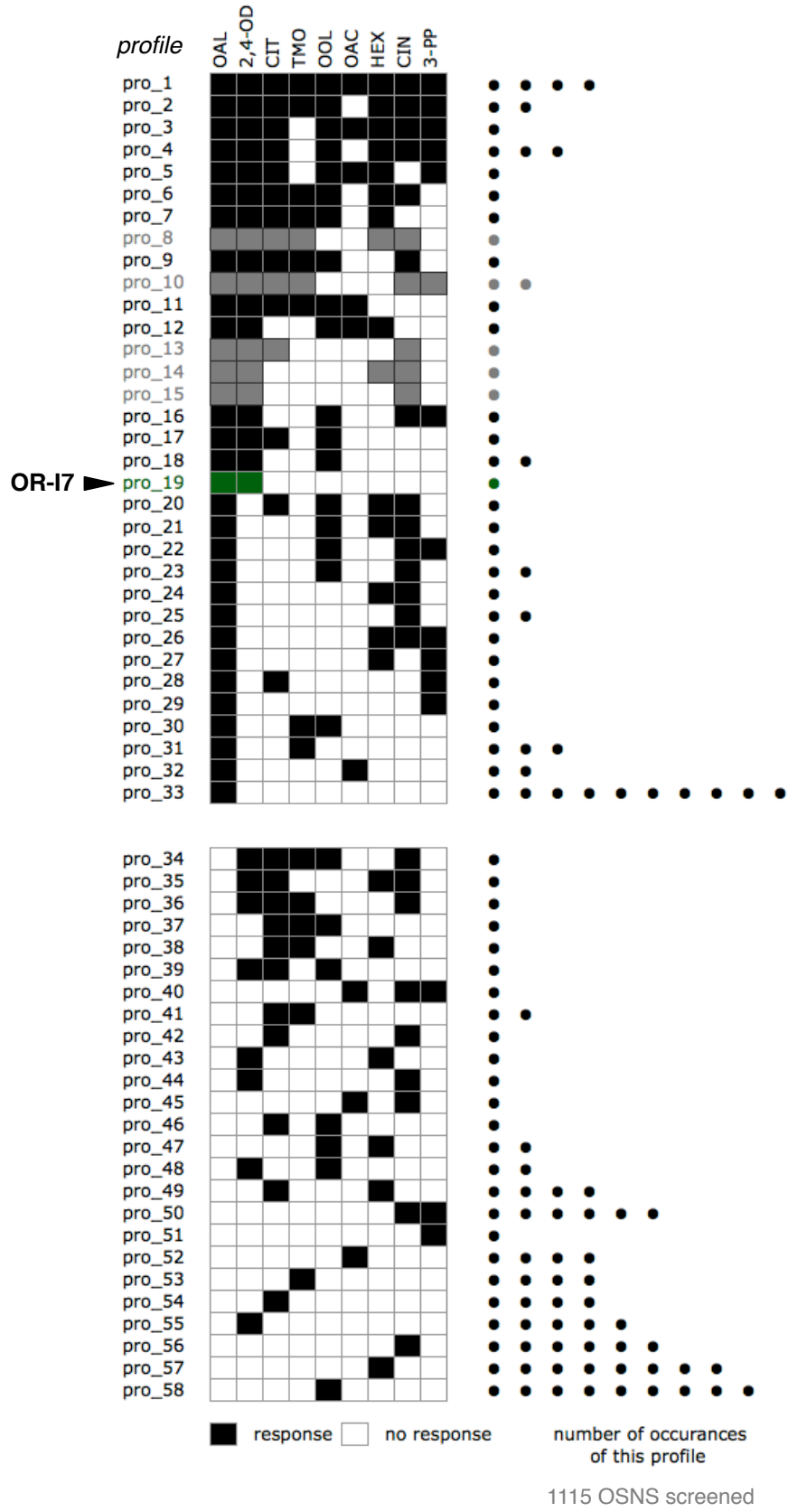


Table 2.2**frequency of activation by a given odorant given the status of the response to octanal**

name	abbrev.	OAL+	OAL-
trans,trans-2,4-octandienal	2,4-OD	0.49	0.19
citral	CIT	0.40	0.26
2,5,7-trimethyl-2-octenal	TMO	0.31	0.14
octanol	OOL	0.47	0.25
octanoic acid	OAC	0.18	0.09
hexanal	HEX	0.38	0.25
cinnamaldehyde	CIN	0.51	0.28
3-phenyl propanal	3-PP	0.35	0.12

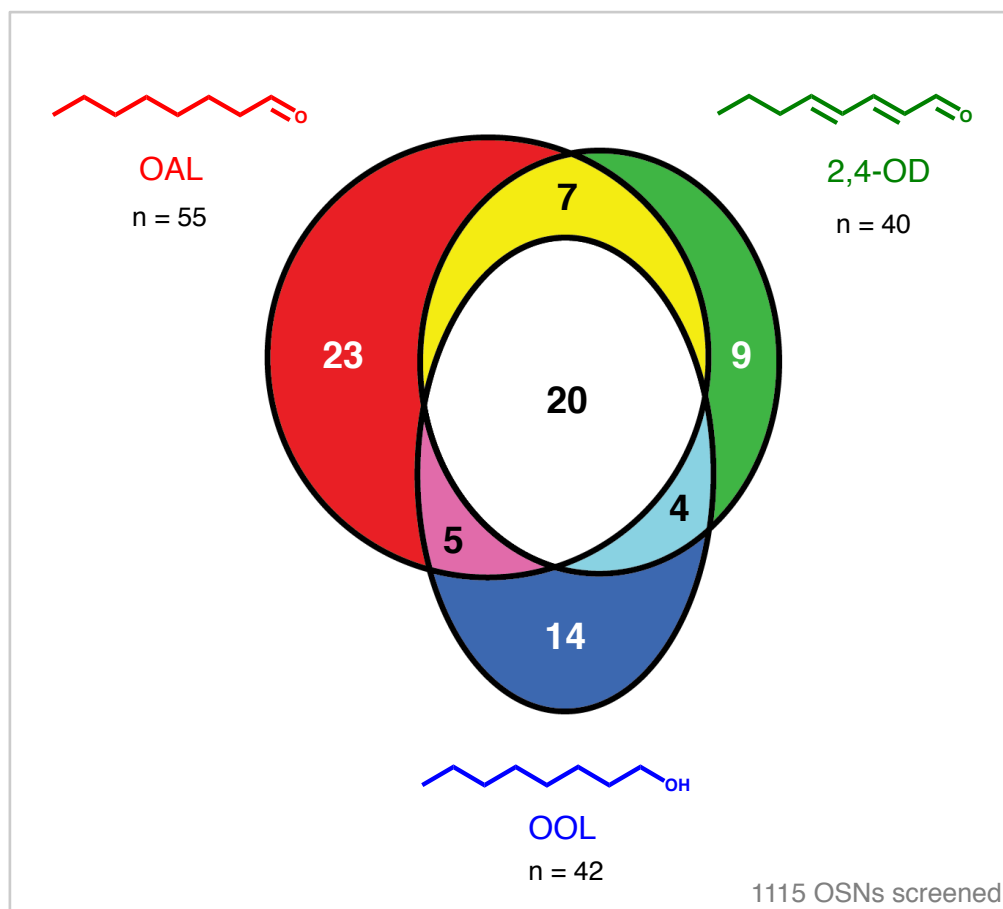
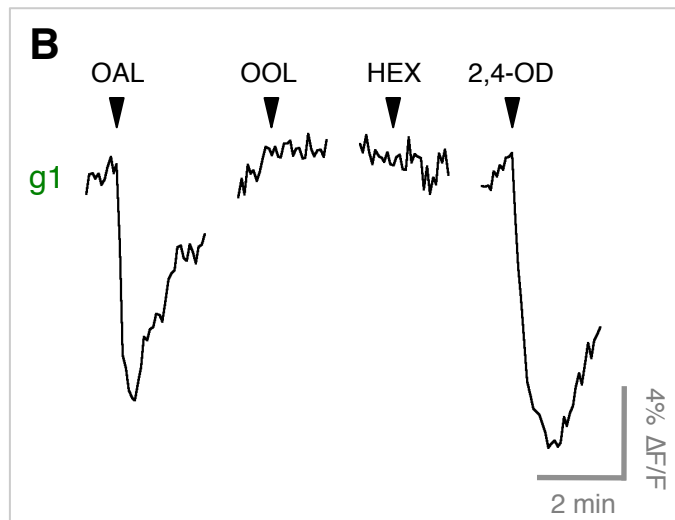
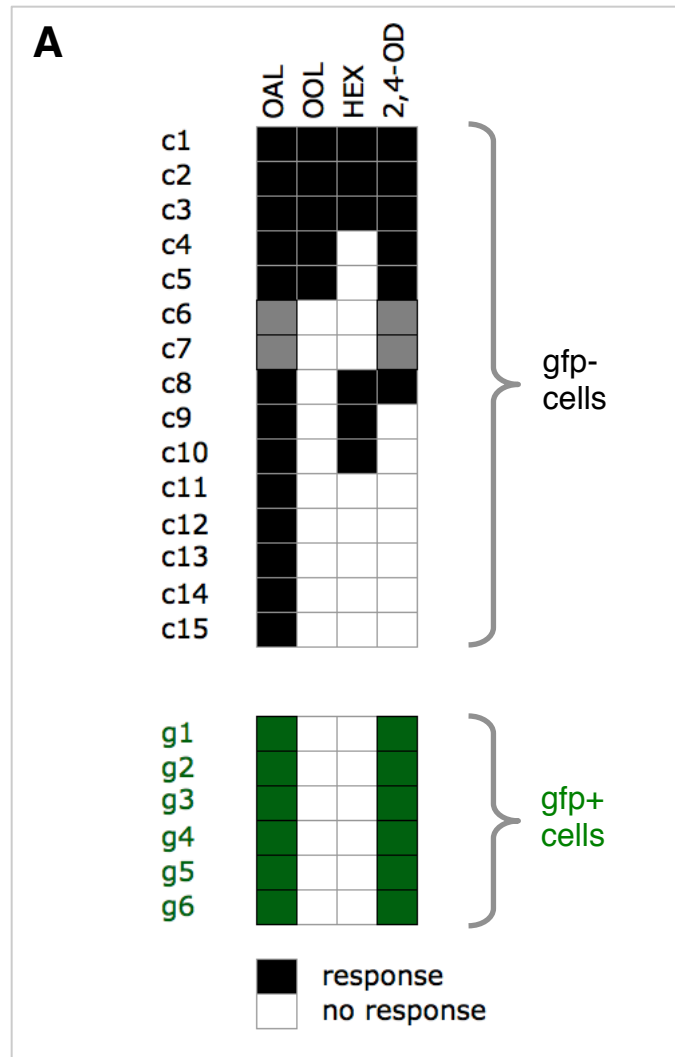
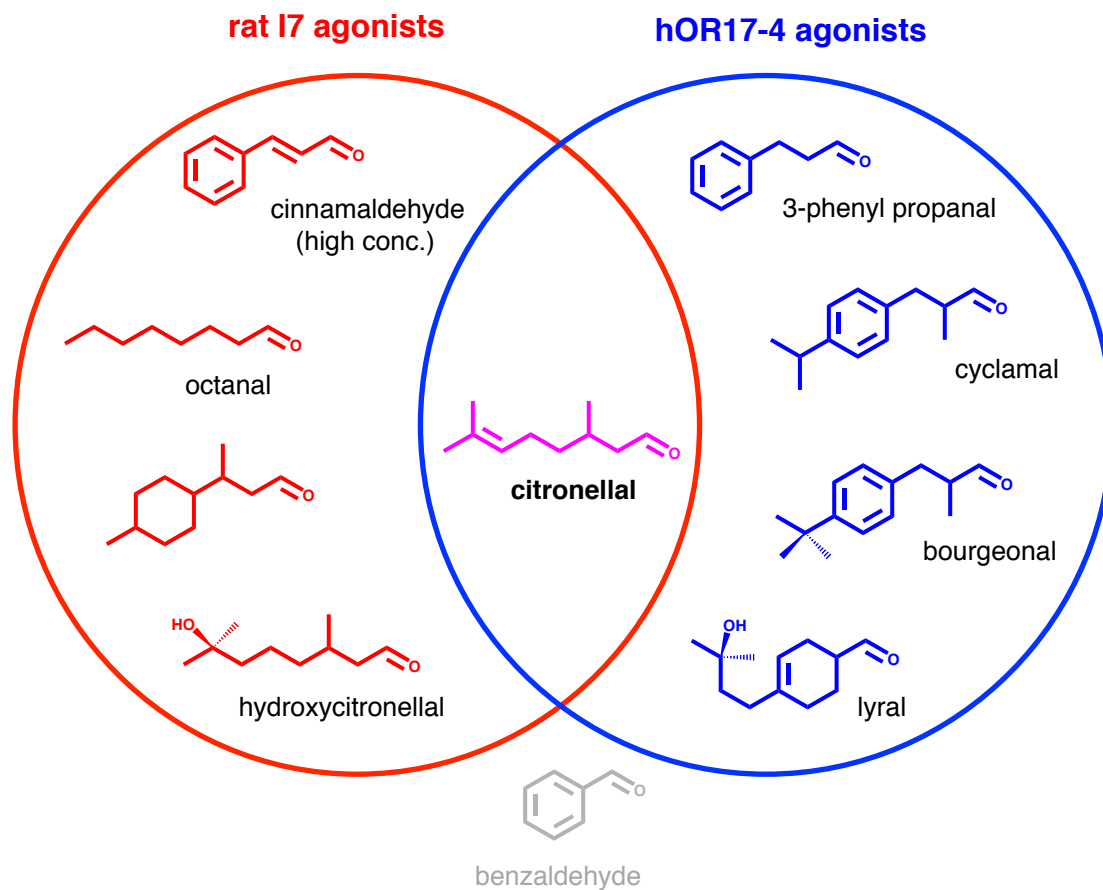


Figure 2.9 - visualization of overlap patterns. Venn diagram showing the number of OSNs from Figure 2.8 that responded with each activation pattern. OOL activates nearly half of the OAL+ population, thus leaving half of the OAL+ population OOL- (red plus yellow sectors). This is a substantial portion of the entire OAL+ code. 2,4-OD also activates nearly half of the OAL+ population, but because of high levels of co-recognition between OOL and 2,4-OD only a small portion of cells are able to discriminate between 2,4-OD and OOL while still recognizing OAL. As a result, the I7-like mini-fingerprint of OAL+/2,4-OD+/OOL- (yellow sector) is rare.

Figure 2.10 - response patterns in the retrovirally-induced I7 system. (A) Response profiles to the mini-fingerprint odor set among GFP+ OSNs (green shading) and GFP- but OAL+ OSNs (black shading) that were present within the same field of view as GFP+ OSNs. While only a few of the GFP-/OAL+ OSNs display the truncated I7-like fingerprint (cells c6 and c7, grey shading), every GFP+/OAL+ OSN displayed the expected profile. (B) Representative trace from a GFP+ cell.





Supplemental Figure 2.1 - partial receptive fields for rat I7 and hOR17-4

demonstrate near mutual exclusivity. Although rat I7 and hOR17-4 are both activated by citronellal and fail to be activated by benzaldehyde, they lack concordance for any other ligand that has currently been tested on both receptors. (hOR17-4 data from Triller et al. (2008), rat I7 data from Zhao et al (1998), Araneda et al. (2000), Araneda et al. (2004) and unpublished observations.) Using the panel presented in Figure 2.8, the functional profile expected for hOR17-4 would match to only one observed rat OSN profile (pro_51).

CHAPTER 3**DUAL MODES OF ALDEHYDE RECOGNITION BY ODORANT RECEPTORS**

ABSTRACT

In aqueous environments such as the mucus, aldehydes exist in equilibrium between a carbonyl and its hydrate, a geminal-diol form (referred to hereafter as simply “diol”). Although only a small amount of diol is typically present, certain odorant receptors (ORs) may exploit the greater hydrogen-bonding capacity offered by its dual hydroxyls. To probe whether this alternate binding mode is used, we stabilized this normally transient and non-isolatable state by adding two electronegative fluorines on carbon C2 of octanal (8AL). The induced partial positive charge on the C1 carbon of the carbonyl promotes nucleophilic attack by water, thus shifting the chemical equilibrium to “trap” the odorant in the diol state. Using calcium imaging of rat olfactory sensory neurons (OSNs), we find that a surprisingly high percentage of 8AL+ ORs are capable of being activated by the fluorinated diol. This includes the well-studied 8AL+ OR, rat I7. 47% of 8AL+ ORs could bind the diol with 16% of these absolutely requiring the second hydroxyl group for activation. The necessity of the diol was demonstrated by their failure to respond to otherwise matched but singly hydroxylated 2,2-difluorooctanol. 24% of 8AL+ ORs reject the diol, indicating that they require the carbonyl form of an aldehyde for activation. Thus, there are at least two intrinsically distinct modes for aldehyde recognition available to ORs. Surprisingly, only those ORs that strictly employ the diol-mode for aldehyde binding were able to discriminate between aldehyde and alcohol functional groups, thus providing a unique signature within the combinatorial code.

INTRODUCTION

Aldehyde-containing odorants are important components of human olfactory perceptual space, constituting over 10% of the entries in the Flavornet database (Acree, T. and Arn, H. www.flavornet.org). In aqueous environments, aldehydes exist in equilibrium with their hydrate, a geminal-diol (Figure 3.1A). The diol is the rarer form. Hexanal, with a hydration equilibrium constant of 0.41 (Buschmann 1980) exists ~30% in the diol form at pH 7.4; the longer octanal would be predicted to form less. Human nasal mucus is slightly acidic, however, (Washington, Steele et al. 2000), and this may promote conversion to the diol. A specialized microenvironment has been shown to stabilize the diol (Rawashdeh, Thangavel et al. 2008), and it is plausible that OR binding pockets might impart a similar niche to allow odorants to assume states more readily than they are normally present in bulk solution. With its two hydroxyl groups, the diol offers more hydrogen-bonding opportunities to stabilize the odorant within the OR.

Is this benefit exploited by ORs, or is aldehyde-sensing relegated to only the carbonyl form that is more prevalent in the bulk solution? It is important to understand if there are indeed alternate means of aldehyde recognition because many of the currently modeled ORs are docked with aldehyde ligands. These include I7 with octanal (Singer 2000; Hall, Floriano et al. 2004; Lai, Singer et al. 2005; Khafizov, Anselmi et al. 2007; Kurland, Newcomer et al. 2010), Olfr43, OR1A1, and OR1A2 with citronellal (Schmiedeberg, Shirokova et al. 2007; Stary, Suwattanasophon et al. 2007), hOR 17-4 with linal and bourgeonal (Doszczak, Kraft et al. 2007), and OR5 with lylal (Afshar, Hubbard et al. 1998).

ORs comprise an exceedingly large gene family, with nearly 1300 intact ORs in the rat genome (Zhang and Firestein 2007). With this size and diversity comes pronounced technical challenges. While heterologous expression systems for ORs continue to improve, so far only 52 of the ~1200 mouse ORs have been assessed in parallel in the most comprehensive screen to date (Saito, Chi et al. 2009). Furthermore, the identity of the G-protein that couples to the OR can dramatically alter activity (Shirokova, Schmiedeberg et al. 2005), leading to different response profiles obtained in a heterologous system (Baud, Etter et al. 2011) versus those recorded directly from native OSNs (Oka, Katada et al. 2006).

Thus, the most reliable and thorough way to survey the full OR repertoire remains calcium-imaging of OSNs. Harvesting the olfactory epithelium tissue from all regions of the nasal cavity eliminates any bias due to the zonal nature of OR expression (Miyamichi, Serizawa et al. 2005). Activation of the olfactory transduction cascade leads to a depolarization-driven somatic calcium influx that can be readily visualized using fluorescent calcium-indicators. Each OSN expresses only a single type of OR (Chess, Simon et al. 1994), and so the cellular response can be taken as a proxy for receptor activation. Thus, optical monitoring of the dispersed tissue permits high-throughput screening while retaining single cell, and thereby single receptor, resolution.

Utilizing this technique, we first identified the suite of OSNs activated by 8AL. The eight carbon length is preferred by rat OSNs (Kaluza and Breer 2000; Araneda, Peterlin et al. 2004). The flexibility of the alkyl backbone allows adoption of a variety of conformations (Peterlin, Li et al. 2008), perhaps contributing to 8AL's effectiveness as a recruiter. Having a large starting pool of n-aldehyde activated OSNs is useful because it

enables us to extract major trends that shape the combinatorial code, and it provides an opportunity to observe potentially rare chemical discrimination patterns.

In our approach, we challenged 8AL+ OSNs with a panel of compounds to assess their ability to accept a diol and to gauge their preference for either the carbonyl or diol form of the aldehyde. The diol form of 8AL cannot be isolated as a distinct species, so two electron-withdrawing fluorine groups were added to carbon C2, adjacent to the carbonyl. The local partial positive charge they induce on the carbonyl carbon makes it more prone to attack by water. This manipulation shifts the hydration equilibrium so dramatically in favor of the diol that 2,2-difluorooctanal (DIF), despite its name, exists almost exclusively in the diol form (Figure 3.1B).

Mere response to DIF thus indicates the capacity of an OR to accept a diol. To determine if the diol was required, we used the mono-hydroxylated 2,2-difluorooctanol (DIFOH). Except for the second hydroxyl, DIFOH is otherwise matched to DIF in terms of sterics and polar topography at C2. Thus, a DIF+/DIFOH- signature demonstrates an absolute requirement for the diol mode of aldehyde binding.

We used two approaches to identify when an aldehyde was recognized strictly in the carbonyl form. 2,2-dimethyl octanal (DIM) provides the ideal probe. As a typical non-halogenated aldehyde, it exists in both carbonyl and diol forms. The equilibrium for DIM is skewed even slightly more to the carbonyl form than is the unsubstituted 8AL because the methyl groups are electron donating. The dimethyls occupy a greater steric volume than the difluorines, so activation by DIM would indicate a physical capacity to dock DIF (provided the polar topology at carbon C2 of DIF did not interfere). A

DIM+/DIF- would suggest that aldehyde binding was occurring through use of a carbonyl.

However, steric occlusion by even just one methyl proximal to the polar functional group of a ligand is detrimental at some ORs, such as MOR-EG (Kajiya, Inaki et al. 2001; Katada, Hirokawa et al. 2005) and hOR17-4 (Spehr, Gisselmann et al. 2003). We were concerned that the even larger dimethyl might prove too great a burden for many ORs. If DIM proved a poor recruiter, it would limit its usefulness as a probe for DIF binding potentiality. We thus used DIFOH as an auxiliary steric probe. OSN activation by DIFOH proves that the difluorines at C2 can be accommodated. A DIFOH+/DIF- signature demonstrates that the second hydroxyl is specifically excluded, implying that the normal 8AL activation is through the carbonyl mode. The presence of unsubstituted 8OH allowed us to assess how the polar topology change and slightly increased sterics at carbon C2 in DIFOH affected a scaffold less dramatically perturbed by the difluorines.

RESULTS

We recorded from 1053 viable rat OSNs, all of which responded to 10uM forskolin. Forskolin directly activates adenylate cyclase, a downstream signal transduction cascade component; OSNs which respond are thus functionally viable and could generate a response if they were provided with an adequate ligand. With ~1300 intact rat ORs predicted (Zhang and Firestein 2007), the number of viable cells we sampled covers a substantial portion of the OR repertoire.

87 OSNs (8.2%) were activated by 30uM 8AL. This is slightly higher than what we have observed in previous studies, perhaps reflecting improvements in our signal to noise ratio. All compounds were applied at equimolar concentrations. The relative size of the responses of the probe odorants was normalized to 8AL by nesting them between 8AL flanks within a continuous movie.

Proximal alkyl substitution is highly disfavored across the 8AL+ population

As had been our concern, the steric load of the two methyls proximal to the polar functional group in DIM severely attenuated activity across the 8AL+ population. Nearly 70% of the 8AL+ cells (61/87) failed to be activated by DIM. Among the 26 OSNs for which DIM did suffice, only 7 OSNs responded as well to DIM as to plain 8AL. The remainder showed diminished response magnitudes. Even though the dimethyl manipulation should only minimally alter the chemical nature of the aldehyde group (slightly destabilizing the carbocation state and mildly disfavoring diol formation), this subtle difference might still be detected by OSNs. Among the 17 OSNs that were subsequently classified as diol-requisite, 15 (88%) failed to respond to DIM. This is higher than the overall attrition rate.

The smaller difluoro moiety was better tolerated on the alcohol scaffold even though it also altered local polar topography along with sterics. Still, DIFOH induced 20% attrition of the 8OH code. Unlike DIM, which uniformly diminished the response of those OSNs capable of detecting it, DIFOH+ OSNs showed a more even distribution in terms of preference for occluded versus un-occluded versions of the alcohol.

Fluorination was favored in 15 DIFOH+ OSNs and disfavored in 9 DIFOH+ OSNs.

Only cell c41 showed substantial activation by DIFOH while lacking activation by 8OH.

The ability of a large number of alcohol-responsive ORs to maintain a substantial response in the face of the difluoro substitution lets DIFOH serve as a comparative probe during aldehyde mode usage assessment.

Using DIM, DIF, and DIFOH we interpreted the preferred activation mode of 8AL+ OSNs. The octanal-normalized activation profiles are presented in Figure 3.2. Strikingly, nearly 50% of 8AL+ OSNs (45/87) were activated by DIF, demonstrating a widespread ability to accommodate the more bulky diol.

A diol-mode requisite 8AL+ subpopulation

For 18% of the total 8AL+ population, the diol-mode of aldehyde recognition was either strictly required or highly preferred. Cells c27-c37 were robustly activated by DIF to equivalent or greater magnitudes as 8AL. Yet they failed to respond to the mono-hydroxylated but otherwise matched DIFOH. The contribution of the second hydroxyl, available only in the diol, is thus critical for activation. The response trace for the diol-requiring cell c27 is shown in Figure 3.3A. Cells c38-c40 responded to the mono-alcohol DIFOH, but only marginally. Their level of activation by DIFOH was ~13% that by DIF. While they could technically stabilize a ligand containing one hydroxyl, these cells need the diol for robust activation. We suggest that at these cells 8AL is preferentially recognized in its diol form. Cell c41 was included as a member of this subpopulation,

even though it could be well activated by DIFOH, because the diol DIF elicited a three-times greater magnitude response.

Cells c25-c26 provide further support that the second hydroxyl present in the diol can help stabilize a ligand. These cells responded to 8OH but lacked a response to DIFOH, revealing that the proximal fluorination was detrimental. Yet DIF overcame the challenge of the difluoro manipulation, presumably due assistive interactions via the second hydroxyl. Because these ORs can competently respond to the unsubstituted 8OH, we cannot unambiguously assign their preferred binding-mode for aldehydes. However, we hypothesize that if presented with structurally complex aldehydes, where the alkyl scaffold is less readily adaptable than the promiscuous n-alkyl chain of 8AL, these ORs might require the subsidiary stabilization afforded only by the diol form.

A carbonyl-mode requisite 8AL+ subpopulation

38% of 8AL+ ORs highly disfavored the diol, and thus we deduce that aldehydes assume the carbonyl form to activate them. OSNs in subclass c65-c74 respond to DIM. Recall that DIM, like 8AL, exists in equilibrium between the carbonyl and diol forms. Cells c65-c68 were activated by the more bulky DIM yet completely failed to respond to the smaller substituted DIF. Note that all these cells could respond to DIFOH, demonstrating that they could handle the polar topology imparted by the C2 fluorines. Thus, it seems that rejection of DIF is based on its being a diol, and these cells are thus carbonyl-mode requisite. The trace for the carbonyl-requiring cell c65 is shown in Figure 3.3B.

Another signature of the strongly carbonyl-preferring cells c69-c74 was their “reversal” in response strength between DIF and DIM. ORs tend to respond smoothly when stimuli vary in a graded manner. For example, ORs activated by hexanal and octanal, rarely ever fail to respond to heptanal. Thus, the weaker response to the smaller DIF is an anomaly from a purely steric standpoint. Tellingly, among these cells the fluorinated DIFOH exhibited at most a modest decrease in activity relative to 8OH; the drop-off between fluorinated DIF versus 8AL was far more dramatic. Both lines of evidence support that it is the diol as opposed to fluorination which is disfavored. Thus, carbonyl-recognition of aldehydes predominates at these ORs.

Using DIFOH as probe, we suggest that two subclasses of DIM- OSNs also prefer the carbonyl form of aldehydes. For cells c42-c57, the difluoro substitution either had a minimal detrimental effect (c42-c46) or was actually a favored epitope (c47-c57). Yet all these OSNs failed to respond to DIF. Even when the difluoro epitope is present it is outweighed by an absolute intolerance for the second hydroxyl. Thus, these OSNs likely recognize only the carbonyl form of the aldehyde.

Cells c58-c63 treated the difluoro substitution equivalently or favorably when carried on the alcohol scaffold. Although these OSNs could be weakly activated by DIF, the reduction in strength between 8AL and DIF was far greater than that observed between 8OH and DIFOH. If 8AL was naturally being recognized in the diol form, such that the only difference between the two compounds was the steric or polar topology impact of the difluorine substitution, the degree of drop-off should have been better matched. Our tentative interpretation is that these cells prefer the carbonyl over the diol form, but they can still flexibly accommodate both.

Population-specific response broadening of DIF suggests beneficial diol pre-formation

DIF occasionally generated responses that decayed more slowly than 8AL (Figure 3.4A). This effect only occurred at OSNs that utilized the diol-mode of aldehyde recognition; OSNs that were diol-accommodating, but not diol-requisite, never showed this broadening (Figure 3.4B). Response broadening has been observed at the I7 receptor when stimuli are presented at concentrations well above the threshold saturating concentration level (Araneda, Peterlin et al. 2004). In our screen, all compounds were given at equimolar concentrations (30 μ M). The observation that broadening occurred only among diol-requisite OSNs suggested that DIF, which pre-formed the diol, was serving as a more potent ligand than 8AL. This phenomenon is analogous to how pre-organizing the alkyl backbone of a flexible odorant into a preferred conformation can increase its potency at select receptors (Peterlin, Li et al. 2008).

Only diol-mode requisite OSNs can selectively discriminate aldehydes

Unexpectedly, we found that among the OSNs to which we could assign an aldehyde usage mode, only the diol-requisite cells could discriminate between 8AL and 8OH. Conversely, nearly all cells that discriminated between 8AL and 8OH (and which were amenable to our probes) utilized the diol-mode of aldehyde recognition. Only cell c64 achieved discrimination between these functional groups while recognizing the aldehyde in its carbonyl form.

Rat I7 is an OR that utilizes diols for both activation and antagonism

Given that I7 is an 8AL+ OR renowned for its selectivity for aldehydes over other functional groups (Zhao, Ivic et al. 1998; Araneda, Kini et al. 2000; Bozza, Feinstein et al. 2002; Peterlin, Li et al. 2008), we asked whether I7 utilizes the diol-mode for aldehyde recognition. Using adenoviral infection to express GFP along with I7 in OSNs, we confirmed that DIF could indeed activate I7 (Figure 3.5). Failure of I7 to respond to DIFOH, even at concentrations up to 300uM, confirmed I7 as an OR that primarily employs the diol-mode for activation by aldehydes. However, I7 was different from most ORs in our panel in that it was very sensitive to proximal steric occlusion and/or the polar presence of the C2 fluorines. Even pre-organization of DIF into the diol could not fully overcome the impact of the added difluorines (EC_{50} DIF 11 +/- 4uM ; EC_{50} 8AL 1.8 +/- 0.2uM). Increasing the steric bulk to the dimethyl severely reduced activity, such that at the solubility limit of 1mM, DIM could activate I7 only to 50% of its maximum capacity.

For diol-requiring ORs, the second hydroxyl is clearly necessary to achieve activation. But is it also needed simply to allow the ligand to reside in the binding pocket? If this tethering can be achieved by a single hydroxyl, the inactive alcohol might serve as an antagonist. On the other hand, if mere ligand stabilization requires contributions from both hydroxyls, the alcohol would be completely filtered out. An antagonist screen of this nature cannot be carried out in a population survey were the cells in a field possess different sensitivities to 8AL. I7 allowed us to address this question at a defined receptor whose sensitivity to 8AL is well established.

We examined the impact of co-application of high concentrations (100uM) of DIFOH and 8OH on a just saturating level of 8AL (10uM) at I7. While 8OH is inactive at 30uM (Araneda, Peterlin et al. 2004; Chesler, Zou et al. 2007), it proved marginally active at 100uM (0.26 +/- 0.09 of the response to 10uM 8AL) (Figure 3.6). The shorter six-carbon alcohol hexanol, neither activates nor antagonizes I7 when tested at 100uM (Peterlin, Li et al. 2008). The optimal eight-carbon alkyl tail in 8OH might thus partially compensate for what is effectively only half of the preferred diol form. Despite 8OH's weak binding of I7, neither 8OH nor DIFOH could maintain an adequate presence at the receptor to counteract a saturating concentration of 8AL (Figure 3.7). Co-application of 8AL with 100uM 8OH was 92 +/- 5% the response to 10uM 8AL alone, and the combination of 8AL with DIFOH was 94 +/- 3%. This reduction in response magnitude is not below the 90% preservation of plain 8AL response level that we take to be a reliable signature of true antagonism. I7 thus appears to require that all its robust ligands, be they agonists or antagonists depending on their alkyl composition (Araneda, Kini et al. 2000; Araneda, Peterlin et al. 2004; Peterlin, Li et al. 2008), provide a diol for stabilization.

DISCUSSION

The olfactory code is combinatorial with a given odorant activating multiple receptors and multiple odorants activating a given receptor (Malnic, Hirono et al. 1999). From the earliest surveys of the OR repertoire, a high degree of co-recognition of homologous aliphatic compounds possessing different functional groups has been

observed. This effect has been well documented for n-alcohols, n-aldehydes, and n-acids (Sato, Hirono et al. 1994; Malnic, Hirono et al. 1999; Ma and Shepherd 2000; Araneda, Peterlin et al. 2004). Yet populations of OSNs exist that can discriminate between functional groups, perhaps serving as important contributors to the distinctive perceptual signatures of each odorant. For example, 8AL and 8OH are both characterized by a waxy, green, and orange-citrus body. However, 8AL is harsh and “peely” while 8OH has floral and sweetly-fatty notes (www.thegoodscentcompany.com).

However, the mechanism by which any OR achieves functional group selectivity has not yet been described. Noting that aldehydes (and to a much lesser extent, ketones) have the exclusive ability to form a diol in solution, we examined whether any ORs are capable of exploiting this feature, particularly as a means of selectively recognizing this class of compounds.

Diols cannot be isolated, but manipulating the local electronic environment can shift the natural equilibrium to trap the aldehyde in that state. We challenged a large population of diverse OSNs with the difluorinated aldehyde DIF, which is forced to exist almost entirely in the diol form. Surprisingly, nearly half of all 8AL+ OSNs were activated by the diol. For 21% the diol form was the exclusive or highly preferred means of recognizing the aldehyde. In contrast, 38% of the 8AL+ OSNs could be classed as exclusively or strongly preferring the carbonyl form. Thus, two distinct modes exist for activation of ORs by aldehydes.

Requiring a diol for activation appears to be the primary means of conferring the ability to discriminate between aldehydes and alcohols. 15/17 of the diol-preferring 8AL+ OSNs failed to respond to equimolar concentrations of 8OH whereas only 1/33 of

the strongly carbonyl-preferring OSNs made that distinction. The ability of aldehyde-selective ORs to filter out alcohols thus appears to occur through titration of the number of hydroxyl groups required to stabilize the ligand in the binding pocket. The inability of 8OH or DIFOH to outcompete 8AL in an antagonism assay at the rat I7 receptor further supports this hypothesis.

As our probe, we used a compound where the aldehyde was attached to the terminus of a plain aliphatic scaffold. This strategy enabled us to recruit the broadest possible subset of ORs. However, our findings should be applicable to more complex aldehyde-containing odorants. We expect this to readily extend to cases where the aldehyde is well separated from other epitopes by an alkyl linker region. But the diol mode of aldehyde recognition still remains feasible for conjugated aldehydes, despite their altered electronics. The values of the hydration equilibrium constant in the bulk solution are comparable between n-hexanal (0.41 (Buschmann 1980)) and the electron-rich trans, trans-2,4-hexadienal (0.40 (Ferreira, Hernandez-Ortega et al. 2010)). Benzaldehyde is also hydrated (0.1; (Ferreira, Hernandez-Ortega et al. 2010)).

Nearly 50% of the 8AL+ OSNs in our screen responded to the diol, demonstrating that they accept bifurcation of a ligand at carbon C1. This raises the intriguing possibility that some of these OSNs may have a large proximal cavity or prefer branching near their polar anchor. Some of these OSNs may accept secondary alcohols such as 2-nonanol, and possible also ketones such as 2-nonanone though in this latter case geometries would differ. Both ligands, however, introduce a hydrophobic terminus into an expected diol slot. Another potential ligand whose recognition frequency may be biased among the diol-accepting subgroup of ORs are the n-acids. The acid would place two polar moieties

in a branched arrangement, albeit a planar one as opposed to pyramidal. Understanding the relationship between diol acceptance, requirement, and intolerance relative to the response to acids will allow a fuller characterization of the chemical rationale behind the “electronegativity spectrum” between alcohols, aldehydes, and acids (Araneda, Peterlin et al. 2004).

METHODS

Isolation of Olfactory Sensory Neurons

All animal procedures were approved by the Columbia University Institutional Animal Care and Use Committee and performed in compliance with relevant national guidelines and regulations. Procedures for isolating OSNs and the infection of male Sprague Dawley rats with an adenovirus encoding OR-I7 and GFP as separate proteins were performed as described previously (Peterlin, Li et al. 2008). For the OR-I7 experiments, infected tissue was micro-dissected to enrich the number of GFP-labeled OSNs. For the primary panel survey, the entire olfactory epithelium from uninfected rats was used.

Calcium Imaging of Olfactory Sensory Neurons

Calcium imaging recordings were performed as previously described (Araneda, Peterlin et al. 2004). Briefly, cells adhered on glass coverslips were loaded with the fura-2AM calcium indicator, prepared by dissolving in rat ringer (138mM NaCl, 5mM KCl, .5nMMgCl₂, 10mM HEPES, and 10mM glucose; pH 7.4) supplemented with pluronic acid. Loading took place for 45 minutes in the dark at room temperature. The coverslip was then placed into a recording chamber where it was constantly perfused with rat ringer at a rate of 1 mL/min. At designated times, 400uL of an odorant solution was injected into the continuous perfusion stream. The odorant concentrations reported are those as prepared in the stimulus syringes. Neat odorants were stored at 4 degrees under argon until use. Y. Li synthesized DIF, DIFOH, and DIM specifically for this study. Other odorants were purchased from Sigma-Aldrich. 8AL was purchased from Sigma-Aldrich, but re-distilled by Y. Li before use. After warming to room temperature, stock solutions of odorants in DMSO (0.5M) were prepared. These were subsequently diluted to the final concentration in ringer. Ringer with a matched concentration of DMSO alone was also applied as a stimulus, and those rare cells that responded to vehicle alone were excluded from further analysis.

Fura-2AM loaded cells were imaged at 380nm excitation and 510nm emission. NIH Image software and custom macros were used to drive data acquisition and provide initial analysis. Due to the slow nature of recovery of the somatic calcium transients, images were acquired only every 4s to minimize bleaching. Each image represents the average of three frames. Data are shown as the fractional change in fluorescent light

intensity, $(F-F_0)/F_0$ where F is the intensity at any each time point and F_0 is the value of the emitted light at the start of the movie prior to any stimulus application. The magnitude of the response was measured from baseline to peak deflection. To account for baseline drift, the stimulus series was flanked by 8AL applications. When three applications of the same odorant are given, the magnitude of the middle application is reliably >90% that predicted by the normalization trend-line drawn connecting the maximal deflections of the two flanking applications. This method allows us to accurately assess the relative response levels of the various analogs compared to the 8AL stimulus. At the end of each experiment, the adenylate cyclase activator forskolin (10uM) was given to strongly stimulate the transduction cascade downstream of the OR and validate the viability of the OSN.

ACKNOWLEDGEMENTS

Y. Li in the laboratory of K. Ryan synthesized and validated the fluorinated and dimethylated compounds. K. Ryan underscored the possible role for differential hydration modes during several useful discussions. Both contributors are affiliated with the City College of New York.

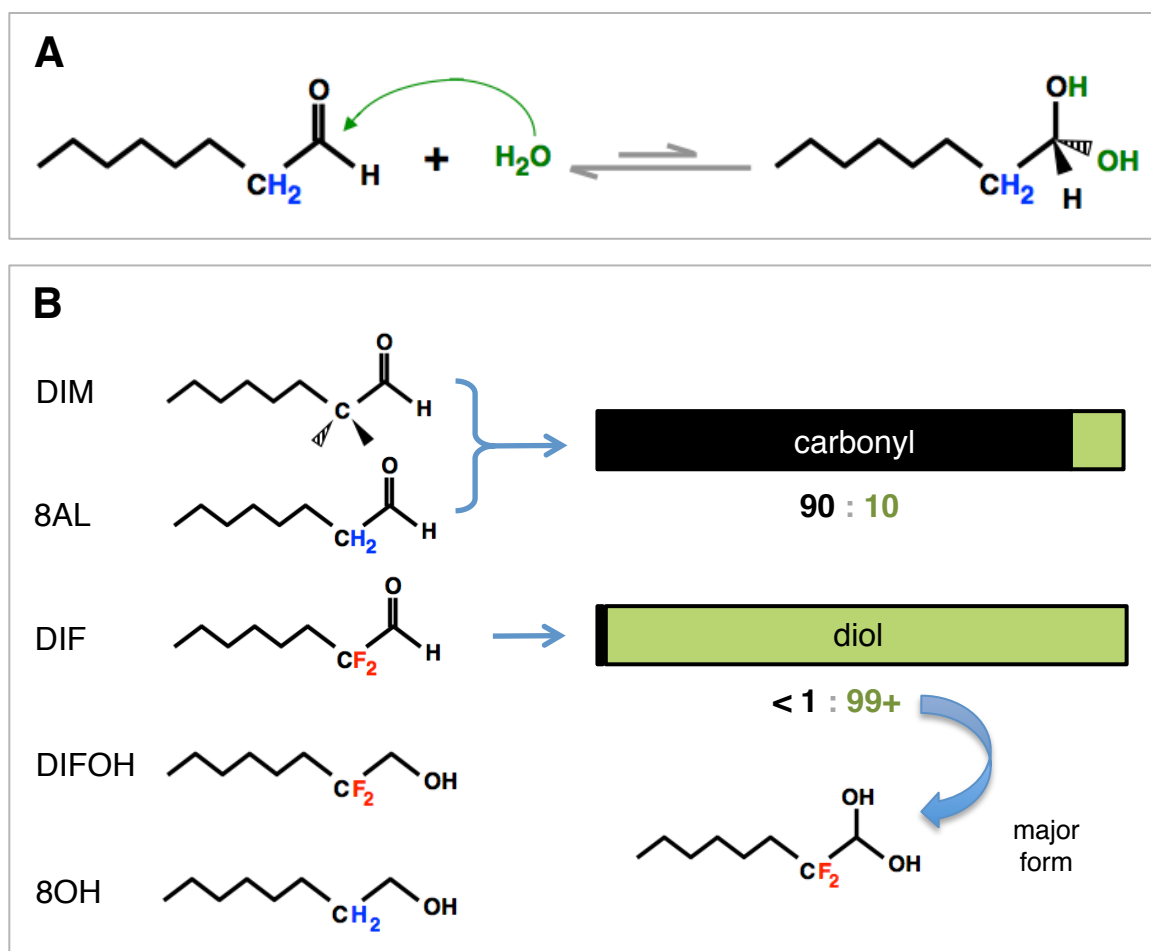


Figure 3.1 - schematic of how proximal fluorination of aldehydes shifts the hydration equilibrium. (A) Nucleophilic attack by water on a regular aldehyde leads to formation of a geminal-diol, but the diol readily converts back to the carbonyl form. (B) Dimethyl appended (DIM) and regular n-octanal (8AL) reside primarily in the carbonyl form in the bulk state (large black bar). The electron-withdrawing nature of the difluorination in DIF increases susceptibility to attack by water, leading to effectively all the compound residing in the diol state (green bar). Structures of the mono-hydroxylated odorants used as controls are shown below.

Figure 3.2 - panel screen for the mode of octanal binding. 87 octanal-responsive cells were detected out of 1053 viable OSNs screened. In the panel, each row corresponds to a different OSN. The columns list the odorants assayed, all at 30uM. Shaded boxes denote a response to an odorant; white boxes denote that an odorant was tested, but it did not elicit a response. “na” denotes when responses to the tested compound were so small given that cell’s baseline fluctuation that they could not be assigned. Responses to the test odorants are normalized within each cell to the response elicited by octanal. The heatmap scale extends above one because octanal need not be the optimally tuned ligand for any given OR. Dots at left mark cells which exhibited response broadening to the fluorinated version of octanal versus the normal form. See text for interpretation of the various grouped response classes.

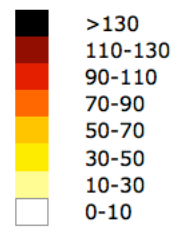
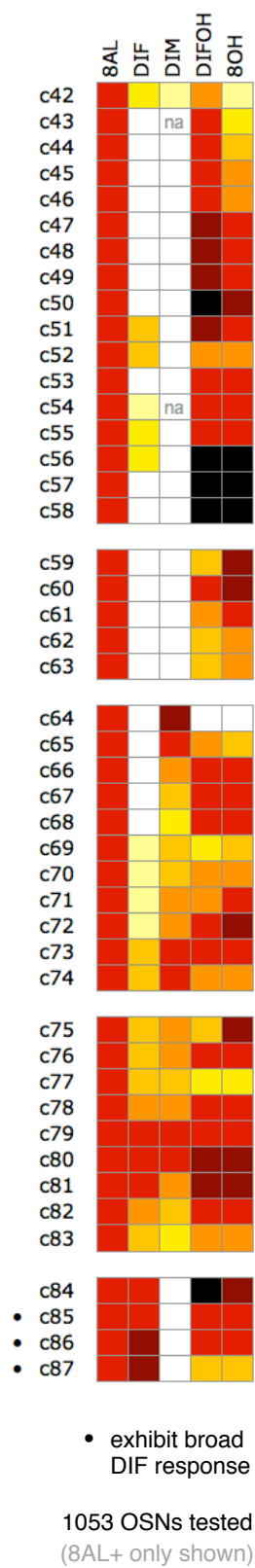
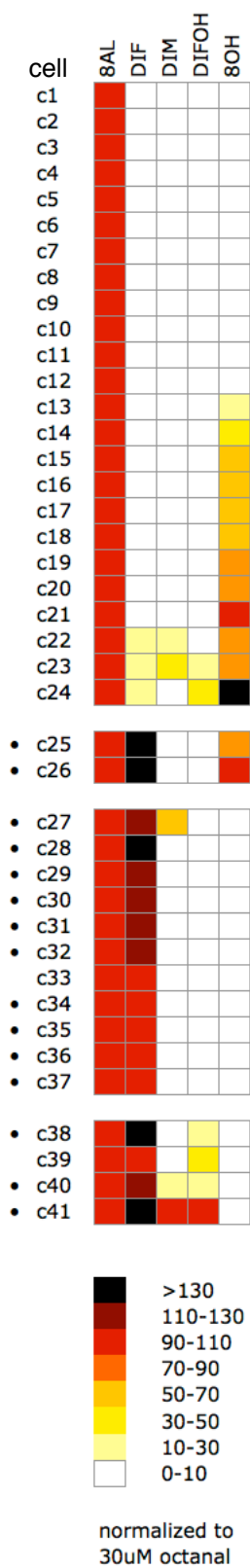


Figure 3.3 - octanal-responsive OSNs can selectively recognize either form of the aldehyde. All compounds were compared at 30uM. The dashed line drawn between the peaks of the responses to the flanking octanal applications is used to assess the relative response strength for the nested compounds and to correct for any baseline deflections.

(A) Cell 27 responds robustly to the diol DIF but fails to respond to DIFOH. This marks an absolute requirement for two hydroxyls for activation. This cell's response to 8AL and DIM must occur through the naturally produced diol formed from these aldehydes.

(B) Cell 65 is quite capable of accommodating steric bulk at carbon 2, as underscored by its response to DIM. The fluorinated alcohol DIFOH is also a robust agonist, even better than the bare 8OH. But adding another hydroxyl to DIFOH to create DIF completely abolishes the activity. This indicates that 8AL and DIM cannot be recognized as the diol, but instead must be recognized in their carbonyl form.

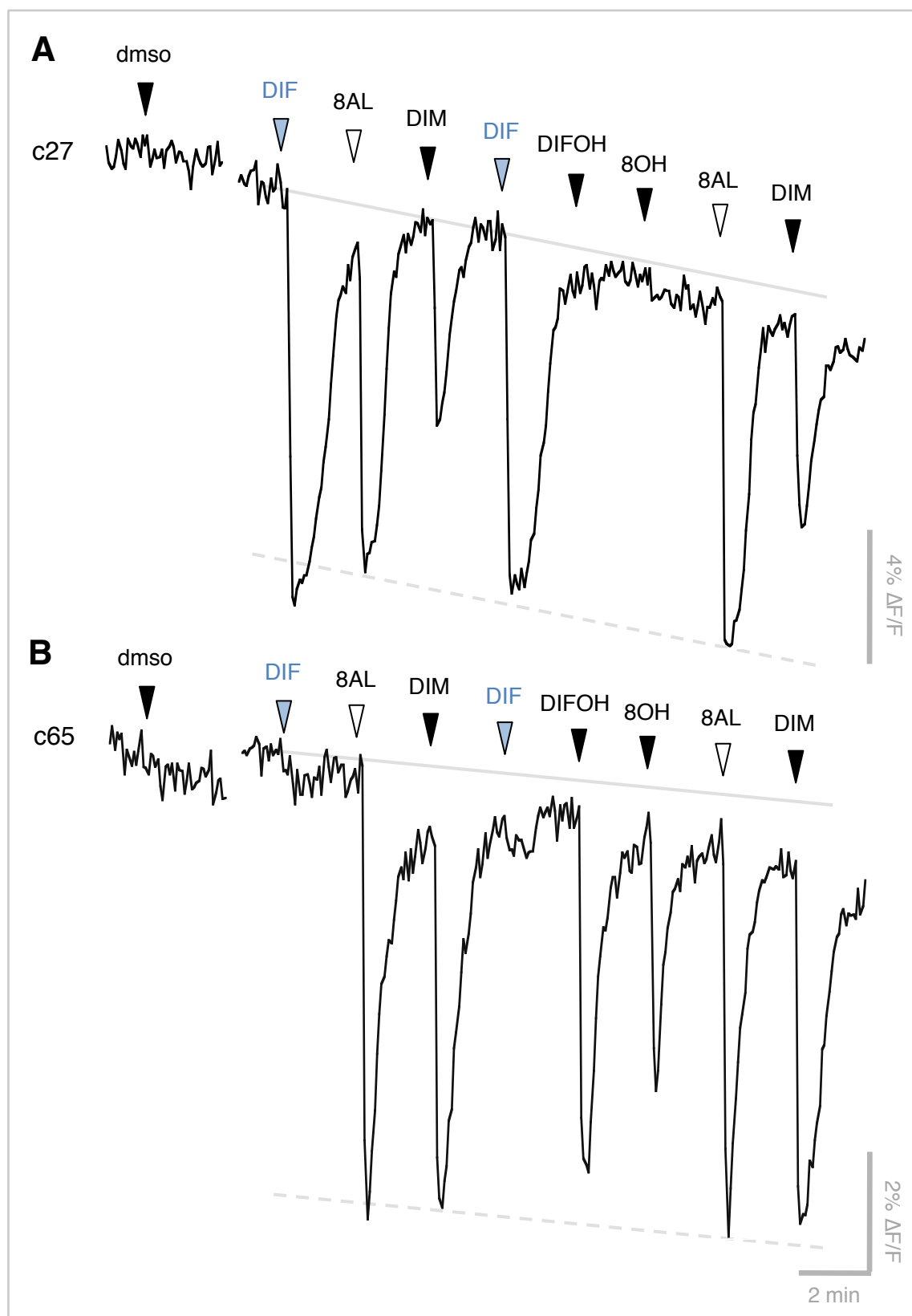
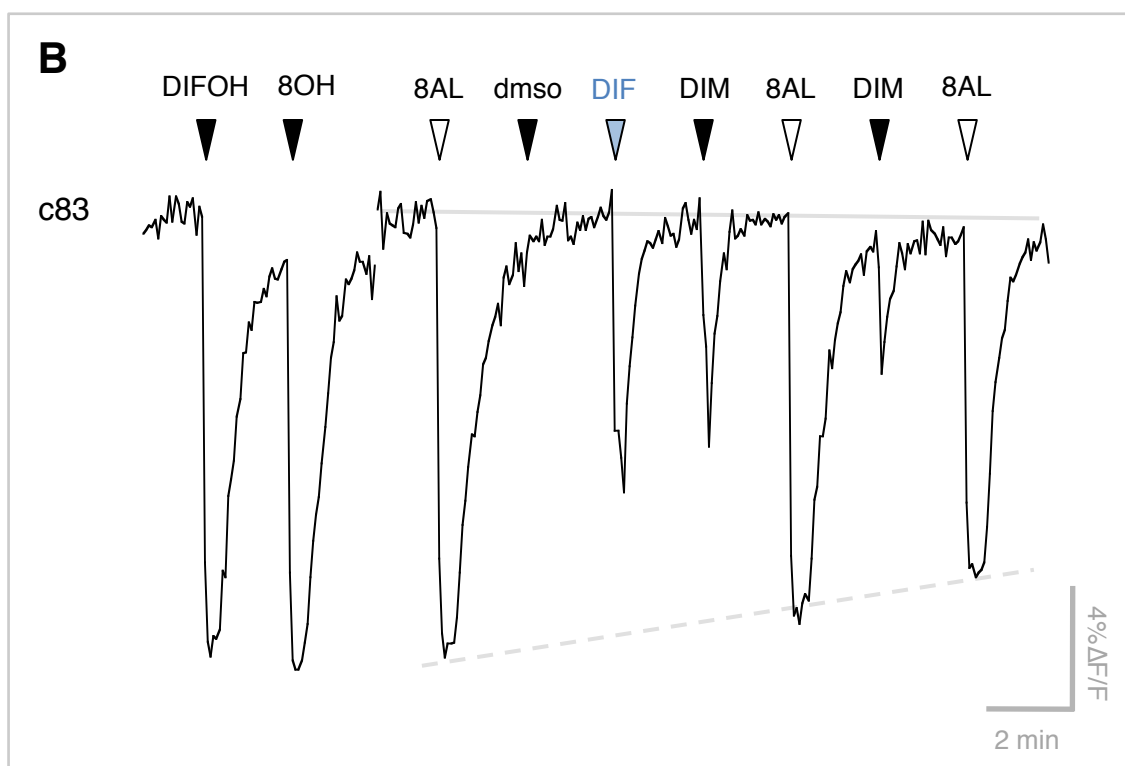
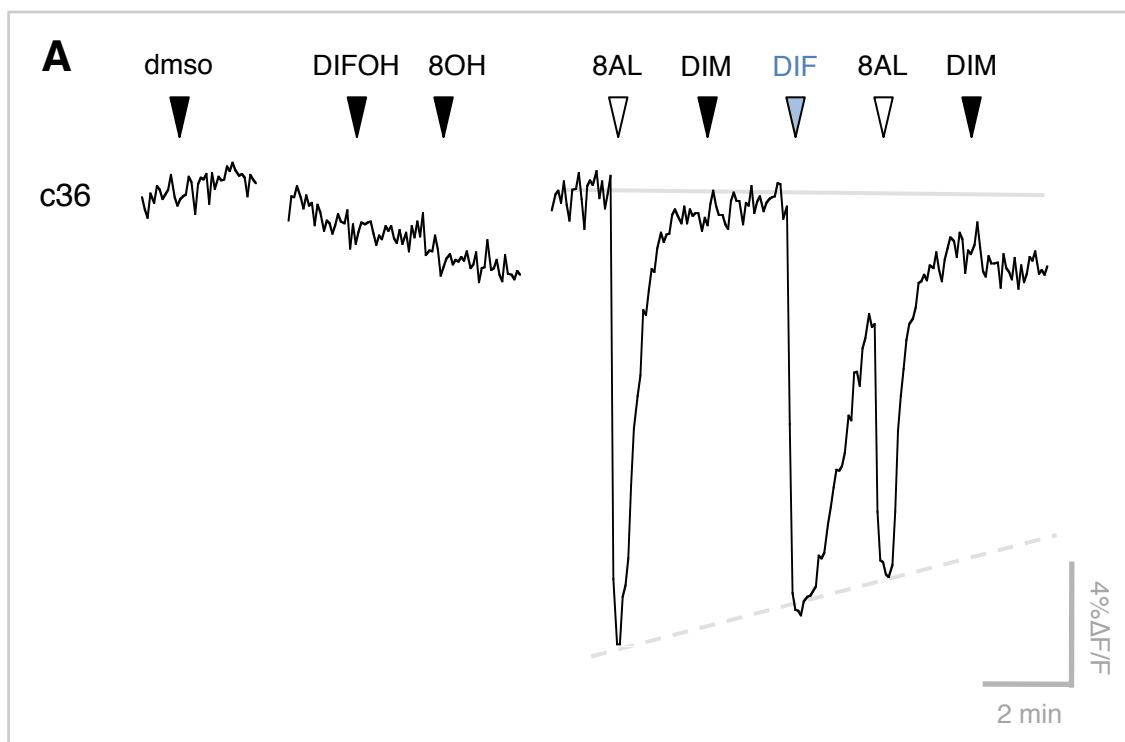


Figure 3.4 - response broadening displayed by DIF appears only among diol-mode requisite OSNs. (A) Among diol-requisite OSNs with a DIF+/DIFOH- signature, the response to DIF sometimes displayed response broadening. This behavior resembles the effect seen of applying an odorant well above a receptor's saturating level. However, in our experiment, all compounds were applied at equimolar concentrations for the same duration. We suggest that for the cells exhibiting the response broadening, the diol of DIF represents a pre-formed preferred state, leading to higher potency. (B) The broadening of the DIF response was not seen among OSNs that did not strictly require the diol for activation. For example, cell 83 was robustly activated by the mono-hydroxylated DIFOH and the response to DIF in this cell is narrow.



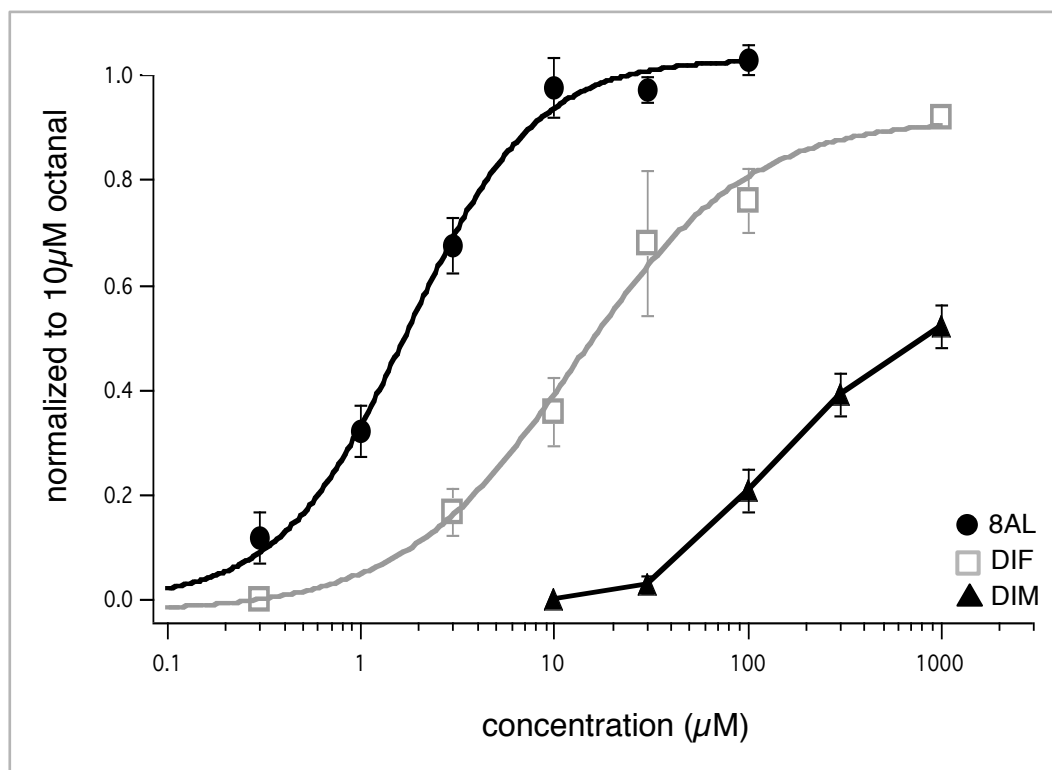


Figure 3.5 - rat I7 primarily uses the diol form for activation: Dose response curves for rat I7-expressing OSNs for the three aldehydes tested in this study. Responses were normalized to 10uM octanal and fit by the Hill equation. (closed circle, 8AL ; $EC_{50} = 1.8 \pm 0.2 \mu M$) ; (open square, DIF ; $EC_{50} = 11 \pm 4 \mu M$) ; (closed triangle, DIM ; $\sim EC_{50}$ is the saturation limit, $1000 \mu M$). Although I7 has a DIF+/DIFOH- signature and is thus classed as diol-requisite, it is especially sensitive to difluorine perturbation at C2 that outweighs any benefit of diol pre-organization. This penalty was also observed in the comparison between DIFOH and 8OH where the fluorination has less impact on polar group identity (see Figure 3.6). The pronounced diminishment of the DIM response shows that I7 has great sensitivity to proximal steric bulk, even when there are no alterations in polar topology nor any double bonding in this region.

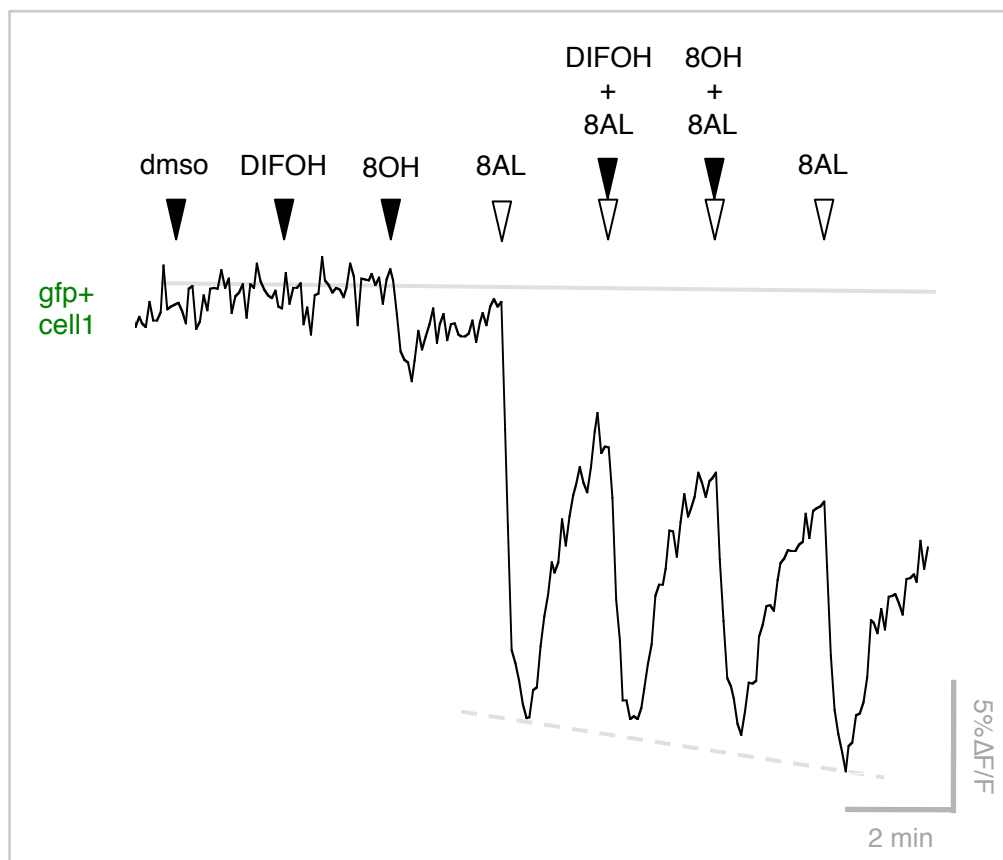


Figure 3.6 - I7 antagonists must be able to assume a diol form. Previously, we have shown that among varied functional groups appended to a six-carbon tail only aldehydes could antagonize I7 (Peterlin et al, 2008). Even when there is an optimal-length eight carbon unconstrained alkyl tail, it appears that the diol form, which can be only be provided by an aldehyde, is necessary for a compound to serve as an effective antagonist. Small responses to 8OH were observed at high concentrations (100uM), but this was eliminated upon fluorination. The marginal binding by 8OH was insufficient to significantly reduce the magnitude of co-applied 8AL (10uM) (residual response 0.92 ± 0.02 ; $n=4$). DIFOH at 100uM was also ineffective as an antagonist (0.94 ± 0.01 ; $n=7$). Because the response of the combination was not reduced to below 90% of the response to 8AL alone, neither 8OH nor DIFOH meet our criteria as a reliable antagonist of I7.

(this page intentionally left blank)

CHAPTER 4

THE IMPORTANCE OF ODORANT CONFORMATION TO THE BINDING AND ACTIVATION OF A REPRESENTATIVE ODORANT RECEPTOR

this chapter has previously been published as

“The importance of odorant conformation to the binding and activation of a representative olfactory receptor.” Peterlin Z*, Li Y*, Sun G, Shah R, Firestein S, Ryan K. Chem Biol. 2008 DEc 22;15(12):1317-27. PMID 19101476

* co-author contributions: ZAP performed all physiological experiments and analyses
YL synthesized and validated the novel cyclic compounds

ABSTRACT

Odorant receptors (ORs) form a large family of G protein-coupled receptor proteins responsible for sensing the ambient chemical environment. The molecular recognition strategies used by ORs to detect and distinguish odorant molecules are unclear. Here, we investigated the variable of odorant carbon chain conformation for an established odorant-OR pair: n-octanal and rat OR-I7. A series of conformationally restricted octanal mimics were tested on live olfactory sensory neurons (OSNs). Our results support a model in which unactivated OR-I7 binds aliphatic aldehydes indiscriminately, and then applies conformational and length filters to distinguish agonists from antagonists. Specific conformers are proposed to activate OR-I7 by steric buttressing of an OR activation pocket. Probing endogenously expressed rat OSNs with octanal and constrained mimics furnished evidence that odorant conformation contributes to an odorant's unique olfactory code signature.

INTRODUCTION

The sense of smell begins with molecular recognition of a chemical odorant by one or more odorant receptors (ORs) expressed in the olfactory sensory neurons (OSNs) of the nasal epithelium (Firestein 2001; Touhara 2002; Reed 2004). The ORs are members of the G protein-coupled receptor (GPCR) family of membrane-bound proteins (Buck and Axel 1991). OR activation by an odorant agonist initiates the transduction of

chemical structure information into a neural activity code that ultimately gives rise to the perception of an odor. An odorant may also bind an OR without triggering signal transduction, contributing to the olfactory code by competitively antagonizing a receptor's activation by other odorant agonists present in a mixture (Araneda, Kini et al. 2000; Araneda, Peterlin et al. 2004; Oka, Omura et al. 2004). The rodent and human genomes encode over 1000 ORs (Malnic, Godfrey et al. 2004; Zhang and Firestein 2007), though in humans many of these are pseudogenes (Niimura and Nei 2007). The combinatorial use of the set of ORs enables an individual to detect and distinguish far more airborne chemicals than there are individual ORs (Malnic, Hirono et al. 1999; Oka, Omura et al. 2004).

Olfactory GPCRs have had to evolve to recognize small molecules that disperse into the air. Hence, odorants are typically low molecular weight and uncharged. Many odorants are hydrocarbons or very hydrophobic molecules containing a single heteroatom, most often oxygen. Many olfactory GPCRs must consequently bind odorants without the benefit of multiple polar interactions common to other small molecule-protein associations such as enzyme-substrate associations, or those pertaining to the aminergic GPCRs (Shi and Javitch 2002). Like rhodopsin and other class A GPCR family members, ORs are predicted to have seven transmembrane (TM) α helices and to bind their ligands in a site bounded by TMs 3, 5, 6, and possibly 4 and 7 (Pilpel and Lancet 1999; Singer 2000; Hall, Floriano et al. 2004; Katada, Hirokawa et al. 2005; Abaffy, Malhotra et al. 2007). ORs exhibit a high degree of sequence variability within these helices as expected for a family of proteins that binds diverse ligands. In the hypervariable TM regions where contact with odorants is predicted to occur, there is a

strong bias toward hydrophobic aliphatic and aromatic residues, a weaker bias toward polar uncharged residues, and a bias against charged residues (Pilpel and Lancet 1999). Difficulties obtaining atomic level structural information on transmembrane proteins have prevented a detailed understanding of the strategies used by olfactory GPCRs to discriminate their odorant ligands.

It has long been known that a single OSN can be activated by a range of related odorants (Sicard and Holley 1984; Firestein, Picco et al. 1993; Sato, Hirono et al. 1994; Ma and Shepherd 2000). Evidence continues to accrue in support of the idea that each OSN expresses only one of its ~1000 genomic ORs (Chess, Simon et al. 1994; Malnic, Hirono et al. 1999; Serizawa, Miyamichi et al. 2004). It follows that each OR must be able to recognize multiple odorants. This has been demonstrated experimentally, though the structural relatedness of the activating odorants varies from receptor to receptor (Raming, Krieger et al. 1993; Krautwurst, Yau et al. 1998; Zhao, Ivic et al. 1998; Malnic, Hirono et al. 1999; Araneda, Kini et al. 2000; Kaluza and Breer 2000; Touhara 2001). Perhaps to ensure coverage while surveying as much of chemical space (Dobson 2004) as possible, the receptive ranges of ORs overlap, with a single odorant typically activating multiple ORs. Different odorants, even those that are structurally related, appear to activate unique subsets of ORs, ultimately giving rise to a unique olfactory experience and forming the basis of the olfactory code (Malnic, Hirono et al. 1999).

To understand the olfactory code at the chemical level will require a precise understanding of the chemical determinants responsible for activating and blocking each OR. Several studies have cited molecular “length” as one such determinant (Malnic, Hirono et al. 1999; Mori, Nagao et al. 1999; Araneda, Kini et al. 2000; Kaluza and Breer

2000; Ho, Johnson et al. 2006). Length studies have focused mainly on odorants containing aliphatic carbon chains (Malnic, Hirono et al. 1999; Araneda, Kini et al. 2000; Kaluza and Breer 2000; Ho, Johnson et al. 2006). These studies used homologous series of conformationally flexible n-alkyl acids, aldehydes, ketones, and alcohols. However, the conformational flexibility of such odorants leaves unclear the true molecular length required for activation because aliphatic odorants exist in large ensembles of conformational isomers. This uncertainty also raises the question whether ORs bind odorants in preferred conformations—such as an extended conformation, as implied in the previous studies—but disfavor the same odorants when presented in other conformations. Moreover, GPCR binding and GPCR activation may have different conformational requirements. To address the variable of odorant conformation as a factor in the molecular receptive range of a representative OR, we have assayed a series of conformationally restricted analogs of octanal, the primary agonist for the rat I7 olfactory receptor (OR-I7). Testing these compounds has provided insight into the activation and blocking of the OR-I7 receptor, and has demonstrated how conformational flexibility influences the total number of ORs activated by a single odorant.

RESULTS

The rat OR-I7 receptor is one of the few ORs to have been cloned, expressed in neurons, and functionally characterized by probing with a large collection of odorants (Zhao, Ivic et al. 1998; Araneda, Kini et al. 2000; Araneda, Peterlin et al. 2004). OR-I7 is activated by multiple aliphatic aldehydes having a length between ~ 8 Å and ~ 12 Å

(Araneda, Kini et al. 2000). We note that multiple conformations are possible for aliphatic aldehydes. We therefore define length here to mean the length of the longest attainable (and typically lowest energy) conformation (see Experimental Procedures). The most potent OR-I7 ligand found thus far is octanal, referred to hereafter as **C8** (for 8 carbon n-alkanal; likewise for **C7**, **C6**, etc.). Like many ORs, OR-I7 is activated by odorants with successive carbon chain lengths centered on the most potent ligand (Malnic, Hirono et al. 1999; Kaluza and Breer 2000). In the rat nasal epithelium, **C8** activates more cells and elicits a greater cAMP (the signal transduction second messenger) response than do shorter and longer homologs (Kaluza and Breer 2000), indicating that the dimensions of the OR-I7 binding site are likely close to average. OR-I7 is thus typical and well characterized, ideal for a systematic investigation of the effect of odorant conformation on its receptive range.

A series of conformationally restricted eight-carbon aldehydes

C8 is highly flexible, having six rotatable bonds that can each adopt three different conformations: one anti, or one of two gauche. The maximum number of formally possible conformational isomers is $3^6 = 729$, though symmetry makes some equivalent and undoubtedly reduces this number. Nothing is known about the bound conformation of **C8**. On the one hand, were **C8** to bind and activate OR-I7 in one or a small subset of favored conformers, it would incur a conformational entropy penalty in the free energy of binding due to the loss of conformational flexibility. In this case, preorganizing **C8** to resemble the bound conformation should improve binding by

minimizing the loss of entropy. On the other hand, a previous study compared the calculated lowest energy conformation of a group of activating ligands and concluded that OR-I7 may tolerate a number of structural variations at the carbons most distant from the aldehyde (Araneda, Kini et al. 2000), possibly indicating that many different **C8** conformers are capable of activating OR-I7. To gain insight into the activating conformation(s) of **C8**, we made a series of eight-carbon aldehydes with restricted conformations (Figure 4.1A). Conceptually, carbon 8 (denoted as C₈) of **C8** was tied back by establishing a new bond successively to C₇ through C₂, yielding compounds **1–6**, respectively. Unlike the previously studied series of homologous n-alkanals, in which the partition coefficient and other physical properties vary with the number of carbons in the chain, we expect to maintain throughout our eight-carbon series similar physical-chemical properties while reducing the number of possible conformations. This strategy should enable us to study effects that occur at the level of the OR binding pocket while minimizing receptor-independent effects. In this series the maximum length of the aldehydes is also progressively shortened. Due to the conformational restriction, the maximum length is now a better estimation of this dimension compared with the n-alkanal series. The synthesis of these analogs was straightforward and is summarized in Figure 4.1B.

OR-I7 activation: octanal uses a semi-extended conformation

The eight-carbon aldehydes were tested via calcium imaging of dissociated rat neurons (Araneda, Peterlin et al. 2004). As an example, the activation of OR-I7 by analog

3 is shown in Figure 4.2A. Responses were concentration dependent and saturating. At high concentrations, the magnitude of the response to analogs **1**, **2**, and **3** saturated with efficacies comparable to that of **C8**; no partial agonists were detected. Analog **4**, **5**, and **6** failed to reach saturation over this concentration range. Activation curves for the entire series, including **C8**, are shown in Figure 4.2B, which also tabulates the concentrations at which half-maximal activation is reached (EC_{50}). The compounds segregate into two groups. Compounds **1**, **2**, and **3**, which have smaller rings and four to six freely rotatable bonds, all strongly activated OR-I7, whereas compounds **4**, **5**, and **6**, which contain larger rings and one to three rotatable bonds, activated OR-I7 weakly or not at all. The greatest difference in activity, 163-fold, was observed between compound **4** (6.3 Å, $EC_{50} = 748$ μM) and compound **3** (7.0 Å, $EC_{50} = 4.6$ μM). The n-alkanals of 5–12 carbons (**C5–C12**) were previously tested against OR-I7 in the vapor phase using electroolfactogram (EOG) recordings (Araneda et al., 2000; Zhao et al., 1998). By that method, the largest difference in activity in the series fell similarly between **C6**, (no activation, 6.4 Å) and **C7** (activation, 7.6 Å). Thus, using the new series of **C8** analogs, we confirmed that there is a minimum length requirement for activation, and further narrow it down from 6.4–7.6 Å to 6.5–6.9 Å. We interpret the finding that an aldehyde of only 7.0 Å is sufficient to activate the receptor, compared with the extended length of **C8** (8.9 Å), to mean that **C8** does not activate OR-I7 in its fully extended conformation, but rather adopts one or more semi-extended conformations to do so. The poor activity in the eight-carbon aldehydes **4–6**, where the variables of total carbon number and length are separated, defines the shorter end of the activating length cutoff, and provides evidence that **C8** does not activate OR-I7 while in compact conformations approximating those mimicked by **4–6**.

Small cycloalkyl rings enhance OR-I7 activation

To test whether maximum length is solely responsible for the difference in activity observed among compounds **1–6**, we obtained the full activation curves for **C7** and **C6** by calcium imaging (Figure 4.3). Although **C7** and compound **2** have identical extended lengths, **2** was 40-fold more potent (Figure 4.3A). Compound **2** was even more potent than **C8**.

Similar to previous OR-I7 EOG recordings (Araneda, Kini et al. 2000), calcium imaging revealed a sharp increase in activity (145-fold) in the step from **C6** to **C7** (Figure 4.3B). The maximum length of compound **3**, which contains the cyclobutyl group, falls between those of **C7** and **C6** (Figure 4.3C). Based on a correlation with maximum length, the activity of **3** should also fall between that of **C7** and **C6**. However, **3** was more potent than both (Figure 4.3B), providing a second example where a small cycloalkyl ring increased potency beyond what was expected based on length alone. Thus, though the activity of the cyclic compounds generally required a certain minimum length, restricting the rotation of the terminal two or three bonds enhanced potency, indicating that specific conformations or shapes at the end opposite the aldehyde are preferred by the activating form of OR-I7.

An activating octanal conformation

We next explored conformational restriction of **C8** toward the middle of the chain. In examining the data shown in Figure 4.2B, we noted that all of the active

compounds had a rotatable bond between C₄ and C₅, whereas in all inactive compounds this bond was locked in a ring (Figure 4.2A, inset). Although this observation might merely reflect the variable of length, in another study the same bond in *trans*-2-*cis*-6-nonadienal, an OR-17 activating compound, was implicated as a potential pivot point important for activation (Araneda, Kini et al. 2000). In the extended conformation, all of **C8**'s C-C bonds adopt the anti conformation (Figure 4.4A, left). Rotation of the C₄-C₅ bond by 120° into a gauche conformation (Figure 4.4A, middle) reduces the total length of **C8** from 8.9 Å to 8.0 Å, provided the other bonds remain in the anti conformation. Changes of this nature could serve to reduce the actual length of the molecule into the type of semiextended conformation proposed herein. To test the effect of this particular alteration, we installed a two-carbon bridge from C₃ of **C8** to C₆ (Figure 4.4A, right). The resulting six-member ring locked **C8** into a gauche conformation around C₄-C₅. Imagining this process beginning with a rotation of the same bond in the opposite sense produces the same structure, due to symmetry. Compared with the 729 hypothetical conformations that **C8** can sample, the resulting **C8** analog, **11**, can exist in only ~10 closely related conformers. **11** was synthesized as a ~2.4:1 mix of the *trans*:*cis* isomers, as outlined in Figure 4B and described in Experimental Procedures.

Unable to separate these two isomers, we tested **11** as a mixture. In the case where one isomer is inactive—or perhaps even an antagonist—testing the mixture incurs the risk of underestimating the true response of the other isomer. Despite this concern and the introduction of a six-member ring into the middle of **C8**, the isomeric mixture of **11** was more active than **C8**, shifting the activation curve slightly to the left (Figure 4.4C). Just as **C8** is two carbons longer than the much less potent **C6**, compound **11** is two carbons

longer than the nearly inactive **5**, and the gain in activity might appear to correlate merely with the increase in extended conformation length (the *cis* isomer of **11** is ~ 7.4 Å and the *trans* is ~ 8.0 Å). However, in contrast to **C8**, the two terminal carbons of **11** are fixed by the ring in their relation to the aldehyde group, though in slightly different locations in the two isomers. If we assume that the orientation of the aldehyde group with OR-I7 is fixed in the odorant binding site, then the three-dimensional coordinates of the ethyl group of **11** must likewise be fixed and occupy a distal (to the aldehyde) activating region in the receptor. **11** may therefore resemble an, or the, activating conformation of **C8**, just as **4**, **5**, and **6** are constrained to resemble inactive conformations.

Conformational determinants of OR-I7 antagonism

In nature, odorants are typically encountered in mixtures. In this context, each odorant can activate one set of receptors while simultaneously antagonizing a subset of receptors activated by other components, leading to great complexity in the olfactory code at the level of sensory input (Malnic, Hirono et al. 1999; Araneda, Kini et al. 2000; Araneda, Peterlin et al. 2004; Oka, Omura et al. 2004). Most OR antagonists discovered to date are structurally related to the agonists whose activity they suppress (Araneda, Kini et al. 2000; Araneda, Peterlin et al. 2004; Oka, Omura et al. 2004). Interestingly, natural product fragrances typically contain structurally related odorants (Arctander, 1960) suggesting a potential evolutionary significance.

We thus set out to systematically probe the length and conformation requirements for antagonism of OR-I7 by simultaneously applying a saturating concentration of **C8** (10

μM) and increasing concentrations of either the inactive **C8** analogs **5** and **6** or the similarly inactive **C4** and **C5**. The marginally active **C6** and **4** were also used. Unexpectedly, nearly all were capable of antagonizing **C8** activation, suggesting a broad antagonist receptive field with regard to the hydrophobic portion of short aldehydes. A representative calcium imaging trace is shown in Figure 4.5A. Here, analog **6**, which itself cannot activate OR-I7, is shown to antagonize **C8** activity. Inhibition curves for **4**, **5**, **6**, **C4**, **C5**, and **C6** are shown in Figure 4.5B with the concentration of each required for 50% inhibition (IC_{50}) tabulated in Figure 4.5C. Among the n-aldehydes, antagonist potency increased with the number of carbons in the chain. The failure of **C4** (3.9 Å) to antagonize **C8** activation may indicate a minimum n-aldehyde chain length requirement for antagonism between 4.0 Å and 5.1 Å, but we cannot rule out receptor-independent effects, such as reduced hydrophobicity and increased water solubility due to the small size. Among the cycloalkyl ring-containing aldehydes, where the constant number of carbons should control for receptor-independent effects, all were moderate antagonists but without apparent length dependence (Figure 4.5C). In fact, the IC_{50} s for the cyclic compounds were remarkably similar and each was a more potent antagonist than its closest length-matched n-alkanal. This result may indicate a dependence of antagonism on odorant surface area or carbon number in combination with a maximum length below 6.5–6.9 Å. Taken together with the activation data, aldehydes that resemble **C8** in a compact conformation appear to be able to bind OR-I7 in its unactivated state, blocking subsequent activation by **C8**, whereas those that can extend beyond 6.5–6.9 Å appear able to bind and stabilize OR-I7 in its activated state. Held close to the aldehyde, the large cycloalkyl groups appeared to enhance antagonism, just as the small cycloalkyl

rings, held distant, enhanced activation. Overall, these results provide an example where a structural trait, namely maximum attainable length, is correlated in a systematic way with the transition from antagonism to agonism.

Functional group determinants of OR-I7 antagonism

The strict requirement of an aldehyde group for activation of OR-I7 is well established (Araneda, Kini et al. 2000). The results described herein prompted us to ask whether antagonism also requires the aldehyde group. As shown in Figure 4.5D, replacement of the aldehyde function in **C6** with a variety of other functional groups resulted in loss of antagonism. In combination with the activation data, this result means that the aldehyde group is necessary but not sufficient for binding to OR-I7. The attributes of the carbon chain complete the requirements for binding and determine whether binding leads to activation or antagonism.

Conformational flexibility contributes to the activation range of an odorant

OR-I7 is not the only **C8** receptor in the rat genome; **C8** is estimated to activate between 33 and 55 of the ~1300 predicted (Gibbs, Weinstock et al. 2004; Zhang and Firestein 2007) functional rat ORs (Araneda, Peterlin et al. 2004). It has long been suspected that highly flexible odorants activate more ORs than do less flexible odorants (Amoore 1970; Kaluza and Breer 2000). However, this possibility has previously only been examined using a series of odorants that vary in carbon number and thus in multiple

physical properties (Kaluza and Breer 2000). Our series of conformationally restricted **C8** analogs provided the opportunity to examine this question in a controlled manner, using **C8** as a representative odorant.

We assayed 1190 viable rat OSNs with 30 μ M **C8** and (individually) analogs **1–6**. The cells were also probed with forskolin, an activator of the signal transduction cascade that bypasses the OR to provide an internal standard for normalization of the OSN response to each odorant. Figure 4.6A represents the entire population of cells that responded to at least one compound, showing how each cell discriminated among the eight-carbon aldehydes. The activation traces of three representative cells are shown in Figure 4.6B. Overall, 5.9% of OSNs (70/1190) were activated to some extent by **C8**, in close agreement with the earlier study (Araneda, Peterlin et al. 2004). **C8** and the less constrained (more rotatable bonds) analogs **1**, **2**, and **3** activated approximately twice as many cells as did the most constrained analogs, **5** and **6** (Figure 4.6C, filled circles; 5.6%, 6.2%, and 6.2% versus 3.4% and 3.6%, respectively). These data support the idea that, in general, the greater the flexibility of an odorant, the greater the number of ORs it will activate, even when the odorant's functional groups and number of carbons are held constant.

With the exception of one cell (Figure 4.6A, cell 53), all **C8**-sensitive cells also responded to at least one of the cyclic analogs, consistent with the idea that our analogs sample subregions of the conformational space occupied by the ensemble of **C8** conformers detected by OSNs. None of the cells activated by **C8** responded equally to all analogs, which we interpret as evidence that conformational preference is a general underlying feature among **C8**-responding ORs, and not unique to OR-I7. Of the 70 cells

that responded to **C8**, 39 (56%) responded more strongly to a cyclic analog than to **C8**. This high percentage was unexpected because **C8** is the only natural product in the series. One explanation is that for these OSNs, the most strongly activating cyclic analog is preorganized into a region of **C8**'s conformational space that binds and stabilizes the activating form of the single ORs expressed in these cells, so that less conformational entropy is lost upon activation. The overall free energy of binding should become more favorable and lead to greater potency versus **C8**. For each OSN that preferred a cyclic analog to **C8**, we calculated the difference in the normalized response magnitudes between its best-tuned analog (i.e., the most highly activating analog) for the OSN and that of **C8** (Figure 6D). Organizing the data in this way revealed a clear trend in which the difference in activation grew as the analogs became more conformationally restricted (fewer rotatable bonds). The more conformationally restricted compounds **5** and **6** may be viewed as frozen in conformations that mimic relatively high-energy, rarely populated conformations of **C8**. The difference in strength of activation shown in Figure 4.6D should reflect both the preorganization inherent in the analog and the difficulty **C8** has in adopting the conformation preferred by these OSNs. Rings are common in natural product odorants. Ring-containing odorants may achieve some of their odorant qualities by simulating conformations rarely adopted by acyclic compounds that otherwise contain a similar number of carbons and the same functional groups.

DISCUSSION

Rhodopsin, the most frequently studied GPCR, evolved to respond to photons, but its activation is in fact triggered by the isomerization of a covalently held ligand (Sakmar, Menon et al. 2002). We consider this isomerization to be analogous to a conformational change, though one that depends on light. From this perspective, rhodopsin can be considered to exemplify the importance of ligand conformation to GPCR activation. ORs, which like rhodopsin belong to the class A GPCR subfamily, have evolved to report on the chemical space of airborne molecules. An important variable in chemical space is shape, which in molecules with rotatable bonds is determined by conformation. Flexible molecules constantly change conformation, but to respond to all possible odorant conformations would be a stringent demand to place on an OR, which needs to maintain a degree of tuning specificity to contribute to the olfactory code. It is reasonable then to expect that molecular conformation is an important determinant of the receptive range of ORs and that, like rhodopsin, ORs will be stabilized in their activated and unactivated states by specific but divergent odorant conformations. The prevalence of carbocyclic rings in distinctive fragrance molecules, such as the santalols and terpenoids, among many others, reinforces this expectation. However, the difficulty in obtaining structural information on membrane-bound proteins has made this expectation impossible to verify experimentally.

We chose OR-I7 to investigate the importance of conformation to OR activation because it can be expressed recombinantly in OSNs and because its primary ligand, **C8**, has many rotatable bonds that can be selectively restricted in synthetic analogs designed

to address specific hypotheses. In the **C8** analogs presented here (Figure 4.1A), we chose to begin by keeping the number of carbons constant. This choice enabled us to progressively restrict the rotatable bonds of **C8** and to systematically shorten its length while maintaining similar physical properties such as lipophilicity. Using this series, we confirmed that molecular length is important to activity when the number of carbons is held constant (summarized in Figure 4.7A): analogs **1**, **2**, and **3** activated OR-I7, but **5**, **6**, and, for the most part, **4** were too short to activate it, even though competition experiments demonstrated that they bound OR-I7. A previous rat OR-I7 study using n-alkanals had noted that **C8**'s activity was greater than that of **C7**, and that **C6** was inactive (Araneda, Kini et al. 2000). We noted a similar trend here (Figure 4.7A) using a different method that permitted greater control over the concentration of applied odorant. The finding here and elsewhere (Araneda, Kini et al. 2000) that **C7** (7.6 Å) produces significant OR-I7 activity can be taken as evidence that **C8** need not adopt its longest possible (and lowest energy) conformer (8.9 Å) to activate OR-I7. The potent activity of **C8** analogs **2** (7.6 Å) and **3** (7.0 Å) further support the idea that **C8** activates OR-I7 in a shorter-than-extended conformation. The inability of the eight-carbon aldehydes **5** (5.4 Å), **6** (4.7 Å), and, with the exception of very high concentrations, **4** (6.3 Å) to activate OR-I7 indicates, however, that extreme deviations from the extended conformation are inconsistent with activation, though not binding. This finding appears to rule out the possibility that OR-I7 is activated by tightly bent **C8** conformers resembling those mimicked by **4–6**. OR-I7 appears therefore to be activated by **C8** in a conformation whose length falls in a window somewhere between its extremes.

The restricted **C8** analogs also revealed that odorant length is not the sole characteristic of the carbon chain that determines OR-I7 activity. Within the window of activating lengths, the activity of compounds **2** and **3** was anomalously high when compared with the n-alkanal series. For example, **C7** and **2** have the same maximum length, yet **2** was 40-fold more potent. This anomaly indicates that the rotational restriction of the last two or three carbons of a sufficiently long aldehyde enhanced its ability to activate OR-I7. OR-I7-activating aldehydes were previously thought to be insensitive to structural variability in this region because the predicted lowest energy conformations of a group of activating ligands showed variability there but not in the proximal C₁–C₄ region (Araneda, Kini et al. 2000). Our results using restricted eight-carbon aldehydes show that terminal cyclopropyl and cyclobutyl groups can be potent substructures for OR-I7 activation. We speculate that the terminal methyl group in **C8** and **C7** can rotate away from a distal activating hydrophobic binding pocket through rotation of the C₅–C₆ or C₆–C₇ bonds, whereas in **2**, the analogous bonds are fixed by the cyclopropyl ring, perhaps forcing a portion of the ring to persist in contact with the pocket. (**C6** apparently reaches this hypothetical binding pocket much less efficiently.) In this regard, the receptive range of OR-I7 appears to be fine-tuned through the application of length and conformational filters, as the receptor binds a wider range of aldehydes than can proceed to activation.

What, then, is the activating **C8** conformation of OR-I7, and how does it stabilize activation? Using our activation data and information from a previous study (Araneda, Kini et al. 2000), we focused on the conformation around the C₄–C₅ bond. A 120° rotation of this bond from the more stable anti to the less-stable gauche conformation shortens and

kinks the chain slightly. When locked into this conformation, the resulting **C8** analog **11** was more active (as a *cis/trans* mixture) than **C8**, despite the extra steric bulk of the two-carbon bridge. The closer of these two bridging carbons resembles a 3-methyl group, which in the context of similar aliphatic aldehydes is well tolerated by OR-I7 (Araneda, Kini et al. 2000). Unlike the acyclic aldehydes, the stereochemical relationship between the aldehyde and the last two carbons of **11** is fixed by the ring to a small number of conformations. Because activity was preserved we conclude that **11** resembles an activating conformation of **C8**. Separate testing of the *cis* and *trans* isomers, and the synthesis of other analogs restricted in this part of **11**, will tell us if it resembles the only activating conformer, or if OR-I7 tolerates some conformational heterogeneity here.

A comparison of **11** to compound **5** is also informative (Figure 4.4C). Compound **5** lacks the ethyl group of **11** but is otherwise identical. The addition of this ethyl group to **5** was sufficient to convert it from an antagonist into an agonist of greater potency than **C8**. The ethyl group is therefore responsible for activation, though not for binding, and must somehow stabilize an activated conformation of OR-I7. It is unlikely that the ethyl group directly adds to the enthalpy of binding the activated OR-I7 because it cannot form hydrogen bonds or engage in other polar noncovalent interactions with the receptor. Nevertheless, the ethyl group triggers activation. One explanation is that the last two carbons of **11**, analogous to those of **C8**, fit into a hydrophobic pocket of the active form where they function as a steric buttress to prevent OR-I7 from reverting to inactive forms (Figure 4.7B). This pocket may be closed off in the inactive forms of OR-I7. Because most odorants are hydrophobic, the steric buttress effect may be a general means of stabilizing activated OR forms, as it does not require a polar interaction between the OR

and odorant, but can nonetheless generate binding enthalpy by the formation of new intramolecular contacts within the reorganized and activated OR (Kobilka and Deupi 2007).

Our finding that tightly bent **C8** analogs bind OR-I7 silently suggests that OR-I7 does not use conformational selection to bind only activating conformers of **C8**, but rather that OR-I7 can bind **C8** in many conformations. Proceeding to receptor activation, however, appears to require a double-induced fit, with the agonist unfurling or kinking, as the case may be, to adopt a specific semiextended conformation that stabilizes the activated form of the receptor. Thus, to be an OR-I7 agonist, an aldehyde must be capable of adopting a conformation in which it can simultaneously plug into two pockets, one specific for the aldehyde functional group and one about 7 Å away having some preference for small hydrophobic rings. The intervening carbons appear to add binding energy, though to be an agonist, C₂-C₃ must not be substituted when doubly bonded, as previously found (Araneda, Kini et al. 2000).

Matching an OR with an activating odorant is the first step toward understanding the structural basis of an OR's contribution to the olfactory code. Once a ligand is identified, rhodopsin-based homology modeling can be used to formulate a structural hypothesis for the interaction. Several groups have recently used site-directed mutagenesis within the transmembrane regions to experimentally test predicted odorant-OR interactions (Katada, Hirokawa et al. 2005; Abaffy, Malhotra et al. 2007; Schmiedeberg, Shirokova et al. 2007). These studies have obtained experimental support for rhodopsin-based structures, and have generated insightful details into the nature of the OR's binding site. Based on our work, we propose that for ligands with rotatable bonds

there will exist conformations favored by the activated and inactive forms of the OR. Experimental evaluation of conformationally restricted odorant analogs may therefore improve homology modeling, as the agonist can be kept in the preferred conformation during the modeling process.

It is not yet clear how many ORs are typically activated by a single odorant, though this question is fundamental to understanding the olfactory code. It has been suggested that flexible odorants can activate more ORs than do constrained odorants (Amoore 1970; Kaluza and Breer 2000). Our series of eight-carbon aldehydes enabled us to study this question in a controlled manner, and we found that there was a correlation between greater flexibility and the percentage of OSNs activated. Furthermore, we found that a high percentage of **C8**-responding OSNs were activated more potently by conformationally restricted **C8** analogs than by **C8** itself, indicating that many **C8**-detecting ORs, and not just OR-I7, possess some sort of conformational filter. Thus, in analogy to rhodopsin, many ORs appear to be activated or antagonized by specific ligand shapes, even though the ligand may adopt multiple forms (isomers or conformations). The conformationally restricted rings often found in natural fragrance molecules may mimic subsets of conformations in related but more flexible odorants. Some of these mimicked conformers may be high energy and rare, thus contributing to uncommon signatures in the olfactory code.

SIGNIFICANCE

The molecular recognition of airborne chemicals is challenging because volatility requires low molecular weights and a minimum or absence of polar functional groups, yet this is the subset of chemical space that the odorant receptors (ORs) have been charged by evolution to monitor. Nearly all odorants have rotatable bonds and can adopt multiple conformations. In a representative system, we have investigated the variable of octanal conformation as a molecular determinant of OR-I7 activation and antagonism. We show that OR-I7 binds a variety of aliphatic aldehydes, but then applies length and conformational criteria that lead either to activation (longer than 6.5–6.9 Å) or antagonism (shorter than 6.5–6.9 Å). Using a series of octanal mimics, we chart the transition from antagonism to agonism as a function of increasing length. For octanal, the apparent primary agonist for this receptor, we deduce that long and short conformers bind the resting state of OR-I7 and, through a double-induced fit, cooperate to produce the activating odorant-OR pair. In mixtures, various OR-I7-bound aldehydes, whether activating or antagonizing, contribute to the olfactory code either positively or negatively, enabling I7 to respond in a gradual manner to mixtures of aliphatic aldehydes rather than to only the best-tuned ligands. By studying nearly 1200 rat olfactory sensory neurons (OSNs), we find evidence that the molecular conformation of flexible odorants appears to be a common determinant of activation, and that fewer OSNs are tuned to rare conformers. For OR-I7, we also find that small cycloalkyl groups at the distal end of an aldehyde enhance activation potency. We propose that they fit into and buttress a small hydrophobic pocket present only in the activated form of the receptor, sterically

preventing reversion to the unactivated form. The steric buttress may be a common strategy for recognizing nonpolar odorants, such as the hydrocarbons.

EXPERIMENTAL PROCEDURES

Method to estimate the maximum extended length of aldehydes

Chem3D Ultra 10.0 software (CambridgeSoft; Cambridge, MA) was used. The structure of the aldehyde was drawn in its most extended conformation. The energy was minimized using the MM2 force field. The length was then measured from the carbonyl carbon to the most remote carbon.

Synthesis of octanal analogs

See Supplemental Data available online for detailed synthetic procedures and compound characterization.

Isolation of olfactory sensory neurons

All animal procedures were approved by the Columbia University Institutional Animal Care and Use Committee and performed at Columbia University in compliance with relevant national guidelines and regulations. Procedures for isolating rat OSNs were performed as described in detail elsewhere with minor modifications to the dissociation solution (Araneda, Peterlin et al. 2004). For OR-I7 experiments, male Sprague-Dawley

rats 6–7 weeks old were infected with an adenovirus that encoded OR-17 and GFP as separate proteins (Zhao, Ivic et al. 1998). Two to three days following infection, regions of the olfactory epithelium exhibiting dense GFP fluorescence were dissected out. For the panel screening in Figure 4.6, uninfected rats were used, and the entire olfactory epithelium was collected. The olfactory epithelium was dissected free from the underlying bone under chilled divalent cation-free Ringer (145 mM NaCl, 5.6 mM KCl, 10 mM HEPES, 10 mM glucose, and 4 mM EGTA [pH 7.4]), minced, and then incubated for 45 min in 2.5 ml of divalent cation-free Ringer containing 5 mg/ml bovine serum albumin (B4287; Sigma-Aldrich; Milwaukee, WI), 1 mg/ml collagenase (17100-017; GIBCO; Carlsbad, CA), 2.4 U/ml dispase (04-942-078-001; Roche; Basel, Switzerland), and 100 µg/mL deoxyribonuclease II (D8764; Sigma-Aldrich). Following, the tissue was dispersed in a small volume of culture medium (typically 150–200 µl) and plated onto concanavalin A-coated coverslips. Cells were kept in a 32°C incubator until use.

Calcium imaging of olfactory sensory neurons

Calcium imaging recordings were performed as described in detail elsewhere (Araneda, Peterlin et al. 2004). Briefly, cells were rinsed with normal rat ringer (138 mM NaCl, 5 mM KCl, 1 mM CaCl₂, 1.5 mM MgCl₂, 10 mM HEPES, and 10 mM glucose [pH 7.4]) and loaded with fura-2AM plus pluronic acid for 45 min at room temperature. The coverslip was placed into a recording chamber and imaged at room temperature at 380 nm excitation and 510 nm emission. Due to the slow nature of the calcium response,

images were only acquired every 4 s with each image representing the average of three frames. NIH Image software was used for data acquisition and analysis.

Ringer was continuously pumped through the recording chamber at a rate of 1 ml/min. Odorants were presented to the cells by injecting 400 μ l of the stimulus solution into the chamber over the course of 4 seconds, exchanging the volume of the recording chamber two to three times. Odorants had been recently synthesized and stored at 4°C under inert atmosphere while awaiting testing. All odorants not specifically synthesized for this study were purchased from Sigma-Aldrich. Stock solutions of the odorants in DMSO (0.5 M) were prepared fresh daily. Stock solutions were subsequently diluted in Ringer to the indicated concentrations with DMSO supplementation as necessary so that all stimuli were matched for the amount of DMSO; cells did not respond to DMSO alone at this level. Odorants were typically applied 3.25 minutes apart with the exception of the panel screening in Figure 4.6, where spacing was increased to 5 minutes apart. Because the cells shown in Figure 4.6 all likely express different ORs, the adenylyl cyclase activator forskolin (10 μ M) was applied at the end of the series to strongly stimulate the downstream signal transduction path and thus provide a means of comparing responses between cells. The response to forskolin also serves as a measure of the functional viability of an OSN because adenylyl cyclase III, like the ORs, is localized to the cilia.

Data are shown as the fractional change in fluorescent light intensity, $(F-F_0)/F_0$, where F is the fluorescent light intensity at each point and F_0 is the value for the emitted fluorescent light at the start of each movie before the first stimulus application.

Responses were measured between the baseline and peak $\Delta F/F$ change. To account for drift due to alterations in fluid level or incomplete return of intracellular calcium levels,

flanking normalization stimuli (typically **C8** or compound **1** at 10 μM) were applied at the beginning and end of each movie. A trend line could then be drawn between the peak responses of the flanking applications. Responses to intervening odorants were normalized by taking the ratio of the measured magnitude over the predicted (to trend line) magnitude. Measured in this manner, we found repetitions of the same stimuli meet or exceed 0.90. Accordingly, for the tuning choice in Figure 4.6A, we classified two responses as being effectively the same magnitude if they were within 90% of each other, and in Figure 4.5D the combination of a putative antagonist with **C8** needed to be less than 90% that of **C8** alone to be classed as an antagonist. Values for the antagonist ratio reported in Figure 4.5D represent the average \pm SEM. Dose response curves were fit using the Hill function in Igor Pro with each point plotted as the average value from at least three independent GFP-expressing cells \pm SEM. EC_{50} and IC_{50} values are reported as \pm SD. For marginally activating aldehydes (**C6** and compound **4**), EC_{50} values are extrapolated from the best fit curve.

ACKNOWLEDGEMENTS

This work was funded by the City College of New York Division of Science, the Professional Staff Conference-City University of New York (PSC-CUNY), and the National Institutes of Health National Institute of Deafness and Other Communication Disorders (NIH NIDCD). Additional support was provided by the City College Research Centers in Minority Institutions (RCMI).

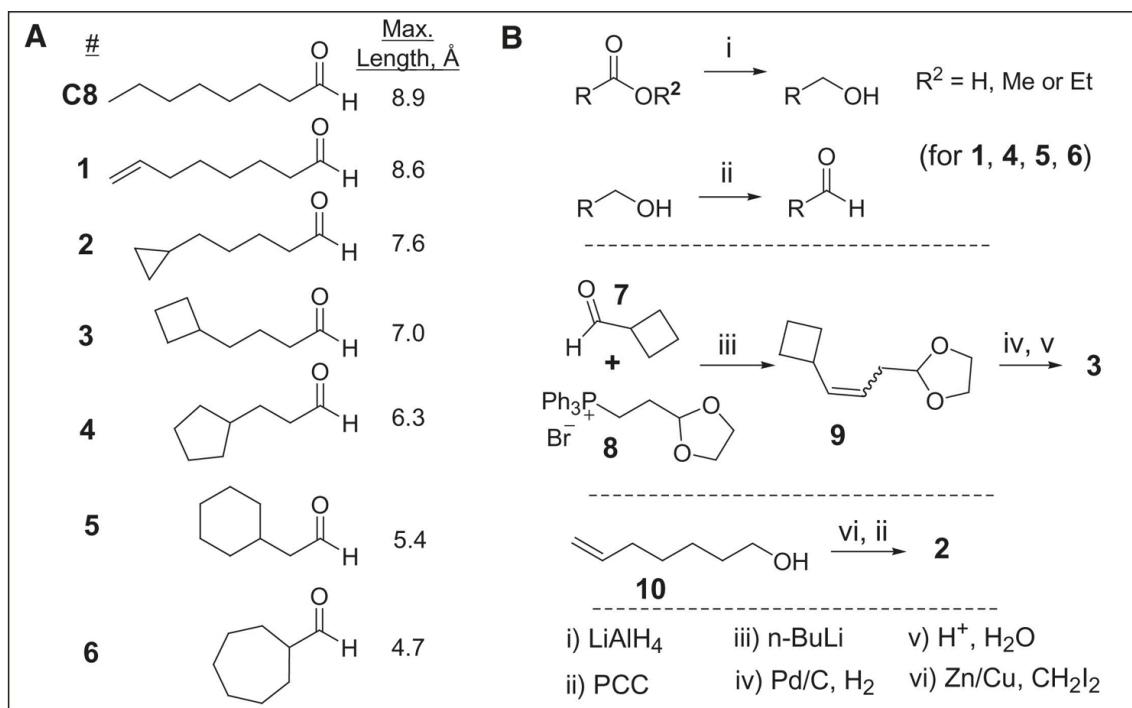
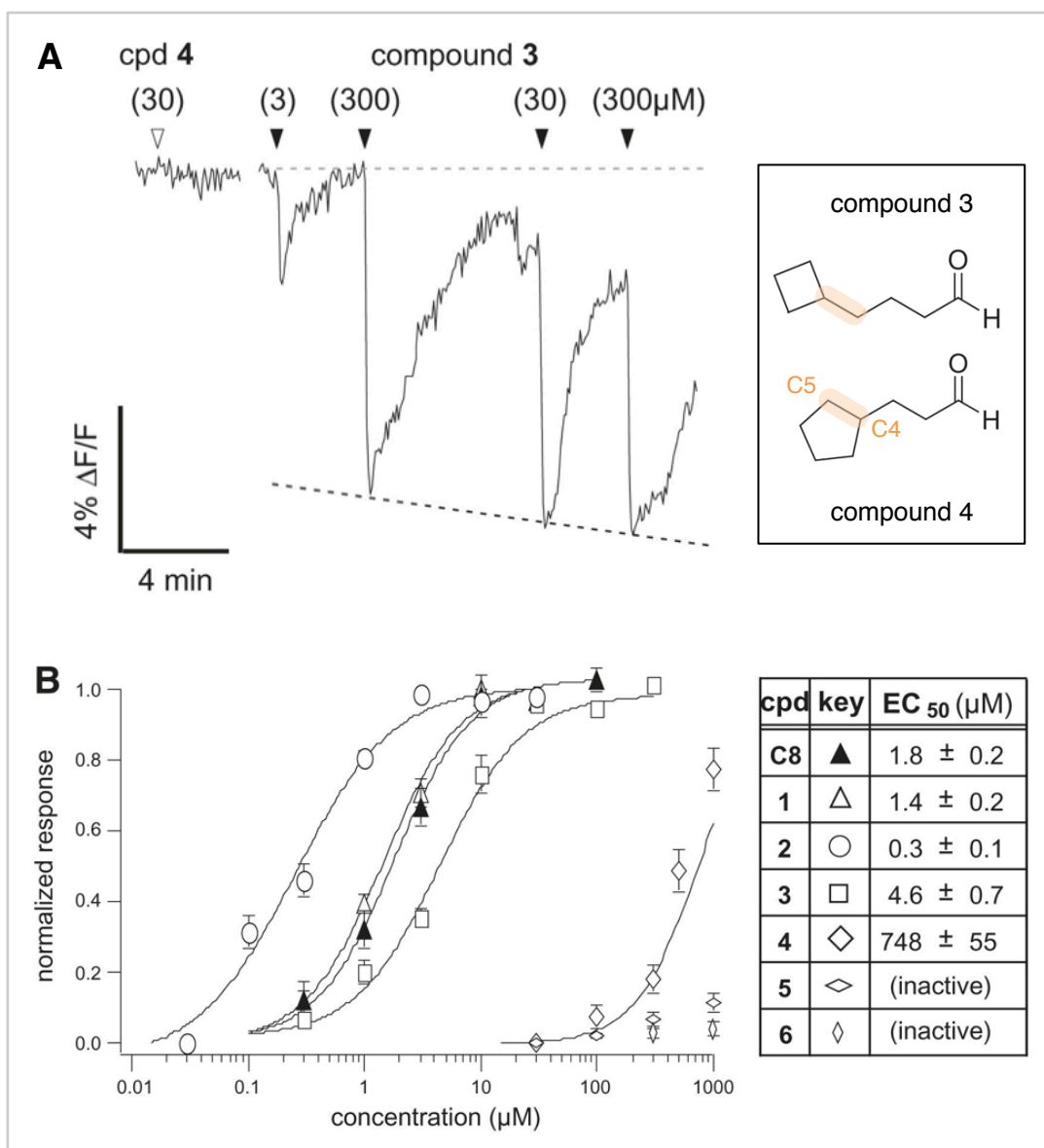


Figure 4.1 - conformationally restricted octanal analogs. (A) Structures of the constrained octanal analogs used in this study. Lengths refer to the distance measured from the carbonyl carbon to the most distant carbon as described in Experimental Procedures. (B) Schematic of the synthetic routes to compounds **1-6**.

Figure 4.2 - OR-I7 activation by cyclic octanal analogs. (A, left) Calcium imaging traces from a GFP+ OSN. Grey dashed line denotes baseline, black dashed line denotes a trend line for normalization (See Experimental Procedures). OR-I7 responds at a near saturating level to 30 μ M of compound **3**, but is unresponsive to compound **4** at the same concentration. (inset, right) The critical C4 and C5 carbons are not part of the ring system in compound **3** but they are constrained in compound **4**. (B) Activation dose-response curves for the cyclic compound series (open symbols). The activation dose-response curve for octanal (**C8**) is also provided for reference (filled symbol). Octanal and compounds **1-3** saturated over this range and are thus normalized to their respective maximal responses. Compounds **4-6** are shown normalized to the response to 10 μ M octanal.



(this page intentionally left blank)

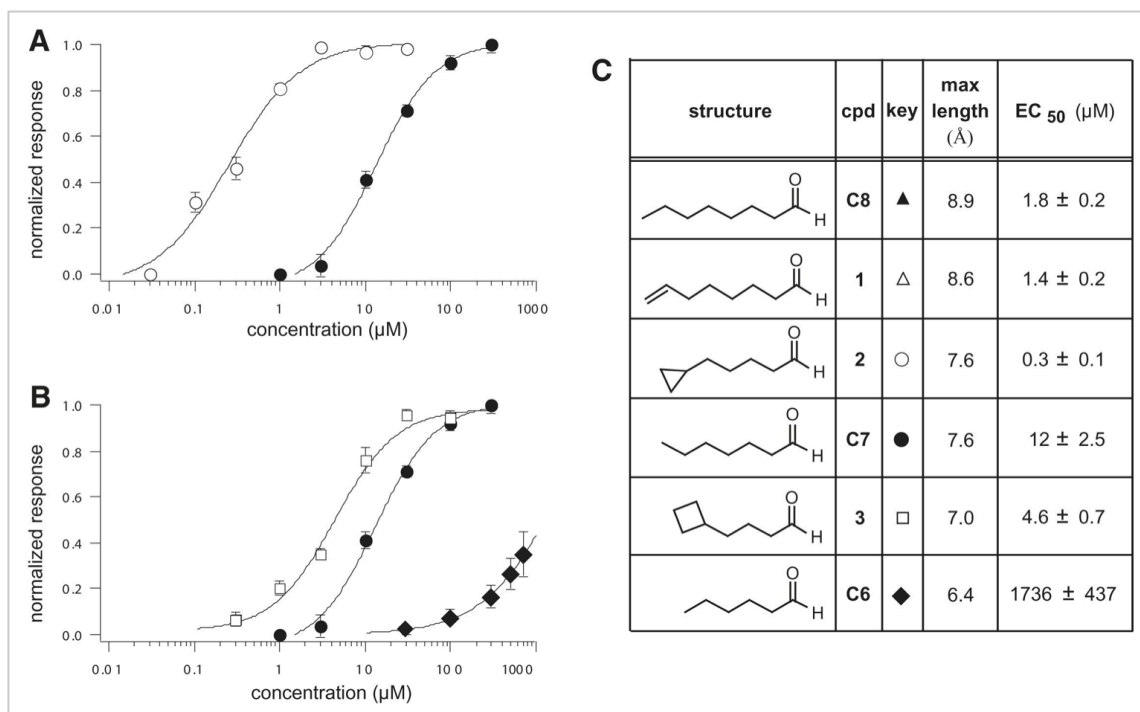


Figure 4.3 - cyclopropyl and cyclobutyl ring-containing analogs are more potent than predicted from their maximal lengths. (A) Activation dose-response curves for cyclic compound **2** (open circles) and the n-aldehyde of identical length, **C7** (filled circles). (B) Activation dose-response curves for cyclic compound **3** (open squares) and the n-aldehydes of flanking lengths **C7** (filled circles) and **C6** (filled diamonds). (C) Summary of maximal lengths and EC_{50} of activation for the strongly activating cyclic and n-aldehydes. The relative activation of **C8** and compound **1** can be found in Figure 4.2B.

Figure 4.4 - a semi-extended octanal conformation activates OR-I7. (A) Line structures (top) and Newman projections (bottom) depicting rotation around the C₄-C₅ bond in octanal, and how it was locked in the gauche conformation in compound **11**. Only the trans isomer's Newman projection is shown. (B) Synthetic route to compound **11**. (C) Activation dose-response curves for octanal (**C8**, filled triangles) and the cis/trans mixture of compound **11** (open inverse triangles). The related compound **5**, which lacks the 4-ethyl group, has no substantial activity (open compressed diamonds).

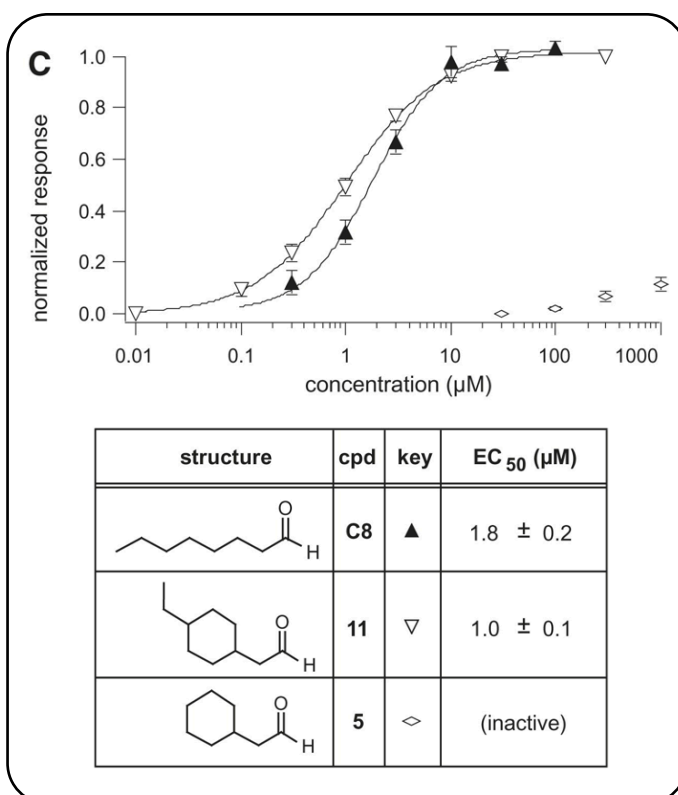
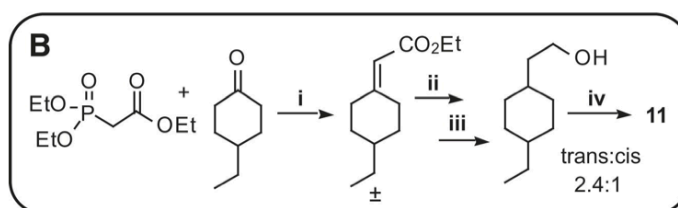
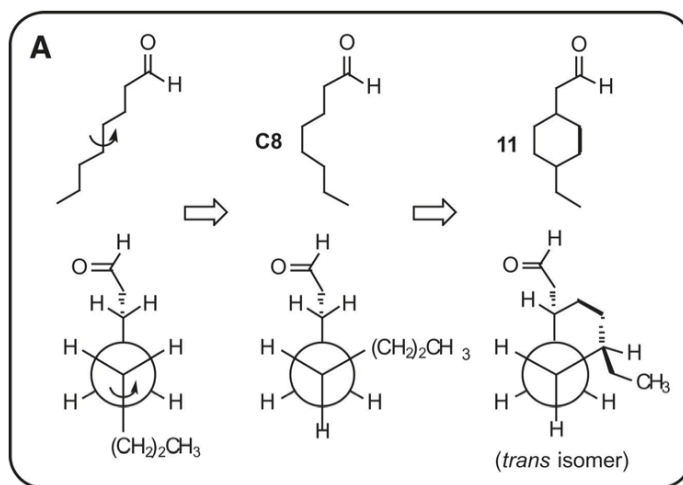


Figure 4.5 - inhibition of OR-I7 activation by short octanal analogs. (A) Calcium imaging traces from a GFP+ OSN, showing the dose-dependent antagonism of compound **6** against a saturating dose of octanal. Black arrowheads denote the application of 10 μ M octanal either with or without co-application of **6** (open arrowheads). The black dashed line is the trend line, indicating the predicted response magnitude if the co-application had no effect. (B) Inhibition dose-response curves for cyclic analogs and n-aldehydes of similar lengths, tested at various concentrations against a 10 μ M octanal stimulus. The cyclic compounds (open symbols) all display very similar potencies regardless of length, while the n-aldehydes (filled symbols) show length dependence for antagonism. Dashed lines indicate extrapolation used to estimate IC_{50} . (C) Summary of maximal lengths and IC_{50} values for the antagonizing aldehydes. (D) An aldehyde group is required for OR-I7 antagonism. Dashed line indicates where the combination of potential antagonist and octanal elicited 90% of the signal produced by 10 μ M octanal alone; only compounds that show a reduction to or below that level are classified as antagonists (black bars). Only hexanal met this criteria. Non-aldehydes of similar size were unable to antagonize octanal activation of OR-I7.

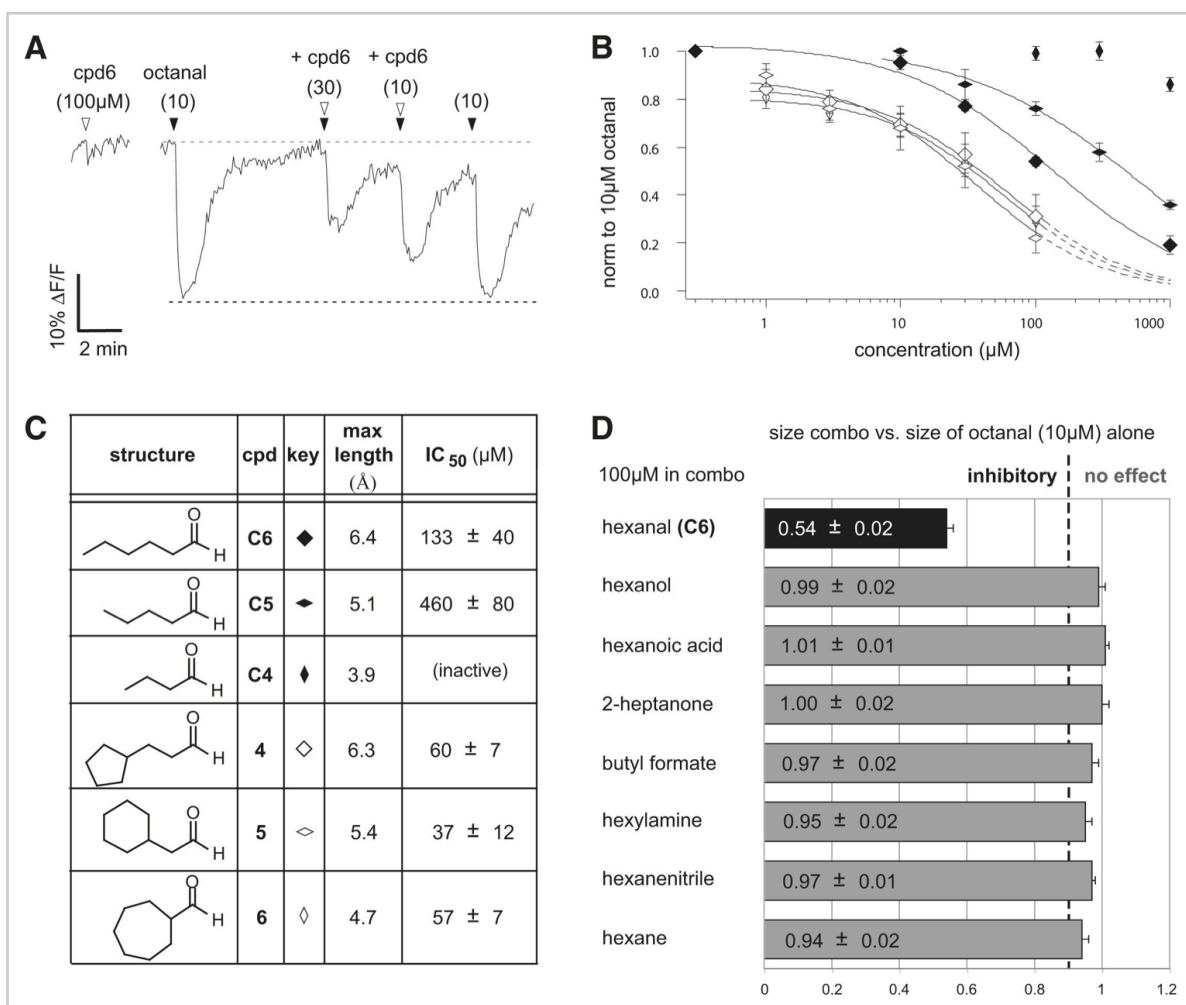
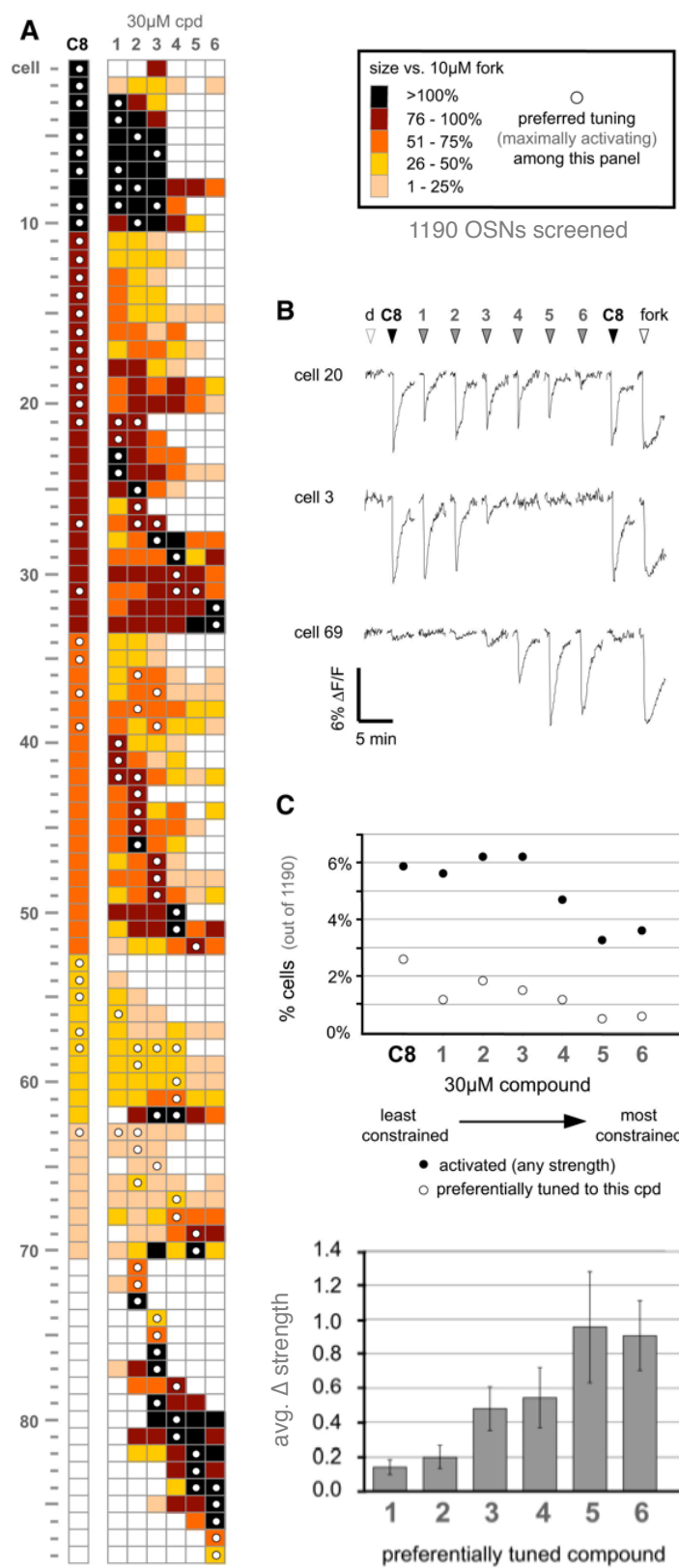


Figure 4.6 - conformational preference among octanal receptors. (A) Response profiles of the entire population of OSNs activated by 30 μM octanal (**C8**) or the cyclic analogs **1-6** out of 1190 tested OSNs. Response strength was normalized within each cell to 10 μM of the drug forskolin which elicits near maximal activation of the signal transduction cascade. The compound generating the greatest response by the cell (i.e. its preferred tuning among this panel) is denoted by a white dot. (B) Representative calcium-imaging traces from three selected cells exposed to aldehydes **1-6**, each given individually at 30 μM . Compounds were tested in random order, but have been rearranged for presentation clarity. The open arrowheads denote application of the DMSO vehicle (d) or forskolin (fork). (C) Percentages of OSNs responding to 30 μM of the indicated compound (filled circles) and percentages of cells preferentially tuned to the indicated compounds (open circles). (D) Average difference in activation strength between analogs and octanal. For the cells whose preferred tuning included a cyclic analog, the response to octanal was subtracted from the response to the preferred analog. This difference was then averaged over all cells tuned to that same analog. Because all responses are normalized within each cell to forskolin activation, the maximum possible difference is 1.0 (i.e. the case where a cell responds as robustly to the preferred analog as forskolin but fails entirely to respond to octanal).



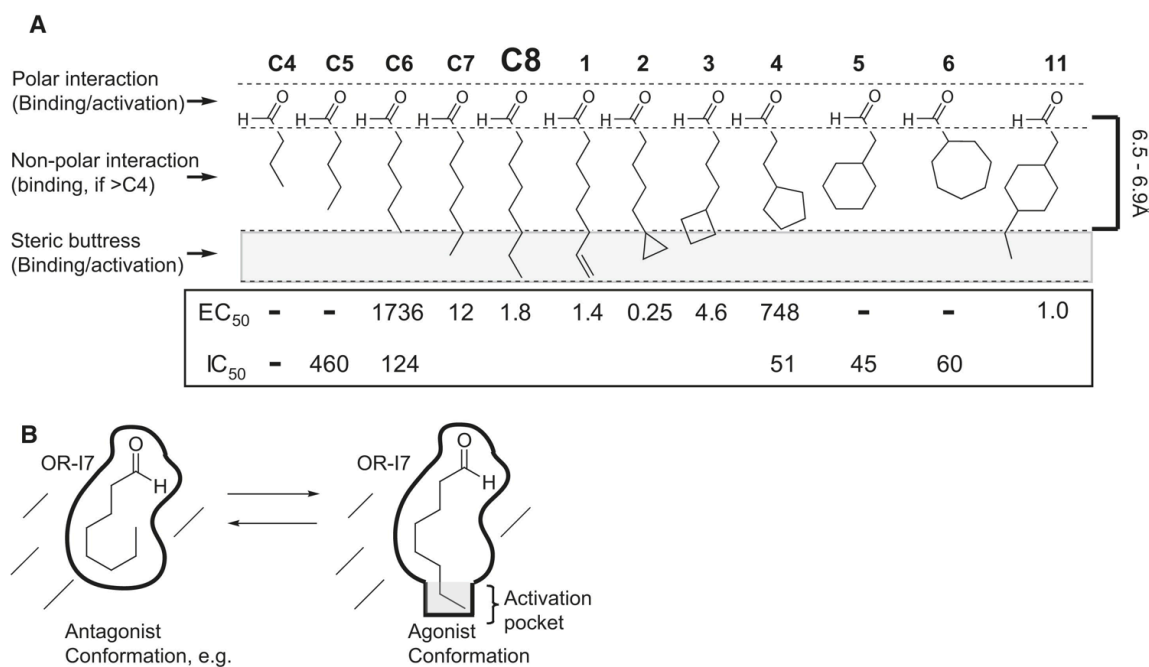
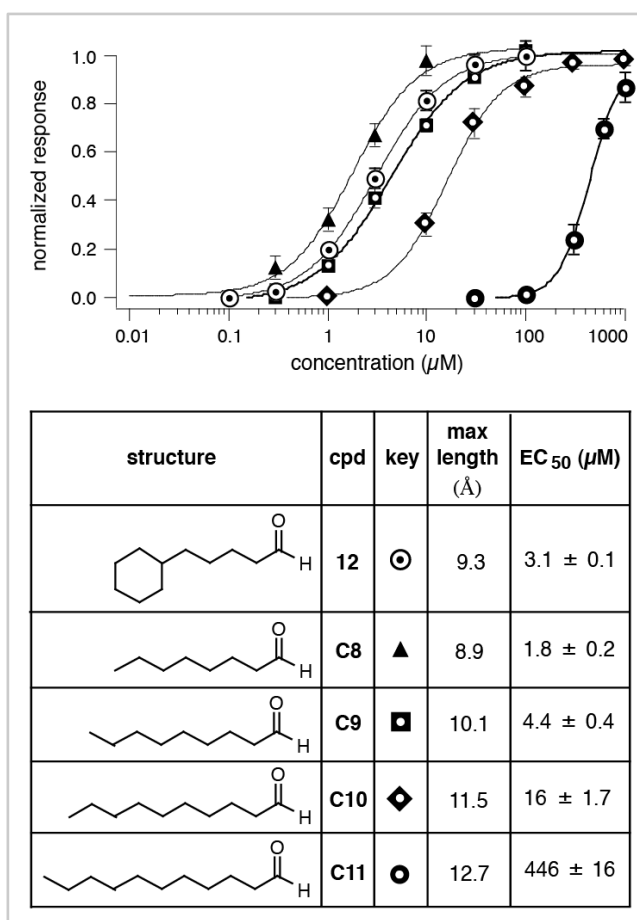


Figure 4.7 - summary of OR-I7 binding and activation by octanal conformation mimics. (A) Structures, maximum lengths, and inhibition/activation constants. Regions of the structures responsible for binding and activation are indicated (left), as is the 6.5-6.9Å length requirement for activation (right). Dashes in EC₅₀ row indicate the compound had no activity within its solubility range. **C4** also failed to antagonize OR-I7 within its solubility range. Gaps in the IC₅₀ row indicate that the compound was not tested for antagonism because it is strongly activating. (B) Schematic depiction of octanal's conformation on OR-I7's activation.



Supplemental Figure 4.1 - OR-I7 activation by longer aldehydes and compounds with a more bulky terminus. Activation dose response curves for long n-aldehydes at OR-I7. Compound **12** can be viewed as a constrained analog of undecanal (**C11**), or a modified version of the cyclic octanal compound **2** where the small cyclopropyl ring is replaced with a larger cyclohexane ring. The spooling of the tail in compound **12** (white background, black dot) greatly improved potency over the unconstrained n-aldehyde **C11** (black background, white dot). The similar potency for compound **12** compared to octanal (black triangle) demonstrates substantial steric tolerance in the distal region of the binding pocket in OR-I7.

(this page intentionally left blank)

CHAPTER 5**IDENTIFICATION OF ACYCLIC, ACTIVITY-GRADED HEDIONE MIMICS**

ABSTRACT

As previously demonstrated with octanal at the I7 receptor, rings can be used to conformationally restrict a flexible odorant and set up receptor-requisite spatial relationships between key activating epitopes (Peterlin, Li et al. 2008). Viewing ring systems as a means of freezing defined geometries of odorants and not as the overriding feature per se can help explain odorant receptor (OR) receptive fields populated by compounds that initially seem structurally discrepant. Here, we report on a panel screen centered on Hedione (HED). HED is a ring-containing synthetic derivative of a jasmonate plant signaling compound. Only one of its four stereoisomers elicits a pronounced percept in humans. In this pilot, we conceptually remove the ring and determine how acyclic compounds without this chiral-imparting feature activate HED+ olfactory sensory neurons (OSNs) as compared to the general OR code. We found that methyl nonanoate (MENON), a fully flexible ester that matched the backbone of HED, was treated by the HED+ OSNs as the most similar odorant. Not only did it recruit almost the full HED+ sub-population, but MENON activation magnitudes were very similar to that elicited by HED in the same cell. The response patterns elicited by MENON and the probe odorants in our panel indicate that neither HED's bulky cyclopentane ring nor its appended ketone are required to elicit activation; a terminal blunt ester and a long flexible alkyl backbone is sufficient. The trajectory of the two arms in HED thus appears to be recreated even without the assistance of the ring. Curiously, there was a graded level of activity elicited by neryl acetate (highest), followed by HED, MENON, and distantly by cis-3-hexenyl acetate; this pattern was conserved across most

of the HED+ subpopulation. This series highlights how a commonly available scaffold can be manipulated into a highly targeted signal.

INTRODUCTION

Hedione (HED) is a synthetic chemical closely related to the plant hormone methyl jasmonate (Cheong and Choi 2003). Two arms attach to the cyclopentanone ring, creating two chiral centers for four stereoisomers total (Figure 5.1). The chiral center formed by the ester arm is designated as (1) and the chiral center formed by the alkyl arm is designated as (2). The extremely challenging task of purifying each stereoisomer of HED revealed that the relative geometry of the ester and alkyl arms dramatically impacts human perceptual sensitivity (Werkhoff P. 2002). The most potent stereoisomer is (1R,2S), a cis configuration that causes both arms to project to the same face of the ring. This stereoisomer has a detection threshold of 15ppb. Relative to this base arrangement, altering the geometry of the alkyl arm decreases the potency ~15 fold. Altering the geometry of the ester arm, however, results in a 1,000 fold drop! The chiral center at the ester arm thus appears to be weighted more strongly across the relevant subset of odorant receptors (ORs) that respond to HED.

This dependence for potent activation on the relative position of two epitopes is highly reminiscent of the behavior of a conformationally locked version of octanal at the I7 receptor (Peterlin, Li et al. 2008)(Figure 5.2A). While both octanal and the cyclic variant can place a methyl terminus at a geometrically localized site, the cyclic variant “pre-molds” the octanal backbone to the proper geometry. By analogy, we hypothesized

that for HED the core backbone was really methyl nonanoate (MENON) and the cyclopentanone ring served merely to shunt the trajectory of this long ester backbone through stabilizing a cis-kink at carbons C3-C4 (Figure 5.2B). Achieving this through the use of a ring, versus a double bond, imparts chirality to the arms of HED. The appended ketone might be a dispensable polar anchor given the presence of the ester as an alternate.

We predicted that MENON would still be recognized by many HED+ olfactory sensory neurons (OSNs), although probably with at least slightly diminished potency. However, there were many uncertainties. For example, if MENON was a poor agonist would only the most sensitive HED+ OSNs generate a residual detectable response to this unlocked compound? Or would only the HED+ cells that were structurally broadly tuned, regardless of their individual sensitivity to HED, be the ones that would continue to respond to MENON after the chiral destruction?

To address these questions, we conducted a pilot with odorants that probed which features could elicit robust co-recognition by HED+ OSNs. The panel members varied in the degree to which they could readily mimic the cis-kink induced by the cyclopentanone ring and/or which included fragments of the ring found in HED (Figure 5.3). Methyl nonanoate (MENON) was fully unconstrained. Neryl acetate (NERAC) sculpted the backbone trajectory via its cis double bond. This bend might align with the inner wall of the cyclopentanone ring in HED and offer greater “pre-molding” relative to MENON. NERAC also contributes a methyl that overlays part of the ring architecture in HED. Coniferan (CONIF) offered a true ring (albeit a 6-membered one) that restored chirality to the arms. However, CONIF could not match the length of either arm. In contrast,

MENON and NERAC can trace out a path that will localize their terminal methyls at the same region as Hedione.

A specific challenge facing CONIF as a HED mimic was the dimethyl load on the alkyl arm. This motif was only two carbons away from the attachment point to the ring. In a study of *n*-aldehydes, similar dimethyl placement close to an important polar anchor was a severe detriment to odorant detection, resulting in 70% attrition of the octanal code (see comparison of DIM versus 8AL in Chapter 3). The dimethyl in CONIF is located close to the secondary chiral center in HED, and this burden could thus prove influential.

Cis-3-hexenyl acetate (cis3-HEXAC) was the final member of the panel. Its alignment to HED was more ambiguous. Its short length would not permit it to meet both alkyl termini in any alignment. Nor did cis3-HEXAC contain a formal ring. Previously, we had characterized the cis-3-hexenyl moiety as a modestly accepted substitute for an aromatic ring in benzyl acetate across the OR repertoire (Supplementary Figure 5.1). We reasoned that cis3-HEXAC might serve as an even better replacement for an alkyl ring. Thus, we predicted that cis3-HEXAC would most likely localize its double bond to the outer perimeter of the cyclopentanone ring in HED. This alignment is related to that achieved by CONIF. Alternatively, the kink in cis3-HEXAC might, as in NERAC, align with the proximal wall of the cyclopentanone ring in HED. However, this scenario seemed unlikely because it would displace the polar anchor in cis3-HEXAC two units away from where HED normally has its carbonyl group. Cis-HEXAC's preferred conformation among the HED+ population would need to be deduced from its response pattern across the ORs relative to odorants with more readily predicted alignments.

A caveat of this study is that while HED and MENON are methyl esters, the remaining panel members are acetate esters. We had turned to acetate esters since methyl esters with the desired features were not commercially available. This seemed a reasonable compromise since acetate esters retain the short distance from the carbonyl to the nearest alkyl terminus. Acetate esters can also be viewed as retroesters of methyl ester, so formed via a “cassette swap” (Figure 5.4). In a cassette swap, the functional group is flipped as a unit; the carbonyl site now houses the ether oxygen, and the ether oxygen position is occupied by the carbonyl. Although this manipulation shifts the carbonyl laterally by one atom, the general polar topology of the compound is retained. In contrast, other potential rearrangements leave polar vacancies and create ectopic polar loci. In addition to being the least perturbing, substitution with retroesters is a well recognized strategy that is often employed in medicinal chemistry because it commonly preserves compound function at the desired drug target (Ciapetti 2008).

METHODS

The full olfactory epithelium from C57Bl6 mice was harvested and OSNs were prepared for fura-2 calcium-imaging as previously described (Araneda, Peterlin et al. 2004; Peterlin, Li et al. 2008). All odorants were prepared as 30uM in the application syringe and delivered as in prior studies. We used the commercial high-cis grade HED that is a blend of enantiomers in a 10 cis: 90 trans ratio. HED was treated as a single-component odorant in calculations. At the conclusion of the screen, 10uM forskolin was delivered to maximally activate the transduction pathway. This allows for normalization

of response magnitudes within a cell, thus providing an analog measure of odorant sensitivity. In total, 103 intact forskolin+ OSNs were screened during this preliminary pilot.

RESULTS

Subclasses among the HED+ population

Results of the panel screen are presented in Figure 5.5A. Although the sample size of the pilot is small, the trends that emerged were robust and intriguing, warranting discussion and providing encouragement for further study. Several functional subclasses of HED+ OSNs could be distinguished.

Subclass 1 : The cyclopentanone ring is a required epitope

25% of HED+ cells (c1-c2) failed to respond to the unlocked flexible esters in our panel. These ORs appear to require some aspect imparted by the cyclopentanone ring. It is possible that cell c1 requires the ketone as a primary or necessary subsidiary anchor, but cell c2 can forego this polar group as indicated by activation by CONIF. It is notable that CONIF was the only ester to suffice at cell c2; this is the only compound with a formal ring and may thus indicate requirement for a rigid steric buttress.

The CONIF+/HED+ profile was exceedingly rare. The only two cells to display it utilized different odorant detection strategies. Both cells c2 and c8 had matched

activity between CONIF and HED. Cell c2 was highly activated by these two compounds yet filtered out all other panel members, demonstrating narrow tuning. In contrast, cell c8 was activated by CONIF and HED but only at a modest level. This cell detected and preferred multiple flexible esters, thus exhibiting broad tuning. The two profiles cannot be accounted for by global difference in sensitivity, and thus they reflect distinct discrimination strategies.

Subclass 2 : Reliably graded activation by unconstrained esters

The majority of HED+ OSNs (75%) were activated by MENON. Recognition was still achieved even by those OSNs that were only modestly activated by HED (c6-c8). Across this subclass, on a cell-by-cell basis the activation elicited by MENON was closely matched to that elicited by HED. The stripped backbone of MENON was thus quite effective in molding into a kinked mimic of the ring-constrained HED.

The terpene ester NERAC activated the same HED+ population as MENON. NERAC consistently activated the HED+ OSNs equivalently or stronger than HED. Intriguingly, MENON / NERAC discrimination could only be achieved by HED- cells.

Somewhat surprisingly, cis-3-HEXAC also targeted the same HED+ subpopulation as had NERAC and MENON. The strong MENON+/HED+ signature across this suite of ORs had indicated that a formal ring was not required. As cis-3-HEXAC was predicted to most likely align to the ring pocket, we no longer expected it to activate HED+ cells. Instead, we found that the same HED+ OSN subpopulation was still targeted, but the cis-3-HEXAC responses were markedly weaker.

Among the majority of HED+ OSNs (c3 to c7), MENON could be classed as an “equi-morph” odorant in its ability to mimic Hedione; that is, the magnitude of the response to MENON in a given cell is within 20% of that elicited by HED. NERAC, then, is an activity “hypermorph” and cis3-HEXAC an activity “hypomorph”. Over the NERAC / HED / MENON span, there was a gentle activity decline or a plateau. However, there was always a marked drop in response magnitude between that elicited by MENON and that by cis3-HEXAC. What is most striking is that this activity gradation was preserved over the entire HED+ sub-population, meaning that a whole subcode can be manipulated in a concerted and predictable way.

The NERAC+ / MENON+ / cis3-HEXAC+ response profile, even when considered as a simple binary profile, was nearly exclusive to HED+ cells. It can thus serve as a useful functional fingerprint in experimental design should one wish to reserve application of HED until the end of the recording set.

Responsiveness to HED impacts the pattern of MENON/NERAC discrimination

Among HED- cells activated by the esters of our panel, recruitment levels and relative activity levels adopt very different patterns. One striking case involves MENON and NERAC discrimination. HED- cells consistently failed to co-recognize NERAC and MENON. Cell c10 represents the only ambiguous case. There were ample opportunities for the HED- population to obtain a potential NERAC+/MENON+ patterning based strictly on availability; one third of MENON’s and NERAC’s recruited repertoires fall outside the HED+ subpopulation. This clean and complete segregation of the

MENON+/NERAC+ profile to the HED+ population underscores that gaining the ability to recognize some critical characteristic feature of HED comes with the penalty of no longer robustly performing certain other chemical discriminations.

The conformer adopted by cis3-HEXAC may depend on the OR's response to MENON

Selection of odorants for the panel had been guided by two motifs. MENON and NERAC had the ability to mimic the full dual arm structure of HED. Their length is sufficient to allow their alkyl termini to plug into the same locations as HED if these flexible compounds will assume a hairpin bend. But the ring of HED might serve as a rigid steric buttress aside from its role in conformational restriction. CONIF was the only member of the panel that provided a fixed ring with a pendant alkyl arm.

Intriguingly, whether HED+ or HED-, there appeared to be a marked partitioning of ORs based on whether they responded to MENON or CONIF. With only two exceptions (cells c17, c8), all CONIF+ OSNs excluded MENON and vice versa. (Figure 5.6A).

Cis3-HEXAC, however, could activate both MENON+ and CONIF+ cells. Cis3-HEXAC also recruited the largest number of cells of any panel member. Cis3-HEXAC can contribute only a partial length arm when in a hairpin configuration, and it provides only the perimeter of a “phantom-ring” and not the mechanical benefits of a true ring. The large cis3-HEXAC+ population was split in half by the ability to detect MENON. Such ORs, accommodating the longer MENON, may thus present an adequate environment for adoption of a more “unspooled” conformation of cis3-HEXAC. At the

ORs accommodating the compact CONIF, cis3-HEXAC may assume its more tightly wound conformer. The amplitude of the responses to cis3-HEXAC were consistently higher among MENON⁻ cells than MENON⁺ cells, and they were particularly robust if a cell was CONIF⁺. Cis3-HEXAC may thus preferentially assume a more compact conformer, but it will adapt to a more open one among HED⁺ OSNs.

DISCUSSION

The opening of rings and simplification of the alkyl scaffold is a common first step in medicinal chemistry, particularly when working with natural compounds (Wermuth 2008). The native plant hormone, Methyl jasmonate, and its synthetic derivative, HED, both retain the same scaffold and differ only in the presence of a single double bond in the alkyl arm. Commercially available HED is a mix of stereoisomers, only one of which is particularly potent to humans (Werkhoff P. 2002). The ring in HED imparts the chirality, but at what cost if 3 of 4 enantiomers don't contribute markedly to the perceptual bouquet? We wondered if taking a "reverse conformational restriction" approach and eliminating the ring would allow a more flexible compound to meet the preferred geometry more readily.

The backbone of HED is the long ester MENON. It was uncertain how frequently MENON would assume the properly located kink. Our previous work with cyclic octanal analogs had demonstrated that many OSNs preferentially bind n-octanal in other than its lowest energy, fully extended state (Peterlin, Li et al. 2008). Provided that the free energy of the receptor/ligand system decreases, binding of higher energy odorant

conformations is possible. A panel survey surprisingly revealed that 75% of the HED+ OSNs also detected the fully unconstrained MENON. Moreover, they did so with similar levels of activation. Appropriate conformational adaptation and stabilization of MENON thus seemed readily promoted by the binding pockets of the ORs in these cells.

HED+/MENON+ cells tended to respond to multiple other panel members of our assay, but the HED+/MENON- cells largely rejected the remaining panel members. Expanded testing is needed to identify what aspect is so critical in imparting such stringent filtering.

While conformationally adaptable, cis3-HEXAC can weakly mimic an aromatic ring if more tightly furled, or mimic the gentle bend between the arms of HED if unfurled. Both conformations appeared evenly populated as judged by the split of the cis3-HEXAC subpopulation with respect to responsiveness to MENON. We interpret that cis3-HEXAC activates MENON+ cells weakly in an unfurled form whereas it activates MENON- cells strongly in a compact form. Only cis3-HEXAC+ cells that were MENON- could respond to CONIF, an odorant with a formal cyclohexyl ring. Cis3-HEXAC may thus preferentially adopt the more tightly furled form, but like n-octanal cis3-HEXAC will adapt its conformation depending on the individual receptor.

One would expect that the most flexible odorant would be the most promiscuous, seeing that it can conform to the greatest number of binding pocket shapes. MENON is more flexible than cis3-HEXAC and it has a longer alkyl tail, granting it more potential conformations. Yet cis3-HEXAC recruited nearly double the number of ORs as did MENON. Cis3-HEXAC has an end-to-end span of 9 atoms, while MENON spans 11 atoms. Intriguingly, amyl acetate, an ester long used as a robust activator (Zhao, Ivic et al. 1998; Duchamp-Viret, Chaput et al. 1999; Araneda, Kini et al. 2000; Ma and

Shepherd 2000), has an overall span of 8 atoms. Among n-compounds a tail length preference of 8 to 9 carbons has long been recognized to be the optimum in terms of recruitment (Sato, Hirono et al. 1994; Kaluza and Breer 2000; Araneda, Peterlin et al. 2004). A similar “biological fovea” for esters falling near a span of 8 may contribute to cis3-HEXAC’s more robust activation relative to MENON.

While several of the flexible esters could activate HED+ cells, they did so with differing relative activation levels. NERAC was a “hypermorph”, activating more robustly than HED at the same concentration, while the majority of MENON responses were nearly equivalent to HED or only slightly lower. Cis3-HEXAC was a decisive “hypomorph”. Further tests will be needed to determine if cis3-HEXAC is merely a weak agonist or if it can serve as a partial antagonist. The graded activity series of NERAC / MENON / cis3-HEXAC provides a unique chemical toolkit to “dial-in” a desired level of activity among HED+ cells. Probing local ester space in more detail, by changing the length of each arm, the total compound length, the orientation of the ester functional group, and converting the ester to a ketone is likely to uncover even more nuanced gradations of activating odorants that can expand the dynamic range of this novel physiological toolkit.

FUTURE DIRECTIONS

Rationale for expanding the scope of this study

The results from the initial pilot are encouraging, and further expansion is warranted. The members of the revised panel are shown in Figure 5.7. These additions will permit a detailed probe of the basis of the NERAC “hypermorphism” among the HED+ subpopulation to clarify whether this is a receptor-subtype specific effect or if it reflects a biased treatment of terpenes by the olfactory system in general. In this panel, the characteristic terpene features of NERAC are gradually stripped away. Given the trends in the initial pilot, I would expect these “partial terpene” odorants to elicit activation intermediate between that of NERAC and MENON among the HED+ population. Several other pairings within this expanded panel will provide initial evaluation of the impact of ester orientation and whether cis/trans geometric preference can be predicted given a particular alignment of another ligand.

Current status of terpene encoding among other functional groups

The modified panel provides an important foray into terpene chemical space. Terpenes are prevalent in natural products but they have received only scattered assessment at the OR receptor repertoire level. Hamana et al. (2003) reported on the

frequency of co-recognition between carvone-responsive OSNs with other cyclic terpenes and the linear terpenes neral and geranial. However, only pairwise comparisons are available. Saito et al. (2009) conducted a survey of the impact of hydrogenation of carvones, but only across 52 ORs. Linear terpenes represent a joining of two isoprene units, but most studies have only examined modifications of the proximal isoprene architecture. In aldehyde space, we have examined the impact of planarity of the C3-appended methyl (citral to citronellal) and the impact of stripping all terpene motifs to yield the bare backbone (citral/citronellal to octanal) across the OR repertoire (Araneda, Peterlin et al. 2004) (Supplementary Figure 5.2A). Saito et al. (2009) have investigated the same changes in alcohol space, but only for 52 ORs (Supplementary Figure 5.2B). Investigation of chiral preference for the C3-methyl has yet to be surveyed at a population level, but chiral discrimination has been recognized as an important characteristic for the OR1A1 and OR1A2 citronellol receptors (Schmiedeberg, Shirokova et al. 2007).

In the proposed alignment of the terpene acetate esters with HED, these most commonly manipulated sites are located at the branch point forming the cis kink that may be key for HED recognition. Using this model, specific terpenes are predicted to exhibit bias for activation among the HED+ cells that are unlikely to extend to the HED- OSN population. Confirming this bias would support the proposed alignments of the terpene esters with HED.

For this study, where effects may be particularly subtle, careful analog measures will be required. To achieve this resolution, HED flanks should surround the probe odor sets. This nesting will provide internal ratios that are more resilient to cell rundown.

Forskolin will still be given at the end to determine the maximal transduction pathway activation and confirm functional viability of the OSNs.

Proposed modified panel

Panel members, all presented @ 30uM (Figure 5.7)

(HED)	Hedione	(S-CITAC)	(S)-citronellyl acetate
(NERAC)	neryl acetate	(ISONAC)	isononyl acetate
(GERAC)	geranyl acetate	(OCTAC)	octyl acetate
(R-CITAC)	(R)-citronellyl acetate	(MENON)	methyl nonanoate
-----		-----	
(cis3-HEXAC)	cis-3-hexenyl acetate	(CONIF)	coniferan

Comparisons of particular note within this panel

Contrasting the relative response magnitudes of the cis-kinked NERAC and trans-held GERAC will provide the first repertoire-wide assessment of this geometric preference for any functional group. Previously, during analysis of I7 antagonism (Araneda, Peterlin et al. 2004) the aldehydes neral and geranial were delivered to a small number of non-I7 expressing OSNs. This revealed, rather unexpectedly, that OSNs tend to treat both geometric isomers equally or with only marginal preference (Supplementary

Figure 5.3). However, we predict that HED+ cells should form a subpopulation that exhibits exclusive or heavily biased activation by the cis neryl ester. NERAC shunts the long alkyl arm towards the proper terminus slot, but GERAC's alternate geometry would route the arm towards the ketone (Figure 5.7). Any attempts to guide GERAC's arm towards a trajectory resembling HED would lead to steric clashes between GERAC's C3 and C7 methyls. HED+ OSNs are thus expected to display a NERAC >> GERAC bias that need not be shared by the terpene ester-activated population as a whole.

NERAC's hypermorphism at HED+ receptors may partly arise because the planarity created by the C2-C3 double bond eliminates chirality of both the ester and alkyl arms. At first, this may seem detrimental since it means that NERAC cannot mold to mimic HED's most perceptually potent (1R,2S) arrangement. However, planarity also prevents NERAC from adopting any of the disfavored stereoisomers. Should any of the three alternate stereoisomers of HED serve as antagonists against the (1R,2S) version, the standard formulated HED blend would not reflect the full potential activity that could be achieved if each element was presented individually.

The impact of chiral reinstatement can be addressed using R-CITAC and S-CITAC. These compounds have the potential to restore chirality to the long alkyl arm. However, because there is no ring it is difficult to assign whether the protruding C3 methyl or the longer alkyl arm will take precedence in determining relative ligand positioning. Figure 5.7 shows the projection of the alkyl arms as if the C3 methyl was held fixed in plane with the phantom cyclopentanone ring. S-CITAC generates the alkyl arm stereochemistry found in the most perceptually potent stereoisomer of Hedione; it may thus be strongly favored over R-CITAC in terms of activation strength among

HED+ cells. As with the NERAC and GERAC pairing, this HED+ skewed S-CITAC / R-CITAC ratio preference need not be maintained among the general population of terpene-ester activated OSNs.

Comparing NERAC versus R/S-CITAC examines the same type of modification of proximal terpene features that has already been studied in alcohol and aldehyde space. However, with our panel of acetate esters we can probe additional stripping of the terpene scaffold, now at the distal isoprene module. ISONAC removes the electron density in the terminus but retains the branched bulk. Unfortunately, due to the loss of the C3 methyl as well, ISONAC cannot be directly related to R/S-CITAC.

The terminal methyl of the HED alkyl arm can rotate freely. Adding an auxiliary methyl at the terminus near the proposed “capture” location for the alkyl arm may increase potency by increasing the chance of “capture”. This is analogous to how a diacid of a given concentration would change the pH of the solution twice as much as a monoacid of the same concentration. Comparing ISONAC to OCTAC activation among HED+ OSNs can test this proposal. Reliance on a “terminal capture” mechanism, particularly when stabilizing ligands that lack a formal ring, would lead HED+ cells to show a preference for ISONAC over OCTAC.

OCTAC is the bioisosteric “cassette-swap” retro-ester pairing for MENON. Fine dissection of this polar tether is crucial for future probe design. If the HED+ population demonstrates greater activation by the acetate ester OCTAC over the length-matched methyl ester MENON, it would suggest that converting our acetate panel members to methyl esters should result in weaker forms that would “dial down” activation of HED+ OSNs. Conversely, should MENON prove more robust an activator than OCTAC, this

signals that methyl ester versions of our panel members have the potential to be more active than the already “hypermorphic” NERAC at HED+ OSNs.

Together, the initial panel and the proposed extension panel provide an opportunity to clarify the features that appear to operate in a near uniform manner across the suite of HED+ OSNs to provided graded levels of activity. This effect offers an intriguing physiological toolkit to finely set the activity of OSNs activated by a commercially relevant compound.

(this page intentionally left blank)

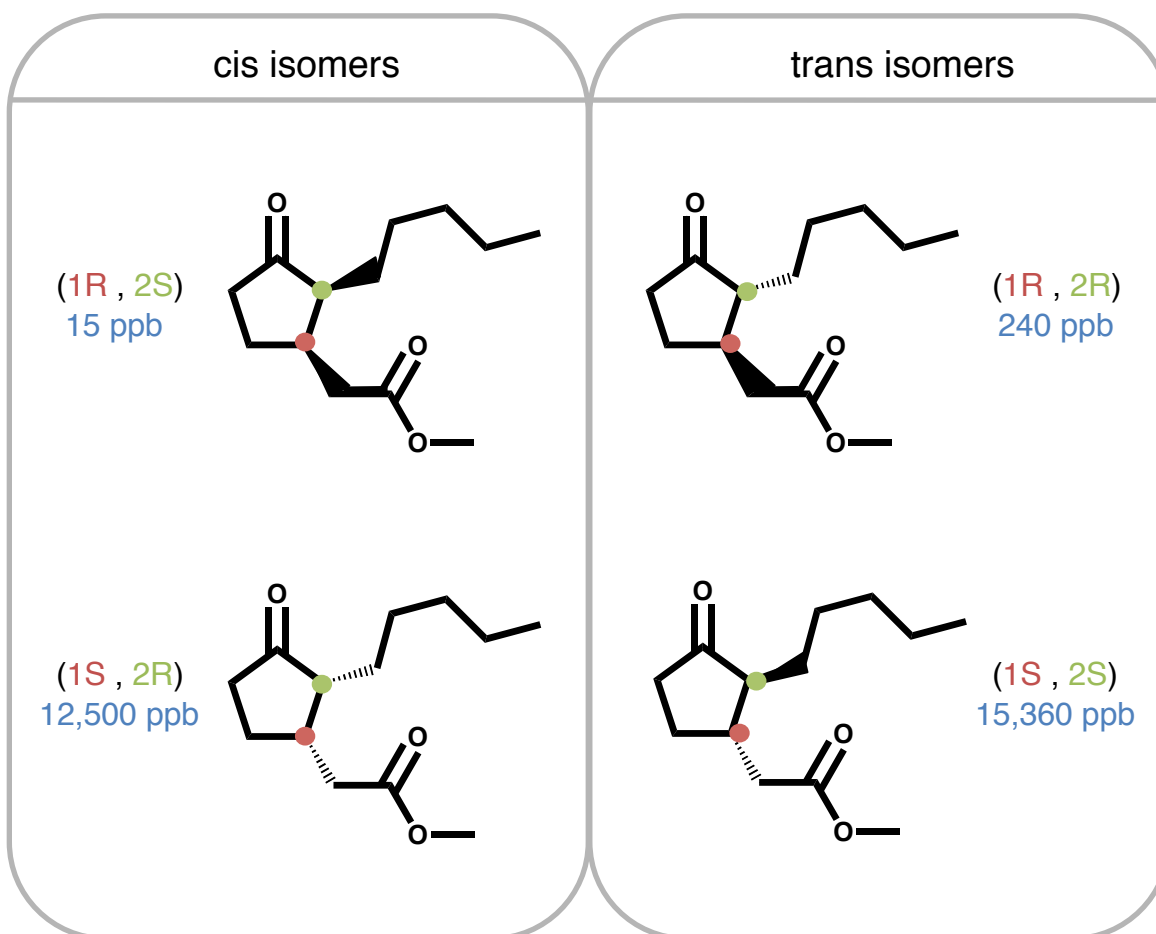


Figure 5.1 –Hedione stereoisomers. Structures of the four Hedione stereoisomers showing the relative position of the two arms and the designation for those orientations. Below is the human recognition threshold as reported by Werkhoff et al. (2002). The commercial version of Hedione used in the study that follows is a ratio of 10 cis : 90 trans.

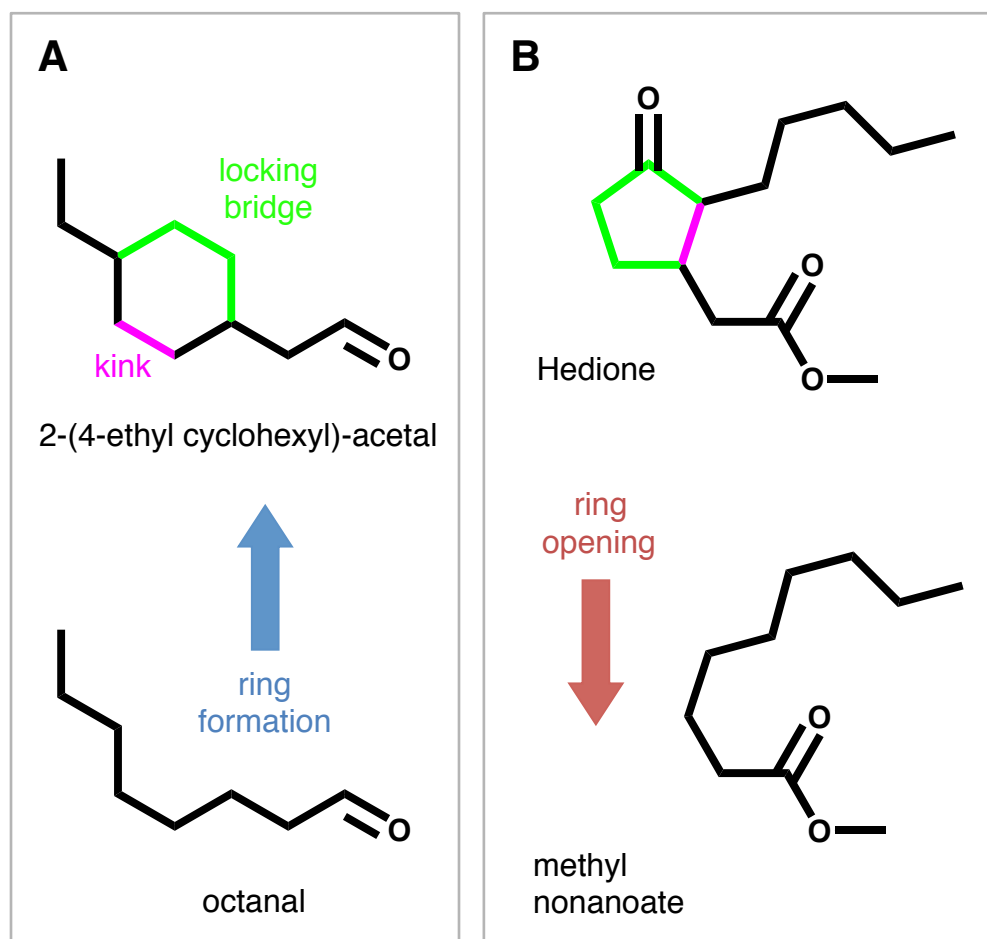


Figure 5.2 - ring closing and ring opening relationships. (A) As part of an investigation of the preferred conformation of octanal by the rat OR-I7 receptor, a strategically located cis kink (pink) was held in place by addition of a two carbon bridge (green), thus forming a cyclohexyl ring (Peterlin et al., 2008). This constrained the terminus of octanal into a particular orientation relative to the aldehyde group. (B) Hedione can be viewed as a conformationally-locked, cis-kinked version of methyl nonanoate. In this model, the cyclopentanone ring serves to maintain the cis conformation of the long backbone. The key epitope is postulated to be the relative geometry between the ester group and the distal alkyl terminus.

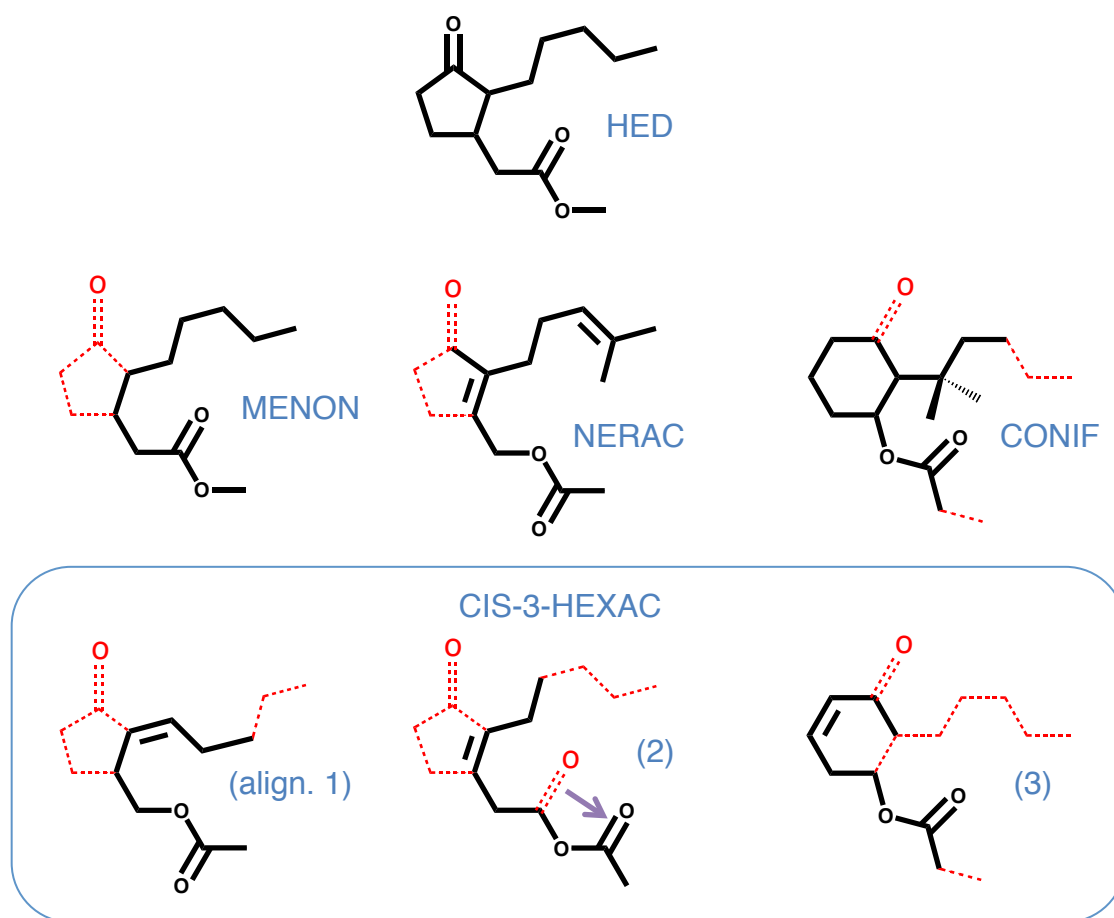


Figure 5.3 - structures of compounds used in this study. The compounds are in black, with their putative alignment to the Hedione scaffold shown in red (dashed lines). Abbreviations are as follows: HED, Hedione; MENON, methyl nonanoate; NERAC, neryl acetate; CONIF, coniferan; cis3-HEXAC, cis-3-hexenyl acetate. The alignment of cis3-HEXAC is particularly ambiguous and three possibilities are provided.

Figure 5.4 - altered polar topology of the ester arm. Potential arrangements, relative to the wall formed by the ring in HED, of the carbonyl and ether oxygens of the ester. The compounds that exhibit each polar topology, should they adopt the alignments suggested in Figure 5.3, are listed to right. Only the “cassette swap” leaves an oxygen at each of the original positions. All other alterations introduce polar groups in sites previously filled with hydrophobic substituents in HED (red arrows), or replace polar sites in HED with hydrophobic groups (open circles). Not enough is known about ester recognition to gauge the functional impact of these more pronounced alterations in polar topology.

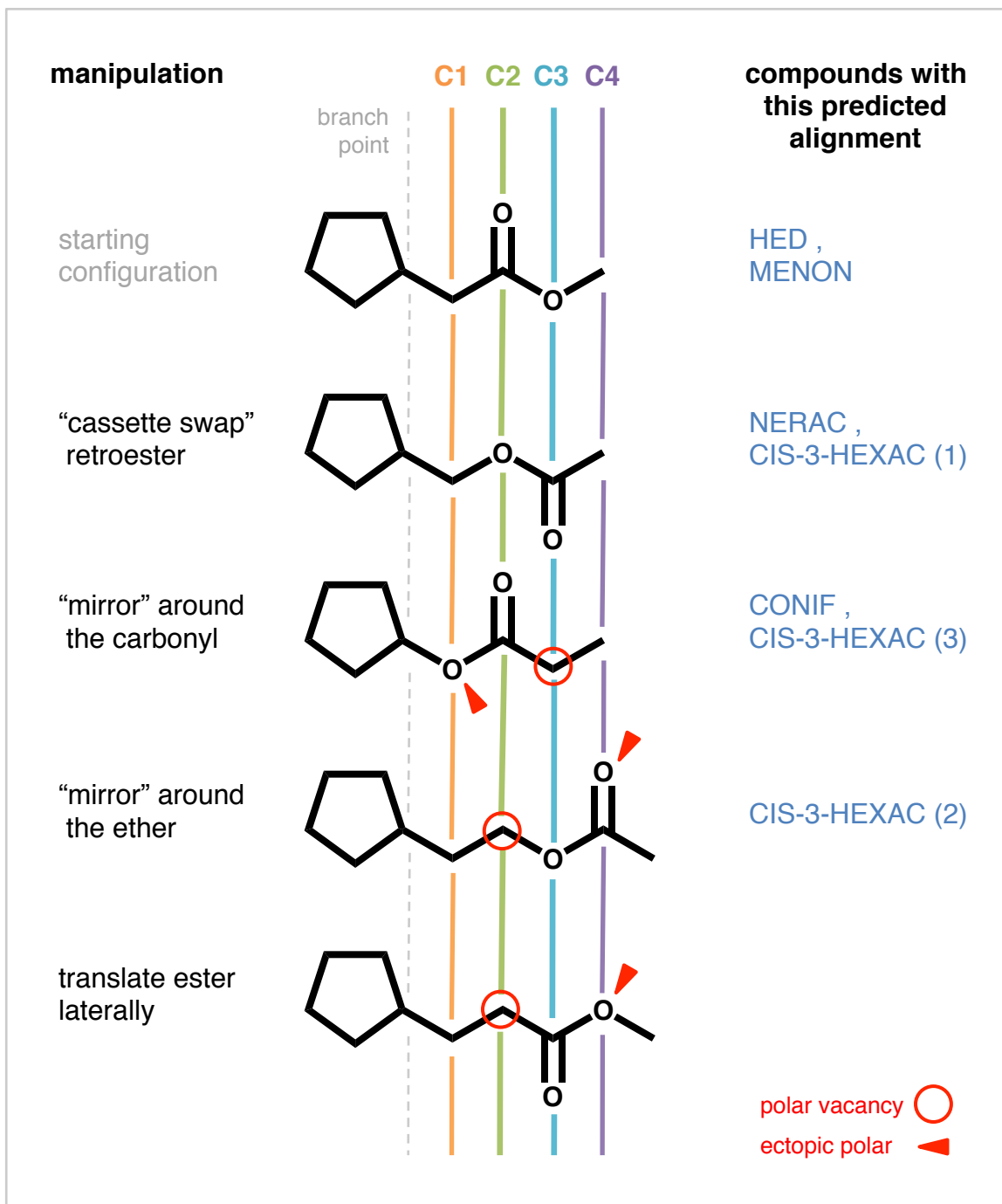
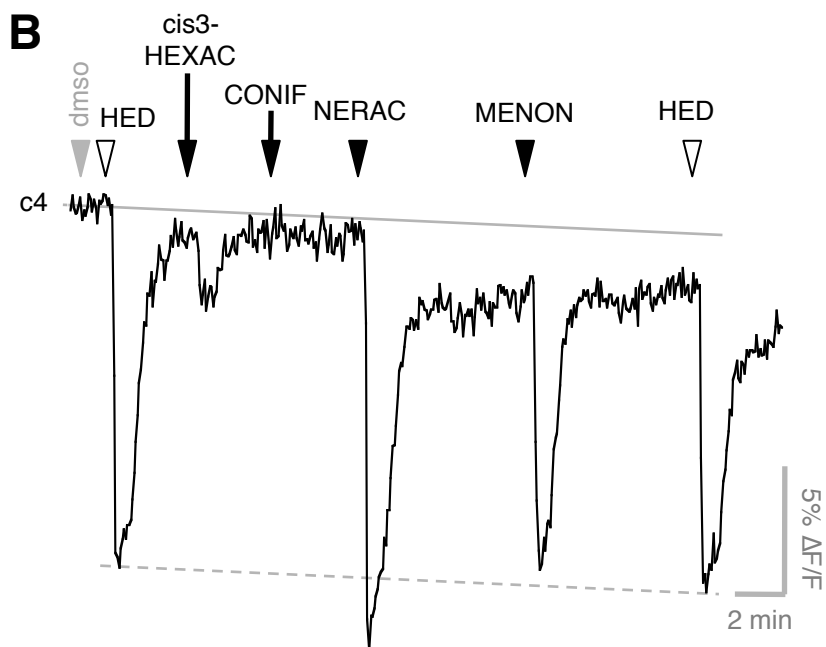
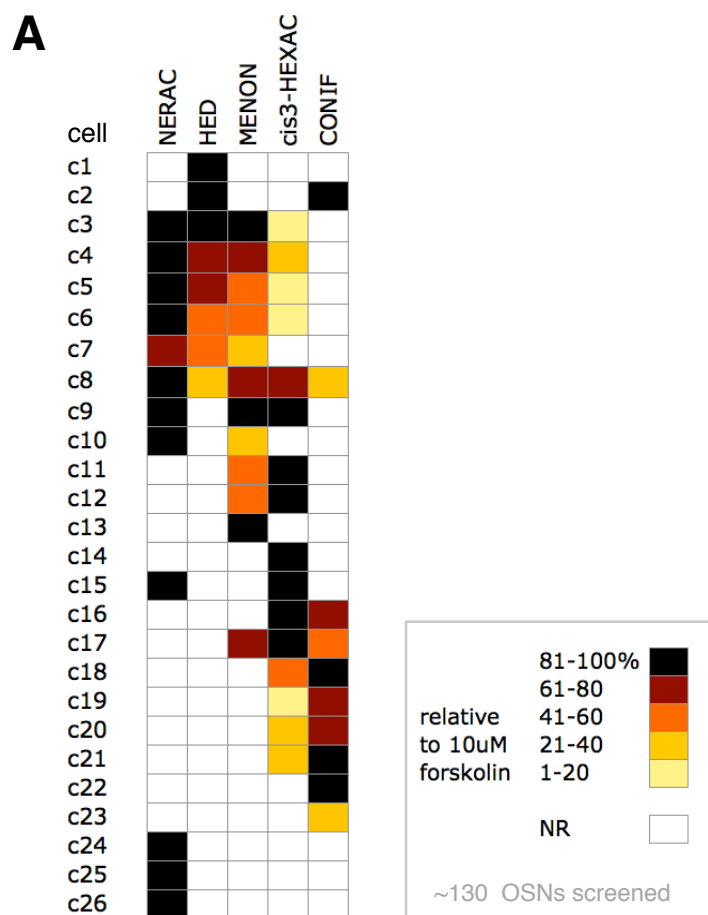


Figure 5.5 - response profiles of cells to the Hedione fragment mimics. (A) Results from a pilot probe on 103 OSNs. All odorants were delivered at 30uM. Each horizontal row is the response profile for an individual cell. Filled boxes denote a response to an odorant, with white boxes indicating that the odorant was tested but it did not elicit a response. Response magnitudes are scaled relative to the the response to 10uM forskolin, a drug that acts downstream of the OR to achieve maximal activation of the signal transduction cascade. (B) Representative calcium-imaging trace from a HED+ OSN. The dashed gray line between the HED flanks allows for assessment of the relative activation compared to HED for the compounds nested inside. NERAC elicited a greater magnitude response than HED, MENON a near equivalent response, and cis3-HEXAC a marked lower yet still present response. This was the most common pattern observed among HED+ OSNs.



(this page intentionally left blank)

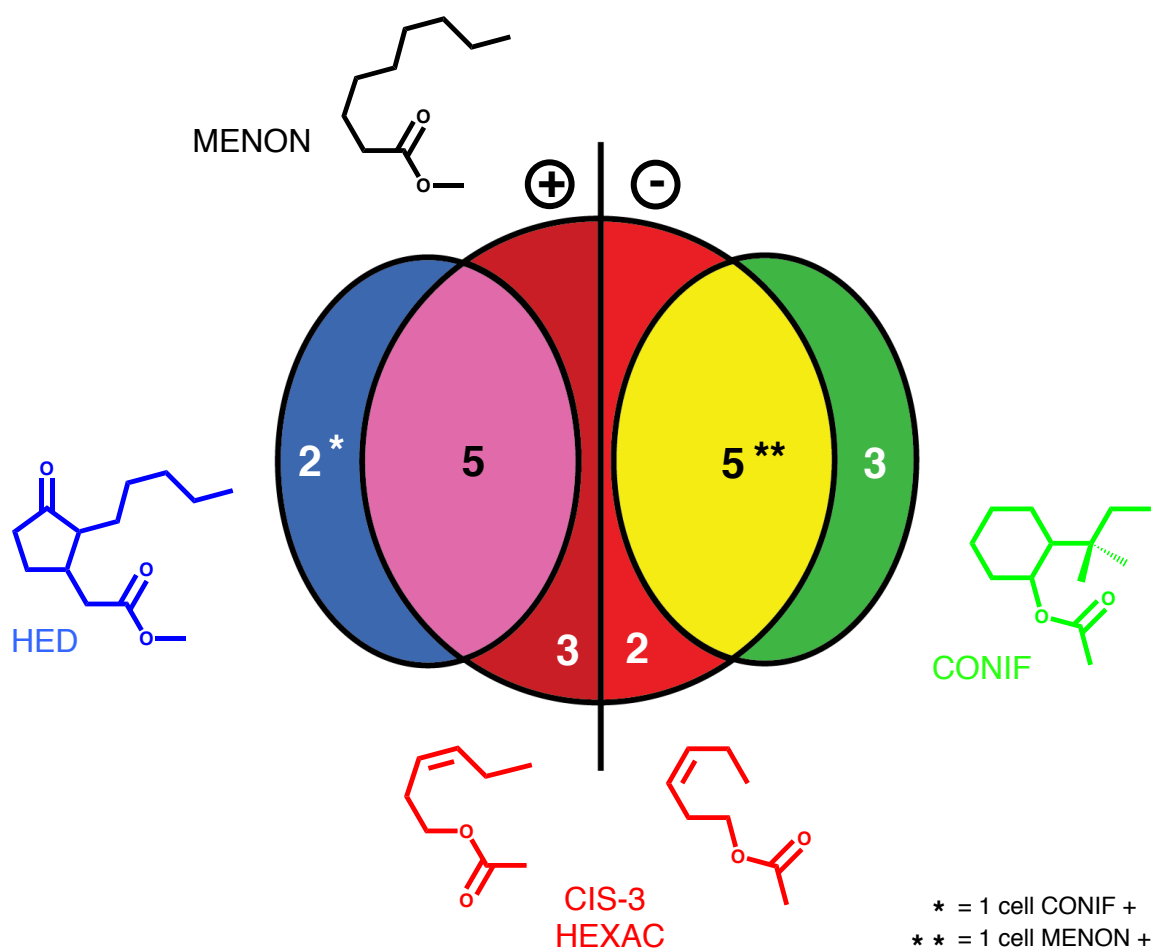
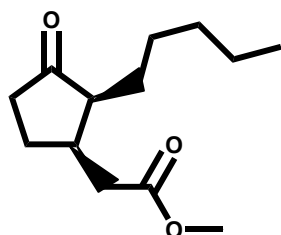
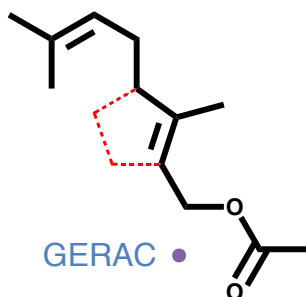


Figure 5.6 - Venn representation of response trends. Four-way Venn diagram of compound detection patterns. The HED and CONIF recruitment hardly overlaps, but cis-3-HEXAC can activate both OSN populations to equivalent degrees. When binding among the MENON+ population, the adaptable cis-3-HEXAC may assume a more open conformation, whereas at CONIF+ cells (and possibly also among MENON- cells) cis-3-HEXAC may assume a more compact form.

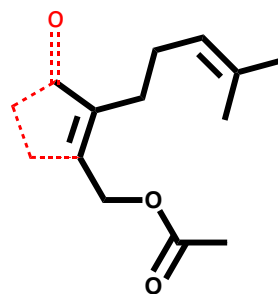
Figure 5.7 - Structures and relationships within the proposed extension panel. This extended panel allows more subtle characterization which features are critical to allow a flexible odorant to mimic the activity levels induced by HED. Emphasis is on stripping elements of the terpene scaffold of the highly active NERAC and probing the impact of the geometry of the alkyl arm. Compounds are shown in black and their proposed alignments to HED in red (dashed lines). Colored dots indicate additional relationships that can also be examined using this extended panel. HED, Hedione; NERAC, neryl acetate, GERAC, geranyl acetate; S-CITAC, (S)-citronellyl acetate; R-CITAC, (R)-citronellyl acetate; ISONAC, isononyl acetate; OCTAC, octyl acetate; MENON, methyl nonanoate.



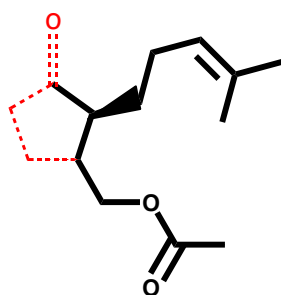
HED



GERAC •



NERAC • •



S-CITAC • •

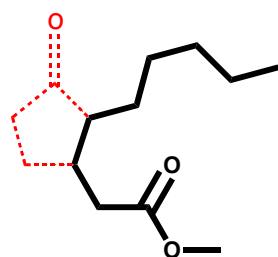
sets to examine:

cis / trans

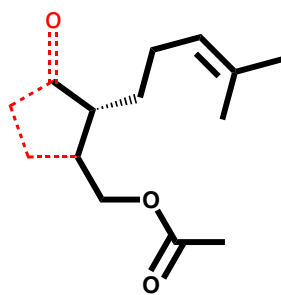
terpene stripping

chirality

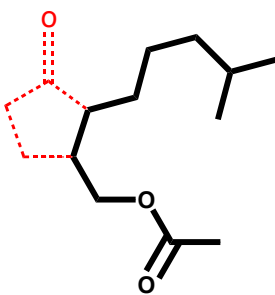
bioisosterism



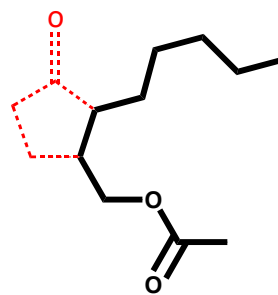
MENON •



R-CITAC • •



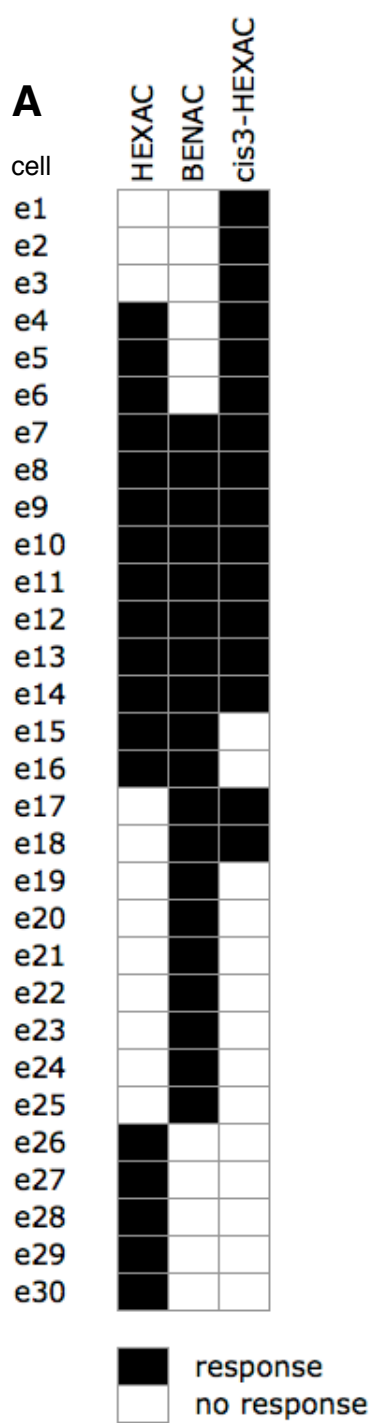
ISONAC •



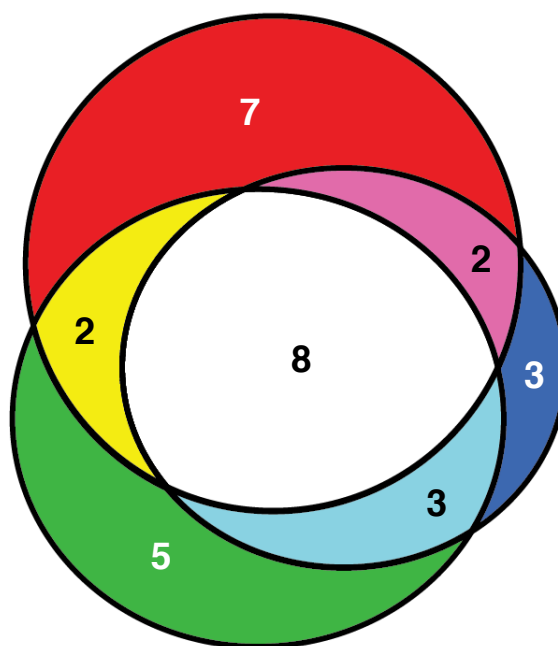
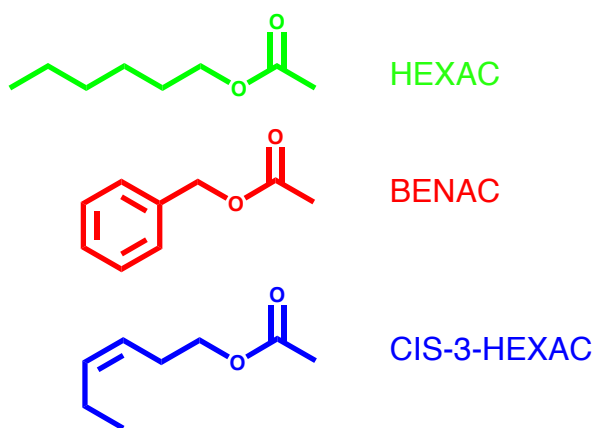
OCTAC • •

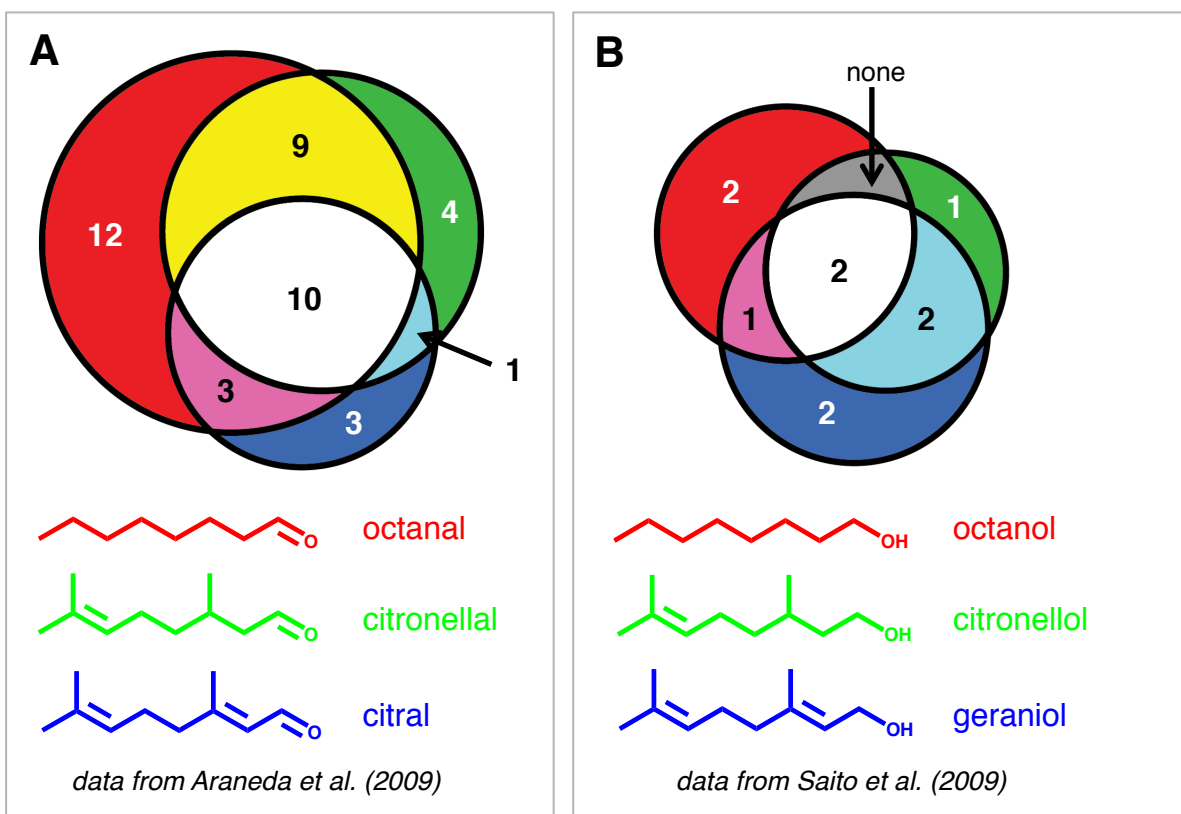
Supplemental Figure 5.1 - cis-3-hexenyl acetate as a weak mimic of a benzene ring.

(A) Results from a panel screen of 634 mouse OSNs comparing the three esters whose structures are shown in (B). Abbreviations: HEXAC, hexenyl acetate; BENAC, benzyl acetate; cis3-HEXAC, cis-3-hexenyl acetate. All compounds were tested at 30uM. Each row denotes the response pattern of a given cell. A shaded box indicates activation and a white box indicates that the odorant was tested but it did not elicit a response. (B) Structures of the panel compounds. HEXAC is fully flexible while cis-3-HEXAC has a kink that could align with the distal curve of the benzene ring in BENAC. (C) Venn diagram visualization of the data in (A). The number of OSNs exhibiting each response profile is given in the appropriate sector. HEXAC and cis-3-HEXAC both recruited many BENAC+ cells, demonstrating a surprisingly robust link between aliphatic and aromatic space. The aromatic nature of BENAC is thus not a crucial feature for at least 63% (12/19) of the responding population. HEXAC and cis-3-HEXAC each could activate nearly 50% of the BENAC+ OSN population. However, the cis-3-HEXAC+ population as a whole was more deeply embedded within the BENAC+ population (ie: there were fewer cis3-HEXAC+/BENAC- than HEXAC+/BENAC- cells). We interpret this as the pre-sculpted cis-3-HEXAC providing a mild improvement as a benzene ring mimic over the fully flexible HEXAC.

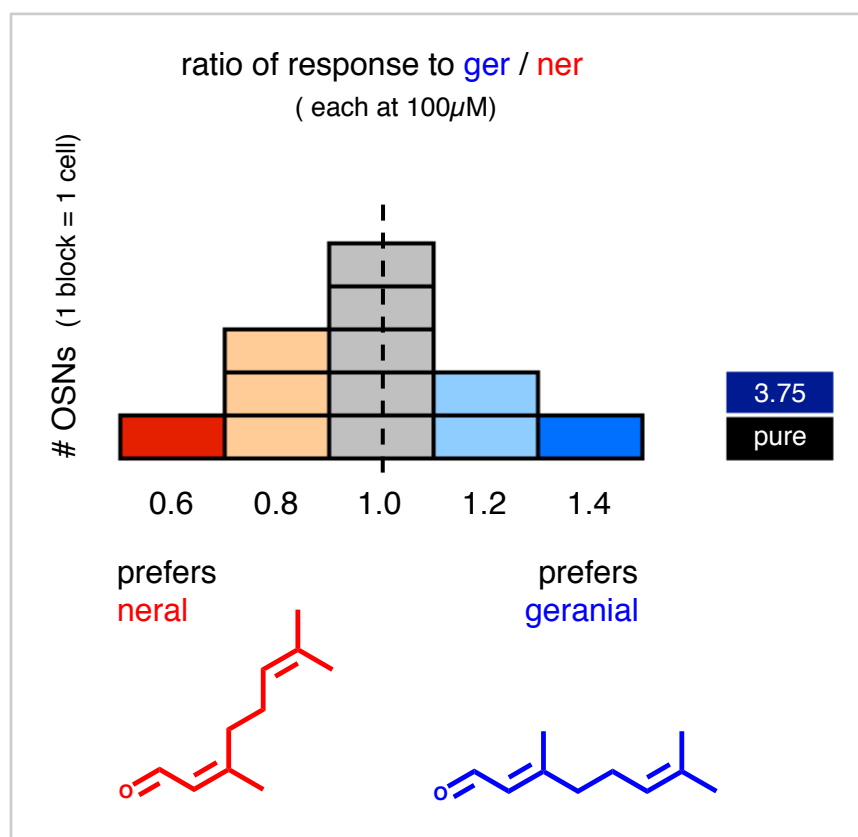


634 OSN screened

B



Supplementary Figure 5.2 - assaying terpene bias in olfactory space. Venn diagrams showing the impact of appending terpene features to a flexible octane scaffold for two functional groups. The number in each sector is the number of OSNs with that response profile out of the group tested. For n-compounds the eight carbon length is preferred; octanal and octanol each provide this core. The citronellal scaffold has a chiral methyl on C3, but it does not interfere with either functional group. The citral scaffold has a planar methyl on C3. This manipulation leads to some interference with the planar aldehyde functional group but not with the alcohol functional group. The identity of the functional group impacts the extent of co-overlap with the bare octane scaffold. This difference was most pronounced for the citral scaffold. The more permissive citronellal scaffold could be appended to either functional group and elicit similar levels of co-recruitment.



Supplementary Figure 5.3 - cis/trans preference for the isomers of citral. Citral is a blend of neral and geranial, differing in their stereochemistry between carbons C2-C3. Despite the marked difference in proximal chain trajectories, both isomers were detected by the majority of these cells. Moreover, a third of all responsive cells (5/14) exhibited magnitudes that differed by 20% or less.

(this page intentionally left blank)

CHAPTER 6**BENZENE BIOISOSTERISM AT ODORANT RECEPTORS**

ABSTRACT

Medicinal chemists utilize a variety of fragment exchanges that seem to majorly alter a compound. However, these changes actually retain key physicochemical properties such that the modified molecule continues to act on the same or similar targets. This phenomenon is called bioisosterism. One important type of bioisosterism involves exchanges of aromatic rings. Specific exchanges emphasize retention of either the electronic or steric aspects of the aromatic ring. To query whether bioisosteric principles translate well to odorant receptors (ORs), in a way that could help explain confusing and broad receptive fields, we quantified the efficacy of various replacements for benzene across the suite of ORs using acetophenone as a lead odorant. We demonstrate a robust alkyl-for-aromatic exchange between the cyclohexene ring and benzene. As both aromatic rings and cyclohexene rings are very common motifs in odorants, our results suggest intriguing new directions for rational odor design. Probing classical aromatic-for-aromatic ring transformations confirmed that the sulfur-containing heteroaromatic thiophene ring could substitute effectively for benzene at ORs. However, the OR repertoire nearly completely rejected the nitrogen-containing heteroaromatic ring odorants in our panel. This is surprising given the success of nitrogen-containing cores in pharmaceuticals; ORs, as dedicated chemoreceptors, may thus obey different rules guiding ligand recognition. Effective bioisosteric exchanges highlight how considering more abstract features can help consolidate seemingly broad receptive fields. Identifying when expected bioisosteric exchanges fail may reveal signature rules of chemical discrimination by ORs.

INTRODUCTION

Bioisosteric replacements provide the means to modestly shade some aspect of a lead compound and yet still retain the same or related receptor targeting (Patani and LaVoie 1996; Ciapetti 2008; Meanwell 2011). The selection of the specific bioisostere will depend on the property that is desirable to preserve. Such qualities can embrace steric size and shape, electronic distribution, polarity, or conformation. Aromatic rings are multifunctional functional groups that can contribute to a compound in several different ways. They can provide a unique planar topology, constrain the conformation of an appended double bond-containing arm, lock a bend in a hypothetical longer backbone, and stabilize a ligand through pi-stacking or on-edge hydrogen bonds. Different bioisosteres for benzene emphasize different aspects (Supplemental Figure 6.1). For example, the non-aromatic MOIMM moiety retains similar electronics (Patani and LaVoie 1996). But benzene rings can also serve structural functions. In benzolouge series the ring serves as an electron conduit as well as a spacer (Wermuth 2008). However, benzene has also been successfully replaced by purely alkyl rigid spacers such as propellane (Meanwell 2011). At ORs, identifying which features of an aromatic ring are critical for activation by a given ligand may provide a useful means of deciphering that receptor's contribution to the greater combinatorial code.

Over half of the currently deorphaned mouse ORs have a benzene-ring containing odorant as one of their activating ligands. These ORs can be loosely grouped into three clades based on the putative role of the aromatic ring (Supplemental Figure 6.2). In one group, MOR29A (Tsuboi, Imai et al. 2011), MOREG (Kajiya, Inaki et al.

2001), and affiliated ORs recognize multipolar odorants. Here, the benzene ring can provide electronic integration between the directly attached polar substituents. A second group of ORs, including hOR17-4 (Spehr, Gisselmann et al. 2003) and mouse I7 (Bozza, Feinstein et al. 2002), recognize odorants such as bourgeonal and cinnamaldehyde. In these ligands, the benzene ring may help shunt the alkyl backbone into a defined conformation. A third group of ORs, such as m139-3 (Yoshikawa and Touhara 2009) and M71 (Bozza, Feinstein et al. 2002), recognize compact monopolar aromatics such as m-cresol and acetophenone. Because the aromatic ring forms the bulk of these odorants, the ring's role is more obscure.

The recent heterologous screen that identified seventeen novel ORs that respond to acetophenone (ACE) also revealed a staggering variety of co-activating ligands (Saito, Chi et al. 2009). Their breadth of response greatly challenges the concept of what it means for odorants to be “similar”. Bioisosterism may provide a useful framework for conceptualizing cross-recognition of diverse functional groups and hydrocarbon scaffolds. Indeed, bioisosterism invites reconsideration of the label “broadly tuned” because it underscores that the essential features for activation may be more abstract.

Through the lens of bioisosterism and medicinal chemistry, the high overlap of ACE+ ORs with 4-chromanone and coumarin (Saito, Chi et al. 2009) seems less surprising. 4-chromanone can be viewed as an isosterically-substituted and conformationally locked ACE. Coumarin can be viewed as a modified vinylogue of ACE. Both of these frequently co-activating odorants are aromatic.

But strikingly, nearly 50% (9/17) of ACE+ ORs were co-activated by carvones (Saito, Chi et al. 2009). This suggests a privileged relationship between a benzene ring

and the cyclohexene ring that forms the core of the carvones. Another relationship between aliphatic and aromatic space was revealed during expanded testing of the ACE+ receptor M72. Short tiglate esters were shown to be quite effective agonists (Soucy, Albeanu et al. 2009). Intriguingly, the tiglyl group can be viewed as a distally “trimmed” cyclohexene ring. As the tiglyl and cyclohexene groups do not afford aromaticity, it suggests that some minimal rigid scaffolding combined with simple conjugation of the carbonyl can often suffice in lieu of a benzene ring, at least in the acetophenone context.

To better assess these potential bioisosteric substitutions, we screened odorants matched to the ACE scaffold against a large and unbiased population of olfactory sensory neurons (OSNs) that represent a sizable portion of the mouse OR repertoire. For comparison, we assayed classical heteroaromatic ring isosteric transformations. Replacing benzene rings with heteroaromatic rings preserves the electronic and steric aspects but it introduces the issue of ring polarity. The presence of electronegative heteroatoms sets up dipole moments of varying magnitude in the core (Supplemental Figure 6.3). The placement of appended arms relative to the heteroatom can thus permit tuning of functional group strength in a conjugated system. This strategy provides an unprecedented palette for the pharmaceutical chemist. By assaying representative heteroaromatic rings across the OR repertoire, we can gauge whether these tools are suited for the fragrance chemist as well.

METHODS

All procedures were conducted in accordance with Columbia University's Institutional Animal Care and Use Committee, following relevant national guidelines and laws.

Details of the preparation, perfusion, and imaging have been described previously (Araneda, Peterlin et al. 2004; Peterlin, Li et al. 2008). Briefly, calcium imaging was performed on isolated mouse OSNs, taking advantage of expression of only one OR type per OSN (Chess, Simon et al. 1994; Malnic, Hirono et al. 1999). The cellular activity can thus be taken as a proxy for the receptor activity. The entire olfactory epithelium from 6 week old, male C57BL6 mice was harvested, enzymatically treated, and dispersed onto coverslips as previously described. Odors were applied by aqueous delivery to ensure that compounds are compared at equimolar concentrations (30uM). All solutions were prepared fresh daily. OSNs were loaded with the calcium indicator fura-2AM to monitor responses to acute applications of odorant solution into the constant perfusion washing over the cells. Stimuli were applied every 5 minutes. Acetophenone was given intermittently to assess cell health, and forskolin (10uM) was applied at the end to elicit maximal pathway transduction and assess viability of the cells.

RESULTS

Alkyl ring substitutions

The set of odors assayed are presented in Figure 6.1. In selecting potential alkyl bioisosteres for the benzene ring in ACE, we reasoned that the conjugation of the aromatic ring with the carbonyl might be an important feature. We positioned the methyl ketone arm to retain this coupling, and thus the scaffolds are matched electronically, varying only in steric bulk. The tiglyl core has a methyl branch off the double bond, enabling it to rigidly mimic the proximal half of the aromatic ring. However, it cannot provide distal steric buttressing. The cyclohexene ring has a greater hydrophobic surface area to better match the benzene ring. However, it assumes a half-chair conformation that causes the distal carbon to veer sharply out of plane and resemble cyclopentane (Herdewijn and De Clercq 2001). Bioisosteric exchanges with this ring may thus demonstrate pronounced position-dependent effects. The cyclopentene ring fills an intermediate surface area, but the proximal carbons to the ketone arm do not align as precisely as in the other two scaffolds.

Cyclohexene as an effective alkyl bioisostere for a benzene ring

We find that both ACE and 1-acetyl-1-cyclohexene (CYC6) were effective recruiters across the OR repertoire, activating ~3.0% of OSNs. The two OSN populations demonstrated mutually similar ability to recognize the converse compound,

with 63% (21/33) of the ACE+ cells responding to CYC6 and 65% (21/32) of the CYC6+ cells responding to ACE (Figure 6.2A). Cyclohexene thus can serve as an effective bioisostere for benzene. Still, the retention of a substantial population of OSNs able to make the discrimination between ACE and CYC6 means that each compound retains an independent signature despite the high degree of co-activation.

Analogues of CYC6 which have an altered distal geometry were more impaired in their ability to substitute for ACE. Reducing the ring size to yield 1-acetyl-1-cyclopentene (CYC5) had a more profound impact on overall recruitment than did clipping off the distal portion of the cyclohexene ring to yield a tiglyl moiety. CYC5 activated only 1.0% of OSNs, while the smaller 3-methyl-3-penten-2-one (TIG) recruited 2.2% of OSNs. This is somewhat surprising; among n-odorants, lower molecular weight compounds tend to be more poorly recruiting (Sato, Hirono et al. 1994; Kaluza and Breer 2000). We speculate that the structural openness of TIG may grant it access to sterically occluded sites in OR binding pockets that would exclude full rings.

A steric spectrum between three alkyl mimics of benzene

Despite lower global recruitment, CYC5 was a better mimic of CYC6, co-activating 6 out of 11 CYC6+ cells (55%). TIG only activated 3 out of 11 CYC6+ cells (27%) (Figure 6.3A). We also noted a spectrum for activation ranging from TIG to CYC5 to CYC6 (Figure 6.3B). OSNs could respond exclusively to the TIG or CYC6 flanks, and they could respond to either flank in combination with CYC5. However we did not observe any CYC5-exclusive cells or cells that responded to both CYC6 and TIG

while rejecting CYC5. While intriguing, we caution that the population tested with all three alkyl scaffolds is currently small and these trends await extended validation.

Heteraromatic ring substitutions : selection of aromatic cores

To provide a frame of reference for the frequency with which we observed these bioisosteric alkyl substitutions, we performed classical isosteric heteroaromatic ring exchanges for benzene (Ciapetti 2008). We compared the responses of ACE to a series of analogs with the ketone placed adjacent to the heteroatom. The probe odorants consisted of the sulfur containing 2-acetyl thiophene (THIP), the nitrogen containing 2-acetyl pyridine (PYRD) and acetyl pyrazine (PYRZ) compounds, and the mixed sulfur-nitrogen substituted 2-acetyl thiazole (THIZ) (Figure 6.1).

These aromatic cores each possess different properties (Supplemental Figure 6.3). Thiophene is the most apolar heteroaromatic ring after benzene, but the sulfur sets up a small intrinsic dipole. The symmetrical positioning of the two nitrogen groups in PRYZ leads to absence of a core dipole, and so the strength of the appended carbonyl group should be identical in strength to ACE. However, a pyrazine ring has a markedly different polar topology than does a benzene ring. THIZ could be considered a secondary isostere of either THIP or PYRD. We also included the oxygen-containing 2-acetyl furan (FUR) for comparison to THIP. Although a sulfur and oxygen are isosteric in an alkyl context, aromatic furans and thiophenes are distinct; sulfur has an expanded valence shell that enables THIP to achieve more resonance structures (Bradlow HL. 1947). The core of FUR has a slightly greater dipole than in THIP, but both align in the same direction.

The orientation should theoretically improve the partial negative charge on the carbonyl and assist with ligand stabilization.

OR repertoire-wide rejection of nitrogen-containing heteroaromatic cores

Nitrogen-containing heteroaromatic rings are highly successful substitutions for benzene rings among pharmaceuticals (Sheridan 2002). But while well tolerated by common drug targets, such exchanges were rejected by the ORs. Only 1 / 664 OSNs was activated by PYRD (Figure 6.4A), and only 1 / 501 OSNs was activated by PYRZ (Figure 6.4B). The single PYRZ+ OSN failed to respond to ACE, despite the similar lack of a core dipole in both compounds. This suggests that ORs are sensitive to polar topology, with the binding pocket architectures generally disfavoring such polar intrusions. THIP elicited a robust 2.0% recruitment, but this collapsed to 0.2% recruitment upon introduction of the nitrogen to the ring in THIZ. The one cell that was marginally THIZ+ failed to respond to THIP (Figure 6.4C).

Thiophene as the best bioisostere for benzene among ORs

Figure 6.5 compares the cellular response profiles for the four most successful isosteres for benzene among ORs. Thiophene and benzene isosterism was well conserved, with 60% (19/31) of ACE+ OSNs responding to THIP (Figure 6.5B). The THIP recruitment was well embedded in the ACE activation code with only 10% of THIP+ cells demonstrating exclusion of ACE (2/21). Thus, even though THIP and CYC6

elicited the same overall degree of recognition by ACE+ OSNs, there are far fewer “residual” THIP+/ACE- cells, than CYC6+/ACE- cells. This arrangement makes a THIP+ signature a more reliable indicator of ACE detection and cleanly demarcates a subpopulation of the ACE+ code.

A suspected polar filter underlying a “spectrum” among heteroaromatic rings

As expected from differences in their physicochemical properties (Bradlow HL, 1947), the thiophenes and furans were well discriminated by the ORs. 71% of THIP+ OSNs rejected FUR (Figure 6.5C). The few FUR+ ORs that rejected THIP also rejected ACE (Figure 6.5A, cells c36-37). This creates a “spectrum” going from ACE to THIP to FUR. Along this spectrum the odorants became more challenging to detect. There was significant attrition at each step, with 40% of ACE+ OSNs failing to respond THIP and 40% of THIP+ OSN failing to respond to FUR. Based on our results with the nitrogen-containing heteroaromatic rings and the failure of PYRZ to activate ACE+ cells in particular, we suggest this graded attrition may be due to increased polar topology of the ring. One result of this arrangement is that if an ACE+ OR could tolerate FUR, then it always accommodated THIP (Figure 6.5A c29-33 and Figure 6.5C). Furthermore, there were no THIP-exclusive cells; all responded to at least one of the flanking members of the spectrum.

Extensive cross-recognition between aliphatic and aromatic space

Comparing the most effective isostere of each type (the aromatic THIP and aliphatic CYC6) against the lead compound ACE revealed that ~75% of ACE+ cells (21/29) accepted at least one alternate scaffold with the overwhelming majority of ACE+ OSNs tolerating both (Figure 6.6). This large OR population, however, should not be confused as having broad tuning for they very restrictively excluded highly polar rings and were selective with regards to alkyl ring geometry.

DISCUSSION

When manipulating drugs to improve their pharmacological profiles, medicinal chemists often use targeted bioisosteric exchanges. These chemical fragment swaps may look discrepant, but they are designed to retain key physicochemical properties. When effective, these manipulations create a range of compounds that are still active at the designated target. In olfaction, it may be useful to consider this process in reverse. Some ORs exhibit receptive fields populated by odorants with diverse functional groups and hydrocarbon scaffolds. Approaching this cohort of chemicals from a bioisosteric viewpoint may help highlight which features are truly crucial for ligand recognition.

The high degree of co-recognition of acetophenone and carvones (Saito, Chi et al. 2009) suggested that comparing benzene ring and aliphatic cyclohexene ring cores could prove particularly informative. Over half of the ORs deorphaned to date have agonists

containing a benzene ring. The cyclohexene ring is present in a number of odorants used in perfumery, such as lylal and beta-ionone (Supplementary figure 6.2, bottom).

We elected to examine the exchange of a cyclohexene ring for a benzene ring by using simple conjugated methyl ketones. We found that the aliphatic cyclohexene ring is indeed a potent bioisostere for benzene. CYC6 co-activated 63% of the ACE+ OSN population and likewise, ACE was recognized by nearly 65% of the CYC6+ OSN population. This is the same approximate level that we noted for the classical isosteric substitution between THIP and ACE (60%). This is an important standard; among pharmaceuticals, the thiophene replacement for benzene ranks as the 11th most frequent out of 18,275 exchange pairs analyzed in the 2001 MDL Drug Data Report database (Sheridan 2002).

Cyclohexene demonstrates unusual geometry with the distal-most carbon bending sharply out of plane (Herdewijn and De Clercq 2001). Intriguingly, the aldehyde of one isomer of lylal falls at this specialized point. Some ORs may prefer this geometry over the full planar arrangement offered by benzene. In the screen conducted by Saito et al. (2009) screen, 2 out of 17 ACE+ ORs responded more potently to the cyclohexene-containing carvone than to ACE. Occasionally, we noted ACE+ cells with a 1.5 to 3-fold greater response magnitudes to CYC6 (data not shown). Exploration of whether regioisomerism contributes to this effect is underway.

While CYC6 had the most prior support in literature for being a potential bioisostere for benzene, we also investigated the role of ring geometry and necessity for a formal ring by testing the five-membered alkene version CYC5 and the distal terminal “trimmed” version TIG. We noted an interesting spectrum of recruitment by these

compounds arrayed by geometric size / surface area in the order CYC6 to CYC5 to TIG. CYC6 and TIG could both be selectively recognized. However, CYC5-exclusivity was never observed, nor was the ability of a TIG+/CYC6+ cell to reject CYC5. This finding further adds to a growing “rule set” concerning the alkyl scaffold portion of odorants and how they critically shape boundaries of the receptive field.

TIG provides better alignment with the proximal portion of CYC6 and it offers equivalent electronics. Yet CYC6+ cells only modestly recognized the smaller TIG. This suggests a need for a certain degree of hydrophobic contact area or the ability to fill a distal terminal hydrophobic position among these OSNs. At the I7 receptor, we have found that short-chain n-aldehydes and long-chain constrained aldehydes of comparable extended length can both be antagonists, but the short-chained compounds have weaker potencies (Peterlin, Li et al. 2008). This further supports that hydrophobic surface area is an important feature to attend to.

Rearrangement of the tiglyl group to a prenyl group offers an additional way to probe the CYC6+ and ACE+ OSNs populations. Conceptually, the prenyl group can be viewed as a methyl-displaced tiglyl group. Two alignments can place the electron density in prenyl acetate within an imagined aromatic ring. One alignment pairs prenyl acetate with benzyl acetate while the other pairs prenyl acetate with phenyl acetate. Support for both exists at a handful of receptors (Saito, Chi et al. 2009), but this relationship needs to be evaluated on an OR repertoire-wide level.

A very unexpected finding of this study was that nitrogen-containing heteroaromatic ring exchanges that are a staple in medicinal chemistry failed to demonstrate compatibility at ORs. The exchange between benzene and a 2-position

attached pyridine ranks 20th out of 18,275 exchanges compiled in the MDL Drug Data Report (Sheridan 2002). However, we found almost no recruitment across the mouse ORs when using this substitution. The other nitrogen heteroaromatic analogs of ACE that we tested were equally poor activators. This even included PYRZ, which has no intrinsic core dipole and thus the strength of its ketone is unperturbed relative to ACE. Disfavor of aromatic nitrogens extended to secondary isosteres where other heteroatoms were present. In our screen THIP proved to be a robust isostere, co-activating ~60% of the ACE+ population. However, inclusion of nitrogen to generate THIZ abolished this activity. The pronounced abrogation that we see using methyl ketones parallels that reported for bare cores. Using intrinsic activity to monitor OR activity in the dorsal olfactory bulb, thiophene was found to activate a substantial number of glomeruli but only a scant fraction of these were activated by thiazole (Matsumoto, Kobayakawa et al. 2010).

Tentatively, we suggest that the binding pocket of ORs may be sensitive to polar intrusions unless these can be offset by hydrogen bonding. The underlying effect that filters out the nitrogen-containing heteroaromatic rings may also contribute to the attrition we see along the spectrum ACE to THIP to FUR. The oxygen-containing FUR has a slightly stronger dipole than THIP, a feature that would amplify the partial negative charge on the appended carbonyl and permit a stronger hydrogen bond. However, FUR was excluded from the majority of THIP-accommodating pockets. It appears that polar constitution of the ring outweighs the expected benefit of improved ligand stabilization.

In summary, by applying the pharmaceutical chemistry concept of bioisosterism we were able to identify a robust link between aromatic and aliphatic chemical space via

two moieties that are common among odorants: a benzene ring and a cyclohexene ring. We identified a population-wide spectrum for recruitment across ACE, THIP, and FUR that we believe relates to ring polar topology and another spectrum across CYC6, CYC5, and TIG relating to alkyl scaffold geometry. Such rule systems underscore how mechanisms of OR ligand binding can strongly constrain the combinatorial code.

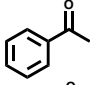
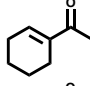
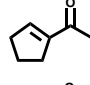
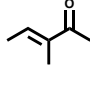
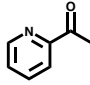
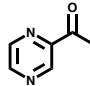
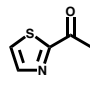
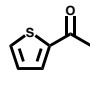
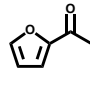
name		abbr.	% active	# responding / # viable OSNs
acetophenone		ACE	3.1 %	(33 / 1046)
1-acetyl-1-cyclohexene		CYC6	3.1 %	(32 / 1046)
1-acetyl-1-cyclopentene		CYC5	1.0 %	(4 / 382)
3-methyl-3-penten-2-one		TIG	2.2 %	(12 / 545)
2-acetyl pyridine		PYRD	0.2 %	(1 / 664)
acetyl pyrazine		PYRZ	0.2 %	(1 / 501)
2-acetyl thiazole		THIZ	0.2 %	(1 / 545)
2-acetyl thiophene		THIP	2.0 %	(21 / 1046)
2-acetyl furan		FUR	0.8 %	(8 / 1046)

Figure 6.1 - compounds used and their recruitment frequencies. Structures and abbreviations for all odorants used in this study. At far right is the number of OSNs each compound was tested on, and how many of those cells responded. Levels of recruitment vary dramatically; ACE and CYC6 performed nearly 10 times better than the nitrogen-containing heteroaromatic compounds PYRZ, PYRD and THIZ.

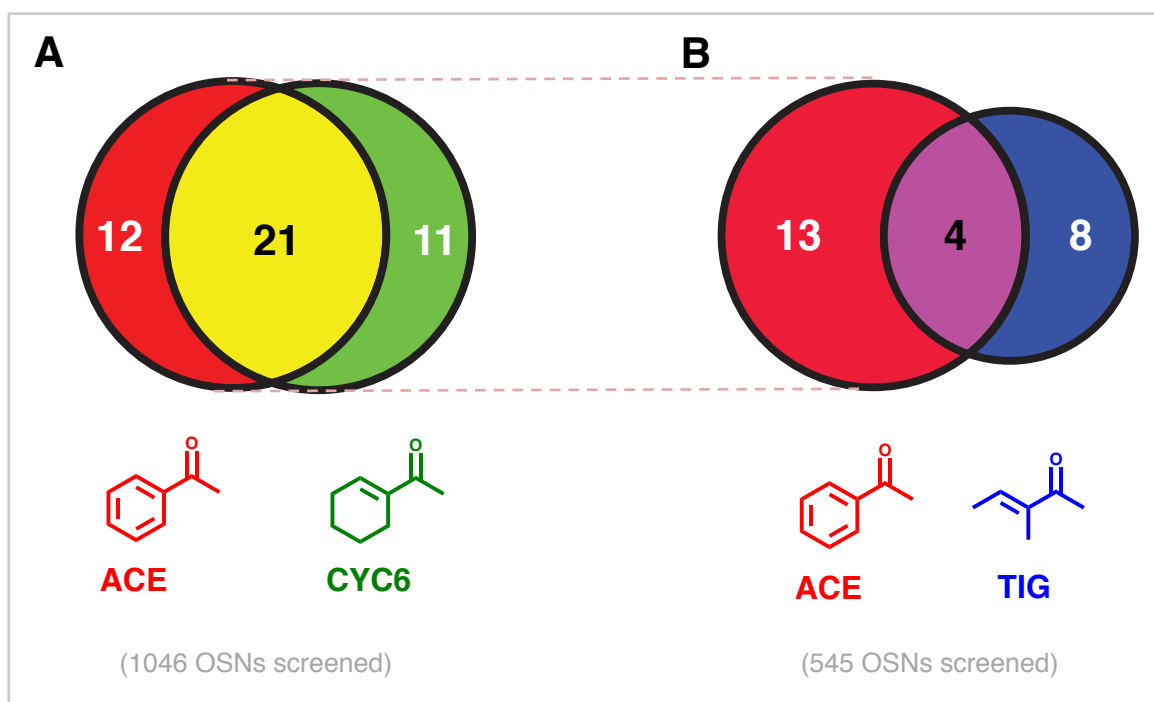


Figure 6.2 - overlap between aromatic and aliphatic odorant space. Venn diagram showing the population analysis of the recruitment by ACE with CYC6 and a truncated analog. The numbers in each sector correspond to the number of OSNs with that activation profile. **(A)** ACE and CYC6 each activated populations of similar sizes and the members could recognize the alternate compound with similar frequencies. **(B)** Conceptual truncation of CYC6 to yield the acyclic but rigid TIG reduced the recruited population size and also altered the extent of overlap with ACE. Only 23% of ACE+ OSNs can also respond to TIG, whereas 63% of ACE+ OSNs responded to CYC6. This marks CYC6 as the preferred alkyl bioisosteric replacement for a benzene ring.

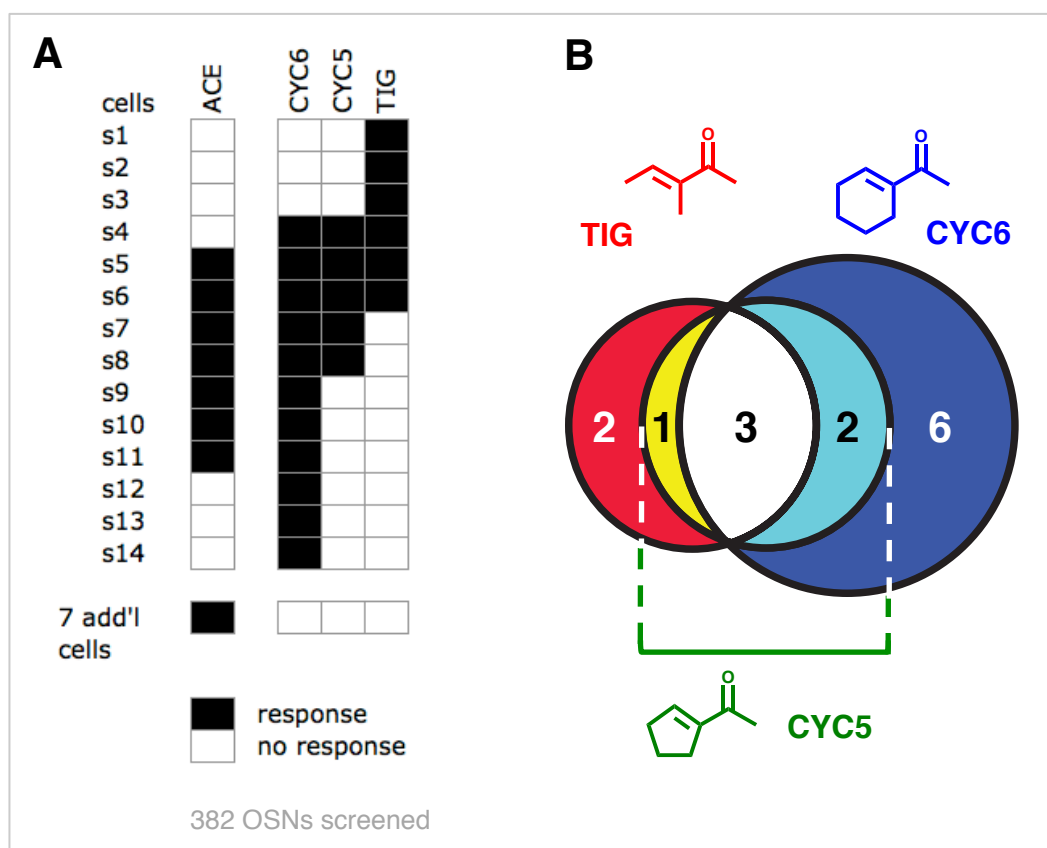


Figure 6.3 - co-recognition among the alkyl scaffolds. (A) Response profiles from a screen of 382 OSNs challenged with all three alkyl scaffolds. The scaffolds, in terms of decreasing steric size, are listed at right. The response to the aromatic ACE is provided for comparison at left. Each row denotes a different OSN. Shaded boxes denote a response and white boxes denote that a compound was tested but it did not elicit a response. A steric “spectrum” was observed in terms of activation, with no cells able to achieve a CYC6+/TIG+ signature without also responding to CYC5. (B) Venn diagram providing an alternate visualization of the overlap in recruitment between the three alkyl scaffolds. The number in each sector corresponds to the number of OSNs with that response profile. The fully embedded aspect of CYC5 is evident.

(this page intentionally left blank)

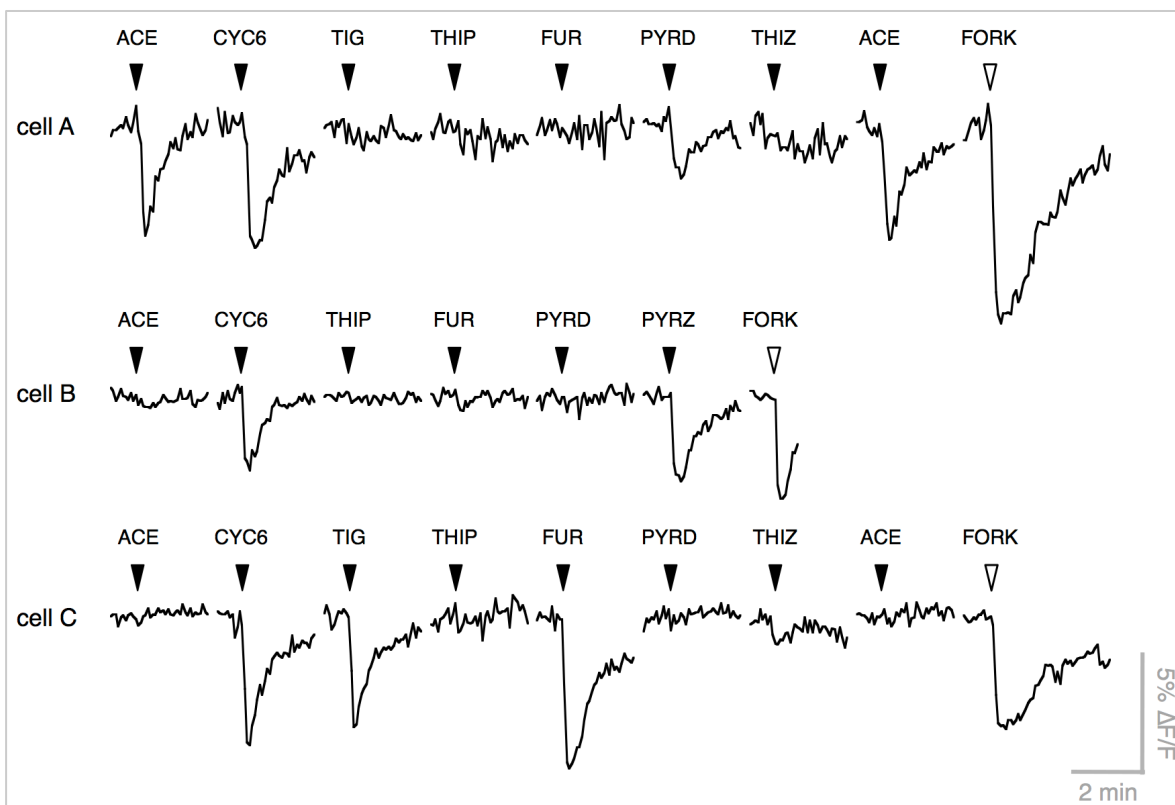
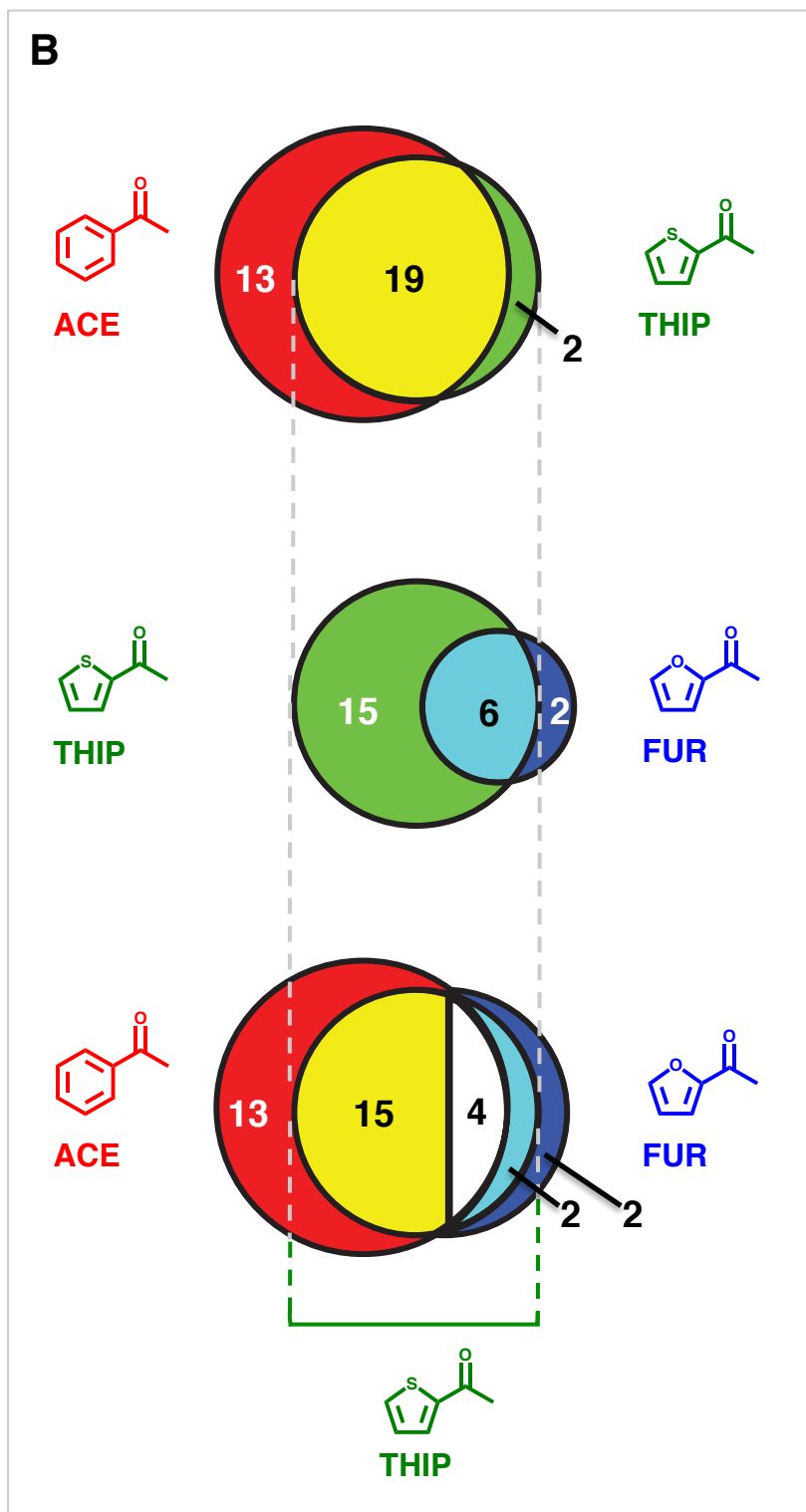
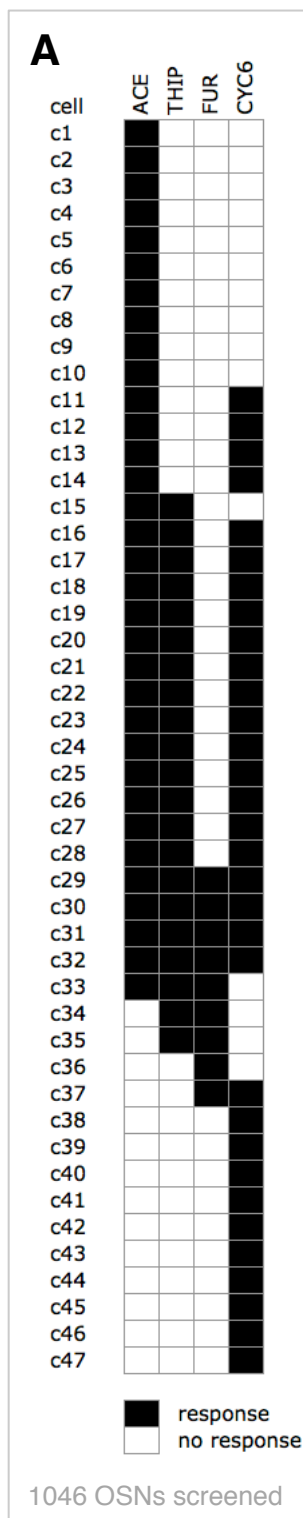


Figure 6.4 - response profiles for OSNs responding to nitrogen-containing heteroaromatic compounds. These three OSNs were the only ones to detect nitrogen containing compounds out of over 500 OSNs screened. Surprisingly, CYC6 was a robust activator for all three. (A) PYRD, which can be viewed as a nitrogen substituted ACE, could robustly activate this ACE+ cell. THIZ can be considered an isostere of PYRD in which one carbon is replaced by sulfur. However, this alteration eliminated activity. (B) This cell required the dual nitrogens of PYRZ, failing to respond when only one nitrogen was present in PYRD. While the pyrazine core has no dipole, this is not the primary determinant for activation; benzene also has no dipole, yet ACE did not exhibit a response. (C) This cell showed a very small but reproducible response to the sulfur and nitrogen-containing THIZ. Presenting the heteroatoms in isolation (THIP and PYRD) did not improve the response strength.

Figure 6.5 - co-recognition between ACE and other aromatic odorants. (A)

Response profiles from screening 1046 viable OSNs. Each row denotes a different OSN. A shaded box indicates a response and a white box indicates that the compound was tested but it did not elicit a response. ACE, THIP, and FUR are the aromatic compounds. CYC6 is an alkyl compound listed for reference at far right. **(B, top)** Venn diagram representation of response patterns. The number in each sector denotes the number of OSNs with that profile. THIP could recruit many ACE+ OSNs, and the THIP+ population was nearly completely embedded within the ACE+ population. **(middle)** Only modest overlap exists between THIP and FUR activation, as expected from the different degree of aromaticity and magnitude of the intrinsic ring dipole. THIP+ cells could very effectively exclude FUR (71% exclusion), but FUR+ cells could not readily exclude THIP (25% exclusion). **(bottom)** Three-way comparison shows that the THIP+ population can be fully recruited by a combination of ACE and FUR. That is, an OSN cannot respond to ACE and FUR without also responding to THIP. Much of this overlay is contributed by the high co-recognition between ACE and THIP.



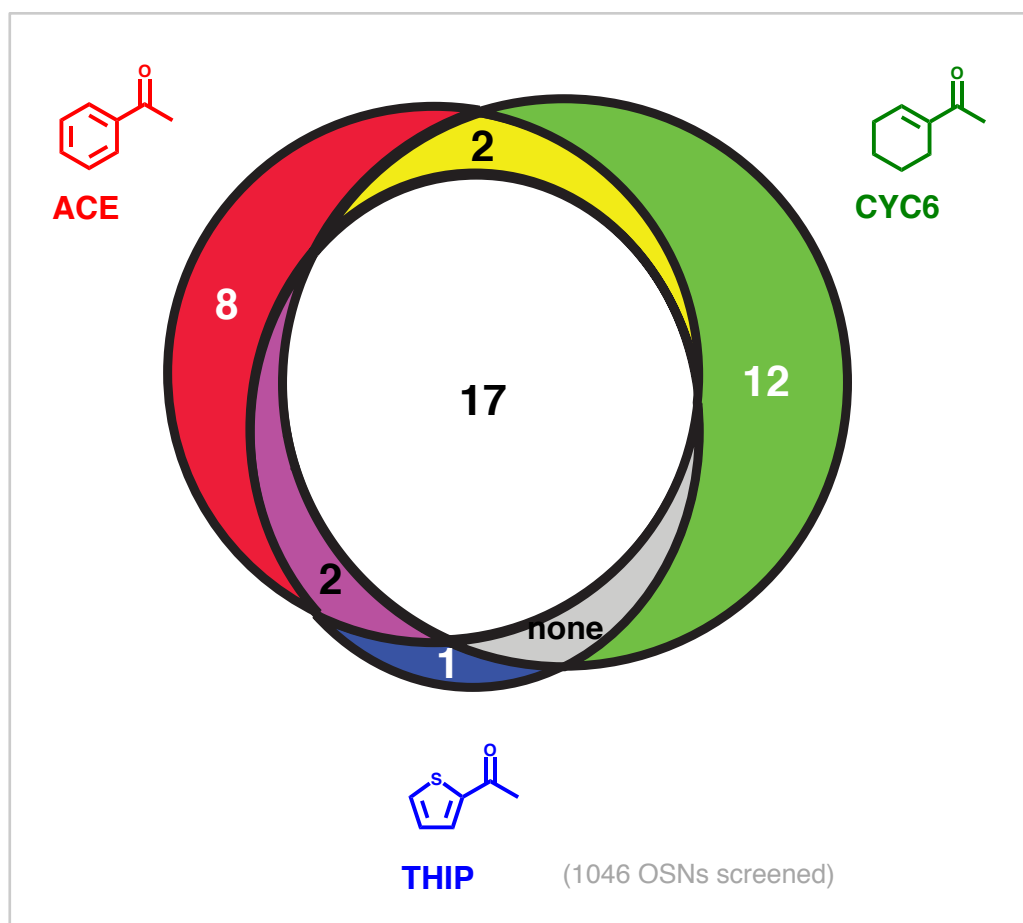


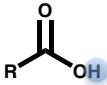
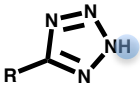
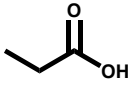
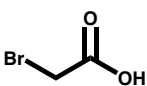
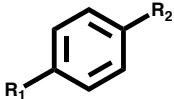
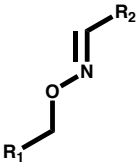
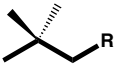
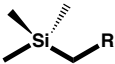




Figure 6.6 - extensive cross-recognition between aromatic and aliphatic cores. Venn diagram for the data in Figure 6.5 (A), contrasting recruitment by the best aromatic (THIP) and best aliphatic (CYC6) isosteres of ACE. As seen by the small size of the yellow and magenta sectors and the absence of a cyan sector, the ability of an OSN to accommodate any two cores highly predicts its ability to accommodate the third. While these seventeen OSNs in the white sector can respond to all three cores, they exclude many other similar aliphatic and heteroaromatic cores. Thus, they are not truly broadly tuned. Rather, they recognize a key feature shared by these visually discrepant cores.

CLASSICAL ISOSTERES		BIOISOSTERES	
			
ether	sulfide	acid	tetrazole
			
acid	bromo-acid	benzene	MOIMM
			
4' carbon	4' silicon	benzene	propellane

Supplementary Figure 6.1 - contrasting classical isosteres with bioisosteres.

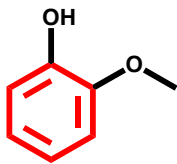
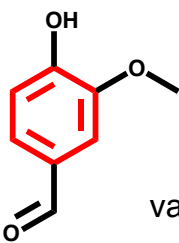
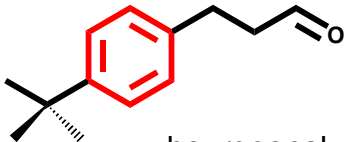
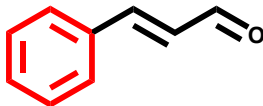
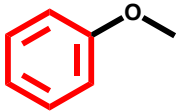
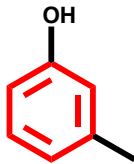
Classical isosteres (left) usually involve single atom exchanges. Overall, the structures appear the same. Bioisosteric exchanges (right) can involve multiple atoms and extensive rearrangements such that the pair is visually discrepant. Yet the members retain similar functionality at the designated target via retention of some key attribute. For example, tetrazole has an acidic proton (shaded blue). For multifunctional functional groups like benzene, different bioisosteres may be employed depending on the circumstance; MOIMM preserves electron distribution while propellane preserves rigid spacing between appended groups.

Supplementary Figure 6.2 - aromatic rings and cyclohexene rings in common odorants. Structures with their cores highlighted in red. Below is a sample OR that responds to that ligand. **(A)** Three general architectures for aromatic odorants. **(top)** Compact compounds integrating multiple directly attached polar groups. **(middle)** compounds with a “ball and chain” organization where the functional group is removed from the ring by an alkyl linker region. Sometimes, as in bourgeonal, the ring can serve as a spacer to impart a specific geometry to an even more distal appended group. **(bottom)** Compact compounds with a single directly attached polar group. Acetophenone would fall in this category. **(B)** Examples of cyclohexene rings in odorants. The red dot denotes the distal carbon that veers out of plane and may thus impact geometry in a specialized way. Odorants where an appendage falls at this carbon may be less amenable for exchanging this core with an aromatic ring.

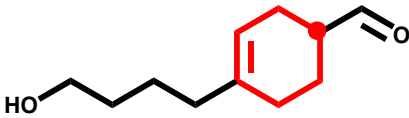
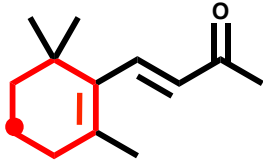
References to the studies characterizing these OR-ligand pairings:

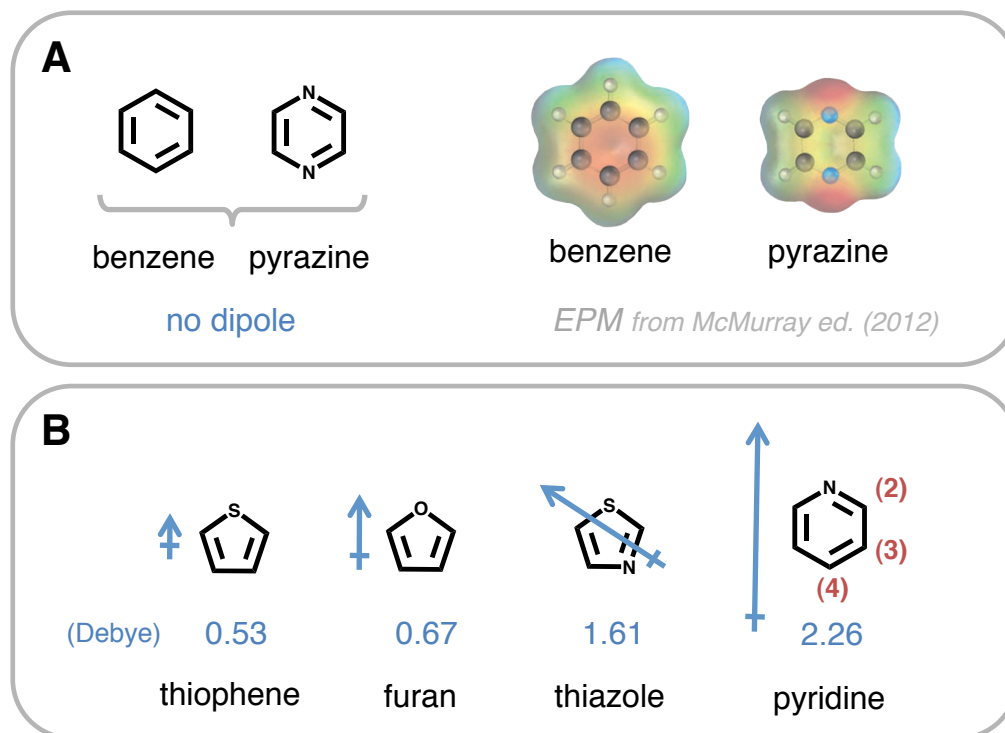
MOR29A	Tsuboi et al. (2011)
MOREG	Kajiya et al. (2001)
hOR17-4	Spehr et al. (2003)
mouse I7	Bozza et al. (2005)
hOR17-209	Matarazzo et al. (2005)
MOR139-3	Yoshikawa and Touhara (2008)
MOR23	Touhara et al. (1999)
OR51E2	Neuhaus et al. (2009)

A

aromatic type 1	 <p>guaicol MOR29A</p>	 <p>vanillin MOREG</p>
aromatic type 2	 <p>bourgeonal hOR17-4</p>	 <p>cinnamaldehyde mouse I7</p>
aromatic type 3	 <p>anisole hOR17-209</p>	 <p>m-cresol m139-3</p>

B

 <p>lylal MOR23</p>	 <p>b-ionone OR51E2</p>
------------------------------------------------------------------------------------------------------------	------------------------------------------------------------------------------------------------------------------



Supplementary Figure 6.3 – some properties of the heteroaromatic cores used in this study. (A) Benzene and pyrazine contain no intrinsic dipole that can interact with that of the appended carbonyl group. However, as seen on the electrostatic potential maps at right, there is greater electron density (red shading) localized around the nitrogens of pyrazine. This imparts a markedly different polar topology. (B) Orientation and magnitude of the intrinsic dipole moments in the other aromatic cores. These ring dipoles mean that the location of the appended group relative to the heteroatom (ex: at positions 2 vs 3 vs 4 in pyridine) can differentially impact the overall polar group strength in a conjugated system.

CHAPTER 7**FUTURE DIRECTIONS : CHARACTERIZING ESTER ENCODING**

INTRODUCTION

Esters are a common functional group, yet they have not been systematically studied at the odorant receptor (OR) repertoire level in mammals. This is surprising given their importance in the flavor and fragrance industry and their attractive chemical organization. Unlike n-odorants, esters bear two alkyl arms. One arm is derived conceptually from an alcohol and is marked with an ether oxygen. The opposing arm, derived from an acid, bears the carbonyl (Figure 7.1A). Esters can thus be ordered into a homologous series via their alcohol-arm length or their acid-arm length. These intersecting series create a “2D” homologous matrix (Figure 7.1B). An unresolved issue is how “1D” n-odorant homologous series relate to each other; esters intrinsically provide this ordering. The matrix organization also introduces new relationships to examine, such the depth of embedding of the functional group and flipping of the functional group. Esters are thus a particularly attractive entry point for exploring how the OR repertoire encodes multidimensional compounds.

BACKGROUND

Reported ester-responsive ORs are broadly tuned

Because esters have only sporadically been included in odor test panels, there are only a few verified ester-responsive ORs whose sequence is known. Many of these are broadly tuned. They exhibit substantial recognition of other functional groups, with a

slight bias towards ketones. For example, MOR256-17 responds to the 12 atom spanning amyl hexanoate, but it also recognizes mid length acids, ketones, di-ketones, and compact aromatics (Saito, Chi et al. 2009). OR2W1, activated by the 8 atom-spanning hexyl acetate, responds with similar potencies to a compact terpene ketone, related cyclic terpenes, linear ketones, and a range of both large and small rigid aromatic compounds (Saito, Chi et al. 2009).

In none of these cases were the ORs assayed with closely related esters. This is unfortunate because the characterization of SR1 suggests that an OR can be broadly tuned with respect to functional group type and hydrocarbon scaffold and yet be quite narrowly tuned with regards to esters. SR1 responds to multiple mid-length acids, aldehydes, and alcohols. Nevertheless, this receptor can make a fine discrimination of a three-carbon difference between the esters amyl acetate and ethyl acetate (Grosmaître, Fuss et al. 2009).

OR1G1 and OR52D1 prioritize different features of esters

Currently, the best view of ester encoding strategies comes from the characterization of the OR1G1 and OR52D1 receptors (Sanz, Schlegel et al. 2005). These two very broadly tuned ORs have been probed with short homologous series of esters and related ketones having alkyl arms ranging from 6 to 10 carbons in length. The activation patterns reinforce that, like SR1, despite being broadly tuned to a diversity of functional groups and hydrocarbon scaffolds OR1G1 and OR52D1 display regular and stringent rules regarding discrimination between esters (Figure 7.2).

OR1G1 prioritizes different features for ketones than for esters. The response pattern suggests that OR1G1 attends to the overall span of ketones, being permissive for the location of the carbonyl group and hence the alkyl arm identity. For ester detection, the situation was reversed. Overall span was no longer the dominant feature; ethyl heptanoate (2:7) and methyl octanoate (1:8) both have a span of 10 atoms, but they exhibited a nearly 6-fold difference in activity. Thus, in OR1G1's discrimination of esters, the length of the acid-derived arm appeared crucial. This is reflected in the close patterning between the methyl and ethyl ester homologous series. The ether oxygen in the ester plays some important shaping role at this receptor, enabling different detection strategies to be used between the two chemical classes.

In contrast, OR52D1 treated ketones and esters equivalently, suggesting use of a measure that is independent of the ether oxygen. This receptor again gave precedence to overall span, preferring a length of 9 to 10 atoms. The reliance on span is seen most clearly in the displacement of the activation patterns of the methyl and ethyl ester homologous series. An ethyl ester's best match is a methyl ester whose acid-derived arm is one carbon longer. Thus, the dramatic cutoff in activity between ethyl heptanoate (2:7) and ethyl octanoate (2:8) falls between methyl octanoate (1:8) and methyl nonanoate (1:9).

PROPOSED INVESTIGATION OF ESTER ENCODING

The differing strategies used by OR1G1 and OR52D1 suggest that there may be important functional subdivisions among the ester-responsive olfactory sensory neurons

(OSNs). Subpopulations, tuned to different features of the alkyl scaffold and monitoring different compound molecular weight ranges, could form a multi-tiered detection system that together leads to complex patterns of activity across the ester matrix. This provides an exciting opportunity to characterize the combinatorial code for a well-organized series of multidimensional odorants. The high throughput dispersed cell calcium imaging method is well suited to monitor the full OR repertoire, as expressed in their native cell type, in an unbiased way. With it, we can systematically probe for rules by monitoring the population trends while preserving individual cell response patterns.

Does the continuity rule transfer from “1D” space to the esters?

Simply screening all members of a homologous series as defined by either the alcohol arm or acid arm, may well hold surprises. One of the most robust rules from “1D” n-odorant space is the continuity rule. That is, if a cell responds to members of a homologous series with carbon chain number X and (X+2), it will also respond to the (X+1) member. At first glance, this rule would seem to be necessarily inviolate, given the physical construction of odorants. But with esters there is reason to be suspicious; certain percepts exhibit gaps along both axes of the ester matrix (Figure 7.3). From medicinal chemistry it is known that some homologous series of drugs demonstrate a serrated pattern of potencies (Wermuth 2008). This has not previously been noted for n-odorants, but it could contribute to a patchy OR-level code among the esters. For this reason, a fully continuous homologous series of esters should be tested around these percept violation locales.

Where is the fovealae of highest recruitment for esters?

One basic characterization that has practical application is identifying whether there is a “biological fovea” (or multiple foveae) for esters the way an eight carbon tail is a biological fovea for homologous “1D” n-compounds. The uneven, bell-like distribution in recruitment levels among a “1D” homologous series is one of the most robust trends in peripheral olfaction. It has been remarked upon from the earliest OR repertoire surveys of n-alcohols (Sato, Hirono et al. 1994; Malnic, Hirono et al. 1999), n-acids (Sato, Hirono et al. 1994), and n-aldehydes (Kaluzza and Breer 2000; Araneda, Peterlin et al. 2004). But how does this concept translate to the “2D” esters, where “length” can be considered that of either of the two arms or the entire span of the compound? A strategy to deal with the breadth of chemical space spanned by esters could be to start with sets that sample the matrix in a loose grid. The information, plotted as a heatmap on the matrix layout, can then be used to triangulate and select the best candidates for subsequent validation.

Investigating bioisosterism can also reveal arm usage bias

Probing how well the bioisosteric exchanges used in medicinal chemistry translate to the ORs can be of great value in gaining new perspectives on OR receptive field organization and what makes these chemosensors so special. The “cassette swap” technique, in which the ester group is excised, flipped, and reinstated, is common in medicinal chemistry (Ciapetti 2008) (Figure 7.4A). Retroester-containing drugs often remain potent at their intended targets. However, the primary reason the cassette swap is

employed is because the retroester orientation makes the drug a less suitable substrate for degradation by esterases. From the point of view of the enzymes, the cassette-swap is far from a well-tolerated exchange and the retroester would thus *not* be considered bioisosteric. How do the ORs respond to this manipulation? This understanding will directly benefit rational odorant design.

The process of analyzing the bioisosteric comparisons should also reveal if ester receptors differentiate between the alkyl arms with a strong bias. If so, the extent of co-recognition of the ester and its retroester will depend on how close the ester polar group is located to the center of the compound (Figure 7.4C). Esters with centrally located embedded groups have arms of nearly the same lengths before and after the swap. However “distal” ester pairs, where the functional group is offset, may be less frequently co-recognized. Biased arm usage should also become apparent when the data from this series is evaluated from the perspective of functional group embedding depth (Figure 7.5). Attribution of “depth” implies an ability to set one particular alkyl terminus as the reference. The ether oxygen creates asymmetry that could serve as the substrate, but is this feature employed?

Esters as a platform for investigating the structure of chemical space

A natural extension of characterizing esters is a comparative study with the other major “2D” odorant class, the ketones. Because ketones lack the signature ether oxygen of esters, they form a “hemi-matrix” where many ketone entries correspond to two ester

entries (Figure 7.6). It will be interesting to see if this ambiguity results in a blurred code for ketones relative to the esters.

Esters can also be contrasted with their cyclic analogs, the lactones.

Conceptually, the terminus of the acid arm from an acetate or propionate ester is tied back to the alcohol arm (Figure 7.7). This covalent bond forces the ester group to lie “cis” versus the normal “trans” configuration that it would assume due to repulsion of the lone pair electrons of the two oxygens. Evaluating ester and lactone co-recognition across the OR repertoire would provide the opportunity to gauge how robust this electronic lock is when considered in the context of the combined ligand-receptor interaction.

But perhaps the most exciting application of esters is to use their grid arrangement as a way to provide orientation within computational models of multidimensional odor space. Two competing models currently plot an array of physicochemical properties of odorants against the response pattern generated by a small subset of OSNs/ORs (Haddad, Khan et al. 2008; Saito, Chi et al. 2009). In this space, the distance between compounds A and B relates to the probability that an OSN responding to A will also respond to B. Commonly, the odorants are plotted in three-dimensions, with the axes representing the three principle components that capture the greatest amount of variance.

These multidimensional models can be powerful tools to describe the general trends within the combinatorial code, but it is not readily apparent how to read this space. Using an online interactive version (Khan, Luk et al. 2007), even a “simple” homologous series of alcohols can be seen to generate a complex and non-evenly spaced curve. Without knowing how different functional groups relate to one another (and compounded by the fact that no homologous series in the database is complete), these short sketches do

little to elucidate the terrain. Esters could change this, making the warping in this space more evident by providing a mesh that is comprised of the same functional group and that spans a gamut of molecular weights. By highlighting the trends operating in multidimensional chemical space, esters can help physiologists gain a greater appreciation of the organization imposed by the combinatorial code.

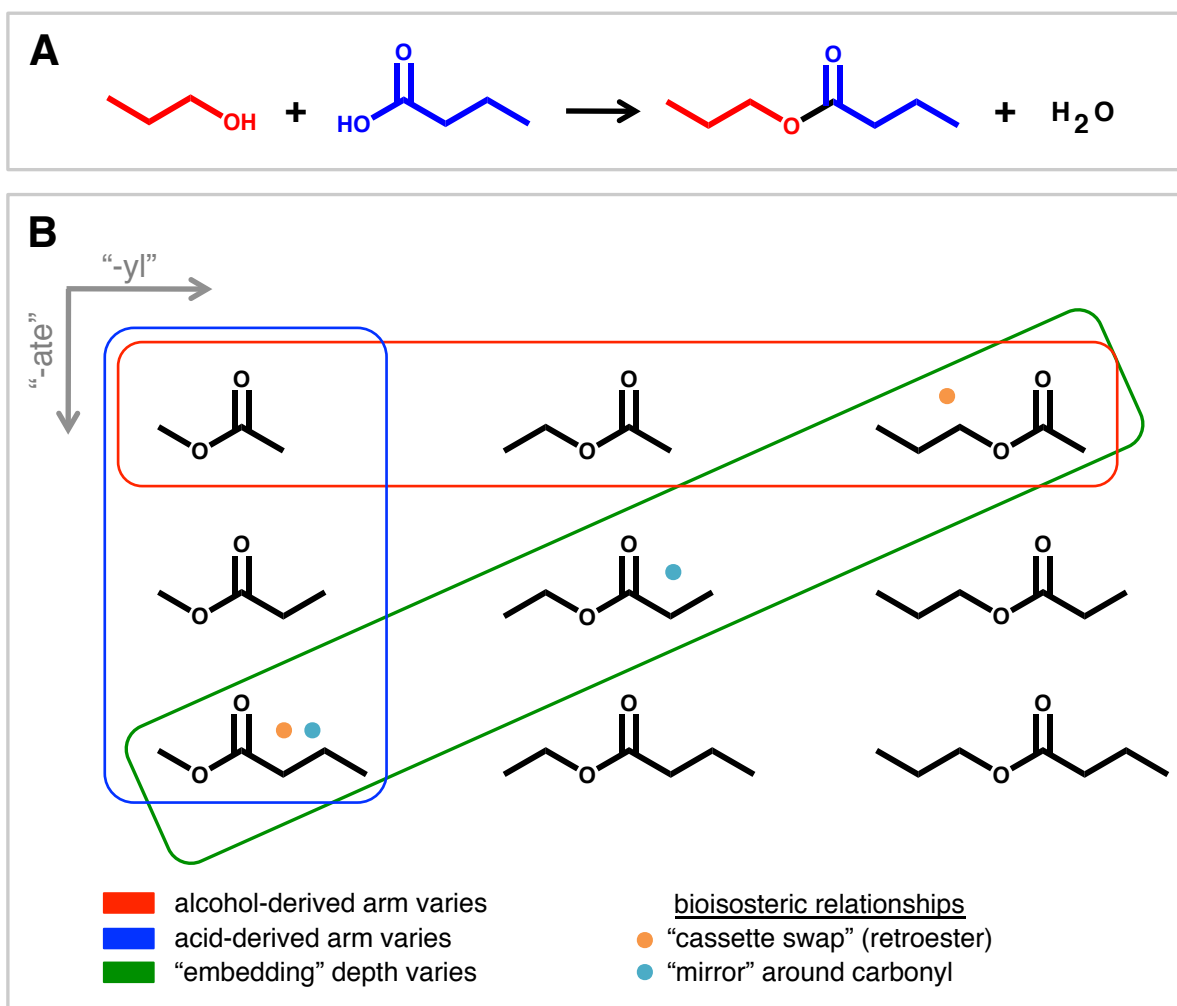
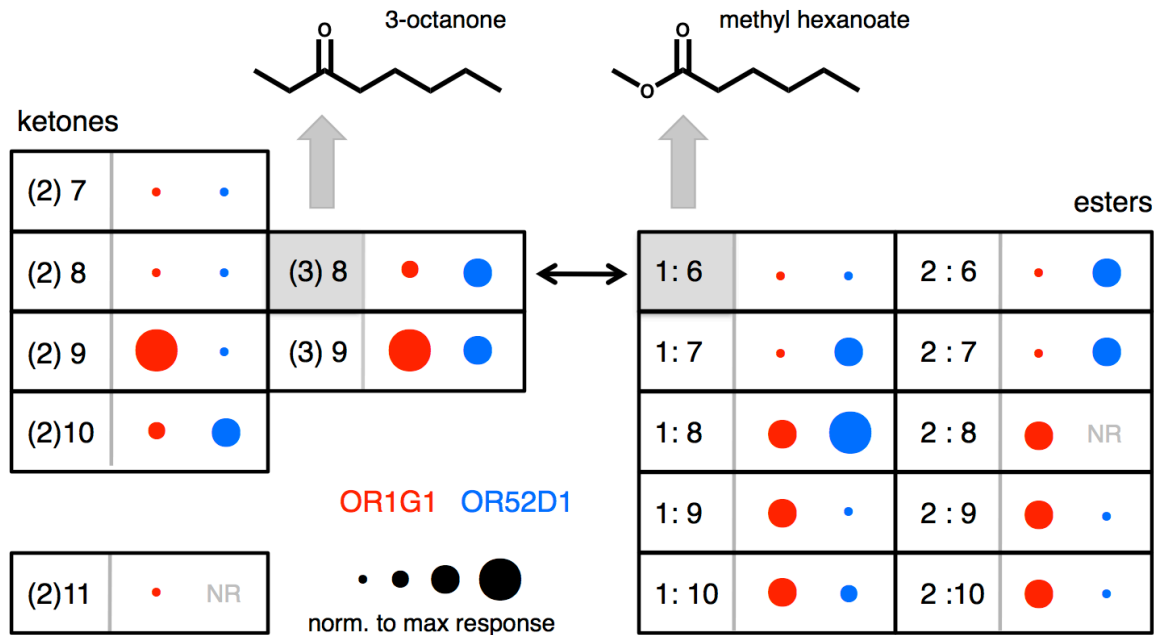


Figure 7.1 – asymmetry of esters sets up a homologous matrix. (A) Synthesis of an ester leads to an alcohol-derived arm (red) that possesses an ether oxygen and an acid-derived arm (blue) that possesses a carbonyl. In abbreviations, the number of carbons in each arm (its “length”) is given. The ester propyl butyrate (shown) would thus be abbreviated (3:4). (B) Esters form multiple homologous series where either the length of the alcohol arm (rows, red) or acid arm (columns, blue) varies. Because these homologous series intersect, they form a homologous matrix. New comparisons are possible due to the matrix arrangement, such as the positioning of the functional group within a series of esters sharing the same overall span (diagonal green).



Adapted from Sanz et al. (2005)

Figure 7.2 - two strategies of ester recognition used by ORs. Section of the receptive field for OR1G1 (red) and OR52D1 (blue). Homologous ketones are listed to the left and homologous esters to the right. The location of the ketone is in parenthesis, followed by the total number of carbons. Thus, 2-heptanone is represented as (2)7. The responses have been scaled based on the largest response within the subset of compounds shown here. “NR” means the compound did not elicit any response above vehicle. The arrow between 3-octanone and methyl hexanoate points out a bridge between these two chemical classes where the compounds share the same overall span and depth of embedding of the carbonyl. OR1G1 appears to give priority to acid arm length when parsing esters as seen in the matched red patterns across the methyl and ethyl esters. OR52D1 appears to give priority to the total compound span as seen in the displaced blue pattern for esters.

Figure 7.3 - an ester percept violating the continuity rule. Ester matrix arrayed as in Figure 7.1. Esters whose percept reported on www.goodscentcompany.com include the descriptor "green" are shaded with a black background. Esters that did not have "green" as a descriptor are in white. Esters where no descriptors were provided are shaded grey and denoted "ND". The elicitation of "green" by every hexyl-alcohol arm ester, regardless of acid arm length (ie: 6:X series) but nearly none of the pentyl-alcohol arm esters (5:X) creates a striking perceptual "cliff". The arrows denote where a homologous stretch of esters fails to uniformly elicit a percept. Such gaps are unexpected based on the pattern of encoding at the OR level for n-compounds that have only a single alkyl tail. Among such compounds, if an OR responds to tails of carbon number X and (X+2), it almost assuredly will respond to a tail length of (X+1). This continuity rule does not extend to the percept level for esters; arrows mark the violations. It will be interesting to examine the OR combinatorial code elicited by the set of esters around each arrow.

“-yl” →

“-ate” ↓

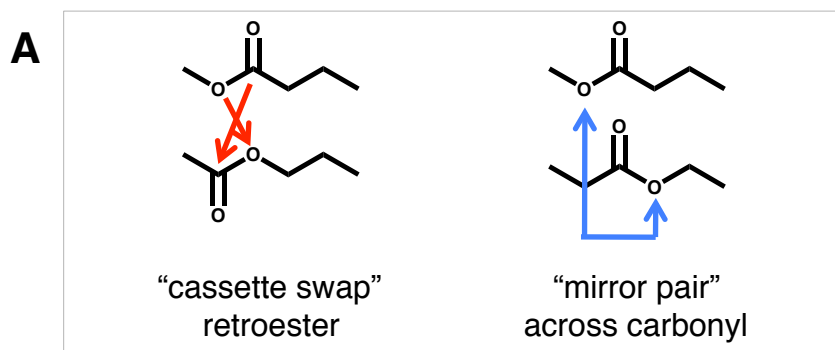
1:2	2:2	3:2	4:2	5:2	6:2	7:2	8:2	9:2
1:3	2:3	3:3	4:3	5:3	6:3	↕↔	8:3	(ND)
1:4	2:4	3:4	4:4	5:4	6:4	7:4	8:4	(ND)
1:5	2:5	↔	4:5	↔	6:5	↕	(ND)	(ND)
↕	2:6	3:6	↔	5:6	6:6	7:6	(ND)	(ND)
1:7	↔	3:7	4:7	5:7	6:7	7:7	8:7	9:7
1:8	2:8	3:8	4:8	5:8	6:8	7:8	8:8	9:8
1:9	2:9	3:9	4:9	5:9	6:9	7:9	(ND)	9:9
1:10	2:10	3:10	4:10	(ND)	6:10	(ND)	(ND)	(ND)

■ alcohol-arm continuity violation ■ elicits “green” percept
■ acid-arm continuity violation ■ no descriptor available

percept descriptors from www.thegoodscentscompany.com

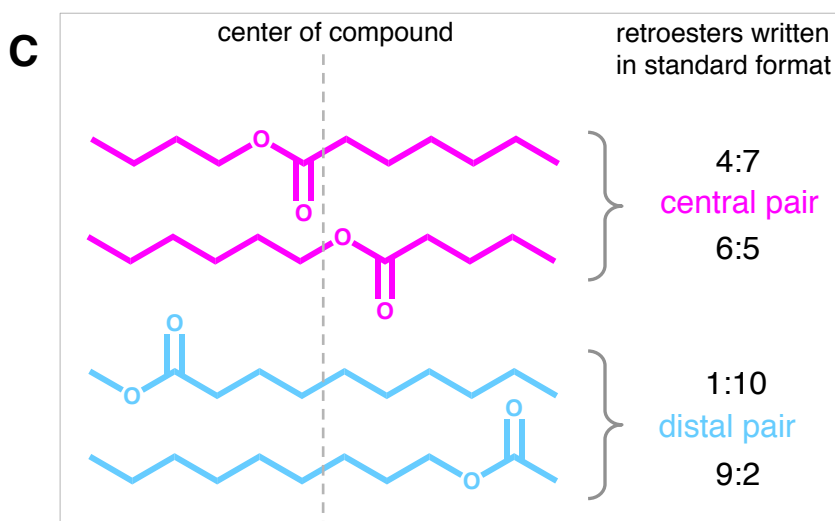
Figure 7.4 - a series of esters with which to explore bioisosteric relationships. (A)

Examples how each of the bioisosteric exchanges impacts methyl butyrate. The “cassette swap” method is the only recognized bioisosteric exchange. The carbonyl is shifted slightly during this exchange. “Mirroring” is an alternate exchange not described in literature. The carbonyl remains in a fixed position during this exchange. **(B)** Ester matrix arrayed as in Figure 7.1, with the formates blocked off in orange as they are the sole esters to lack an acid-arm alkyl terminus and may thus be treated differently. The colored cells represent esters with an overall span of 12. Matched colors denote the bioisosteric retroester pairs using the “cassette swap” relationship. **(C)** Two pairs drawn using the convention of placing the alcohol arm on the left hand side. The grey dashed line is the symmetry line from the point of view of the two alkyl termini. In the pink “central” ester pair, the depth of embedding is fairly consistent and the alcohol arm is of similar length before and after the swap. The blue “distal” pair radically alters the embedding of the ester group from the point of view of the alcohol arm terminus.



B

1:1	2:1	3:1	4:1	5:1	6:1	7:1	8:1	9:1	10:1
1:2	2:2	3:2	4:2	5:2	6:2	7:2	8:2	9:2	10:2
1:3	2:3	3:3	4:3	5:3	6:3	7:3	8:3	9:3	10:3
1:4	2:4	3:4	4:4	5:4	6:4	7:4	8:4	9:4	10:4
1:5	2:5	3:5	4:5	5:5	6:5	7:5	8:5	9:5	10:5
1:6	2:6	3:6	4:6	5:6	6:6	7:6	8:6	9:6	10:6
1:7	2:7	3:7	4:7	5:7	6:7	7:7	8:7	9:7	10:7
1:8	2:8	3:8	4:8	5:8	6:8	7:8	8:8	9:8	10:8
1:9	2:9	3:9	4:9	5:9	6:9	7:9	8:9	9:9	10:9
1:10	2:10	3:10	4:10	5:10	6:10	7:10	8:10	9:10	10:10



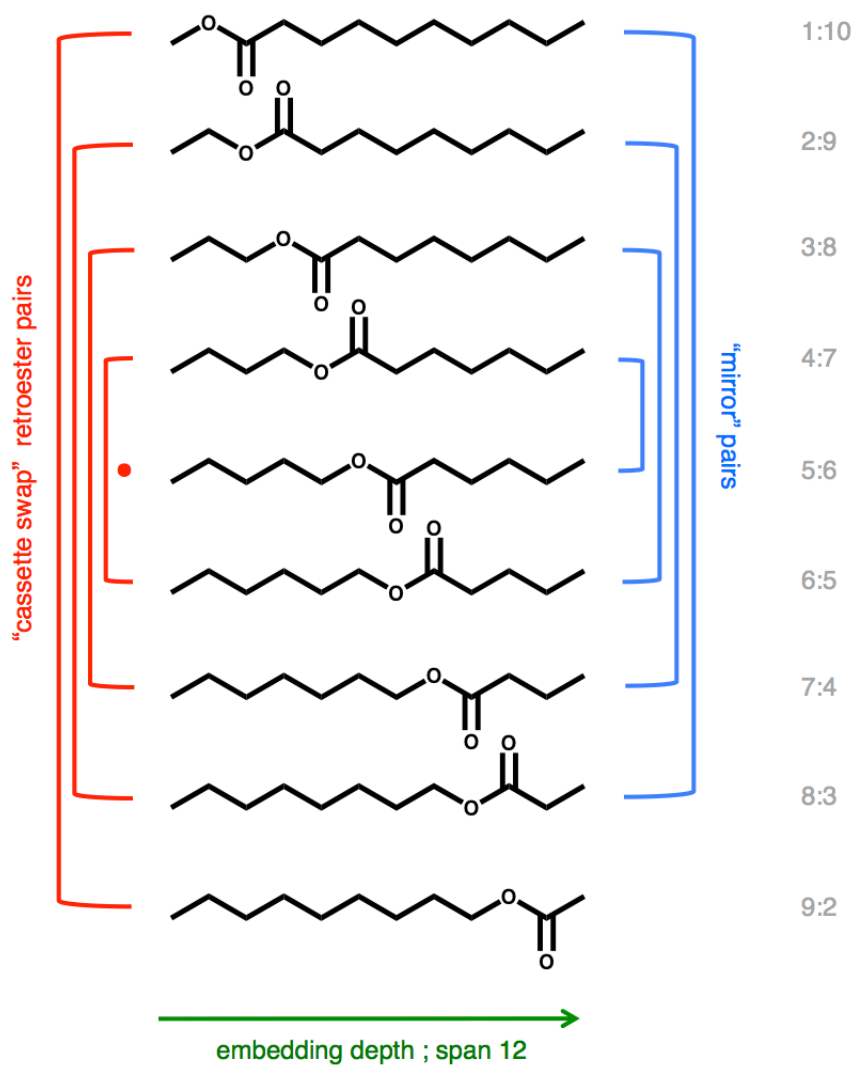


Figure 7.5 – how the bioisostere series of esters also probes embedding depth.

The structures of all esters with a fixed span of 12 from Figure 7.4. Note how the "mirror" and "cassette swap" bioisosteric pairings are offset by one.

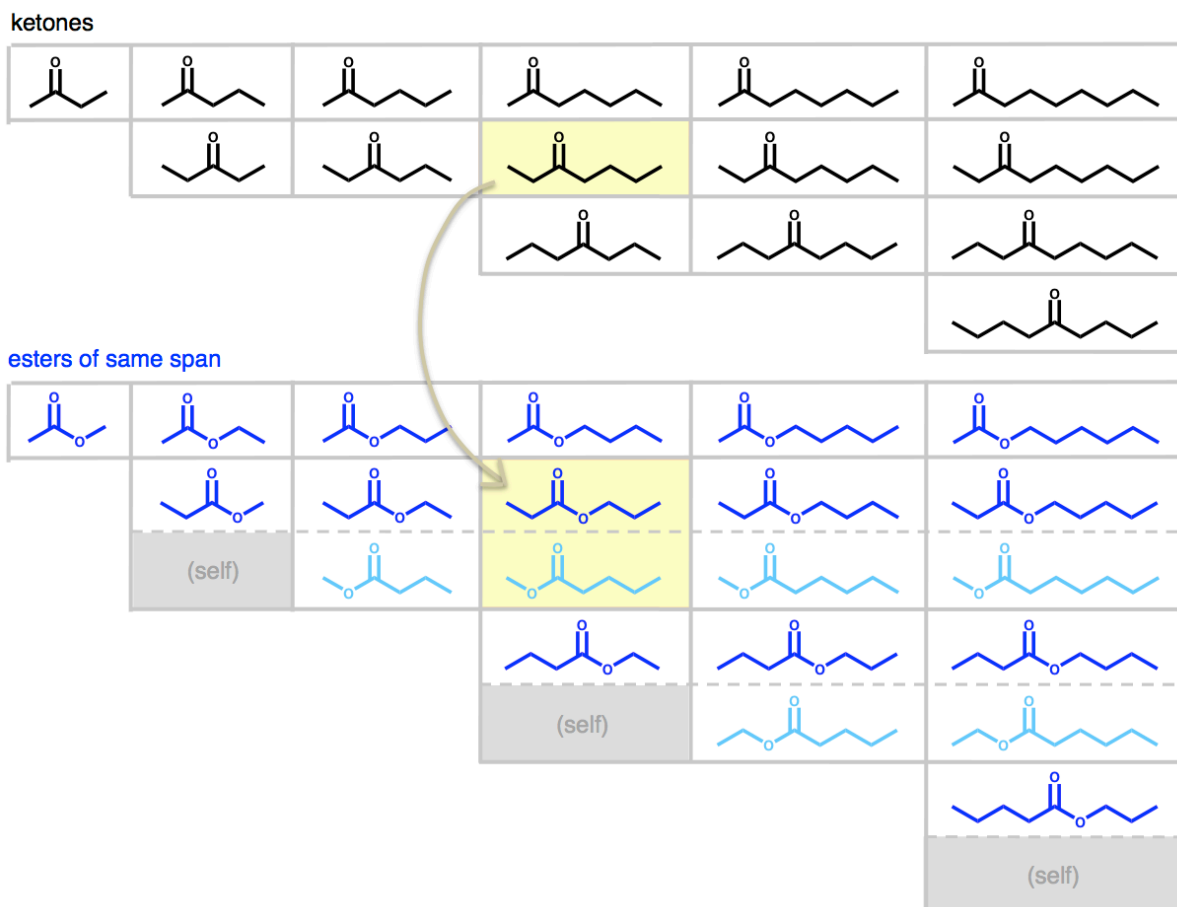


Figure 7.6 - relationship between ketones and esters. The ketone “hemi-matrix” is shown at top in black. Below in blue are esters that correspond to the same overall span and depth of embedding of the carbonyl within that span. Some 2-ketones can be matched to unique esters (ex. all the acetates (X:2)). However, most other ketones are matched to a pair of esters related by a “mirroring” of the ether oxygen around the carbonyl. One example is highlighted in yellow.

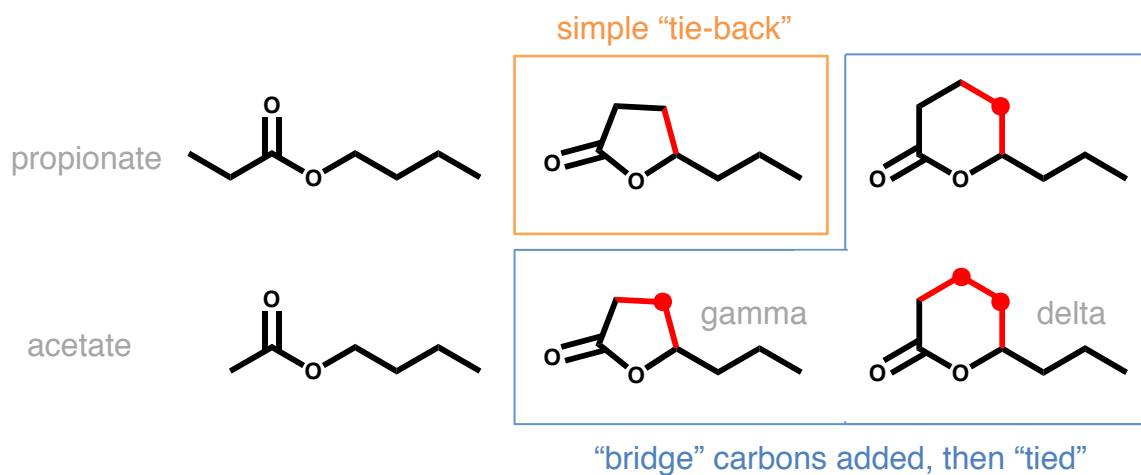


Figure 7.7 - two ways of conceptualizing the relationship between regular esters and lactones. A five-membered ring gamma lactone can be created by forming a bond between the acid arm terminus of a propionate ester (orange box). This requires a sharp kink in the acid arm chain, and the resultant gamma lactone does not extend as far from the carbonyl as the open propionate could. The gamma lactone could also conceptually be formed from an acetate ester if a bridge carbon is included along with the covalent locking bonds (blue box, additional carbons as dots). As the terminus of the acetate ester was held rigid anyway, the gamma lactone extends an equivalent distance from the carbonyl as in the open compound. Formation of six-membered delta lactones require bridging carbons in both cases. This may result in less strained geometries that can be better mimicked by a ketone.

SUMMARY

Using over 1000 odorant receptors (ORs) (Zhang and Firestein 2007) and employing a combinatorial code (Malnic, Hirono et al. 1999), the olfactory system detects thousands of diverse odorants and yet still makes nuanced discriminations between them. Understanding the organization of this code is challenging, but it is a critical task since the activity pattern across the OR repertoire forms the substrate for all higher processing. Careful characterization of the receptive fields of individual ORs remains an important step in this process. However, because ORs work as an ensemble to parse chemicals, understanding the function of any one receptor is incomplete without appreciation of its context. An empirical study of the broad-scale response patterns across ORs is needed to identify biologically meaningful features of odorants. This has been the aim of my thesis.

In my approach, I used high throughput calcium imaging of a large and unbiased population of olfactory sensory neurons (OSNs), mostly from rat, relying on the expression of only a single OR type per OSN (Chess, Simon et al. 1994). This technique allowed me to test a battery of odorants, acquiring population trends while still maintaining single cell and thus single receptor type resolution. The ability to monitor the combinatorial code at both of its levels has let me describe novel features of the distributed response to odorants.

The size of the code can vary greatly between odorants. It does not appear to constitute a labeled line for even the rarest recruiting odorants that I have tested. Among widely recruiting odorants, the code is comprised of a mix of narrowly tuned and broadly

tuned cells. Yet even among this large subpopulation, the chemical recognition strategies of each OSN result in a number of unique functional signatures. Although we do not know the basis of these rare signatures, I showed that they can be employed as useful experimental tools.

Another key finding is that odorants often interact with their cognate ORs while assuming rare forms that would not be predicted from the behavior of these chemicals in bulk solution. A geminal-diol is a specific form exclusive to aldehydes that is typically present in only minor amounts. However, ~15% of the octanal-responsive OSNs absolutely required this form. This suggests that the binding pockets in these ORs may promote assumption of or stabilize this rare form. Strikingly, the strict requirement for the diol form in order to recognize an aldehyde appears to confer the ability to filter out alcohols, providing the first mechanism for functional group discrimination.

Similarly, ORs seem able to stabilize higher energy states of the alkyl scaffold of odorants. I first noted this for a pair of aromatic odorants during a general survey. I pursued this concept further through a targeted study using cyclic analogs of octanal. OSNs activated by normal, flexible octanal also accepted a broad range of compact, higher energy-mimicking analogs of octanal. These observations underscore that there is important interplay between the receptor and odorant, such that binding of an odorant in its lowest energy state is far from a limiting requirement.

The realization that odorants literally need to be viewed more flexibly was the driving motivation for two pilots where I used population trends to rate the biological similarity between odorants that initially appeared highly discrepant. Both studies propose that rings, even aromatic ones, are best viewed as sculpting entities that present

flexible backbones in a more confined conformation. A preliminary assay was conducted using an odorant where the stereochemistry imparted by the ring is known to be important perceptually. Nevertheless, a striking level of activity was preserved among the target OSNs when using flexible odorants. I also demonstrated that aromatic rings could be exchanged for aliphatic rings in the context of the robustly recruiting odorant acetophenone. Often, the electronic nature of aromatic rings has been given precedence when ordering odorants, and aromatic odorants of diverse functional groups are often shunted into the same mix. However, my work suggests that aromatic rings are sometimes better considered as scaffolding elements instead of the primary epitope. Approaching aromatic and alkyl rings in this way invites reconsideration of broadly tuned receptive fields from the point of view of what the ORs report as critical features.

Given the breadth of odor space and the complexity of the combinatorial code, many fundamental questions remain. Systematic study of the combinatorial code has so far been largely based on simple odorants with single alkyl tails. This has left entire classes of odorants that have two alkyl tails, such as the esters and ketones, sparsely characterized at best. Before multidimensional odor space was visualized, the simple single-tailed homologous series appeared to be the most regular set of odorants available. Now recognizing that there is non-uniform spacing of these “1D” homologous suggests that it may be more productive to perform basic characterization of odorants that form “2D” series. The naturally interrelated, mesh-like organization of esters may assist visualization of multidimensional odor space, thus helping physiologists better leverage these new computational models.

(this page intentionally left blank)

REFERENCES

. "www.flavornet.org" curated by Acree, T. and Arn, H.

. "www.leffingwell.com/chirality/chirality.htm" curated by Leffingwell, JC.

. "www.thegoodscentcompany.com."

Abaffy, T., A. Malhotra, et al. (2007). "The molecular basis for ligand specificity in a mouse olfactory receptor: a network of functionally important residues." The Journal of biological chemistry **282**(2): 1216-1224.

Abaffy, T., H. Matsunami, et al. (2006). "Functional analysis of a mammalian odorant receptor subfamily." Journal of neurochemistry **97**(5): 1506-1518.

Afshar, M., R. E. Hubbard, et al. (1998). "Towards structural models of molecular recognition in olfactory receptors." Biochimie **80**(2): 129-135.

Amoore, J. (1970). Molecular Basis of Odour. Springfield , IL, C.C.Thomas.

Anselmi, C., A. Buonocore, et al. (2011). "The human olfactory receptor 17-40: requisites for fitting into the binding pocket." Computational biology and chemistry **35**(3): 159-168.

Araneda, R. C., A. D. Kini, et al. (2000). "The molecular receptive range of an odorant receptor." Nature neuroscience **3**(12): 1248-1255.

Araneda, R. C., Z. Peterlin, et al. (2004). "A pharmacological profile of the aldehyde receptor repertoire in rat olfactory epithelium." The Journal of physiology **555**(Pt 3): 743-756.

Archtander, S. (1960). Perfume and Flavor Materials of Natural Origin. Elizabeth, NJ, Arctander Publishing.

- Bakalyar, H. A. and R. R. Reed (1990). "Identification of a specialized adenylyl cyclase that may mediate odorant detection." Science **250**(4986): 1403-1406.
- Baud, O., S. Etter, et al. (2011). "The mouse eugenol odorant receptor: structural and functional plasticity of a broadly tuned odorant binding pocket." Biochemistry **50**(5): 843-853.
- Bhandawat, V., J. Reisert, et al. (2005). "Elementary response of olfactory receptor neurons to odorants." Science **308**(5730): 1931-1934.
- Bieri, S., K. Monastyrskaia, et al. (2004). "Olfactory receptor neuron profiling using sandalwood odorants." Chemical senses **29**(6): 483-487.
- Billig, G. M., B. Pal, et al. (2011). "Ca²⁺-activated Cl⁻ currents are dispensable for olfaction." Nature neuroscience **14**(6): 763-769.
- Boccaccio, A., L. Lagostena, et al. (2006). "Fast adaptation in mouse olfactory sensory neurons does not require the activity of phosphodiesterase." The Journal of general physiology **128**(2): 171-184.
- Borisy, F. F., G. V. Ronnett, et al. (1992). "Calcium/calmodulin-activated phosphodiesterase expressed in olfactory receptor neurons." The Journal of neuroscience : the official journal of the Society for Neuroscience **12**(3): 915-923.
- Boschat, C., C. Pelofi, et al. (2002). "Pheromone detection mediated by a V1r vomeronasal receptor." Nature neuroscience **5**(12): 1261-1262.
- Bozza, T., P. Feinstein, et al. (2002). "Odorant receptor expression defines functional units in the mouse olfactory system." The Journal of neuroscience : the official journal of the Society for Neuroscience **22**(8): 3033-3043.
- Bozza, T., J. P. McGann, et al. (2004). "In vivo imaging of neuronal activity by targeted expression of a genetically encoded probe in the mouse." Neuron **42**(1): 9-21.
- Bozza, T., A. Vassalli, et al. (2009). "Mapping of class I and class II odorant receptors to glomerular domains by two distinct types of olfactory sensory neurons in the mouse." Neuron **61**(2): 220-233.

- Bozza, T. C. and J. S. Kauer (1998). "Odorant response properties of convergent olfactory receptor neurons." The Journal of neuroscience : the official journal of the Society for Neuroscience **18**(12): 4560-4569.
- Bradley, J., W. Bonigk, et al. (2004). "Calmodulin permanently associates with rat olfactory CNG channels under native conditions." Nature neuroscience **7**(7): 705-710.
- Bradlow HL., V. C., Kleinberg J. (1947). "The concept of Isosterism." Journal of Chemical Education **24**(9): 433-435.
- Buck, L. and R. Axel (1991). "A novel multigene family may encode odorant receptors: a molecular basis for odor recognition." Cell **65**(1): 175-187.
- Buck, L. B. (1992). "The olfactory multigene family." Current opinion in neurobiology **2**(3): 282-288.
- Buschmann, H. F. H. K. W. (1980). "The Reversible Hydration of Carbonyl Compounds in Aqueous Solution. Part I, THE Keto/Gen-diol Equilibrium." Ber Bunsenges Phys Chem **84**: 41-44.
- Bush, C. F. and R. A. Hall (2008). "Olfactory receptor trafficking to the plasma membrane." Cellular and molecular life sciences : CMLS **65**(15): 2289-2295.
- Cheong, J. J. and Y. D. Choi (2003). "Methyl jasmonate as a vital substance in plants." Trends in genetics : TIG **19**(7): 409-413.
- Chesler, A. T., D. J. Zou, et al. (2007). "A G protein/cAMP signal cascade is required for axonal convergence into olfactory glomeruli." Proceedings of the National Academy of Sciences of the United States of America **104**(3): 1039-1044.
- Chess, A., I. Simon, et al. (1994). "Allelic inactivation regulates olfactory receptor gene expression." Cell **78**(5): 823-834.
- Ciapetti, P. G., B. (2008). Molecular Variations Based on Isosteric Replacements. The Practice of Medicinal Chemistry. C. Wermuth. San Diego, CA, Academic Press (Elsevier): 290-342.

- Cometto-Muniz, J. E., W. S. Cain, et al. (1998). "Nasal pungency and odor of homologous aldehydes and carboxylic acids." Experimental brain research. Experimentelle Hirnforschung. Experimentation cerebrale **118**(2): 180-188.
- Dalton, P. (2000). "Psychophysical and behavioral characteristics of olfactory adaptation." Chemical senses **25**(4): 487-492.
- Dalton, P. (2002). Olfaction. Steven's Handbook of Experimental Psychology: Perception and Motivation. New York, John Wiley & Sons: 691-746.
- Deupi, X. and J. Standfuss (2011). "Structural insights into agonist-induced activation of G-protein-coupled receptors." Current opinion in structural biology **21**(4): 541-551.
- Dobson, C. M. (2004). "Chemical space and biology." Nature **432**(7019): 824-828.
- Doszczak, L., P. Kraft, et al. (2007). "Prediction of perception: probing the hOR17-4 olfactory receptor model with silicon analogues of bourgeonal and linal." Angewandte Chemie **46**(18): 3367-3371.
- Doty, R. L. (2009). "The olfactory system and its disorders." Seminars in neurology **29**(1): 74-81.
- Duchamp-Viret, P., M. A. Chaput, et al. (1999). "Odor response properties of rat olfactory receptor neurons." Science **284**(5423): 2171-2174.
- Feinstein, P., T. Bozza, et al. (2004). "Axon guidance of mouse olfactory sensory neurons by odorant receptors and the beta2 adrenergic receptor." Cell **117**(6): 833-846.
- Feinstein, P. and P. Mombaerts (2004). "A contextual model for axonal sorting into glomeruli in the mouse olfactory system." Cell **117**(6): 817-831.
- Ferreira, P., A. Hernandez-Ortega, et al. (2010). "Kinetic and chemical characterization of aldehyde oxidation by fungal aryl-alcohol oxidase." The Biochemical journal **425**(3): 585-593.
- Firestein, S. (2001). "How the olfactory system makes sense of scents." Nature **413**(6852): 211-218.

- Firestein, S., C. Picco, et al. (1993). "The relation between stimulus and response in olfactory receptor cells of the tiger salamander." The Journal of physiology **468**: 1-10.
- Fried, H. U., S. H. Fuss, et al. (2002). "Selective imaging of presynaptic activity in the mouse olfactory bulb shows concentration and structure dependence of odor responses in identified glomeruli." Proceedings of the National Academy of Sciences of the United States of America **99**(5): 3222-3227.
- Fukuda, N., K. Yomogida, et al. (2004). "Functional characterization of a mouse testicular olfactory receptor and its role in chemosensing and in regulation of sperm motility." Journal of cell science **117**(Pt 24): 5835-5845.
- Furudono, Y., Y. Sone, et al. (2009). "Relationship between peripheral receptor code and perceived odor quality." Chemical senses **34**(2): 151-158.
- Gaillard, I., S. Rouquier, et al. (2002). "A single olfactory receptor specifically binds a set of odorant molecules." The European journal of neuroscience **15**(3): 409-418.
- Gangadhar, N. M., S. J. Firestein, et al. (2008). "A novel role for jun N-terminal kinase signaling in olfactory sensory neuronal death." Molecular and cellular neurosciences **38**(4): 518-525.
- Gelis, L., S. Wolf, et al. (2011). "Prediction of a Ligand-binding Niche within a Human Olfactory Receptor by Combining Site-directed Mutagenesis with Dynamic Homology Modeling." Angewandte Chemie.
- Gibbs, R. A., G. M. Weinstock, et al. (2004). "Genome sequence of the Brown Norway rat yields insights into mammalian evolution." Nature **428**(6982): 493-521.
- Goff, S. A. and H. J. Klee (2006). "Plant volatile compounds: sensory cues for health and nutritional value?" Science **311**(5762): 815-819.
- Gonzales, F., A. I. Farbman, et al. (1985). "Cell and explant culture of olfactory chemoreceptor cells." Journal of neuroscience methods **14**(2): 77-90.
- Grosmaître, X., S. H. Fuss, et al. (2009). "SR1, a mouse odorant receptor with an unusually broad response profile." The Journal of neuroscience : the official journal of the Society for Neuroscience **29**(46): 14545-14552.

- Hacquemand, R., L. Jacquot, et al. (2010). "Comparative Fear-Related Behaviors to Predator Odors (TMT and Natural Fox Feces) before and after Intranasal ZnSO₄ Treatment in Mice." Frontiers in behavioral neuroscience **4**: 188.
- Haddad, R., R. Khan, et al. (2008). "A metric for odorant comparison." Nature methods **5**(5): 425-429.
- Hall, S. E., W. B. Floriano, et al. (2004). "Predicted 3-D structures for mouse I7 and rat I7 olfactory receptors and comparison of predicted odor recognition profiles with experiment." Chemical senses **29**(7): 595-616.
- Hamana, H., J. Hirono, et al. (2003). "Sensitivity-dependent hierarchical receptor codes for odors." Chemical senses **28**(2): 87-104.
- Herdewijn, P. and E. De Clercq (2001). "The cyclohexene ring as bioisostere of a furanose ring: synthesis and antiviral activity of cyclohexenyl nucleosides." Bioorganic & medicinal chemistry letters **11**(12): 1591-1597.
- Hilal, R. and A. M. el-Aaser (1985). "A comparative quantum chemical study of methyl acetate and S-methyl thioacetate. Toward an understanding of the biochemical reactivity of esters of coenzyme A." Biophysical chemistry **22**(3): 145-150.
- Hinman, A., H. H. Chuang, et al. (2006). "TRP channel activation by reversible covalent modification." Proceedings of the National Academy of Sciences of the United States of America **103**(51): 19564-19568.
- Ho, S. L., B. A. Johnson, et al. (2006). "Differential responses to branched and unsaturated aliphatic hydrocarbons in the rat olfactory system." The Journal of comparative neurology **499**(4): 519-532.
- Imai, T. and H. Sakano (2009). "Odorant receptor gene choice and axonal projection in the mouse olfactory system." Results and problems in cell differentiation **47**: 57-75.
- Johnson, B. A., S. L. Ho, et al. (2002). "Functional mapping of the rat olfactory bulb using diverse odorants reveals modular responses to functional groups and hydrocarbon structural features." The Journal of comparative neurology **449**(2): 180-194.

- Jones, D. T. and R. R. Reed (1989). "Golf: an olfactory neuron specific-G protein involved in odorant signal transduction." Science **244**(4906): 790-795.
- Juilfs, D. M., H. J. Fulle, et al. (1997). "A subset of olfactory neurons that selectively express cGMP-stimulated phosphodiesterase (PDE2) and guanylyl cyclase-D define a unique olfactory signal transduction pathway." Proceedings of the National Academy of Sciences of the United States of America **94**(7): 3388-3395.
- Kajiya, K., K. Inaki, et al. (2001). "Molecular bases of odor discrimination: Reconstitution of olfactory receptors that recognize overlapping sets of odorants." The Journal of neuroscience : the official journal of the Society for Neuroscience **21**(16): 6018-6025.
- Kaluza, J. F. and H. Breer (2000). "Responsiveness of olfactory neurons to distinct aliphatic aldehydes." The Journal of experimental biology **203**(Pt 5): 927-933.
- Katada, S., T. Hirokawa, et al. (2005). "Structural basis for a broad but selective ligand spectrum of a mouse olfactory receptor: mapping the odorant-binding site." The Journal of neuroscience : the official journal of the Society for Neuroscience **25**(7): 1806-1815.
- Katada, S., T. Nakagawa, et al. (2003). "Odorant response assays for a heterologously expressed olfactory receptor." Biochemical and biophysical research communications **305**(4): 964-969.
- Katritch, V., V. Cherezov, et al. (2012). "Diversity and modularity of G protein-coupled receptor structures." Trends in pharmacological sciences **33**(1): 17-27.
- Kaupp, U. B. (2010). "Olfactory signalling in vertebrates and insects: differences and commonalities." Nature reviews. Neuroscience **11**(3): 188-200.
- Kaupp, U. B. and R. Seifert (2002). "Cyclic nucleotide-gated ion channels." Physiological reviews **82**(3): 769-824.
- Keller, A., H. Zhuang, et al. (2007). "Genetic variation in a human odorant receptor alters odour perception." Nature **449**(7161): 468-472.
- Khafizov, K., C. Anselmi, et al. (2007). "Ligand specificity of odorant receptors." Journal of molecular modeling **13**(3): 401-409.

- Khan, R. M., C. H. Luk, et al. (2007). "Predicting odor pleasantness from odorant structure: pleasantness as a reflection of the physical world." The Journal of neuroscience : the official journal of the Society for Neuroscience **27**(37): 10015-10023.
- Kleene, S. J. (1993). "Origin of the chloride current in olfactory transduction." Neuron **11**(1): 123-132.
- Kobilka, B. K. and X. Deupi (2007). "Conformational complexity of G-protein-coupled receptors." Trends in pharmacological sciences **28**(8): 397-406.
- Kramer, R. H. and S. A. Siegelbaum (1992). "Intracellular Ca²⁺ regulates the sensitivity of cyclic nucleotide-gated channels in olfactory receptor neurons." Neuron **9**(5): 897-906.
- Krautwurst, D., K. W. Yau, et al. (1998). "Identification of ligands for olfactory receptors by functional expression of a receptor library." Cell **95**(7): 917-926.
- Kurahashi, T. and A. Menini (1997). "Mechanism of odorant adaptation in the olfactory receptor cell." Nature **385**(6618): 725-729.
- Kurland, M. D., M. B. Newcomer, et al. (2010). "Discrimination of saturated aldehydes by the rat I7 olfactory receptor." Biochemistry **49**(30): 6302-6304.
- Lai, P. C., M. S. Singer, et al. (2005). "Structural activation pathways from dynamic olfactory receptor-odorant interactions." Chemical senses **30**(9): 781-792.
- Laing, D. G., P. K. Legha, et al. (2003). "Relationship between molecular structure, concentration and odor qualities of oxygenated aliphatic molecules." Chemical senses **28**(1): 57-69.
- Laing, D. G., H. Panhuber, et al. (1989). "Odor masking in the rat." Physiology & behavior **45**(4): 689-694.
- Leinders-Zufall, T., M. N. Rand, et al. (1997). "Calcium entry through cyclic nucleotide-gated channels in individual cilia of olfactory receptor cells: spatiotemporal dynamics." The Journal of neuroscience : the official journal of the Society for Neuroscience **17**(11): 4136-4148.

- Leon, M. and B. A. Johnson (2003). "Olfactory coding in the mammalian olfactory bulb." Brain research. Brain research reviews **42**(1): 23-32.
- Levasseur, G., M. A. Persuy, et al. (2003). "Ligand-specific dose-response of heterologously expressed olfactory receptors." European journal of biochemistry / FEBS **270**(13): 2905-2912.
- Liberles, S. D. and L. B. Buck (2006). "A second class of chemosensory receptors in the olfactory epithelium." Nature **442**(7103): 645-650.
- Lin, W., R. Margolskee, et al. (2007). "Olfactory neurons expressing transient receptor potential channel M5 (TRPM5) are involved in sensing semiochemicals." Proceedings of the National Academy of Sciences of the United States of America **104**(7): 2471-2476.
- Liu, A. H., X. Zhang, et al. (2003). "Motif-based construction of a functional map for mammalian olfactory receptors." Genomics **81**(5): 443-456.
- Ma, M. and G. M. Shepherd (2000). "Functional mosaic organization of mouse olfactory receptor neurons." Proceedings of the National Academy of Sciences of the United States of America **97**(23): 12869-12874.
- Macpherson, L. J., A. E. Dubin, et al. (2007). "Noxious compounds activate TRPA1 ion channels through covalent modification of cysteines." Nature **445**(7127): 541-545.
- Malnic, B., P. A. Godfrey, et al. (2004). "The human olfactory receptor gene family." Proceedings of the National Academy of Sciences of the United States of America **101**(8): 2584-2589.
- Malnic, B., J. Hirono, et al. (1999). "Combinatorial receptor codes for odors." Cell **96**(5): 713-723.
- Man, O., Y. Gilad, et al. (2004). "Prediction of the odorant binding site of olfactory receptor proteins by human-mouse comparisons." Protein science : a publication of the Protein Society **13**(1): 240-254.
- Matarazzo, V., O. Clot-Faybesse, et al. (2005). "Functional characterization of two human olfactory receptors expressed in the baculovirus Sf9 insect cell system." Chemical senses **30**(3): 195-207.

- Matsukawa, M., M. Imada, et al. (2011). "Rose odor can innately counteract predator odor." Brain research **1381**: 117-123.
- Matsumoto, H., K. Kobayakawa, et al. (2010). "Spatial arrangement of glomerular molecular-feature clusters in the odorant-receptor class domains of the mouse olfactory bulb." Journal of neurophysiology **103**(6): 3490-3500.
- Matsunami, H. (2005). "Functional expression of Mammalian odorant receptors." Chemical senses **30 Suppl 1**: i95-96.
- McEwen, D. P., P. M. Jenkins, et al. (2008). "Olfactory cilia: our direct neuronal connection to the external world." Current topics in developmental biology **85**: 333-370.
- McMurry, J. (2012). Organic Chemistry. Belmont, CA, Brooks / Cole.
- Meanwell, N. A. (2011). "Synopsis of some recent tactical application of bioisosteres in drug design." Journal of medicinal chemistry **54**(8): 2529-2591.
- Miesenbock, G., D. A. De Angelis, et al. (1998). "Visualizing secretion and synaptic transmission with pH-sensitive green fluorescent proteins." Nature **394**(6689): 192-195.
- Mills, J. E. and P. M. Dean (1996). "Three-dimensional hydrogen-bond geometry and probability information from a crystal survey." Journal of computer-aided molecular design **10**(6): 607-622.
- Miyamichi, K., S. Serizawa, et al. (2005). "Continuous and overlapping expression domains of odorant receptor genes in the olfactory epithelium determine the dorsal/ventral positioning of glomeruli in the olfactory bulb." The Journal of neuroscience : the official journal of the Society for Neuroscience **25**(14): 3586-3592.
- Mizrahi, A., H. Matsunami, et al. (2004). "An imaging-based approach to identify ligands for olfactory receptors." Neuropharmacology **47**(5): 661-668.
- Mombaerts, P. (1999). "Seven-transmembrane proteins as odorant and chemosensory receptors." Science **286**(5440): 707-711.

- Mombaerts, P. (2004). "Genes and ligands for odorant, vomeronasal and taste receptors." Nature reviews. Neuroscience **5**(4): 263-278.
- Mombaerts, P., F. Wang, et al. (1996). "Visualizing an olfactory sensory map." Cell **87**(4): 675-686.
- Mori, K., H. Nagao, et al. (1999). "The olfactory bulb: coding and processing of odor molecule information." Science **286**(5440): 711-715.
- Mori, K., Y. K. Takahashi, et al. (2006). "Maps of odorant molecular features in the Mammalian olfactory bulb." Physiological reviews **86**(2): 409-433.
- Mucignat-Caretta, C. (2010). "The rodent accessory olfactory system." Journal of comparative physiology. A, Neuroethology, sensory, neural, and behavioral physiology **196**(10): 767-777.
- Murrell, J. R. and D. D. Hunter (1999). "An olfactory sensory neuron line, odora, properly targets olfactory proteins and responds to odorants." The Journal of neuroscience : the official journal of the Society for Neuroscience **19**(19): 8260-8270.
- Nakamura, T. and G. H. Gold (1987). "A cyclic nucleotide-gated conductance in olfactory receptor cilia." Nature **325**(6103): 442-444.
- Nara, K., L. R. Saraiva, et al. (2011). "A large-scale analysis of odor coding in the olfactory epithelium." The Journal of neuroscience : the official journal of the Society for Neuroscience **31**(25): 9179-9191.
- Neuhaus, E. M., W. Zhang, et al. (2009). "Activation of an olfactory receptor inhibits proliferation of prostate cancer cells." The Journal of biological chemistry **284**(24): 16218-16225.
- Niimura, Y. and M. Nei (2007). "Extensive gains and losses of olfactory receptor genes in mammalian evolution." PloS one **2**(8): e708.
- Oka, Y., S. Katada, et al. (2006). "Odorant receptor map in the mouse olfactory bulb: in vivo sensitivity and specificity of receptor-defined glomeruli." Neuron **52**(5): 857-869.

- Oka, Y., M. Omura, et al. (2004). "Olfactory receptor antagonism between odorants." The EMBO journal **23**(1): 120-126.
- Otsuguro, K., S. H. Gautam, et al. (2005). "Characterization of forskolin-induced Ca²⁺ signals in rat olfactory receptor neurons." Journal of pharmacological sciences **97**(4): 510-518.
- Patani, G. A. and E. J. LaVoie (1996). "Bioisosterism: A Rational Approach in Drug Design." Chemical reviews **96**(8): 3147-3176.
- Peterlin, Z., A. Chesler, et al. (2007). "A painful trp can be a bonding experience." Neuron **53**(5): 635-638.
- Peterlin, Z., Y. Ishizawa, et al. (2005). "Selective activation of G-protein coupled receptors by volatile anesthetics." Molecular and cellular neurosciences **30**(4): 506-512.
- Peterlin, Z., Y. Li, et al. (2008). "The importance of odorant conformation to the binding and activation of a representative olfactory receptor." Chemistry & biology **15**(12): 1317-1327.
- Pifferi, S., A. Menini, et al. (2010). Signal Transduction in Vertebrate Olfactory Cilia. The Neurobiology of Olfaction. A. Menini. Boca Raton (FL).
- Pilpel, Y. and D. Lancet (1999). "The variable and conserved interfaces of modeled olfactory receptor proteins." Protein science : a publication of the Protein Society **8**(5): 969-977.
- Pyrski, M., J. H. Koo, et al. (2007). "Sodium/calcium exchanger expression in the mouse and rat olfactory systems." The Journal of comparative neurology **501**(6): 944-958.
- Raming, K., J. Krieger, et al. (1993). "Cloning and expression of odorant receptors." Nature **361**(6410): 353-356.
- Rawashdeh, A. M., A. Thangavel, et al. (2008). "Control of the ketone to gem-diol equilibrium by host-guest interactions." Organic letters **10**(6): 1131-1134.

- Rawson, N. E., J. Eberwine, et al. (2000). "Expression of mRNAs encoding for two different olfactory receptors in a subset of olfactory receptor neurons." Journal of neurochemistry **75**(1): 185-195.
- Reed, R. R. (2004). "After the holy grail: establishing a molecular basis for Mammalian olfaction." Cell **116**(2): 329-336.
- Reisert, J., J. Lai, et al. (2005). "Mechanism of the excitatory Cl⁻ response in mouse olfactory receptor neurons." Neuron **45**(4): 553-561.
- Reisert, J. and H. R. Matthews (1998). "Na⁺-dependent Ca²⁺ extrusion governs response recovery in frog olfactory receptor cells." The Journal of general physiology **112**(5): 529-535.
- Repicky, S. E. and C. W. Luetje (2009). "Molecular receptive range variation among mouse odorant receptors for aliphatic carboxylic acids." Journal of neurochemistry **109**(1): 193-202.
- Ressler, K. J., S. L. Sullivan, et al. (1993). "A zonal organization of odorant receptor gene expression in the olfactory epithelium." Cell **73**(3): 597-609.
- Rossiter, K. J. (1996). "Structureminus signOdor Relationships." Chemical reviews **96**(8): 3201-3240.
- Rubin, B. D. and L. C. Katz (1999). "Optical imaging of odorant representations in the mammalian olfactory bulb." Neuron **23**(3): 499-511.
- Saito, H., Q. Chi, et al. (2009). "Odor coding by a Mammalian receptor repertoire." Science signaling **2**(60): ra9.
- Saito, H., M. Kubota, et al. (2004). "RTP family members induce functional expression of mammalian odorant receptors." Cell **119**(5): 679-691.
- Sakmar, T. P., S. T. Menon, et al. (2002). "Rhodopsin: insights from recent structural studies." Annual review of biophysics and biomolecular structure **31**: 443-484.

- Sanz, G., C. Schlegel, et al. (2005). "Comparison of odorant specificity of two human olfactory receptors from different phylogenetic classes and evidence for antagonism." Chemical senses **30**(1): 69-80.
- Sanz, G., T. Thomas-Danguin, et al. (2008). "Relationships between molecular structure and perceived odor quality of ligands for a human olfactory receptor." Chemical senses **33**(7): 639-653.
- Sato, T., J. Hirono, et al. (1994). "Tuning specificities to aliphatic odorants in mouse olfactory receptor neurons and their local distribution." Journal of neurophysiology **72**(6): 2980-2989.
- Schmiedeberg, K., E. Shirokova, et al. (2007). "Structural determinants of odorant recognition by the human olfactory receptors OR1A1 and OR1A2." Journal of structural biology **159**(3): 400-412.
- Schwobel, J., R. U. Ebert, et al. (2009). "Prediction of the intrinsic hydrogen bond acceptor strength of organic compounds by local molecular parameters." Journal of chemical information and modeling **49**(4): 956-962.
- Serizawa, S., K. Miyamichi, et al. (2003). "Negative feedback regulation ensures the one receptor-one olfactory neuron rule in mouse." Science **302**(5653): 2088-2094.
- Serizawa, S., K. Miyamichi, et al. (2004). "One neuron-one receptor rule in the mouse olfactory system." Trends in genetics : TIG **20**(12): 648-653.
- Sheridan, R. P. (2002). "The most common chemical replacements in drug-like compounds." Journal of chemical information and computer sciences **42**(1): 103-108.
- Shi, L. and J. A. Javitch (2002). "The binding site of aminergic G protein-coupled receptors: the transmembrane segments and second extracellular loop." Annual review of pharmacology and toxicology **42**: 437-467.
- Shirokova, E., K. Schmiedeberg, et al. (2005). "Identification of specific ligands for orphan olfactory receptors. G protein-dependent agonism and antagonism of odorants." The Journal of biological chemistry **280**(12): 11807-11815.

- Sicard, G. and A. Holley (1984). "Receptor cell responses to odorants: similarities and differences among odorants." Brain research **292**(2): 283-296.
- Singer, M. S. (2000). "Analysis of the molecular basis for octanal interactions in the expressed rat 17 olfactory receptor." Chemical senses **25**(2): 155-165.
- Soucy, E. R., D. F. Albeanu, et al. (2009). "Precision and diversity in an odor map on the olfactory bulb." Nature neuroscience **12**(2): 210-220.
- Spehr, M., G. Gisselmann, et al. (2003). "Identification of a testicular odorant receptor mediating human sperm chemotaxis." Science **299**(5615): 2054-2058.
- Sztybel, D., C. Suwattanasophon, et al. (2007). "Differences in (-)-citronellal binding to various odorant receptors." Biochemical and biophysical research communications **361**(4): 941-945.
- Takahashi, Y. K., M. Kurosaki, et al. (2004). "Topographic representation of odorant molecular features in the rat olfactory bulb." Journal of neurophysiology **92**(4): 2413-2427.
- Takahashi, Y. K., S. Nagayama, et al. (2004). "Detection and masking of spoiled food smells by odor maps in the olfactory bulb." The Journal of neuroscience : the official journal of the Society for Neuroscience **24**(40): 8690-8694.
- Tan, J., A. Savigner, et al. (2010). "Odor information processing by the olfactory bulb analyzed in gene-targeted mice." Neuron **65**(6): 912-926.
- Touhara, K. (2001). "Functional cloning and reconstitution of vertebrate odorant receptors." Life sciences **68**(19-20): 2199-2206.
- Touhara, K. (2002). "Odor discrimination by G protein-coupled olfactory receptors." Microscopy research and technique **58**(3): 135-141.
- Touhara, K., S. Sengoku, et al. (1999). "Functional identification and reconstitution of an odorant receptor in single olfactory neurons." Proceedings of the National Academy of Sciences of the United States of America **96**(7): 4040-4045.

- Triller, A., E. A. Boulden, et al. (2008). "Odorant-receptor interactions and odor percept: a chemical perspective." Chemistry & biodiversity **5**(6): 862-886.
- Tsuboi, A., T. Imai, et al. (2011). "Two highly homologous mouse odorant receptors encoded by tandemly-linked MOR29A and MOR29B genes respond differently to phenyl ethers." The European journal of neuroscience **33**(2): 205-213.
- Tsuboi, A., T. Miyazaki, et al. (2006). "Olfactory sensory neurons expressing class I odorant receptors converge their axons on an antero-dorsal domain of the olfactory bulb in the mouse." The European journal of neuroscience **23**(6): 1436-1444.
- Tsuboi, A., S. Yoshihara, et al. (1999). "Olfactory neurons expressing closely linked and homologous odorant receptor genes tend to project their axons to neighboring glomeruli on the olfactory bulb." The Journal of neuroscience : the official journal of the Society for Neuroscience **19**(19): 8409-8418.
- Uchida, N., Y. K. Takahashi, et al. (2000). "Odor maps in the mammalian olfactory bulb: domain organization and odorant structural features." Nature neuroscience **3**(10): 1035-1043.
- Von Dannecker, L. E., A. F. Mercadante, et al. (2006). "Ric-8B promotes functional expression of odorant receptors." Proceedings of the National Academy of Sciences of the United States of America **103**(24): 9310-9314.
- Wachowiak, M. and L. B. Cohen (2001). "Representation of odorants by receptor neuron input to the mouse olfactory bulb." Neuron **32**(4): 723-735.
- Washington, N., R. J. Steele, et al. (2000). "Determination of baseline human nasal pH and the effect of intranasally administered buffers." International journal of pharmaceutics **198**(2): 139-146.
- Wei, J., A. Z. Zhao, et al. (1998). "Phosphorylation and inhibition of olfactory adenylyl cyclase by CaM kinase II in Neurons: a mechanism for attenuation of olfactory signals." Neuron **21**(3): 495-504.
- Werkhoff P., K. G., Brennecke S., Roloff M., Hertram HJ. (2002). "Methylhydrojasmonate and its stereoisomers: sensory properties and enantioselective analysis." Food Reviews International **18**(2&3): 103-122.

- Wermuth, C. (2008). Molecular Variations in Homologous Series: Vinylogues and Benzologues. The Practice of Medicinal Chemistry. C. Wermuth. San Diego, CA, Academic Press (Eselvier): 275-289.
- Wermuth, C. (2008). Ring Transformations. The Practice of Medicinal Chemistry. C. Wermuth. San Diego, CA, Academic Press (Eselvier): 343-362.
- Wetzel, C. H., M. Oles, et al. (1999). "Specificity and sensitivity of a human olfactory receptor functionally expressed in human embryonic kidney 293 cells and *Xenopus Laevis* oocytes." The Journal of neuroscience : the official journal of the Society for Neuroscience **19**(17): 7426-7433.
- Wolf, S., M. Bockmann, et al. (2008). "Simulations of a G protein-coupled receptor homology model predict dynamic features and a ligand binding site." FEBS letters **582**(23-24): 3335-3342.
- Xu, F., N. Liu, et al. (2003). "Odor maps of aldehydes and esters revealed by functional MRI in the glomerular layer of the mouse olfactory bulb." Proceedings of the National Academy of Sciences of the United States of America **100**(19): 11029-11034.
- Yan, C., A. Z. Zhao, et al. (1995). "Molecular cloning and characterization of a calmodulin-dependent phosphodiesterase enriched in olfactory sensory neurons." Proceedings of the National Academy of Sciences of the United States of America **92**(21): 9677-9681.
- Yoshikawa, K. and K. Touhara (2009). "Myr-Ric-8A enhances G(alpha15)-mediated Ca₂⁺ response of vertebrate olfactory receptors." Chemical senses **34**(1): 15-23.
- Yuste R., L. F., Konnerth A. (2000). Imaging Neurons: A Laboratory Manual. New York, Cold Spring Harbor Laboratory Press.
- Zhang, X. and S. Firestein (2002). "The olfactory receptor gene superfamily of the mouse." Nature neuroscience **5**(2): 124-133.
- Zhang, X. and S. Firestein (2007). "Comparative genomics of odorant and pheromone receptor genes in rodents." Genomics **89**(4): 441-450.

- Zhang, X., I. Rodriguez, et al. (2004). "Odorant and vomeronasal receptor genes in two mouse genome assemblies." Genomics **83**(5): 802-811.
- Zhang, X., M. Rogers, et al. (2004). "High-throughput microarray detection of olfactory receptor gene expression in the mouse." Proceedings of the National Academy of Sciences of the United States of America **101**(39): 14168-14173.
- Zhao, H., L. Ivic, et al. (1998). "Functional expression of a mammalian odorant receptor." Science **279**(5348): 237-242.